Investigation of Higher Fullerenes: Trifluoromethylated Derivatives of C_{84} Cage Isomers

D I S S E R T A T I O N

zur Erlangung des akademischen Grades

Doctor rerum naturalium (Dr. rer. nat.)
im Fach Chemie

eingereicht an der
Mathematisch-Naturwissenschaftlichen Fakultät I
Humboldt-Universität zu Berlin

von
Dipl. Chem. Kai-Chin Chang

Präsident der Humboldt-Universität zu Berlin:
Prof. Dr. Jan-Hendrik Olbertz

Dekan der Mathematisch-Naturwissenschaftlichen Fakultät I:
Prof. Stefan Hecht, PhD

Gutachter:
1. Prof. Dr. Erhard Kemnitz
2. Prof. Dr. Konrad Seppelt

eingereicht am: 9. Oktober 2012
Tag der mündlichen Prüfung: 5. Dezember 2012

For my parents Tai-Wen Chang Mei-shu Lee

Abstract

Trifluoromethylation of higher fullerene mixtures with CF_3I was performed in ampoules at 400-420°C and 500-600°C. The obtained product mixtures were separated by multi-step HPLC. Subsequent crystal growth and X-ray diffraction measurements allowed for structural characterization of the CF_3 derivatives of fullerenes C_{84}, C_{86} and C_{88} listed in the following table.

Cage isomer	No. of CF_3 groups	No. of CF_3 derivatives	X-ray data of derivatives
$C_{84}(4)$	12	1	Ref. 1
$C_{84}(11)$	10	1	this work
	12	1	Ref. 2,3
	14	3	this work
	16	1	this work
$C_{84}(16)$	8	1	this work
	14	1	this work
$C_{84}(18)$	10	1	this work
	12	1	this work
$C_{84}(22)$	12	2	this work
	14	2	this work
	16	4	this work
	20	1	this work
$C_{84}(23)$	8	1	this work
	10	1	this work
	12	1	this work
	14	2	this work
	18	1	this work
$C_{86}(17)$	10	1	this work
	16	1	Ref. 4
$C_{88}(33)$	16	1	this work
	18	1	Ref. 5
	20	1	this work

The molecular structures of isolated isomers were discussed in terms of their addition patterns and relative formation energies. DFT calculations were used to predict stable molecular structures of the CF_3 derivatives. Calculated model structures have been compared with the experimental ones. In addition, the reaction pathways from the lower derivatives to higher ones of selected compounds were predicted. The pathways indicate the regioselectivity of additions depending on the fullerene cage isomer. Reaction pathways are presented for four fullerene cages in this work.

$$C_{84}(11)(CF_3)_{10} \longrightarrow C_{84}(11)(CF_3)_{16}$$
$$C_{84}(22)(CF_3)_2 \longrightarrow C_{84}(22)(CF_3)_{20}$$
$$C_{84}(23)(CF_3)_{10} \longrightarrow C_{84}(23)(CF_3)_{18}$$
$$C_{86}(17)(CF_3)_{10} \longrightarrow C_{86}(17)(CF_3)_{16}$$

Keywords: higher fullerenes, trifluoromethylation, multistep- HPLC, X-ray diffraction, DFT calculations, reaction pathway, regioselectivity

Zusammenfassung

Trifluoromethylierung von Mischungen höherer Fullerene mit CF_3I wurde in Ampullen bei 400-420°C und 500-600°C durchgeführt. Die Produktmischungen wurden mittels mehrstufiger HPLC getrennt. In mehreren Versuchen konnten aus den isolierten HPLC-Fraktionen Kristalle für die Röntgenstrukturanalyse gewonnen werden. Die Strukturen der CF_3-Derivate der Fullerene C_{84}, C_{86} und C_{88}, die in dieser Arbeit bestimmt wurden, sind in der nachfolgenden Tabelle aufgelistet.

Käfigisomer	Anzahl der Additionsgruppen	Anzahl der CF_3-Derivaten	Röntgenanalysedaten von CF_3-Derivaten
$C_{84}(4)$	12	1	Ref. 1
$C_{84}(11)$	10	1	diese Arbeit
	12	1	Ref. 2,3
	14	3	diese Arbeit
	16	1	diese Arbeit
$C_{84}(16)$	8	1	diese Arbeit
	14	1	diese Arbeit
$C_{84}(18)$	10	1	diese Arbeit
	12	1	diese Arbeit
$C_{84}(22)$	12	2	diese Arbeit
	14	2	diese Arbeit
	16	4	diese Arbeit
	20	1	diese Arbeit
$C_{84}(23)$	8	1	diese Arbeit
	10	1	diese Arbeit
	12	1	diese Arbeit
	14	2	diese Arbeit
	18	1	diese Arbeit
$C_{86}(17)$	10	1	diese Arbeit
	16	1	Ref. 4
$C_{88}(33)$	16	1	diese Arbeit
	18	1	Ref. 5
	20	1	diese Arbeit

Die Additionsmuster der Strukturen wurden diskutiert. Die experimentell nachgewiesenen Strukturen wurden mit berechneten Modellstrukturen verglichen. Dabei wurde auch die Stabilität der experimentellen Strukturen vorausgesagt. Zusätzlich wurden die möglichen Reaktionspfade für die Bildung höherer Derivate ausgehend von niedrigen Derivaten diskutiert. Sie zeigen, dass die Regioselektivität der Addition vom Käfigisomer abhängig ist. Die Reaktionspfade von vier Fullerenkäfigen werden in dieser Arbeit vorgestellt.

$$C_{84}(11)(CF_3)_{10} \longrightarrow C_{84}(11)(CF_3)_{16}$$
$$C_{84}(22)(CF_3)_2 \longrightarrow C_{84}(22)(CF_3)_{20}$$
$$C_{84}(23)(CF_3)_{10} \longrightarrow C_{84}(23)(CF_3)_{18}$$
$$C_{86}(17)(CF_3)_{10} \longrightarrow C_{86}(17)(CF_3)_{16}$$

Schlagwörter: : höhere Fullerene, Trifluoromethylierung, mehrstufige HPLC, Röntgendiffraktometrie, DFT Berechnung, Reaktionspfade, Regioselektivität

Diese Arbeit wurde mit dem Textsatzsystem TEX unter Verwendung des Softwarepakets LATEX (Version 2_ε) editiert. TEX wurde von DONALD E. KNUTH entwickelt. Informationen zu TEX befinden sich auf der Webseite `http://www.tug.org`. LATEX ist eine Sammlung von TEX-Makros, die von LESLIE LAMPORT entwickelt wurden. Weitere Informationen zu LATEX befinden sich unter `http://www.latex-project.org`.

Die Abbildungen in dieser Arbeit wurden mit folgender Software erstellt:

DIAMOND (Crystal Impact GbR): Bilder von molekularen Strukturen.

INKSCAPE (Informationen unter `http://inkscape.org`): Nachbearbeitung der Bilder, Erstellung der Schemata.

ORIGIN (OriginLab Corporation): Bilder von Chromatograme und Spektrum.

SCHLEGEL (Thermochemistry Lab, Moscow State University): Erstellung der Schlegel Diagramme.

Stand aller Webadressen in der Dissertation:
Oktober 2012

Contents

Chapter 1.

Introduction

The story of fullerenes begins with an extinction spectrum recorded by astrophysicists in the beginning of the 1980's. It was obtained from a galaxy far away from the earth, and contained a mysterious signal. In order to investigate this signal, routine experiments with a lucky incident at the Heidelberger Max-Planck Institute caused a huge revolution in carbon chemistry. An extinction spectrum was obtained by W. Krätschmer and D. R. Huffman. Beside the signals caused probably by ice, graphite and silicate, the undefined signal was observed in the spectrum. It was suggested that this signal was dust ejected from a supernova and absorbed at about 217 nm.[6,7] The same signal is also observed in carbon dust generated in lab. Hence, the astrophysicists supposed that the interstellar matter must contain carbon. There were only two known carbon allotropes at that time, i.e., diamond and graphite. However, both of them exhibited no signal at 217 nm.

1.1. Discovery of fullerenes

Interstellar particles are formed most probably under extreme low temperature, low pressure and high radiation. Based on such astrophysical environment, Krätschmer and Huffman designed a generator (see Fig. 1.1), using a vacuum evaporation technique for the production of amorphous carbon films. The generator consists of a glass bell jar connected to a vacuum pump and a gas inlet. In this glass jar, two pure carbon rods used as electrodes are kept in contact by a sharp tip. The jar is evacuated first and then filled with helium. An electric current is passed through the rods and leads to a bright arc-discharge under high temperatures of 2500-3000°C. Black smoke is observed, cooled in helium and finally condensed on the smoke catcher. The pressure of helium is used not only for carbon vapor cooling but also for particle growth. If the gas pressure is relatively high, carbon vapor concentrates around the contact point of the two rods. Therefore, particles grow fast and form amorphous substance. About 27 mbar have been used by Krätschmer and Huffman at that time yielding a carbon film that exhibits characteristic UV absorption signals at 216, 264 and 339 nm.[8]

Which compound was measured by Krätschmer and Huffman? How does the structure of this substance look like? This question could not be answered until a paper has been published by H. Kroto from University Sussex in Brighton and his American colleagues R. Curl and R. Smalley from Rice University in Huston. They used a Nd-YAG laser to vaporize carbon species from a graphite disc into a high-density helium flow (see Fig. 1.2).[10] The carbon clusters formed in the gas phase have been detected by time-of-flight mass spectrometry (TOF-MS). They contain up to 190 carbon atoms and those clusters with more than 40 carbons consist only of even numbers of atoms. The intensity of the C_{60} peak is much higher than that of others neighboring clusters, and varies by different pressures of the gas flow. In addition, the small fragments detected in the mass spectrum consist of six-membered rings, and can be considered as precursors for the C_{60}. Hence, Kroto constructed a polyhedron made of paper as a model of the C_{60} molecule. The polyhedron has 32 faces with twelve pentagons and 20 hexagons. This molecule with almost spherical structure was later named after Buckminster Fuller, who is famous for his architectural

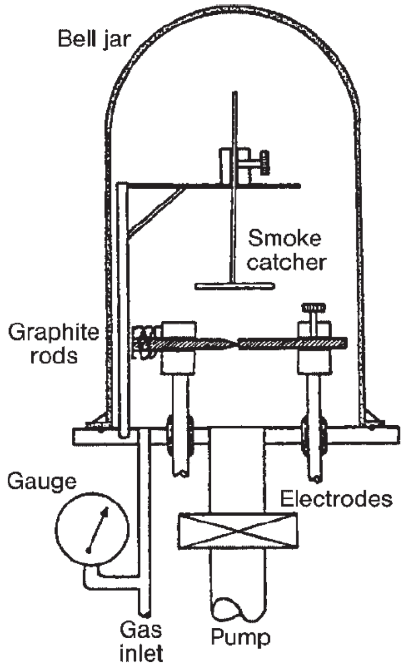

Figure 1.1.: Fullerene generator originally used by Krätschmer.[9]

design of geodesic domes. A completely new allotrope of carbon has been found by Kroto, Curl and Smalley. They have been awarded the Nobel Prize in Chemistry 1996.

1.2. Synthesis of fullerenes

Although the 'spherical' C_{60} molecule had been discovered, it was obtained just in 'academic' amounts. This was sufficient for spectroscopic characterization but not for further synthetic modifications. Increased product yields were not achieved until the end of the 80s. At that time, a routine experiment with a lucky incident made the fullerene production affordable.

The production of the carbon soot, whose spectra is used to explain the absorption of interstellar particles, has always carried out under low pressure and low temperature to simulate the cosmic con-

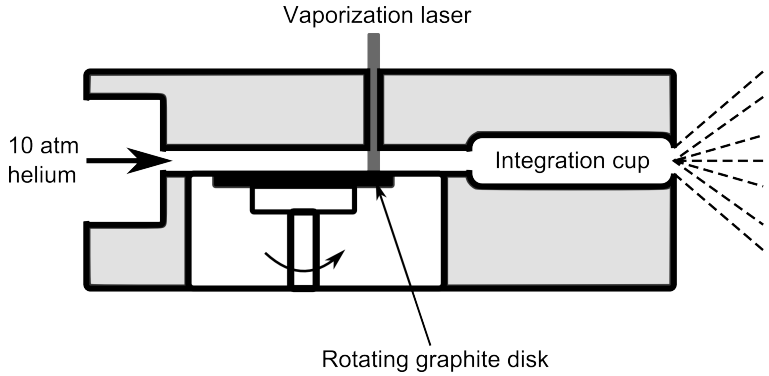

Figure 1.2.: Fullerene generator used by Smalley.

ditions. These reaction conditions were used by numerous researchers in the past. A physics student, Bernd Wanger, has been asked by Krätschmer to repeat the soot experiment changing some parameters. The results were similar to the previous ones until he introduced too much helium into the system. Under pressures around 100 torr (133 mbar), the absorption around 220 nm became pronounced and reproducible. The IR absorption of this product exhibited the pattern of the soccer-ball C_{60}. This high pressure method for the bulk production of C_{60} was reported by Krätschmer, Lamb, Fostiropoulos and Huffman[8], and became a commercial method for fullerene production until now.

1.3. Structure of fullerenes

In fact, the discovery of fullerenes was a lucky incident resulting from the experiments on interstellar-like dusts. In the product soot, C_{60} is the dominating product, while C_{70} and some higher fullerenes, such as C_{76}, C_{78}, C_{84} are minor products. They can be separated chromatographically for further research.[11–14]

Isolated pentagon rule

Each fullerene is a closed carbon cage of twelve pentagons and varying number of hexagons. Different connectivities between pentagons and hexagons lead to various fullerene cage isomers. The cage isomer number grows with the fullerene size. For example, C_{60} has 1812 but C_{84} has 51592 structural isomers.[15] However, only one isomer of C_{60} can be obtained by experiments due to steric strain caused by the cage. An important rule for the construction of fullerene cages proposed by Kroto in 1987 can provide a reasonable explanation.[16] This rule is related to the stability of the fullerene cage, and is known as the *Isolated Pentagon Rule* (IPR). It suggests that, a cage is optimal if all twelve pentagons are completely surrounded by hexagons. This supports that only one experimental structure of C_{60} has been found. The IPR strongly reduces the number of cage isomers, e.g., C_{84} has only 24 IPR isomers compared to 51592 isomers in total.

Spiral code

In order to distinguish the different IPR isomers, the spiral code of fullerene cages was introduced:

The surface of a fullerene polyhedron may be unwound in a continuous spiral strip of edge-sharing pentagons and hexagons such that each new face in the spiral after the second shares an edge with both (a) the first and (b) the last face in the preceding spiral that still has an open edge.[15]

This spiral code can be applied to every fullerene polyhedron. For example, C_{60} can be represented by a sequence of the digits 5 and 6 for pentagons and hexagons, respectively. This sequence gives the positions of the pentagons and hexagons along its spiral path (see Figure 4). The first face in the spiral strip can be any face of the polyhedron. The second face can be any neighboring face that shares an edge with the first one, and the third one shares edges with faces one and two. Hence, the C_{60} spiral is represented by the sequences:

$$5666665656565656656565656666665, \tag{1.1}$$

$$6565656665665656565665665656566, \tag{1.2}$$

$$6656565656656656565665665656656. \tag{1.3}$$

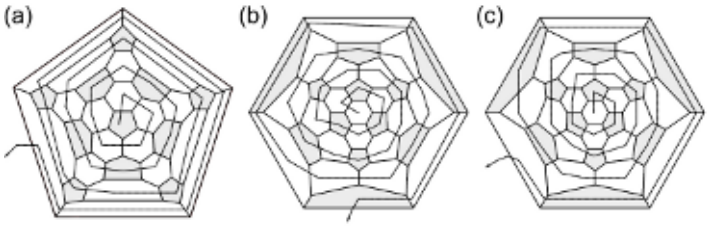

Figure 1.3.: Three spirals of C_{60}.

All of the three sequences consist of 32 digits and describe the same fullerene cage. Each sequence can be read as a number. Thus, the order of these numbers is (1.1) < (1.2) < (1.3). The spiral sequence (1.1) is the smallest number because it begins with a digit 5. In this sequence, the pentagons have positions at

$$1,7,9,11,13,15,18,20,22,24,26,32. \tag{1.4}$$

This sequence of positions of pentagons is the spiral code used to distinguish the geometric structures of fullerenes. The spiral codes of fullerenes C_{84}, C_{86} and C_{88} investigated in this work are given in Appendix D.

Stability of fullerenes

All fullerenes have a common design principle based on the Euler theorem for polyhedrons:

$$vertices + faces = edges + 2. \tag{1.5}$$

For a fullerene C_n, this equation can be represented as

$$faces = \frac{n}{2} + 2. \tag{1.6}$$

Every fullerene contains exactly twelve pentagons, thus the number of hexagons (M) can be presented as

$$M = \frac{n}{2} - 10. \tag{1.7}$$

According to the above equation, C_{20} can be imagined as the smallest fullerene (M = 0). C_{20} without any hexagon is against the IPR and can be considered as highly instable. C_{60} is the smallest stable fullerene which obeys the IPR. According to the IPR, two adjacent pentagons are forbidden. The reasons for this instability are (i) the pentalen-type 8 π electron systems and (ii) the increase of the strain energy.[9] The 8 π electron system is predicted as destabilized by resonance according to Hückel's rule for aromatic hydrocarbons. This steric strain is a result of the enforced bond angles due to limited flexibility of the fullerene cage.

Besides the σ bonds lying on the spherical surface, C atoms of fullerenes connect with each by weak π bonds. The spherical structure of fullerenes leads to the pyramidalization of the sp^2 hybridization as a consequence of the rehybridization. For planar structures, e.g., graphite, the ideal bond angle is 120° which fits perfectly to sp^2 hybridization, and thus rehybridization is not necessary. However, the bond angles in C_{60} are closer to 109° than 120°, yielding a substantial rehybridization in fullerenes.[15] In addition, rehybridization accompanies with the strain energy. Graphite serves here to explain the source of the strain energy. In the case of graphite, p_π orbitala are perfectly aligned, whereas the p_π orbitals of fullerenes are perpendicular to the surface of the cage resulting in weak π bonding (less overlap) (see

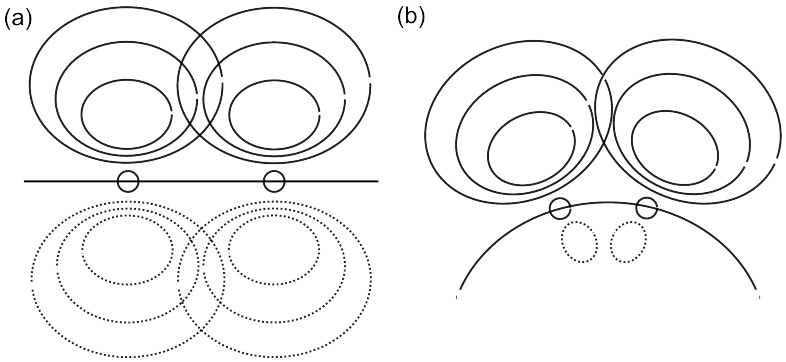

Figure 1.4.: π orbitals of (a) graphite and (b) fullerene. Positive and negative contours are shown with solid and dashed lines, respectively.

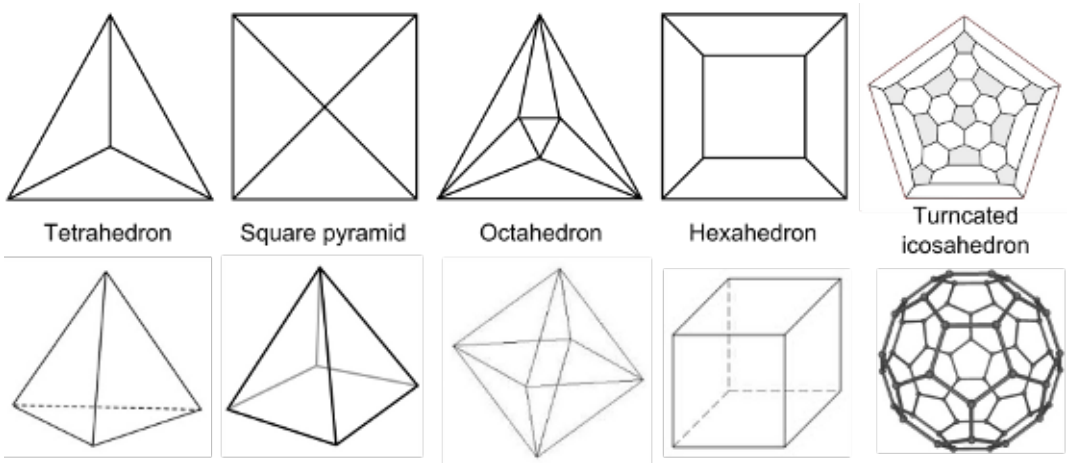

Figure 1.5.: Schlegel diagrams for polyhedrons.

Fig. 1.4). The overlap degree of a π bond in fullerenes is smaller than that one in graphite. In typical fullerenes, the degree of rehybridization varies by the local environment and strain has been released.

Schlegel diagrams and numbering of C atoms of the fullerene cages

In order to illustrate the geometric figures of fullerenes and their derivatives, perspective views have been used. However, it is more convenient to present the fullerene structure as a Schlegel diagram. This is commonly used for illustration of polyhedrons, such as tetra-, hexa-, octahedron and some more complicated structures (see Fig. 1.5). For fullerenes, the Schlegel diagram projects all C atoms of the fullerene cage into a plane with respect to one of its rotation axes, so that some of the C-C bonds appear stretched. The selected reference axis of the projection is usually a principle axis with the highest symmetric order, of which the contiguous helical pathway of the C atoms successfully unwind. Such 2D projections show the same cage connectivities as well as 3D-projections and are used for the structure illustrations of bare fullerenes and their derivatives in this thesis.

The numbering of the fullerenes follows the recommendations of F. Cozzi, W.H. Powell and C. Thilgen which have been published in *Pure Appl. Chem.*, 1995.[17] The basic rules are:

(1) A proper rotation axis (reference axis) has been selected, which is usually a highest-order axis (but not necessarily).

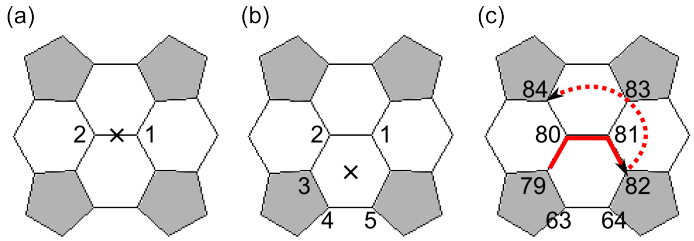

Figure 1.6.: Models of a partial fullerene cage for systematic numbering. Crosses show the principle axis. The beginning position of numbering: a ring (b) is preferred over a bond (a). In (c), the solid line shows the continuous numbering while the dashed line shows the discontinuous numbering.

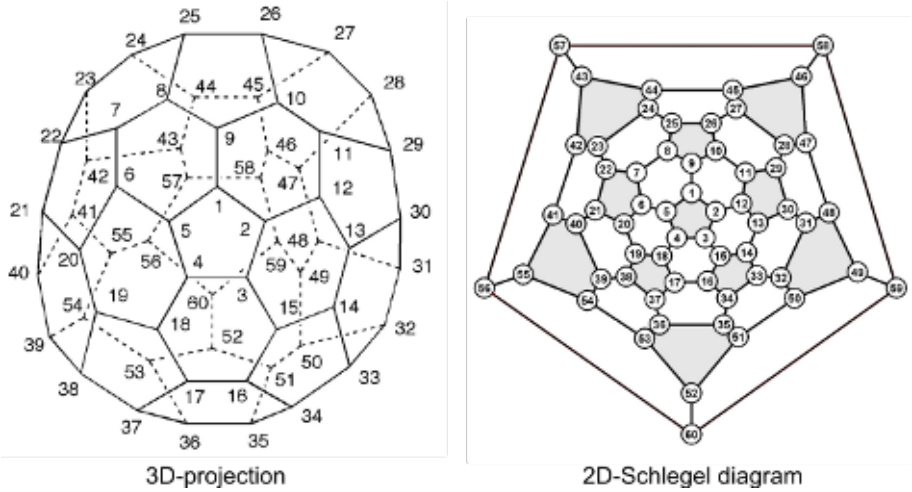

Figure 1.7.: Systematic numbering of the C_{60} fullerene.

(2) Numbering begins at one terminus of the contiguous helical pathway. For the beginning position, a ring is preferred over a bond (see Fig. 1.6). If there are several helical pathways, the preferred pathway terminates as close as possible to the reference axis.
(3) If the pathway breaks, the larger sequential number is preferred for the break. 'Break' means that the helical pathway for numbering is discontinuous. For example $C_{84}(11)$ with a break at position 82 means that the numbering becomes discontinuous at position 82 (see Fig. 1.6).

A example, the numbering of C_{60} will be illustrated in Fig. 1.7.

1.4. Perfluoroalkylated fullerenes

All fullerenes can be considered as three-dimensional analogues of planar aromatics. In contrast to classical aromatic compounds, fullerenes contain no hydrogen atom and thus no substitution reaction can be carried out. Most of known fullerene chemistry refers to electron-transfer and addition reactions on C_{60} and C_{70}.

C_{60} was predicted to be an electronegative molecule based on calculations of orbital energies.[18–22] In agreement with this prediction, cyclic voltammetry (CV) studies demonstrate the formation of the hexaanion C_{60}^{6-}.[23,24] This means that fullerenes behave like electron deficient conjugated polyolefins and can react rapidly with nucleophiles and radicals. In addition, the sp^2 C atoms in fullerenes exhibit a

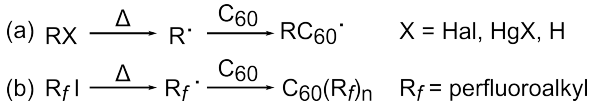

Figure 1.8.: Alkylation reaction.

relative high degree of pyramidalization, i.e., they are strained molecules. Thus the release of strain in the fullerene cage is a driving force for addition reactions. The average CCC bond angle of the fullerene cage is closer to 109° than to 120°, which is **not** ideal for sp^2 hybridization. When a functional group attaches to the cage, the CCC bond angle varies by a small value but it fits better to sp^3 hybridization. Therefore, the cage strain has been released and addition reaction is usually exothermic.

In 1993, Fagan *et al.* at DuPont synthesized perfluoroalkylated nanospheres using the photolysis and thermolysis of C_{60} and perfluoroalkyl iodide (R_fI) in organic solvent at different temperatures. At high temperature (about 200°C) in a sealed ampoule, perfluoroalkyl radicals are generated by thermal decomposition of the iodide precursor. The typical reactions are shown in Fig. 1.8.

Dark-brown product mixtures cintaining $C_{60}(C_6F_{13})_{6-12}$ and $C_{60}(CF_3)_{3-14}$ were observed, dominated by the species $C_{60}(C_6F_{13})_{10}$ and $C_{60}(CF_3)_{8-10}$. In the reaction at room temperature, radicals were generated by photolysis of perfluoromethyl iodide using UV light. The product compositions $C_{60}(C_2F_5)_{9-16}$ and $C_{60}(CF_3)_{1-13}$ were determined by electron-capture mass spectrometry.

Possible reaction paths that yield perfluoroalkylated fullerenes have been reported. In a solid-phase synthesis, fullerenes and silver trifluoroacetate loaded in a nickel boat are placed in a quartz ampoule. The reaction was carried out at 300-350°C for 4-8 h. The product mixture contains $C_{60}(CF_3)_{2-22}$.[25] Another synthesis is carried out in a gas-solid reactor which has been reported by Kareev *et al...*[26] Fullerene and copper powder are heated with gaseous C_2F_5I in a glass tube to 400-430°C under argon atmosphere for 2-4 h. The product mixture contains $C_{60}(C_2F_5)_{9-16}$.

1.5. Applications

Since fullerenes have been discovered in 1990, the most frequent question was how they can be used in applications. Thus, it is rather disappointing that there is still no widespread use of fullerenes beyond academic research. This is in contrast to their numerous fascinating physical, chemical and biological properties. The reason for this lack of applications is found in the limited availability of fullerene mixtures or even pure fullerenes. Current investigations concentrate on C_{60} and C_{70}, in particular on fulleride salts and their exohedral addition products.

In the beginning of the 1990s, fullerene films have been suggested as solid lubricants.[27] However, this is still an academic idea because fullerenes are expensive and unstable compared to commercial lubricants, such as graphite, molybdenum disulphide and boron nitride. In medicine, fullerene cages have been thought of as container for target drugs. So far, this principle is not realized due to the relative small cage size and the complication for opening/closing fullerene cages. Therefore, this *drug delivery system* remains a challenge. Nevertheless, fullerene derivatives are potentially interesting for pharmaceutical use. The attachment of polar groups on bare fullerenes yields water-soluble derivatives. They can be used for molecular recognition due to their spherical shape, e.g., for the HIV Protease inhibitor.[28–30] In addition, fullerene derivatives can be used for anti-tumor therapeutics and radio therapy.[31] Other interesting applications are polymer-fullerene composites used in photovoltaic cells. Photovoltaic cell using pure conjugated polymers achieved energy conversion efficiencies of only 10^{-3} to 10^{-2} % in the 1990s.[32–37] This was improved by using mixtures of conducting organic polymers with C_{60} and its derivatives.[38] Recent studies by Dyakonov *et al.* at *Konarka Technologies, Inc.* show that efficiencies of

9 % can be achieved.[39] This technology was used in the Power Plastic© series solar cell. Other possible applications of fullerenes and their derivatives are, e.g., the production of diamonds, the use as catalysts and antioxidants in cosmetic products and drugs.

1.6. Motivation and objectives

The fullerene chemistry has been dominated by derivatives of C_{60} and C_{70} since their discovery. The research on higher fullerenes with more than 70 C atoms is however hampered by their limited availability and the existence of cage isomers. Improved methods for their synthesis are required at this point. In contrast to C_{60}, there are non-equivalent C atoms in higher fullerenes due to different distributions of pentagons and hexagons. Hence, the regioselectivity of additions on the cages of the higher fullerenes is the major research interest.

In this thesis, the reactivities and regioselectivities of different higher fullerene cage isomers have been investigated. Several trifluoromethylated higher fullerenes are synthesized under varied reaction conditions. The products are purified via multi-step HPLC, and their molecular structures are determined by single crystal X-ray analysis. The structural data, such as molecular structures and addition patterns provide important information for the selection rules of the quantum chemical calculations. Combining the experimental and computational results, the possible reaction pathways are predicted.

Chapter 2.

Basic concepts of used methods and equipments

This chapter is devoted to the general concepts of the methods and the equipments used for separation and analyses of trifluoromethylated fullerene species in this work. The basic principles for every method and the setup for the equipments are briefly described.

2.1. Separation of fullerenes and derivatives: High Performance Liquid Chromatography

For the separation of the bare fullerenes and fullerene derivatives, HPLC is a useful method which is easy to be operated. The most important separation step of this work is based on this technique. The basic principle, the package of the used columns and the chromatograph equipments will be described in this section.

2.1.1. Basic principles

Basically, the HPLC is the further development of the traditional column chromatography under normal pressure. Different than the column chromatography, high pressure is used for HPLC as driving force for the solvent (mobile phase) to flow through the columns filled with the packing materials (stationary phase). The principle of the component separation can be described as following: two compounds dissolved in the mobile phase (MP) have different interaction with the stationary phase (SP). With this interaction, the compound is adsorbed onto the surface of the SP. As a consequence, the compound interacting with SP elutes slowly while the one not interacting with SP elutes quickly. The relationship can be expressed using the distribution coefficient, K.[40]

$$K = \frac{C_s}{C_m} \tag{2.1}$$

where C_s is the concentration of the compound in the SP, whereas C_m is the one in the MP. With the same MP and SP (under the same separation conditions), the compounds can be separated when their K values are different.

In order to describe exactly the compound separation, the retention time (t_R) of the compound is used as the qualitative expression. The retention time is defined as the period that elapses between the sample injection and the recording of the signal maximum by a detector. A typical chromatogram and its characteristic features are shown in Fig. 2.1. Some information on the separation efficiency can be provided here. Here t_0 is the dead time showing the retention time of the unretained compound, i.e., the time requested by the MP to pass through the column. Depending on the retention time and the dead time, a dimensionless factor, i.e., retention factor or k value[40], can be described as

$$k = \frac{(t_R - t_0)}{t_0}. \tag{2.2}$$

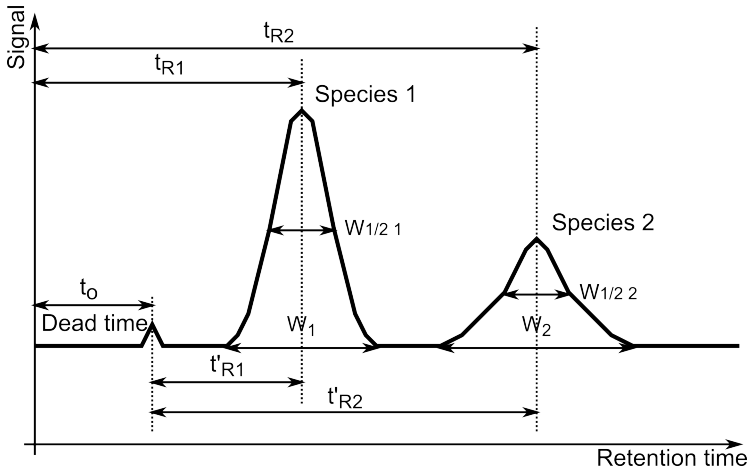

Figure 2.1.: The chromatogram and its characteristic features.

This k value is an indicator to show the degree of the separation. If the k values are too low, the compounds pass through the column too quickly causing no or less retention of the compound, i.e., no separation. Further consideration consists of the separation efficiency. This term can be described with the number of the theoretical plates of the column (N).[40]

$$N = 16(\frac{t_R}{W})^2 = 5.54(\frac{t_R}{W_{1/2}})^2 \tag{2.3}$$

where W is the peak width at the base line (see Fig. 2.1), while the $W_{1/2}$ is the peak width of the half peak height. The larger the numbers are, the better separation can be expected. This value is strongly influenced by the peak width. For example, compounds with long retention times have lower N values than those with shorter retention times due to the possible peak broadening (the peak broadening is discussed in the next section). Otherwise, N also depends on the *column length* (L). The longer is the column, the larger is the N value. So that, the plate height (h) can be described as Some information on the separation efficiency can be provided here. Here t_0 is the dead time showing the retention time of the unretained compound, i.e., the time requested by the MP to pass through the column. Depending on the retention time and the dead time, a dimensionless factor, i.e., retention factor or k value[40], can be described as

$$h = \frac{L}{N}. \tag{2.4}$$

The lower h is, the large N is. In consequence, the better efficiency is.

Two more important indicators of the degree of separation are selectivity and resolution. The selectivity indicates the potential for a separation of two compounds. The separation factor, α[40], is expressed as

$$\alpha = \frac{k_2}{k_1} = \frac{t_{R_2} - t_0}{t_{R_1} - t_0}. \tag{2.5}$$

If α = 1, then there is no separation between two compounds. In order to improve the selectivity, changing the elute compositions or the stationary phase are options.[40]

The resolution, R, of two neighboring peaks can be described as the ratio of the distance between two peak maximum and mean of the peak widths. It is often difficult to measure accurately the peak width,

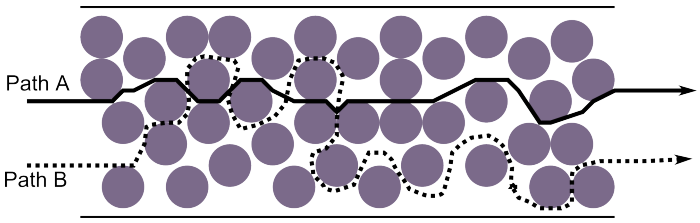

Figure 2.2.: Eddy diffusion in the column.

therefore another approach described with the $W_{1/2}$ are also shown here.[40]

$$R = 2(\frac{t_{R_2} - t_{R_1}}{W_1 + W_2}) = 1.18(\frac{t_{R_2} - t_{R_1}}{W_{1/2_1} + W_{1/2_2}}) \tag{2.6}$$

This value shows how completely two peaks can be separated from each other. If R >1, two peaks are separated. Two peaks are not completely separated when R=1. For R <1, two peaks overlap.

2.1.2. Peak broadening

The peak broadening influences many parameters such as N and R which affect the separation efficiency. It is important to reduce this phenomenon so that better separation can be obtained (N in the column can be kept in high value). Briefly, there are four reasons causing peak broadening: (a) Eddy diffusion and flow distribution, (b) sample diffusion in MP, and (c) mass transfer.

Eddy diffusion is caused by the effects of packing material size and geometry. The analyzed compound or MP molecules can pass through the column by different routes (see Fig. 2.2). The path A results in the narrow peak while the path B in peak broadening. This effect can be reduced by the improvement of the column quality, such as using uniform sized packing, no dead space in the column, etc..[40]

The MP passes through the particles of the stationary phase in the column. In the center of the space between the packing particles the MP molecules can travel faster than near the particles due to friction. The different flow rates belong to the horizontal effect compared to the vertical effect caused by the sample molecules diffusion. This longitudinal diffusion influences directly the plate height (h), i.e., the separation efficiency. This phenomenon is especially obvious if the MP velocity is too low or the sample has a large diffusion coefficient. Both of the flow distribution and the sample diffusion in MP are related to the flow velocity. If the flow velocity is high enough, the effects of the flow distribution and sample diffusion can be neglected.[40]

The stationary phase (packing materials) consists of many particles with pores (Fig. 2.3). The sample molecules can travel into these pores and can only move out the pores via diffusion. This diffusion back to main flux of MP takes times and leads to peak broadening. Otherwise, this diffusion rate depends on the pores size, length and the viscosity of the used MP. The packing material with small particle sizes (smaller pore size and length) and the MP with lower viscosity improve the diffusion of the sample molecules.[40]

In conclusion, three reasons causing the band broadening can be described in form of one equation related with the MP velocity and theoretical plate height (H), i.e., so called the van Deemter equation (Eq. (2.7)). Total plate height is the sum of that caused by (a) Eddy diffusion and flow distribution, (b) sample diffusion in MP, and (c) mass transfer which are shown as A, B and C term. The corresponding Van Deemter curve is shown in Fig. 2.4. In the equation, A term is the component depends on Eddy diffusion and flow distribution. A term is small, if the packing material particle is small and the shape/size uniformed. B term is the component of the sample diffusion. B term is small, if separations are carried

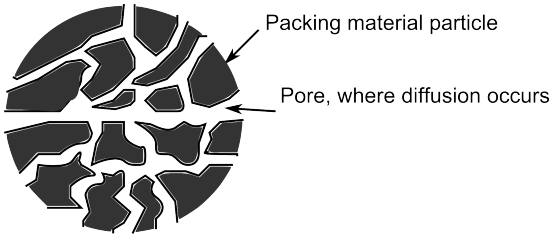

Figure 2.3.: Pore structure of the packing materials (SP).

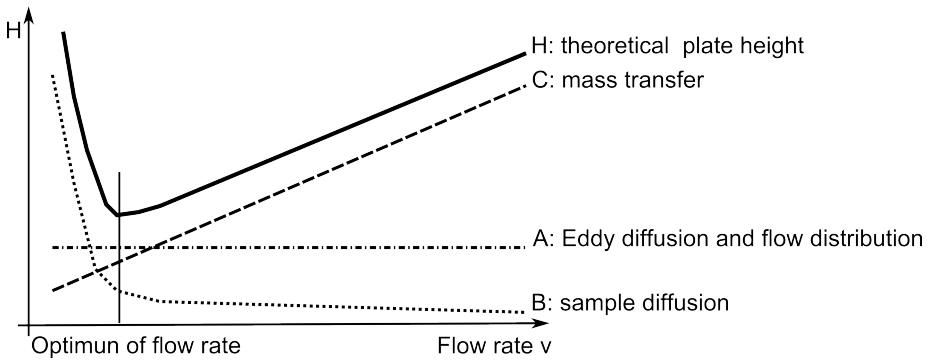

Figure 2.4.: Van Deemter curve: the optimum of the flow rate is obtained via this curve, i.e., the column has the best efficiency under this condition.

out under higher flux rate and use the MP with lower viscosity. C term is component of the mass transfer. C term is small if the flux rate lower.[40]

$$H = A + \frac{B}{v} + Cv \tag{2.7}$$

2.1.3. Packing material

The stationary phase consists of the spherical and porous particles. The size distribution of particles should be narrow. The ratio of the biggest and smallest one should not be bigger than 2 , 1.5 or 1.2 are even better.[40] This is because smaller particles according the Van Deemter curve result in the lower theoretical plate height which leads to better column efficiency. The pore size of the particles is another important parameter for packing material. The pore size is related to the surface area of interaction between sample molecules and SP (pore size / surface area: 30/100; 10/300, and 6/500 (μm / m^2/g)[40]). The smaller pore size, bigger surface area is expected. The bigger surface area, the higher is the retention factor.

Porous silica is one useful option for the packing material in HPLC. Silanol groups (Si-OH, unmodified silica) on the surface of the silica are polar with a slight acidic character, so that basic compounds can be adsorbed here. If using nonpolar organic solvent as MP, it was defined as normal phase (NP) chromatography. Another type of MP is modified silica. Silanol groups on the surface of MP react with organosilanes and resulting in the target products. If the separation is performed using modified silica and polar solvents, it is called reversed phase (RP) chromatography.[40] In this work, two types of columns are used which were developed by *Nacalai Tesque Inc.*, Japan. The packing material of (a) 5-PYE© and (b) Backyprep© column are shown in Fig. 2.5.

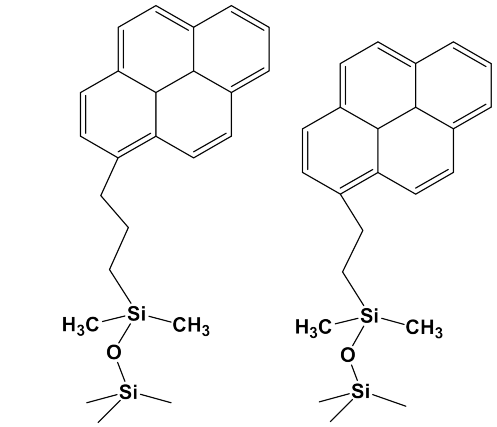

Figure 2.5.: Packing material of the columns.

2.1.4. HPLC equipment

Two different HPLC systems from Shimadzu Prominence series (*Shimadzu Corporation*, Japan) are used in this work. The **single separation** is carried out with System I: solvent delivery module (pump) LC-20AT, degasser DGU-20A5, column oven CTO-20AC, diode array detector SPD-M20A, system controller CBM-20A and injector *Rheodyne* 7725i. A schematic presentation is shown in Fig. 2.6. LC solution version 1.24 SP1 (*Shimadzu Corporation*, Japan) is used for data collection and system control. The **multiple separation** is carried out with System II: solvent delivery module (pump) LC-20AT, degasser DGU-20A5 (share with System I), column oven CTO-20AC (share with System I), UV/VIS detector SPD-20A, system controller CBM-20A, fraction collector FRC-10A, 2 high pressure flow channel selection valve FCV-20AH2 (Valve I and II) and injector Rheodyne 7725i. A schematic presentation is shown in Fig. 2.7.

The two systems are equipped with one guard column (10 mm I.D. x 20 mm) and one packed semi-preparative *Cosmosil* Buckyprep© column (10mm I.D. x 250 mm, *Nacalai Tesque Inc.*, Japan) with 3-(1-pyrenyl)propyl-group bonded silica as stationary phase.

For isomers with similar structures, the isolation within a single separation was not successful. A multi-step HPLC is useful for these cases. Compared with the system of single step separation, two additional recycling valves were developed to introduce the out-flow from the detector back to the pump for a new separation cycle. With this setup, multi step HPLC runs are realized ranging from 3 up to 20 cycles depending on the required resolution and the mixtures employed. After the completion of a selected number of cycles, the mode of two recycling valves is changed which are controlled by the computer and the fractions are transferred to a collector. The multi step HPLC can achieve higher resolutions compared to the single step HPLC. In addition, the multi step HPLC consumes no eluent within the cycling mode and is thus more efficient as the single step HPLC for a comparable number of separation steps.

Note that the capillary between recycling valve II and manual valve [1] should be thinner than other

[1]This manual valve does not exist in the current system yet. There is only one T-piece that connects the reservoirs, the pump and the recycling valve II. Only with this manual valve, a complete closed system for the multiple separations can be set up.

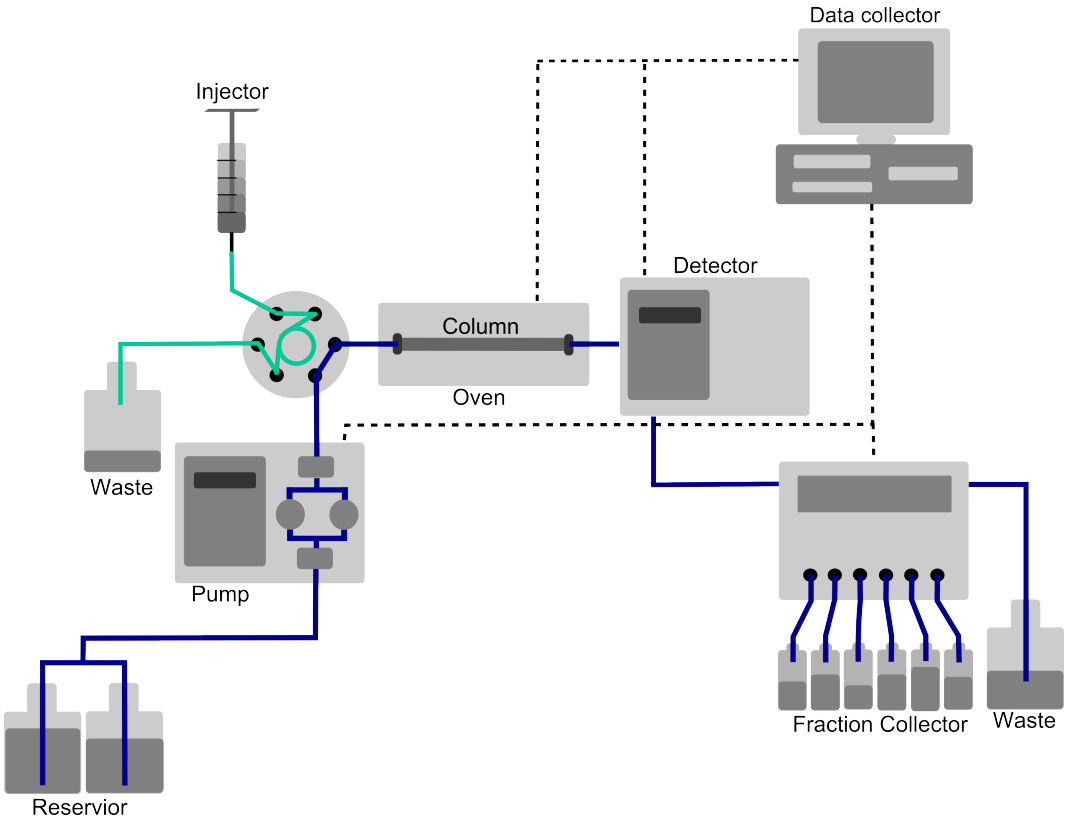

Figure 2.6.: A schematic presentation of **single separation** HPLC system.

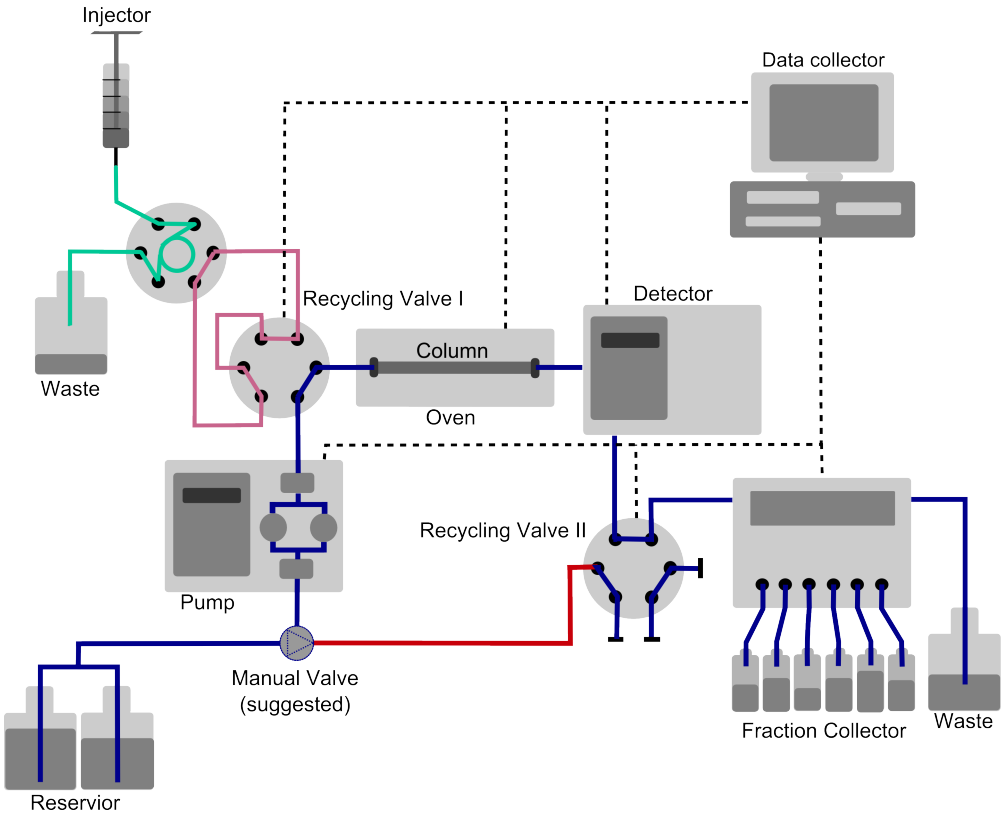

Figure 2.7.: A schematic presentation of **multiple separation** HPLC system.

capillaries used in the system. This avoids mixing of the substances which are already separated within the last separation cycle. This manual valve is a mechanical switch between two modes. Either the mobile phase is supplied with eluent from the reservoir or the system is kept closed for several separation cycles.

Although the multi-step separation is more efficient than the single step separation, there is a limitation. The substance with a short retention time is not always suitable for this method. After few separation cycles, the first peak in the chromatogram (first substance) could be overlapped with the last peak of the last substance. Therefore, it results in no separation between two substances. Few methods can prolong the retention time to avoid this situation, for example, changing the mobile phase, using two columns in series, etc.

2.2. Ultraviolet-Visible Spectrophotometer

The UV/VIS spectroscopy combined with HPLC system is used to identify fullerene species in this work. It is very sensitive, is independent on the temperature fluctuation, has a wide linear range and is suitable not only for isocratic but also for gradient separation. The range of visible spectroscopy is from 400 to 800 nm. The range of UV spectroscopy is from 1 to 400 nm, but measurements below 190 nm are excluded in this work due to the absorption of atmospheric oxygen.[41] (Measurement below 190 nm has to be carried out under the vacuum, i.e., Vacuum-UV-spectrocophy.)

2.2.1. Basic principles

The UV/VIS spectroscopy is, on the one hand, an electronic spectra, and is related to the valence electron promotion from the highest occupied molecular orbital (HOMO) to the lowest unoccupied molecular orbital (LUMO). The procedure of the electron promotion between two orbitals is called excitation of the electrons, and the state of the promoted electron is called excited state. The electron transitions are shown in Fig. 2.8. Only the transition (1) and (2) can be achieved by UV/VIS spectrum, because the photo energies of UV/VIS region is small, i.e., 150-598 kJ/mol in the range of 800-200 nm [2]. Other transitions (3-6) are achieved only in vacuum UV spectroscopy. On the other hand, UV/VIS spectroscopy is an absorption spectroscopy. The absorption takes place above 200 nm if the molecules have following functional groups:[41]

(a) C=C bond adjacent to an atom with a lone electron pair,
(b) Bromine, iodine or sulphur,
(c) C=O, NO_2^- and NO_3^-,
(d) Conjugated C=C bond and
(e) An aromatic ring, e.g. benzene or naphthalene, etc..

When the sample is excited by the light, the electron absorbs energy and can be promoted to the excited state. The wavelength at which absorption occurs and the degree of the absorption are recorded. The degree of the absorption which is measured when the light beam passes through the sample cuvette can be described with the product of the molar absorptivity, ε, sample concentration, c (mg/ml), and the length of the cell, d (cm), so called *Beer Lambert law*:

$$A = \varepsilon c d. \tag{2.8}$$

where A is the absorbance. The absorbance is dimensionless and usually used as the absorption unit in HPLC chromatograms, i.e., 1 absorbance is usually expressed as 1 absorption unit (AU). The UV detector

[2] The energy calculation using the equations $E = h\upsilon = \frac{hc}{\lambda}$, E = energy, h = Planck's constant = 6.6×10^{-27} erg·sec, υ = frequency, λ = wave length, c = velocity of the light = 3×10^{10} cm/sec.

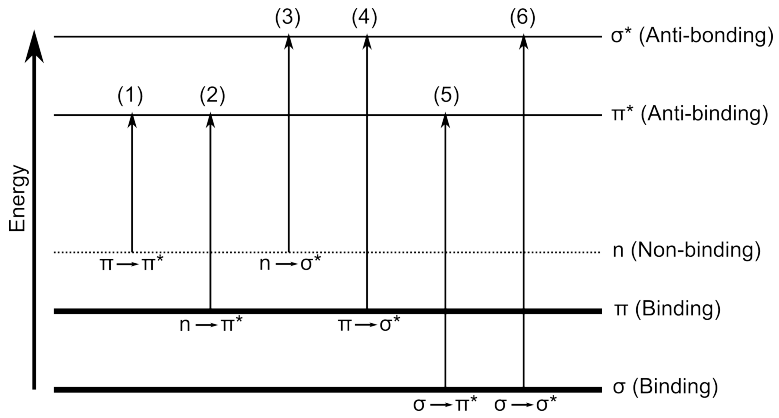

Figure 2.8.: The electron transitions in an organic molecule. Only the transition (1) and (2) occur in the excitation of the UV/VIS light source.

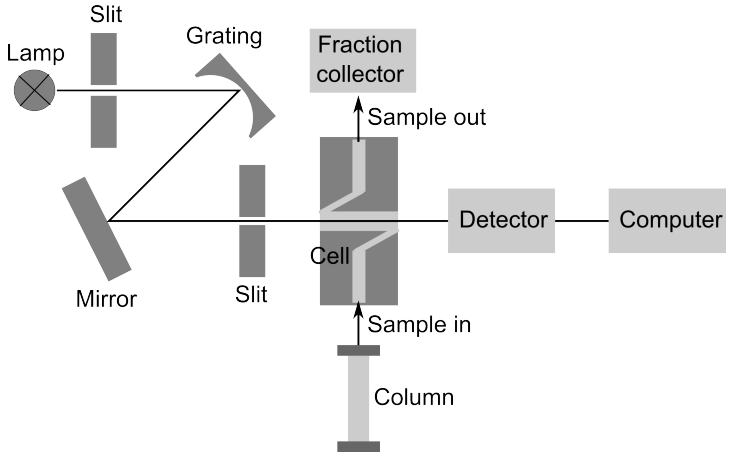

Figure 2.9.: Principle of the multi-wavelength detector connected with HPLC system.

measures the absorption of the eluent. Therefore, the MP should be chosen for optical transparent at the detected wavelength. That means its absorption should be zero or be adjustable to zero electronically, so that a stable baseline can be generated during the separation which is especially important during the gradient elution.

2.2.2. UV/VIS spectroscopy in HPLC system

In a spectrometer, the light is dispersed by a prism or grating monochromator. With the light source of a deuterium lamp, the light wavelength of 180-370 nm for the UV region can be achieved, whereas a tungsten-halogen lamp emits the light of 340-850 nm for the VIS region.[41] The measurements can be presented over the whole spectral range, usually in 190-800 nm. The instrument used in this work is single-beam instrument. The reference and measured sample pass through the sample cuvette one after another. The absorption of the reference, i.e., pure mobile phase, serves as base line in the chromatogram, compared with the one caused by the measured sample. With an optical system, any wavelength in the spectral region can be selected where the sample has the highest absorption. A simple illustration of a dispersive UV/VIS detector is shown in Fig. 2.9.

Another type of spectrophotometer combines the dispersing elements described in the previous part

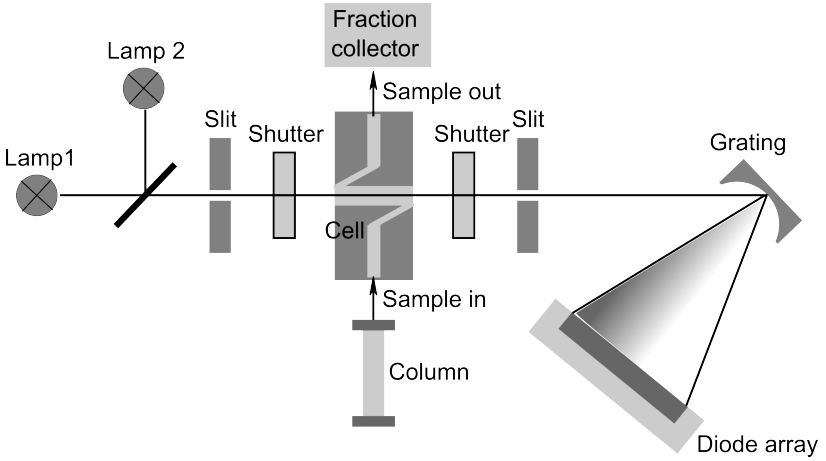

Figure 2.10.: Principle of the photodiode array detector connected with HPLC system.

and the the photodiode array (PDA) as detector. A diagram of the construction is shown in Fig. 2.10. The entering light is controlled by a slit and a shutter, then the light which passes through the sample cell is reflected with a grating and scattered to a multi-channel detector (diode array) which converts optical signals to digital signals.

A spectrum for the whole wavelength range can serve as a comparison tool for similar molecules or isomers even they only have insignificant structural differences. As an example, the spectrum of isomer $C_{84}(22)(CF_3)_{16}$-I to -III are shown in Fig. 2.11.

2.3. MALDI-TOF Mass Spectrometry

MALDI is a soft ionization technique which was developed by Karas, Hillenkamp and coworkers.[42–44] The studies of Tanaka *et al.* were also based on the related technique and used a mixture of the sample and fine metal powder.[45] It is usually combined with a mass spectrometer and widely used in bio-, organic and polymer chemistry. In fullerene chemistry, this technique is very useful due to the following reasons:[46]

(1) soft ionization method and therefore lower degree of the fragmentation,
(2) broad range of the measurements,
(3) short measure time (several seconds per sample spot),
(4) high sensitivity and accuracy.

2.3.1. Basic principles

Matrix

A laser pulse deposits large energy into a sample vaporizing it to an aerosol. Usually, the MALDI-MS sample consists of analyzed molecules and a matrix, due to difficulties in ionization of the pure analytes. The matrix is the volatile acidic substance with strong absorption of photons.[47] When it mixes with the analyte, the ion yield is increased because of the electron transfer between the matrix and less ionizable analyte molecules. The matrix not only enhances the yield of molecular ions but also protects the analyte from being destroyed by the laser. Commonly used matrices are 2,5-dihydroxybenzonic acid (DHB), α-cyano-4-hydroxycinnamic acid (CHCA), picolinic acid (PA), etc., which are dissolved in toluene or 0.1

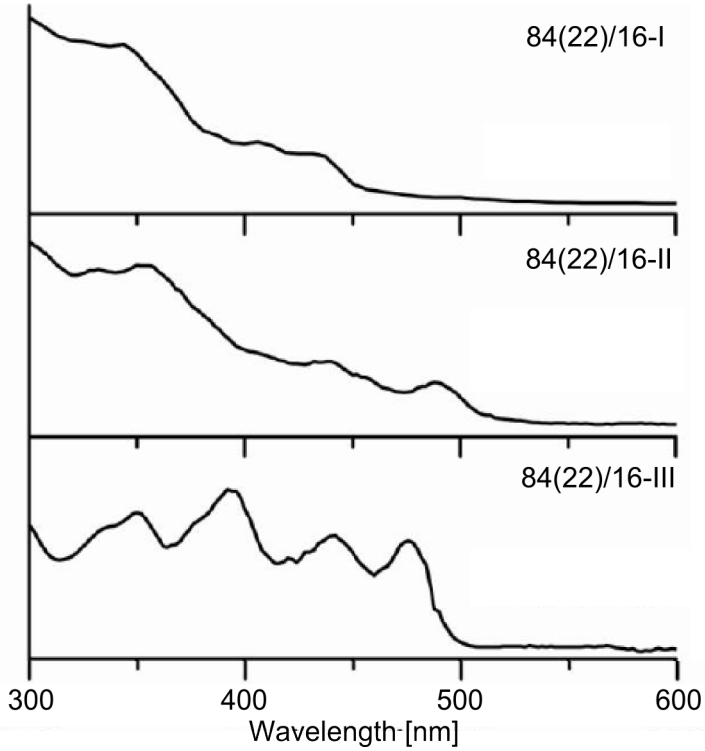

Figure 2.11.: The spectrum of isomer $C_{84}(22)(CF_3)_{16}$-I to -III.

% trifluoroacetic acid (TFA).[48–50] *Trans*-2-[3-(4-butylphenyl)-2-methyl-2-propenylidene]malononitrile (DCTB) was used as matrix in this work. The laser intensity for the ion production of DCTB is extremely low (25 J/m^2 for negative ions), compared with commonly used matrix DHB (100 J/m^2).[51] At such low laser fluence, the tendency to split off addends from fullerene cages is suppressed during the measurement. Therefore, DCTB is an excellent matrix especially for fullerene derivatives.

Time-of-flight (TOF)

After ionizing the sample mixture, the molecular ions are accelerated by an electric field and fly directly to a detector (so called linear TOF-MS, see in Fig. 2.12). The traveling time of ions along the flight tube depends on the ion mass and charge. The smaller the mass of the ion, the faster it arrives at the detector. The motion of ions flying in the tube can described as Eq. (2.9). When the ions are accelerated by the electric field, E (volts), their kinetic energy. E_k, is equal to their potential energy, E_p:

$$E_k = \frac{mv^2}{2} = zeE = E_p. \tag{2.9}$$

where z is the charge of an ion, v is flying velocity and e is the charge of an electron. With the simple rearrangement,

$$v = \sqrt{\frac{2zeE}{m}}. \tag{2.10}$$

If the ion flying distance between the ions source and the detector is d, the flying time (t) can be calculated

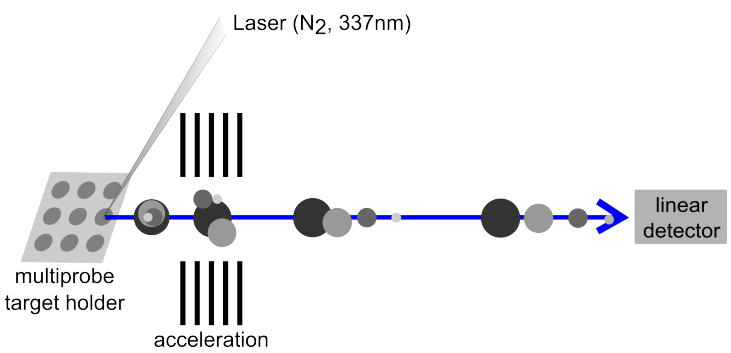

Figure 2.12.: Linear TOF mass spectrometer.

as

$$t = \frac{d}{v} = \frac{d}{\sqrt{2zeE/m}} = \frac{d\sqrt{m/z}}{\sqrt{2eE}} = k\sqrt{m/z}. \tag{2.11}$$

where k is a constant if the fixed electronic filed used during the measurement. Thus the flying time of the ion is proportional to the square root of *m/z*. The recorded flight time can be converted into a mass scale against the ion abundance giving the final mass spectrum.

Resolution and restriction

Based on the Eq. (2.11), the differences in the flight time of two ions can be described as

$$t_m - t_{m+1} = \Delta_t = k(\sqrt{m/z} - \sqrt{(m+1)/z}). \tag{2.12}$$

If m increases, Δ_t will be much smaller, i.e., if the differences of time at the detector between two ions are too small, and it is not possible to distinguish them. Another effect causing decreasing resolution is that not all ions with the same *m/z* value can reach the same velocity after acceleration. The flight time of ions with the same *m/z* is usually not at an exact time but a distribution, i.e., an overlap in arrival time of different ions with similar *m/z* value can be obtained. This effect can be modified using a reflection mode in the measurement. The mass limitation is another restriction of mass spectrometer. Due to the distribution of the arrival time, discrimination of times between two ions becomes more difficult when *m/z* values are higher than 3000. At *m/z* values of 50000, an overlap of 50 mass units is more typical, i.e., mass accuracy is no better than 50-100 mass units.[47] For low mass ranges (<600 Dalton), the measurement is often difficult due to high background.[46]

Reflectron TOF-MS

Compared to the linear TOF-MS, the reflectron TOF-MS has a much better resolution. All of the molecular ions with the same *m/z* value cannot reach the same the same velocity, so results in a distribution of the flight times. To compensate the slight differences in the kinetic energies between the ions with the same *m/z* value, a reflector is set up at the end of the flight tube. The molecular ions will be reflected by the reflector and fly towards the detector. So that the ions with the same *m/z* value are more 'concentrated' in space and in time reach in the detector (see Fig. 2.13). Much more accurate measurements are thereby obtained.

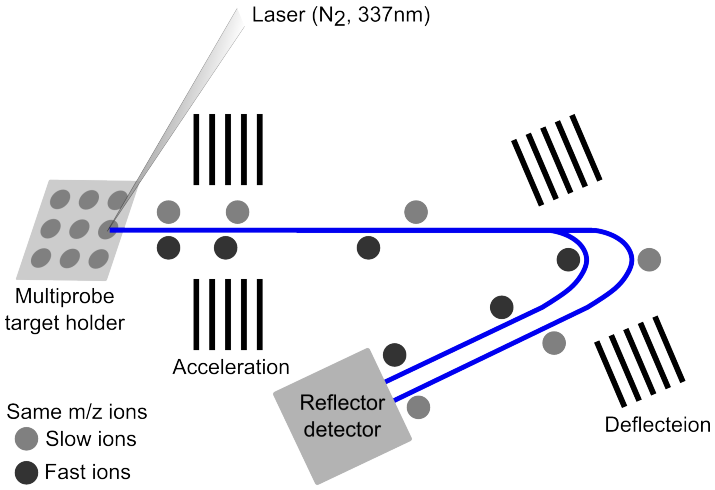

Figure 2.13.: Reflectron TOF mass spectrometer.

2.3.2. Set-up of the TOF mass spectrometer

The mass spectrometer contains three main components: ionizer, mass analyzer and detector. Two common ion sources are MALDI and electrospary, for which J.B. Fenn and K. Tanaka got the Nobel price in chemistry in 2002. The mass analyzer can be iontrap, TOF, quadrupole, Fourier transfer ion cyclotron resonance (FTICR), and so on.[47] For the TOF-MS, the reflecting mode provides higher resolution the linear mode. A schematic representation of the linear and the reflectron TOF MS is shown in Fig. 2.12 and Fig. 2.13, respectively. An Autoflex III smartbeam (*Brucker Daltonik*, Germany) MALDI-TOF Mass Spectrometer has been used in this work.

2.4. Single crystal X-ray diffraction

Single crystal X-ray diffraction is a direct analytical technique which provides detailed information of crystalline substances. The relative location of all atoms within the unit cell can be determined; the connectivity between the atoms, the distance and angles among the atoms can be thereby established.

2.4.1. Basic principles

The constructive interaction between the characteristic X-ray and sample generates constructive interference which satisfy *Bragg's Law*

$$n\lambda = 2dsin\theta (n = 1,2,3...). \tag{2.13}$$

W.H. and W.L. Bragg showed that this incident angle θ must be equal to the angle of reflection and the path difference $2dsin\theta$ is an integral multiple of the wavelength λ.[52] The incoming beam is deflected by an angle 2θ, producing a reflection spot in the diffraction pattern. In a measurement, each reflection requires a unique orientation of the corresponding lattice plane (*hkl*). By the calculation of these orientations, atomic coordinates and coefficients of thermal displacement parameters are provided after measurement. Then it is possible to calculate bonds and bond angles.

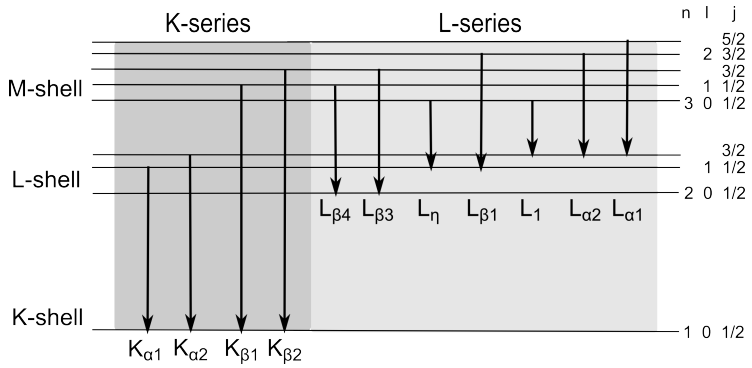

Figure 2.14.: Term transition in the inner electron shells: energy diagram for the individual X-ray emission lines of K- and L-series. n: principle quantum number, l: angular momentum quantum number, j: inner quantum number.

2.4.2. Set-up of a X-ray diffractometer

The diffractometer contains an X-ray tube served as light source, a monochromator for the selection of wavelength, a filter or slit for adjustment of the beam, a sample holder and an X-ray detector. The generated X-ray is filtered to produce monochromatic radiation, collimated and directed toward the sample. In the end, the detector records the reflection to generate reflection pattern.

X-ray tube

X-rays are generated in a sealed high-vacuum tube in two ways. First, a high energetically electron beam hits a metal target, such as Cu, Mo, Fe and so on.[52] The electrons are decelerated and their direction is charged by the field of the metal. Some of its energy is converted into radiation, i.e., general or 'white' radiation.[52] Second, the 'characterized' radiation, which is useful for crystal structure investigation, emitted when an electron transits from the higher atomic energy level to the lower one. If an electron falls from L-shell (principle quantum number $n = 2$) to K-shell ($n = 1$), an X-ray photon with a defined wavelength called K_α radiation is emitted. By the same argument, K_β radiation emitted as the results of electron transition from M-shell to K-shell (see Fig. 2.14). Usually, the radiation caused from the transition from L- or higher shells is weaker, and it is excluded for X-ray diffraction.

There are two types of diffractometers based on the different focus ways. In powder diffraction, the line focus or line source of the tube are used, while point focus is used for single crystal work.[52]

Filter and monochromator

In order to eliminate radiation of other wave length (e.g. K_β radiation), a filter or a monochromator is used. The filter is made of a suitable metal absorbing defined X-ray radiation. For example, to eliminate Cu K_β radiation but allowing Cu K_α to pass, a filter of Ni is suitable.[52] In the same way, Mn filters is suitable for Fe radiation, and Zr for Mo radiation.[52] The monochromator of graphite, quartz, and germanium or lithium fluoride orientates only the desired K_α line to meet the constructive condition.

Synchrotron radiation is another option of the beam source beside the 'characterized' X-ray radiation. It has a very high intensity and a very low divergence. Its tunable wavelength and higher degree of polarization are very useful for structure determinations.[52]. The most fullerene derivatives obtained in this work were structurally characterized using synchrotron radiation from *BESSY* (*Berlin Electronen-Specicherring Gesellschaft für Synchrotronstrahlung*) due to very small crystals.

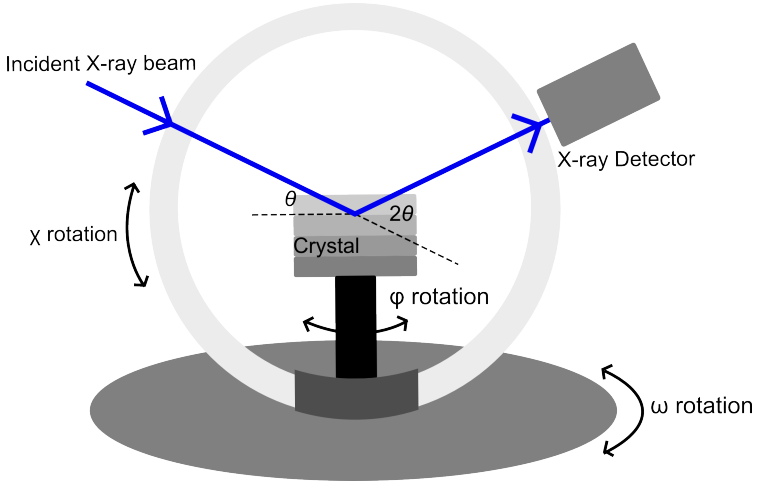

Figure 2.15.: Four-circle Eulerian-cradle diffractometer.

Sample holder

It is a glass fiber, on which a crystal is mounted using some kind of adhesives. The fiber and crystal are affixed on a goniometer so that the crystal is allowed to be oriented. The adjustment of the X, Y, Z orthogonal directions allows centering of the crystal within the X-ray beam. The goniometer used in single-crystal diffractometers can be two types: four-circle Eulerian-cradle or three-circle Enraf-Nonius diffractometer.[52] The four circles refer to the four angles, 2θ, φ, χ, and ω, defining the relationship of the crystal lattices. A simple illustration is shown in Fig. 2.15.

Detector

Many types detectors can be used for diffractometer. According to the development of the sensor technology, they are evolved from one-dimensional sensor, e.g. position-sensitive proportional counters and array scintillation counters, to two-dimensional CCD cameras, such as array proportional counters or image plate. Two currently used types are introduced here:

Charge-coupled device (CCD) system uses 'CCD-chips' to record data, on which a layer of a fluorescent material has been coated. In diffractometer, the chip size is related to the resolution. The larger a chip is, the better is the resolution. The CCD detector provides the fast data record and high quantum sensitivity. However, the relative higher background noise makes it not suitable for weak scattering materials due to the long exposure time. The detector is usually about 95×95 mm. This is not large enough to collect all scattering signals of a crystal in a single position. Thus it has to been mounted on the three- or four-circle diffractometer.[52]

The **image plate system** with a diameter of 180-350 mm serves with a solution for the shortage of the detector surface, and it can be mounted in a two-circle diffractometer (φ and ω). Its surface is coated with a material containing Eu^{2+}. The Eu^{2+} is oxided to Eu^{3+} by the X-rays and then reduced back to Eu^{2+} by the laser. The emission during the reduction is measured to generate 'frames'. For every measurement, numerous frames are generated depending on the exposure time, detected 2θ angle and so on. Compared to the CCD system, the big advantage of the image plate system is its lower background. It is almost only sensitive to the scattered X-radiation, and therefore it is suitable to measure materials with long exposure time, i.e., weak diffracting materials.[52]

Chapter 3.

Results and discussion: Syntheses

In this chapter, the synthesis procedure, the impacts of the reaction times and temperatures are briefly presented and discussed.

3.1. Synthesis procedure

Trifluoromethylated fullerene derivatives (TMF) of higher fullerenes were synthesized in a glass or quartz ampoule because of the different reaction temperature demands. The target product was obtained from the reaction between different fullerene sources and excess CF_3I. Two fullerene sources were used in this work: Source 1 of $C_{82/84}$ (referred to as S1) and Source 2 of C_{76-96} (S2) containing small amounts of C_{60} and C_{70}.

3.1.1. Reaction at low temperature

In a *glass* ampoule, the reaction is carried out at 400-420°C for several days. This reaction yields a mixture containing $C_n(CF_3)_m$ (n = 82-84 or 60, 70, 76-96; m is an even number in the range of 12-20) depending on the composition of reactant fullerene source (1 or 2). Such products deposit as an orange layer in the cold region of the ampoule (Fig. 3.1). According to MALDI-MS results, the major species of the reaction with fullerene S1 were $C_n(CF_3)_{16-20}$ (Fig. 3.2). The product distribution is shown in Tab. 3.1.

The trifluoromethylation of fullerenes involved steps are illustrated as a scheme in Fig. 3.3. The product mixture was produced from the addition of CF_3 radicals on the fullerene cages[53]. The reaction took place in the hot region at first and following steps are: (i) CF_3 radicals are generated for thermolysis of CF_3I; (ii) the solid parent fullerenes are attacked by CF_3 radicals and form the low degree trifluoromethylated fullerenes (TMFs), $C_n(CF_3)_m$ ($m \leq 12$), with lower volatility; (iii) within the reaction time, such compositions are attacked continuously by CF_3 radicals and converted to high degree

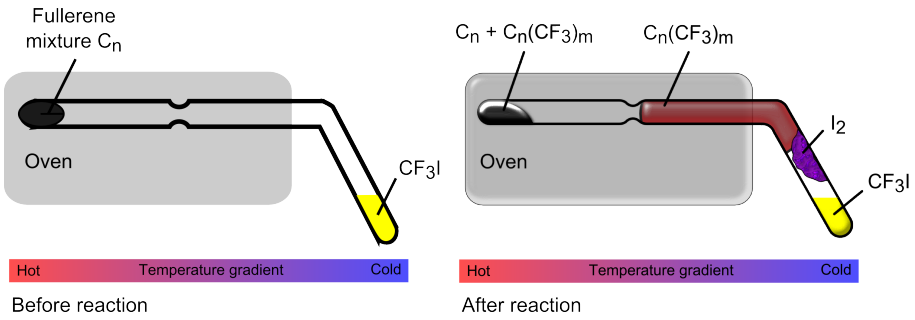

Figure 3.1.: The relative positions of the fullerene mixture and products in a synthesis ampoule.

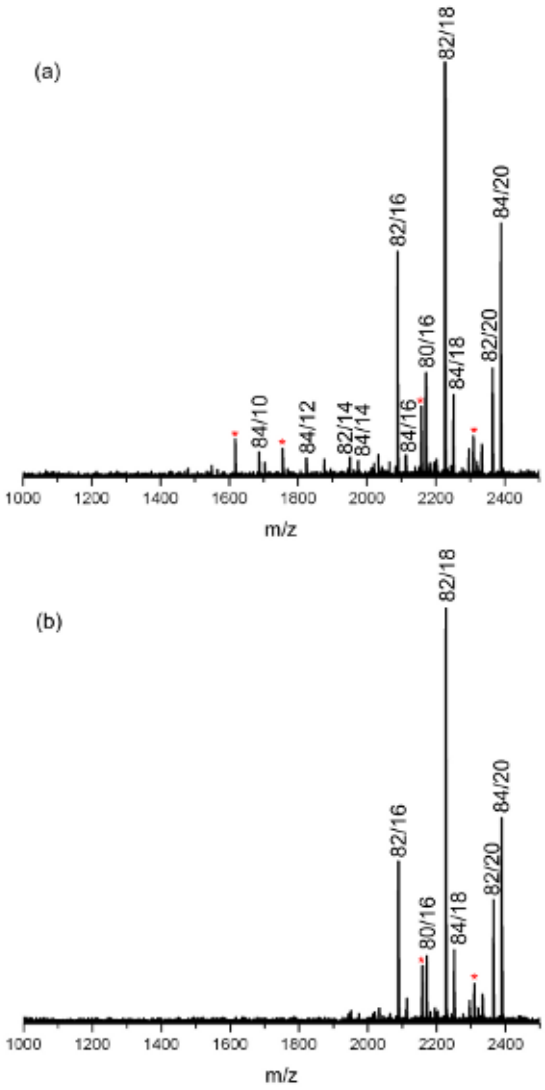

Figure 3.2.: The product distribution is shown in the MALDI-MS spectra of trifluoromethylation of fullerene S1 in a glass ampoule: the rest in the hot zone (a); the sublimate in the cold zone (b). Peaks marked with asterisks correspond to metastable ions.

Table 3.1.: Product distribution of trifluoromethylated fullerenes at 400-420°C.

Reactor	Fullerene source	Product type	$C_n(CF_3)_m$	
			all species, m =	major species, n/m =
glass	1	residue	10-20	82/16-18, 84/20
		sublimate	16-20	82/16-18, 84/20
	2	residue	14-20	76,82,86,90/18, 86,96/20
		sublimate	16-20	76,82,86,90/18, 86/20

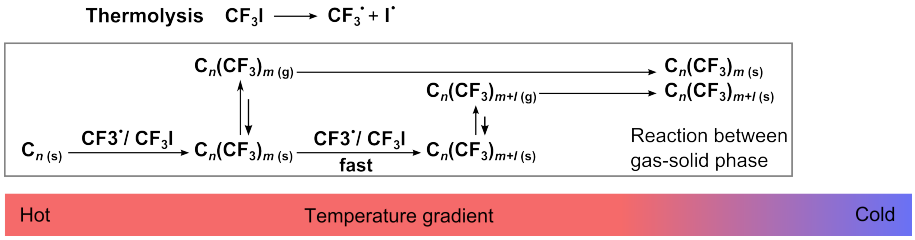

Figure 3.3.: Synthesis of trifluoromethylated fullerenes in glass ampoule at 400-420°C.

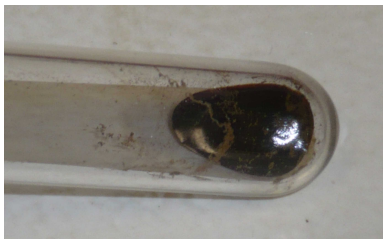

Figure 3.4.: A black-colored melt which was solidified upon the cooling at the end of the ampoule in the high temperature region.

TMFs, $C_n(CF_3)_{m+l}$ ($m+l \geq 10$), with higher volatilities; (iv) the high degree TMFs mixture sublime and condense in the cold region of the ampoule and a deep-colored residue is left in the hot region.

It is noteworthy to mention, that species $C_{82}(CF_3)_m$ present the main sublimed products of trifluoromethylation with fullerene mixture S1, whereas most $C_{84}(CF_3)_{10-20}$ remained in the hot zone (see Tab. 3.1). For trifluoromethylation of the fullerene mixture S2, rather similar results were described earlier in ref[54]. The product distribution of $C_n(CF_3)_m$ in the hot zone is shifted to lower m values and the major species were $C_n(CF_3)_{14,16}$.

After the long reaction time (several days), the corrosion of glass was observed in the hot zone. A white insoluble layer adhered on the inner glass wall. It can be assigned, neither to reactants nor to products of the trifluoromathylated addition reaction because of its color (TMFs are brown/orange while solid parent fullerenes are black) and solubility (TMFs and solid parent fullerenes dissolve well in toluene or dichlorobenzene). Hence this layer consists presumably of some polymer species generated from the reaction of CF_3I with glass. This corrosion phenomenon has never been observed when the reactions were carried out in quartz ampoules.

3.1.2. Reaction at high temperature

In a *quartz* ampoule, the syntheses are performed at higher temperature (510-600°C) for short time (few minutes to 1h). The brown-orange products with large numbers of CF_3 groups ($C_n(CF_3)_{10-20}$) sublimed (MALDI-MS spectra is shown in Fig. 3.5 and summarized in Tab. 3.2) and condensed around the end of the furnace at lower temperature. In contrast, the product mixture of $C_n(CF_3)_{2-20}$ remained as a black-colored melt at the end of the ampoule in the high temperature region (Fig. 3.4). The presence of the melt in the hot zone during the reaction can be understood by the formation of a glassy black layer after ampoule cooling. It was evidenced for the observation of liquid phase, when the ampoule was quickly removed from the furnace during the reaction. The first observation of melted mixtures of trifluoromethylated fullerenes gas has been reported for the case of C_{70}[55].

The suggested addition reaction steps are different than sublimed products obtained in the reaction at 400-420°C. The addition begins from gaseous CF_3 radicals on the surface of solid parent fullerenes and

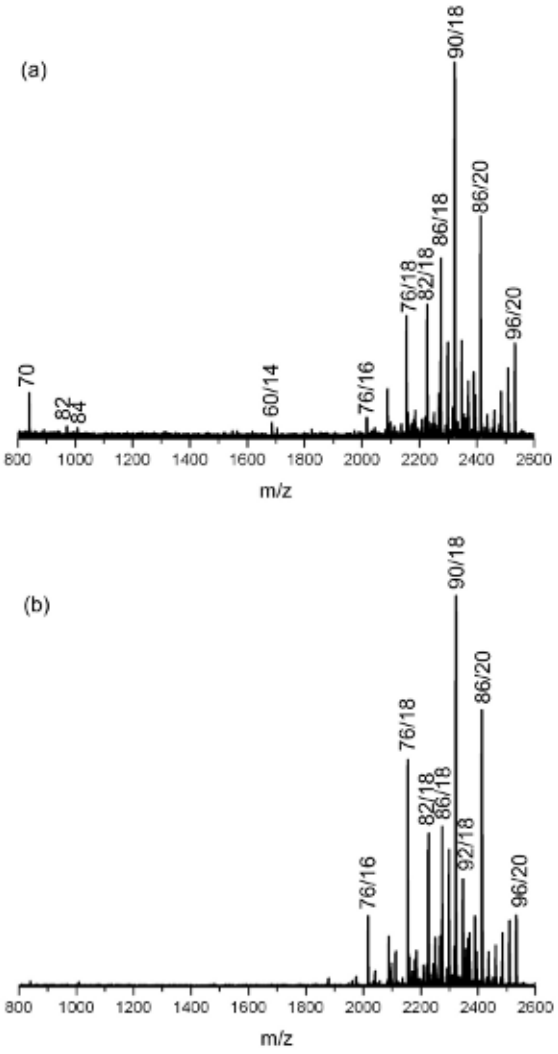

Figure 3.5.: The product distribution is shown in the MALDI-MS spectra of trifluoromethylation of fullerene S2 in a glass ampoule: the rest in the hot zone (a); the sublimate in the cold zone (b).

Table 3.2.: Product distribution of trifluoromethylated fullerenes at 510-600°C.

Reactor	Fullerene source	Product type	$C_n(CF_3)_m$	
			all species, m =	major species, n/m =
quartz	1	residue	2-20	84/6-14
		sublimate	12-20	84/14,16
	2	residue	2-20	84/6-10,14
		sublimate	10-20	84/14-18, 90/14, 76/12

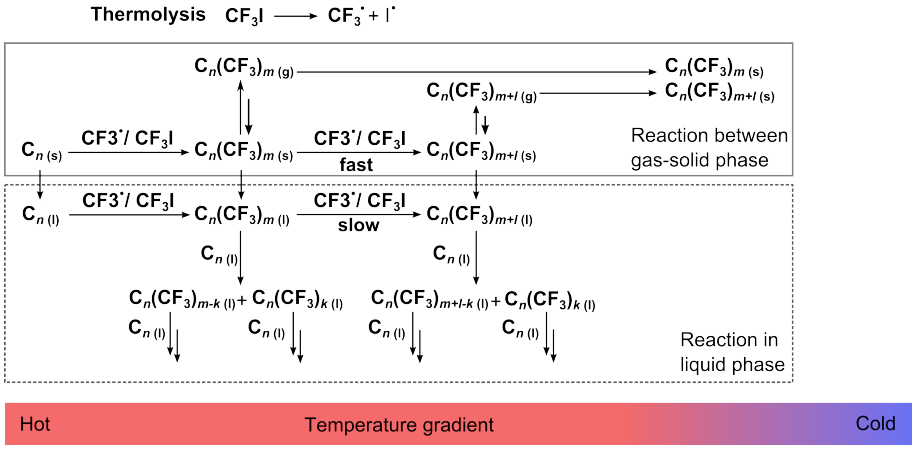

Figure 3.6.: Reaction path of trifluoromethylated fullerenes in a quartz ampoule at 510-600°C.

gaseous CF_3 radicals. Initially, low degrees TMFs are generated. After some minutes, the TMFs and fullerenes mixture begins to melt. Thus, the addition reaction can be performed in 2 ways: (i) in solid-gas phase between CF_3 radicals and solid fullerenes, or (ii) in liquid phase between fullerene derivatives and parent fullerene. The reaction via way (i) is described previously. For the reaction via way (ii), the consequences of this phase transfer are twofold. Firstly, reaction rates in the melt are much higher due to better contact of fullerene particles with fullerene derivatives, and secondly, the sublimation rate of CF_3 derivatives into the colder zone is much lower due to lower surface of a melt compared with a powder. For the same reason, the rate of further trifluoromethylation between the melt substance and gaseous CF_3 radicals in a hot zone decreases. The possible reaction way is shown as a schema in Fig. 3.6.

As a result, the amount of sublimed products with composition $C_n(CF_3)_{16-20}$ was reduced compared to those in a glass ampoule. Thus the distribution of the products which remained in the hot zone in form of a black-colored residue is much wider. Compared to the number of CF_3 groups, the range spreads from 12-20 in the reaction at 400-420°C to 2-20 in that at 510-600°C.

3.2. Reaction parameters of fullerene trifluoromethylation: temperature and time

In this section, the influence of the reaction parameters: temperature and time on trifluoromethylation of fullerenes are discussed. The data of the reaction with fullerene source 1 and source 2 are discussed in this section.

3.2.1. Fullerene mixture C_{82-84}

According to the MALDI-MS results of the syntheses in a glass (400-420°C) (Fig. 3.7) and quartz (550°C) ampoule (Tab. 3.3), the higher reaction temperature affects the composition and amount of the products, especially for products in the hot zone. To prove this phenomenon, some syntheses were carried out in quartz ampoules at different reaction temperatures. The remaining products (a congealed melt) in the hot zone of the reaction with fullerene mixture S1 at 550°C contain the species $C_{84}(CF_3)_{2-20}$, while the species of $C_{84}(CF_3)_{10-18}$ were the majority at 510°C. The main species are $C_{84}(CF_3)_{10-16}$ for the reaction at higher temperature and $C_{84}(CF_3)_{14-16}$ for the reaction at lower temperature. The sublimed products show a temperature dependent distribution with a product composition of $C_{84}(CF_3)_m$ with m

Table 3.3.: Product distribution of the reaction with fullerene S1 at different temperatures. Results are according to MALDI MS spectra shown in Fig. 3.7. The minor products $C_{82}(CF_3)_{6-16}$ are excluded in this table.

Product type	Product distribution $C_{84}(CF_3)_m$, m =		Major species $C_{84}(CF_3)_m$, m =	
	550°C	510°C	550°C	510°C
residue	2-20	10-18	10-16	14-16
sublimate	4-20	14-20	14-18	14-18

Table 3.4.: Product distribution of the reaction with fullerene source 1 with different reaction times. Results are according to MALDI MS spectra (Fig. 3.8). The minor products $C_{82}(CF_3)_{6-16}$ are excluded in this table.

Product type	Product distribution $C_{84}(CF_3)_m$, m =		Major species $C_{84}(CF_3)_m$, m =	
	1h	16 min	1h	16 min
residue	2-20	2-14	10-16	6-10
sublimate	4-20	12-18	14-18	14-18

ranging from 4-20 at the reaction temperatures 550°C and 14-20 at 510°C. The main sublimed species for both reactions at different temperatures are quiet similar with m = 14-18. Noteworthy, the species with m <10 in the hot zone and the species with m <14 in cold zone were not found. Otherwise, the product distribution of the species $C_{82}(CF_3)_m$ are narrower with the range of m = 6-12 in the hot zone and m = 12-16 in the cold zone for the reaction at 550°C. For the reaction at 510°C, there was no significant signal of trifluoromethylated fullerene C_{82} obtained.

The higher reaction temperature significantly affects the composition of the products. The more volatile the trifluoromethylated fullerenes, the higher the tendency to deposit as sublimed products in the colder zone of the ampoule. As a general rule, those fullerene derivatives with a lower number of attached CF_3 groups, are able to sublimate and deposit in the cold zone of the ampoules. In conclusion, the reaction at higher temperatures shows a wider product distribution than at lower temperatures.

Beside the reaction temperature, reaction time can also influence the product species. The results of the reaction at 550°C for 1 h and 16 min supports this thesis. Compared to the residues in the hot zone of the reaction with longer reaction time, the distribution of the species decreases with m ranging from 2-20 (for 1h) to 2-14 (for 16 min) (Results of MALDI analysis are shown in Fig. 3.8 and summarized in Tab. 3.4). After a reaction time of 16 minutes, there is no signal for the species with higher number of attached CF_3 groups ($C_{84}(CF_3)_{16-20}$) as compared to 1 hour reaction. The major species $C_{84}(CF_3)_m$ are changed from m = 10-16 to 6-10. In the sublimed products, the species of the reaction with shorter time are not as complicated as those produced for the longer time. They contained only $C_{84}(CF_3)_{14-20}$ while $C_{84}(CF_3)_{4-20}$ were found in the reaction within 1h. At this point, two observations can be made. First, the species $C_{84}(CF_3)_m$ in the hot zone is shifted to lower m values due to the shorter reaction time. Second: the lower volatile species were not detected in the products in the cold zone of the ampoule in the reaction within 16 min. The major species are C_{84} with 14-18 CF_3 groups, the same as the products of reaction with 1 h. Consequently, we can suspect that the species with 14-18 CF_3 groups are the most stable species with high volatilization. The same product species were found also in the reaction at lower temperature (510°C) which were discussed previously.

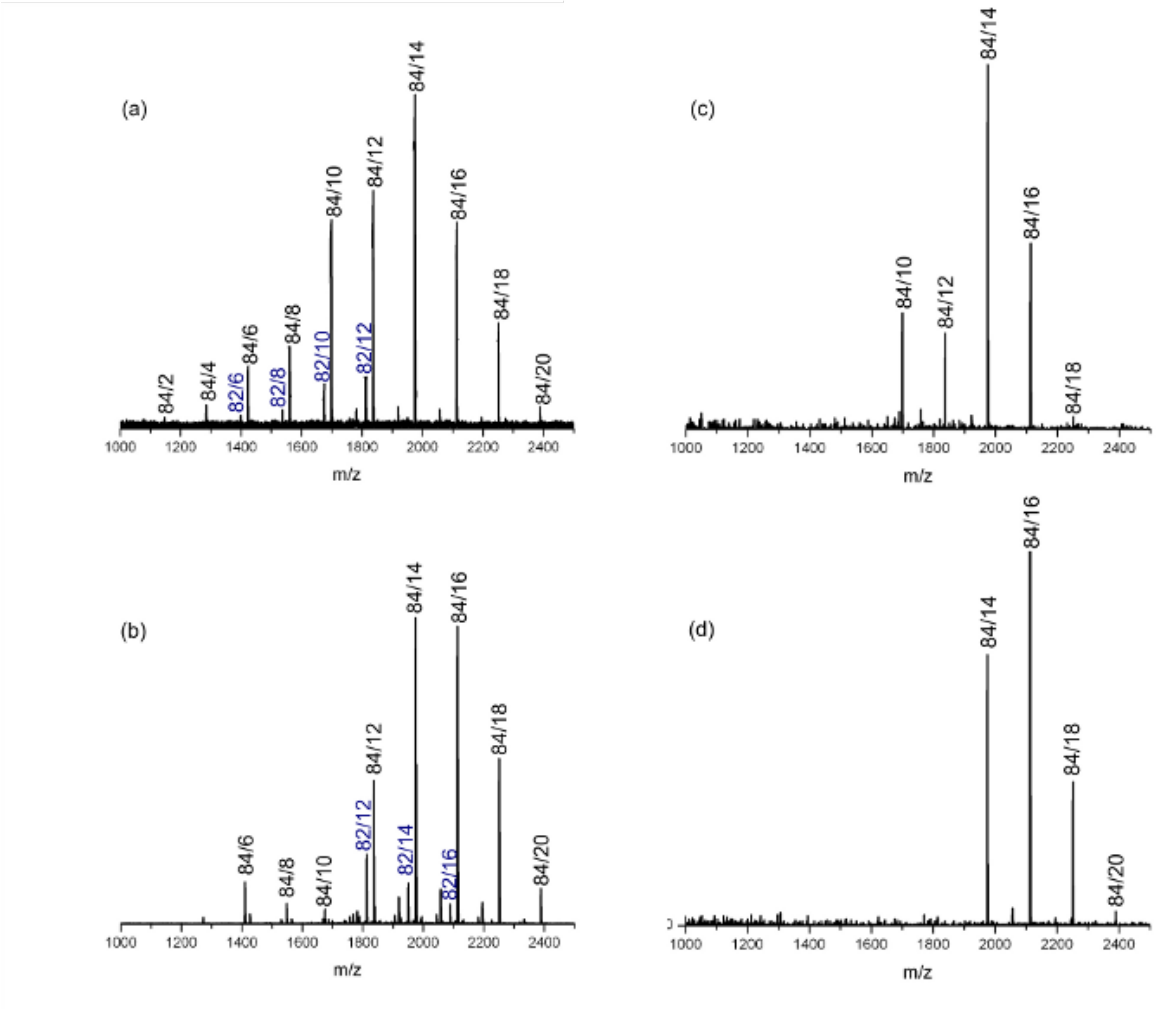

Figure 3.7.: Effect of the different reaction temperatures. MALDI MS spectra of the products obtained by trifluoromethylation of C_{82-84} mixture (S1) in the quartz ampoule for 1h at different reaction temperatures. The left column shows the data of the reaction at 550°C and right column the data of the reaction at 510°C. The residues in a hot zone (a) and (c); the sublimed products in the cold zone (b) and (d). The minor products $C_{82}(CF_3)_{6-16}$ are marked in blue color.

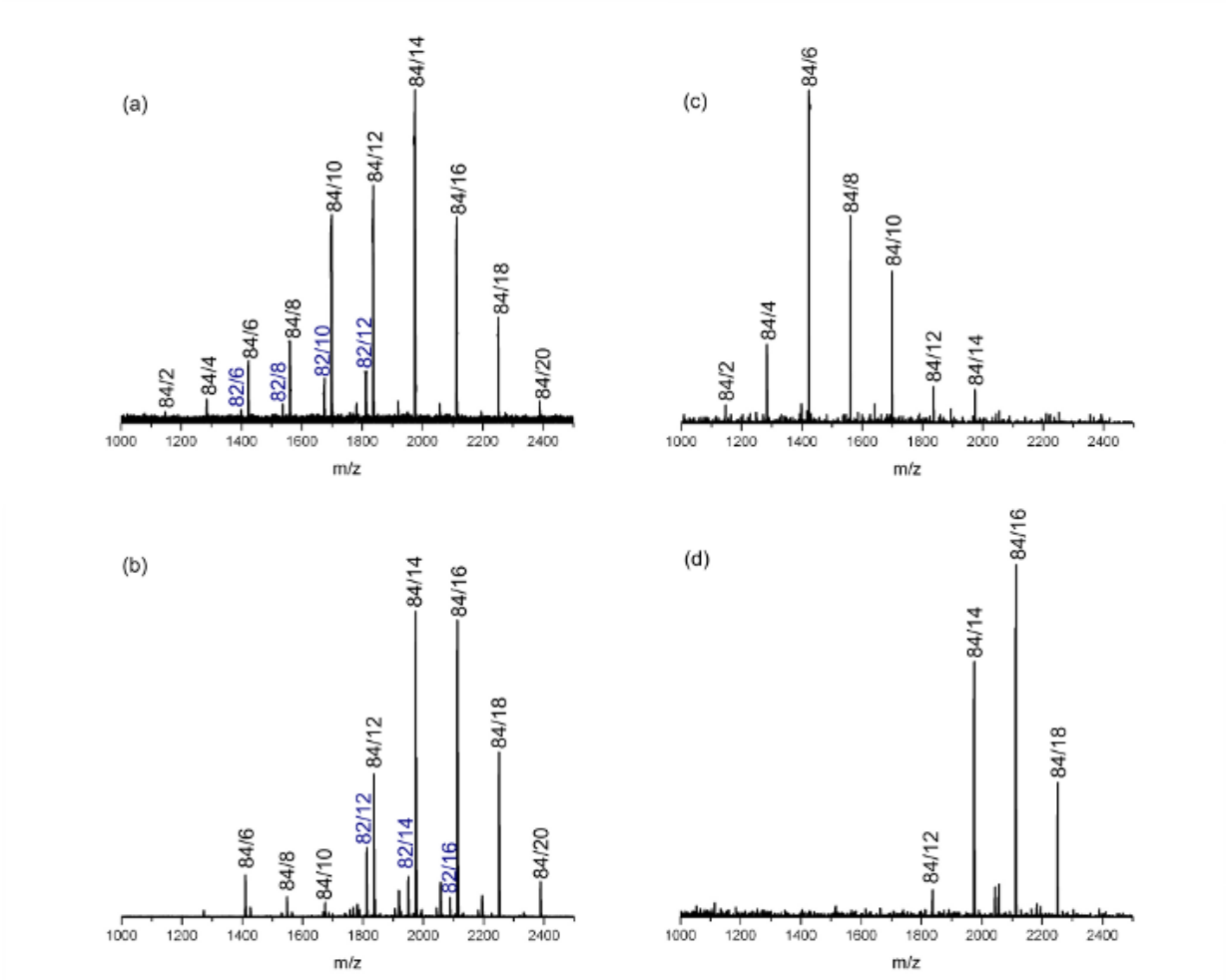

Figure 3.8.: Effect of different reaction times. MALDI MS spectra of the products obtained by trifluoromethylation of C_{82-84} mixture (source 1) in the quartz ampoule at 550°C for different reaction times. The data of the reactions performed for 1 h and 16 min are shown in left and right columns, respectively). The spectra of residues in the hot zone are (a) and (c); the sublimed products in the cold zone are (b) and (d). The minor products $C_{82}(CF_3)_{6-16}$ are marked in blue color.

Table 3.5.: Product distribution of the reaction with fullerene source 2 at 530°C with different reaction times. Results are according to MALDI MS spectra (Fig. 3.9). Only main product of $C_{84}(CF_3)_m$ are shown in this table.

Product type	Product distribution $C_{84}(CF_3)_m$, m =		Major species $C_{84}(CF_3)_m$, m =	
	2.3 h	40 min	2.3 h	40 min
residue	12-20	4-16	16-20	8-10
sublimate	14-20	10-18	16-18	14-16

Table 3.6.: Product distribution of the reaction with fullerene S2 at 600°C. Results are according to MALDI MS spectra (Fig. 3.11). Only main product of $C_{84}(CF_3)_m$ are shown in this table.

Product type	Product distribution $C_{84}(CF_3)_m$, m =	Major species $C_{84}(CF_3)_m$, m =
residue	4-10	6-10
sublimate	4-16	12-14

3.2.2. Fullerene mixture C_{76-96}

The product distribution of the reaction with fullerene source 2 is shown in Tab. 3.5 according to the MALDI-MS spectra which are shown in Fig. 3.9. The similar tendency compared to the reaction with fullerene source 1 is observed. The product species $C_n(CF_3)_m$ (n and m are even numbers) in the hot zone shifts to lower m values with decreasing reaction time and the m range was varied from 14-20 to 4-16. In the sublimed products, the species of $C_{76}(CF_3)_{10-12}$ and $C_{78}(CF_3)_{12}$ are detected with relatively higher intensities compared to the reaction with shorter time, while the amount of C_{84} containing species is strongly increased within a longer reaction time.

One synthesis was preformed at extreme high temperature (600°C) for a long time. The first observation after the reaction was less sublimed products were formed as compared to the reaction at 550°C for 1 h (Fig. 3.10). According to the results of MALDI analysis (Fig. 3.11), the species $C_n(CF_3)_m$ distribution in the cold zone shifted to lower m values (short summary is shown in Tab. 3.6) Many species with lower numbers of CF_3 groups are found in this area, e.g. $C_n(CF_3)_{4-10}$. Two reasons can be responsible for the migration of such species: (1) due to high reaction temperature, the less volatile trifluoromethylated fullerenes are able to sublimate and deposit as sublimed products in the colder zone of the ampoule; and (2) the sublimation (reaction I in Fig. 3.12) is preferred to take place rather than further trifluoromathylation (reaction II in Fig. 3.12) under such reaction conditions. For the species with high number of CF_3 groups, e.g. $C_n(CF_3)_{m>18}$, they are not stable under such reaction conditions. Therefore, no significant singles are obtained in MALDI MS spectrum. The main sublimed products of $C_n(CF_3)_m$ are changed from m = 14-18 to 12-14.

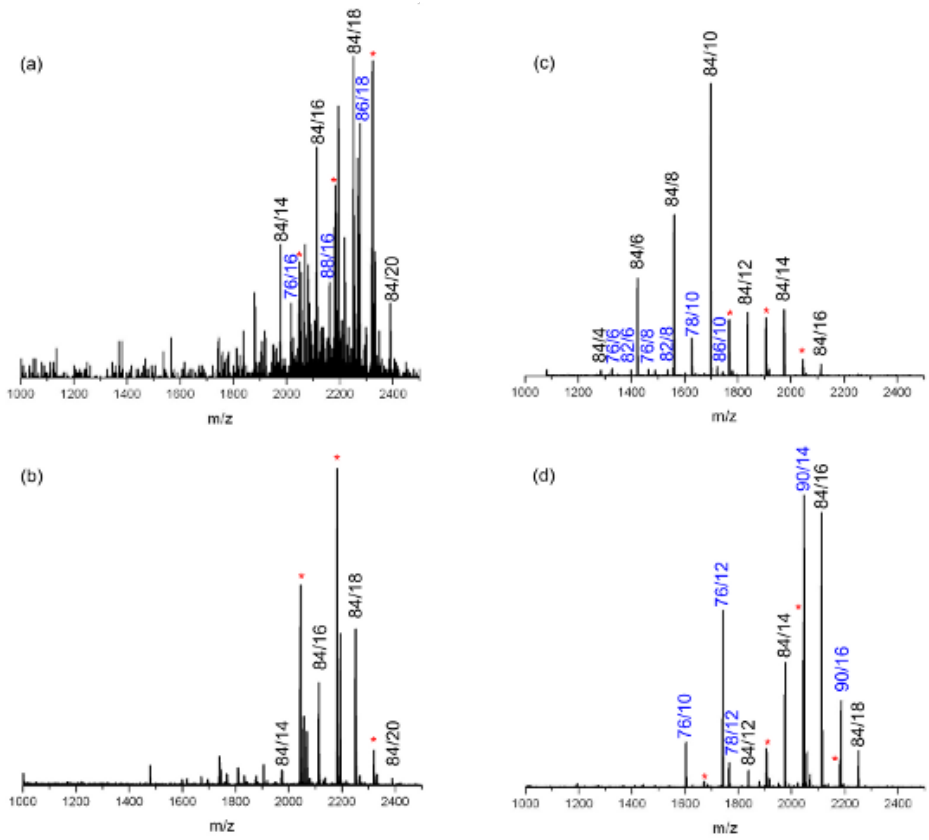

Figure 3.9.: Effect of the different reaction times. MALDI MS spectra of the products obtained by trifluoromethylation of C_{76-96} mixture (source 2) in the quartz ampoule at 530°C for different reaction times. The data of the reactions performed for 2.3 h and 40 min are shown as in left column and right column, respectively. The spectra of residues in a hot zone are (a) and (c); the sublimed products in the cold zone are (b) and (d). The minor products are marked in blue color.

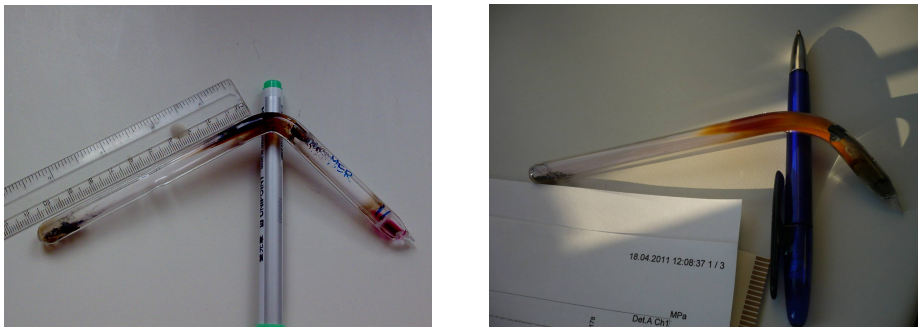

Figure 3.10.: The observation of the ampoule after the reaction with fullerene source 2 at 600°C for 2.75 h (left). The sublimate amount is significant less compared to the one of the reaction at 550°C for 1 h (right).

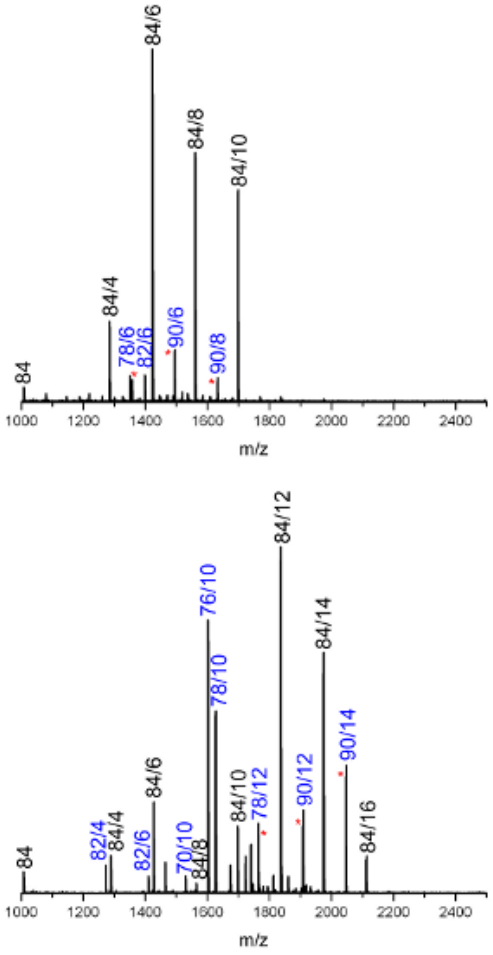

Figure 3.11.: Effect of the high temperature for a long reaction time. MALDI MS spectra of the products obtained by trifluoromethylation of fullerene mixture (source 2) in the quartz ampoule at 600°C for 2.75 h. The spectra of residues in a hot zone are (a); the sublimated products in the cold zone are (b). The products $C_n(CF_3)_m$ beside $C_{84}(CF_3)_m$ are marked in blue color.

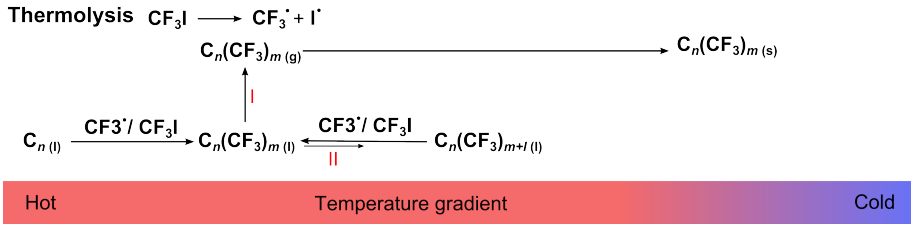

Figure 3.12.: Reaction of trifluoromethylated fullerenes at 600°C for 2.75 h in quartz ampoule.

Chapter 4.

Results and discussion: Separation of the reaction products

The raw products of several syntheses were purified using the HPLC system. This technique is essential to obtain isolated isomers. Only if the isomers have been well separated, they can form single crystals, which allows for the determination of their molecular structures. In this chapter, the optimization of the HPLC techniques utilized in this study and separation details of selected species have been presented.

4.1. General aspects

The HPLC separation consists of several steps illustrated in Fig. 4.1. This sequence multi-step separation is crucial in order to obtain highly purified fullerene derivatives. In step 1, a powder of the product mixture is dissolved in the toluene as eluent and a single separation is performed using the Buckyprep© column at 25°C with a flow rate of 4.6 ml/min.

In step 2, the HPLC separation is carried out with different compositions of the mobile phase in order to achieve a better separation. Before step 2 can be performed, toluene in the fractions of step 1 has to be removed, and the brown residue is dissolved in the mobile phase used in step 2, especially for the fractions with short retention times. The species in such fractions are further isolated with the mobile phase which contains more v % hexane than toluene. Due to different solubility of species in different mobile phases, the species can deposit in the column when the mobile phase is changed from the one with good solubility to one with relative low solubility. This may lead to loss of the products and decreasing separation capacity of the column. This phenomenon of substance deposit can be clearly observed if the mobile phase changes from toluene to hexane. Some insoluble particles of species are visible and should be removed with a membrane filter before injection into the HPLC system. Step 2 of

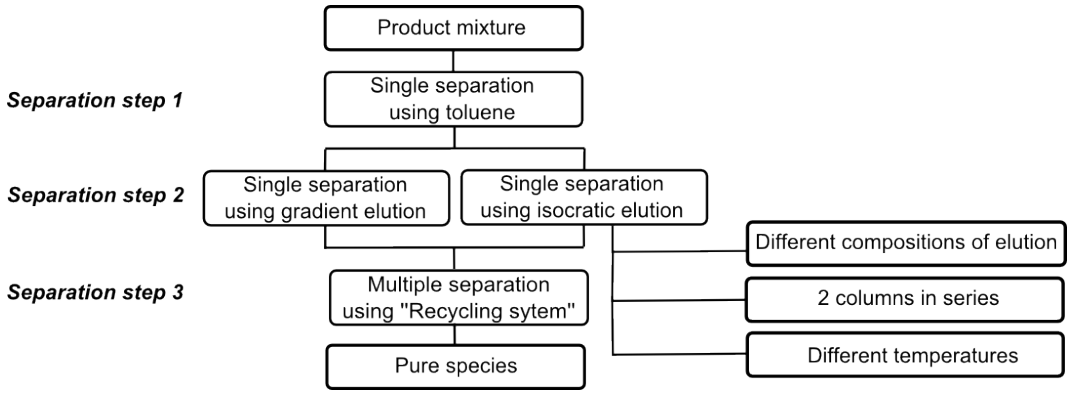

Figure 4.1.: The three main steps of the separation process. Important options which are used for step 2 and 3 are shown on the right.

this procedure is rather time demanding because optimal separation parameters have to be determined, and some separation runs have to be performed repeatedly to assure pure isomer samples. Step 2 is performed in one of two different modes, i.e., with gradient or isocratic elution with the Buckprep© column, flow rate 4.6 ml/min and at different temperatures. Details are shown in Table in appendix B.

The product mixture obtained from the reaction between C_{82-84} (S1) and CF_3I serves as an example to explain step 2 in more detail. For reasons of simplicity, only the main products of $C_{84}(CF_3)_m$ are discussed here. The minor products of $C_{82}(CF_3)_m$ are excluded in this section though they are found in MALDI mass spectra and some of their structures have been determined. [1] The similar procedures are applied to products of reactions between C_{76-96} (S2) and CF_3I. Details are shown in appendix B.

4.2. HPLC optimization with gradient elution

For step 2, a technique is utilized which gradually changes the composition of eluent during the separation. In this work, toluene serves as a strong solvent dissolving the species from the column quickly, while hexane as a weak solvent makes the species stay longer in the column. Hence, the strongly retained species can be eluted quickly and still have enough resolution of separation comparing to isocratic elution. This technique not only improves column efficiency but also reduces the time of separation runs. For example, a peak tailing behavior, which often is observed during long time separation, can be improved. The tail of the peak is minimized by stronger elution comparing to the front of peak. That means that the substance moves quickly and performs as a narrower peak. Some fractions of step 1 were further separated using this technique but with a composition of the eluent (H/T ratio) decreased e.g. from 70/30 to 20/80. This variation of the H/T ratio strongly depends on the retention of fraction in step 1. The optimal eluent composition is determined individually during several test runs.

4.3. HPLC optimization with isocratic elution

Each fraction of step 1 is separated further in a mixture of hexane/toluene as the mobile phase. The ratio of the mixture depends on the retention time of the fractions in step 1. There is no clear rule to describe the variation of the elute ratio, because (i) the raw products are obtained from several syntheses under different reaction parameters, and (ii) the collected time of each fraction in step 1 are slight different. This leads to different species found in a fraction with the same (or similar) retention time between different syntheses. In general, H/T ratio is decreased with increasing retention time in step 1. For example, the fractions with retention time >10 min in step 1, more toluene containing eluent is used. In opposite, more hexane containing eluent is used for the fractions, which were collected between 4-10 min in step 1. Especially, for the fraction with extremely short retention time of 3-4 min in the first step, pure hexane is used as mobile phase. Due to the presence of a large number of different species, the separation with different compositions of eluent is not always successful. In some cases in this work, separation using two columns in series or carried out at different temperatures were other options.

Most species can be separated within the second step of the procedure with gradient or isocratic elution. However, for some cases, a third separation step has to been carried out with different parameters (step 3). This 'recycling system' (see the Chapter 2) is utilized especially for the species with extreme close retention times. For this kind of multiple separations, the eluent typically has small H/T, e.g. 1/9, or is even pure toluene. The separation using the recycling mode may last several hours.

[1] For the results of the trifluoromethylated fullerene C_{82} see the paper in the Crystallography Reports, 2011, 56, 6, 1107-1113

4.4. Details for selected trifluoromethylated fullerenes

In the following, detailed information is provided for the separation of several isomers, which have been isolated and structurally determined. For the isomers that are not shown here, an overview of their separation route are described in Appendix B. The UV/VIS spectra of selected species are given in the same Appendix. The composition of $C_n(X)(CF_3)_m$ is given as $n(X)/m$ in the following discussion (C_n: fullerene; X: fullerene cage isomer; m: the numbers of the attached CF_3 groups); the following Roman number denotes a sequential number of the isomer in order of increasing elution time. The reaction products, which were successfully isolated and structurally characterized, have been denoted with three-symbol code: 1 or 2 for fullerene source; *q* or *g* for synthesis in quartz or glass ampoules and *s* or *r* for the sublimed or residue products, respectively.

A typical chromatogram for the raw products of trifluoromethylated fullerene C_{82-84} in the first separation step is shown in Fig. 4.2. It contains more than 20 fractions within 30 min, and each fraction contains several species that are confirmed with MALDI-MS analysis. The results of this analysis for the corresponding fractions in Fig. 4.2 are shown in Fig. 4.3

4.4.1. C_{84}, cage isomer 4

84(4)/12-I (obtained from 2*gs*) The toluene fraction at 3.01 min is further separated with pure hexane in step 2. The orange fraction is collected at 10.84 min.

4.4.2. C_{84}, cage isomer 11

For cage isomer 11 of C_{84}, six different derivatives have been separated. Their retention times in step 1 range from 3.02 to 16.45 min as shown in Fig. 4.9.

84(11)/10-I (1*qr*) Species of $C_{84}(11)(CF_3)_{10}$ is obtained in two ways. In the first way, the fraction of step 1 at 16.45 min undergoes a single isocratic separation in step 2 with H/T = 35/65, and species 84(11)/10-I elutes at 38.04 min (see Fig. 4.4). In the second way, the fraction of step 1 at 15.18 min is separated with H/T = 90/10 eluent. One fraction is collected at about 20 min. (Its chromatogram is not shown here.) Due to no crystallization, this collected fraction is further introduced to multiple separations in step 3. The separation is performed with H/T = 9/1 eluent and, species $C_{84}(11)(CF_3)_{10}$ is collected at 80.54 min in fourth cycle (Fig. 4.4).

84(11)/12-I (1*qr* and 2*qr*) Isolation of compound 84(11)/12-I has been carried out at different temperatures. First, the fraction obtained from 1*qr* at 10.89 min of step 1 is introduced into step 2 and eluted with H/T = 40/60 at 25°C. This yields the chromatogram shown in Fig. 4.5(a), and it shows that the peak of species 84(11)/12-I at 23.60 min overlaps strongly with a neighboring peak. Therefore, this fraction is collected and further purified under the same conditions (Fig. 4.5(b)). The pure species 84(11)/12-I is collected at 23.56 min. Second, the fraction (obtained from 2*qr*) at 10.48 min of step 1 is also introduced into step 2 with H/T = 40/60 at 40°C. The retention time of species 84(11)/12-I is reduced to 17.9 min due to higher temperature (Fig. 4.5(c)). In both orange fractions, crystals of the species 84(11)/12-I were identified.

84(11)/14-I (2*gs*) In step 1, the retention time of isomer 84(11)/14-I is 3.02 min. This retention time is relative short compared to the dead time [2]. Therefore, the resolution is insufficient. The better resolution

[2] Column dead time (t_0) in the HPLC system is about 2.9 min. It has been determined by injection of an entirely unretained sample.

can be achieved by using two columns in series in step 2. The retention time of the light orange-colored fraction of 84(11)/14-I is collected at 16.55 min using hexane as eluent.

4.4.3. C_{84}, cage isomer 22

In total, nine different derivatives of the cage isomer $C_{84}(22)$ were isolated. Two isomers have been found for each of the compositions with n = 12 and 14. Four isomers were obtained for n = 16 and one isomers for n = 20. The chromatograms of step 1 for nine compounds are shown in Fig. 4.9.

84(22)/12-I (2*qr*) In the chromatogram of Fig. 4.9(b), the isomer I of $C_{84}(22)(CF_3)_{12}$ appears in the peak at 3.12 min. The fraction of this peak is separated in step 2 with H/T = 90/10. The light yellowed fraction collected at 4.8 min contains the isolated isomer I.

84(22)/12-II (2*qr*) For isomer II of $C_{84}(22)(CF_3)_{12}$, there are two different methods used in step 2. In the first method, the fraction of step 1 between 5 and 10 min (Fig. 4.9) is further separated with isocratic elution using H/T = 80/20 where the orange-colored collected at 71.79 min contains more species. This orange fraction is introduced into step 3 using H/T = 50/50. The pure fraction is collected at 24.52 min. The second method uses gradient elution at 35°C. The gradient profile and the chromatogram are shown in Fig. 4.6.

84/22/14-I (1*qr*) For compound $C_{84}(22)(CF_3)_{14}$, isomer I is found in the fraction at 3.60 min of step 1. The separation in step 2 was carried out with two columns in series using H/T = 90/10, an orange solution is collected at 30.35 min.

84/22/14-II (1*qs*) Isomer II is separated using a toluene fraction of step 1 at 8.0 min using H/T = 50/50 and a single column.

84(22)/20-I (1*gs*) This isomer is isolated after several HPLC runs with hexane. The first separation is carried out with flow rate 4.6 ml/min, and the fraction between 3.5 and 5.2 min was collected. This collected fraction is introduced to second separation with flow rate 2.3 ml/min, and fraction between 9.7 and 10.1 min is collected for the third separation. The third separation step is performed under the same condition as the second step. The yellow-colored fraction containing species 84(22)/20-I is collected between 8.2 and 9.7 min for crystallization. The chromatograms for three separation steps are shown in Fig. 4.7.

4.4.4. C_{86}, cage isomer 17

The separation of compound $C_{86}(17)(CF_3)_{16}$ was complicated due to eluent impurity. Therefore, different chromatograms were obtained under the same separation condition. The impact of eluent purity on the separation will be discussed in the next section.

86(17)/16-I (2*qs*) Toluene fraction at 3.01 min of step 1 is introduced to step 2 using 100 % hexane as eluent. The fraction is collected in a wide period (see Fig. 4.9) compared to the normal fraction collection peak by peak that is shown in Fig. 4.2. Hexane fraction between 7 and 15 min of step 2 is purified again with 100 % hexane with two columns in series. The small amount of fraction is collected at 13.98 min, which contains species 86(17)/16-I. HPLC trace is shown in Fig. 4.8.

Table 4.1.: Purity of toluene from different sources. Analysis via Shimadzu GC-2010 under conditions: injector temperature 300°C, HP column (Agilent) with 0.25 mm × 100 m, analysis temperature 120°C, FID temperature 350°C.

	Suppliers	Purity (GC analysis)
toluene 1	Acros	99.995%
toluene 2	toluene 3 distilled with Na(s)	99.920%
toluene 3	Stockmeier	99.556%

4.4.5. Summary

Two chromatograms of product mixtures from different syntheses of fullerene S1 and 2 are shown in Fig. 4.9. The retention times of fractions from which crystals presented in this work are given. In chromatogram (b), only species of fullerene C_{84}, C_{86} and C_{88} are shown. It does not mean that only such perfluoromethylated fullerene is synthesized, but only such species have enough amount to grow crystals. Other trifluoromethylated species of $C_{60,76,78,82}$ are not discussed in this thesis. Furthermore, some trifluoromethylated species of other higher fullerenes, e.g. C_{90-96}, were successfully isolated, but no crystal structure determinations can be performed.

4.5. Impact of the eluent purity

The mixture containing derivatives of higher fullerenes is difficult to separate with HPLC into single species due to their complicated cage isomers and chemical diversity of their additional products. Within the HPLC optimization it turned out that a good separation is only achieved using a mobile phase with high purity. Impurities in the eluent can lead to unexpected effects in the retention behavior of the fullerenes and their derivatives. As an example, the HPLC trace of pure fullerene C_{60} using toluene as eluent is discussed here. Fullerene C_{60} is dissolved in toluene 1 (T1). A single separation has been performed under the same conditions as described in the previous section replacing the eluent by toluene. The different toluene sources employed in this study are shown in Tab. 4.1. The chromatograms of these HPLC separations are shown in Fig. 4.10.

The chromatogram obtained with T1 shows a strong single peak of C_{60} at 8 min while the chromatograms with toluene 2 (T2) and toluene 3 (T3) exhibit several broad peaks between 4-8 min. UV/VIS spectra (Fig. 4.11) have been recorded for the eluent T3 at peaks around 5.33, 6.24, 7.50 and 8.30 min. While the spectrum of the 8.30 min peak is typical for C_{60}[56], no chemical species have been found which could be assigned to the absorption spectra of the peaks at 5.33, 6.24 and 7.50 min. However, the substances in these fractions must be the same according to their UV/VIS spectra.

The purity of the eluents T1, T2, and T3 shown in Tab. 4.1 is determined by GC analysis. The records of gas chromatography and mass spectroscopy (Fig. 4.12 and Fig. 4.13, only chromatograms are shown) provide more information about the chemical impurities of the eluent. This helps to interpret the related HPLC effects. The impurity, which is eluted at 10.5 min, can be removed by distillation over metallic sodium. According to GC-MS results, it can be benzene or benzene containing compounds. While impurities eluted before toluene are removed by distillation, ethyl benzene and xylene with higher boiling points are still detected in T2 (Fig. 4.13). The chromatogram for T2 in Fig. 4.12 shows that this purification is not sufficient to obtain a sharp, single C_{60} peak although the multi-peaked pattern is less pronounced compared to the T3 chromatogram. Therefore, neither T2 nor T3 can be used as eluents for HPLC of fullerenes. The broadening and multi-peak effect of the C_{60} peak can be explained by a partial complexation of the fullerene with the aromatic impurities. This complexation may block *p-p*

interactions between the fullerene/their derivatives and the stationary phase in the column and therefore decreases the retention of a fullerene fraction. This would explain why the C_{60} peak broadens mainly towards smaller retention times.

4.6. Impact of the temperature

According to the previous experience, the different chromatograms are obtained in the summer and winter. They are usually slightly different in retention time or peak form because of the variation of temperature. With a column oven in the HPLC system, this phenomenon can be avoided and the influence of the temperature on the retention and separation can be studied. Some investigations about temperature impact were presented by Zarzycki *et. al.*.[57] Pure fullerene C_{60} and C_{70} have the max retention time ($t_{R_{max}}$) at -20°C using C_{18} alkyl bonded stationary phase (ODS: carbon loaded octadecylsilica). Ohta *et. al.*. expended the tests using C_{30}, C_{18} and C_8 columns and found the $t_{R_{max}}$ at 20°C for C_{30} column.[58] Both investigations confirmed that the best resolution is obtained at a certain temperature; at this temperature the fullerenes have the $t_{R_{max}}$. But using a different column and sample different results can be expected. In this work, the temperature effect on the separation of perfluoromathylated fullerene species is tested using a pyrenylpropyl bonded stationary phase.

For this test, a suitable eluent composition is important. Toluene is a good eluent for separation of pure fullerenes. Pure fullerenes can dissolve well in toluene with up to 2.8 mg/ml for C_{60}. It is not such a strong solvent as 1,2-Dichlorobenzene (27 mg/ml) [3] and not as weak as n-hexane (0.043 mg/ml).[59] But for the derivatives, toluene is still a strong solvent; therefore, toluene and hexane mixture is a possible choice.

The test is carried out with gradient and isocratic elution system. Several chromatograms from the gradient system are shown in Fig. 4.14. Focusing on the marked fraction in gray, its retention time is decreased depending on increasing temperature. Because of longer retention times, the peaks at 15°C broaden compared with peaks at high temperatures. While the marked peak with higher intensity is noticeable, the other species, which have been eluted before and after the marked fraction, with relative lower intensities are not as isolated as the marked ones at low temperatures. With the increasing temperature, the resolution of such species with lower quantities can be improved due to reduced retention times and lower overlap degree. Obviously, the best separation run is preformed at 35°C as the chromatogram shows good resolution and a relative stable background. A background correction is important for the gradient elution, if the eluents have large differences in absorption. The chromatogram in Fig. 4.14(e) shows the increased background in 300 mAU within 35 min under the variation of toluene v % from 30 to 100 %. Under this condition, the peaks after 25 min could not be recognized and leads to sample lost.

The similar tendency in the separation is also obtained by using the isocratic elution. The chromatograms are provided in Fig. 4.15. On the one hand, a better resolution is generally achieved when the separation procedure is performed at higher temperatures, but continuous use of columns under high temperature, e.g. 60°C, purposely can cause column deterioration. Less than 60 °C is the recommended temperature of the column. [4] On the other hand, when the separation is carried out at lower temperatures, e.g. 15°C, the peaks of substances with small content are not observable. So that, the optimal operating temperature used in this work is in the range of 25 to 40°C.

[3] Usually used in fullerenes extraction and washing column because of high solubility of fullerenes.
[4] Recommendation from column producer, Nacalai Tesque Inc.

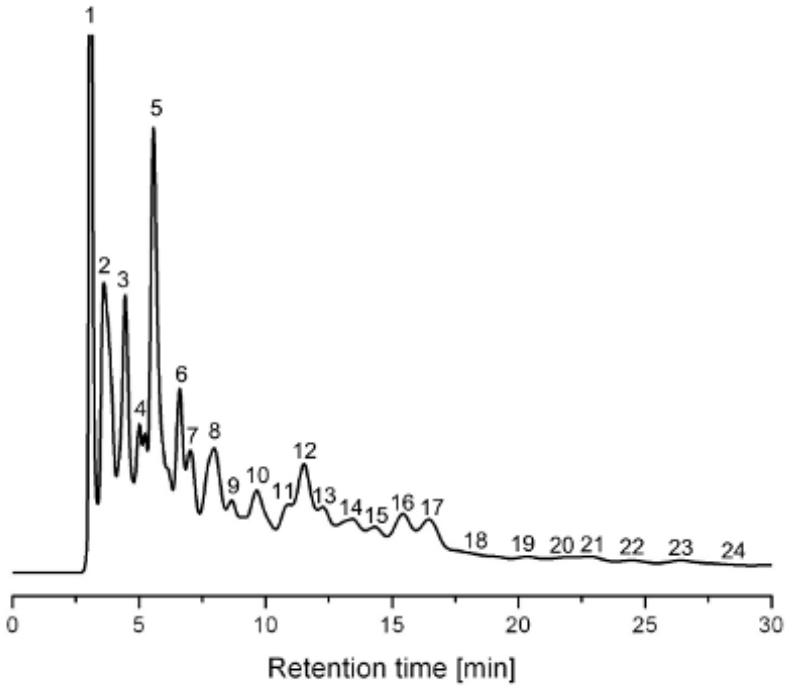

Figure 4.2.: Chromatogram of trifluoromethylated fullerenes C_{82-84} from the raw product. The numbers indicate the sequential number of the collected fractions.

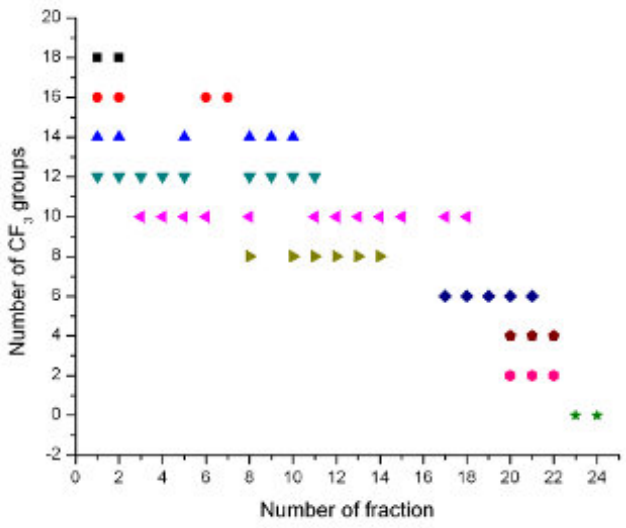

Figure 4.3.: The distribution of the species of $C_{84}(CF_3)_{18-0}$ among the HPLC fractions from Fig. 4.2. The results are obtained via the MALDI MS analysis (the spectra is not shown). The minor products of $C_{82}(CF_3)_{6-14}$, which have been found and structurally characterized in this work, are not shown here.

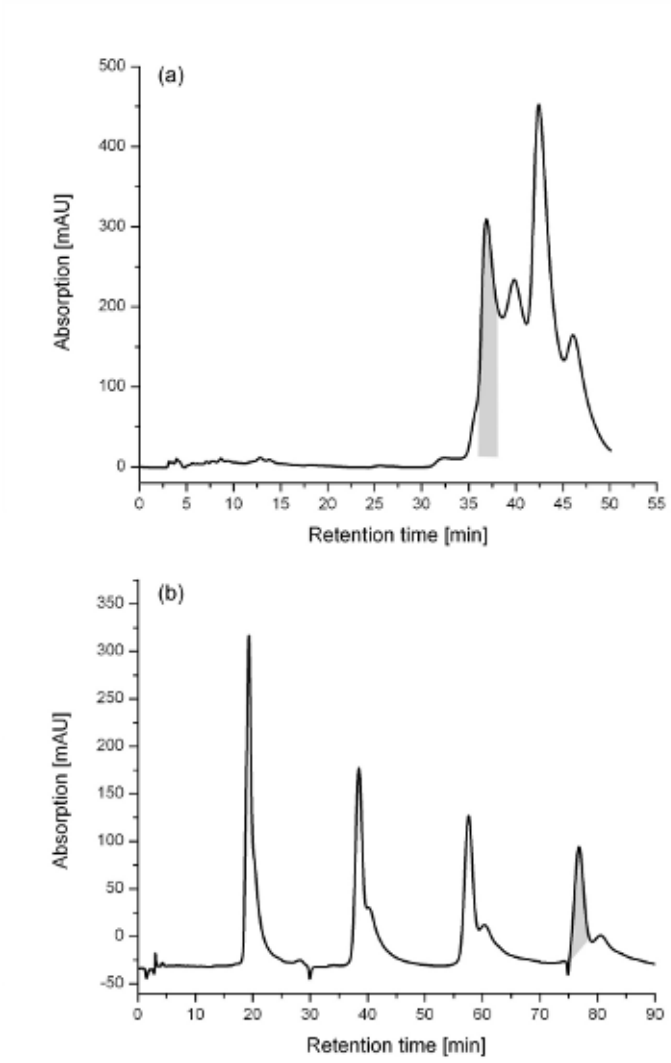

Figure 4.4.: Chromatograms using single (a) and multiple (b) separation technique. The row products were obtained from 1*qr* at 570 (a) and 600°C (b). The pure fraction of compound 84(11)/10-I is highlighted in gray.

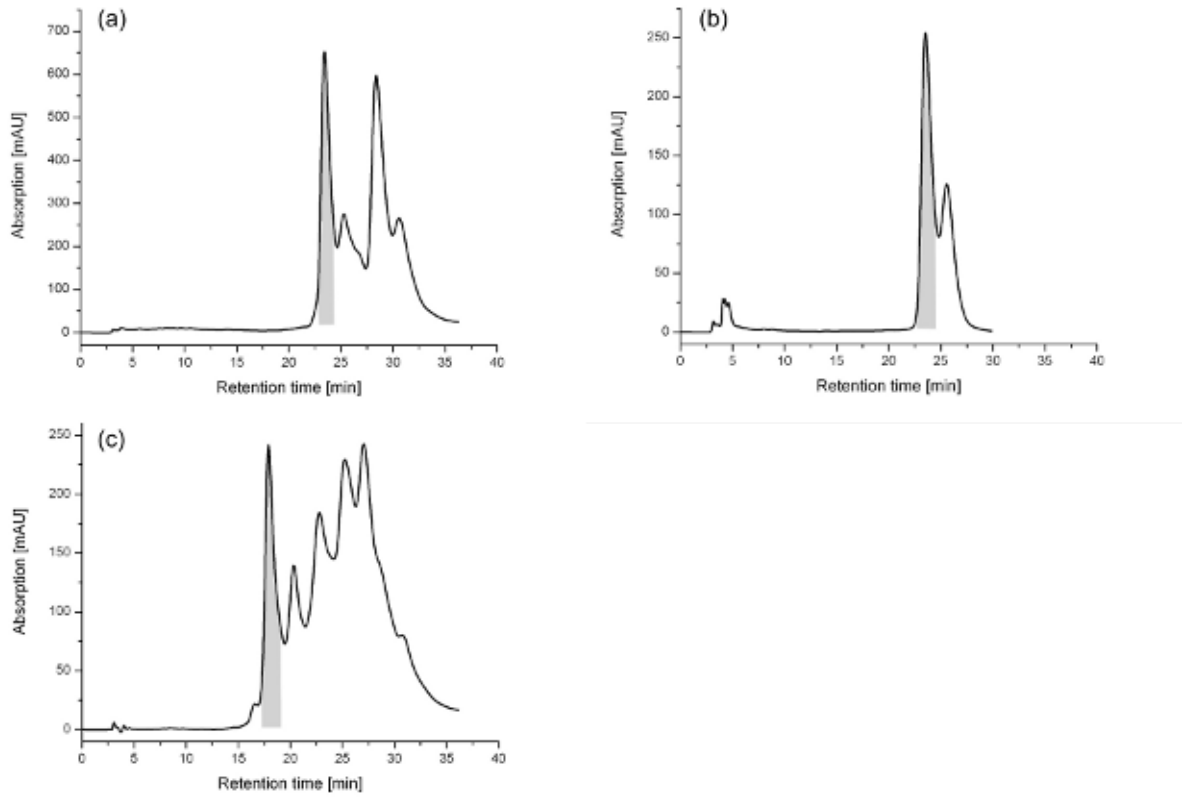

Figure 4.5.: Chromatograms for the isolation of compound 84(11)/12-I at different temperatures. The separation is carried out at 25°C (a) and 40°C (c) with the same eluent. The chromatograms (a) and (c) contain different species due to different fullerene sources during the syntheses (1*qr* and 2*qr*, respectively). Chromatogram (b) shows further purification of gray peak in (a) using the same separation parameters. The collected fractions of 84(11)/12-I are highlighted in gray.

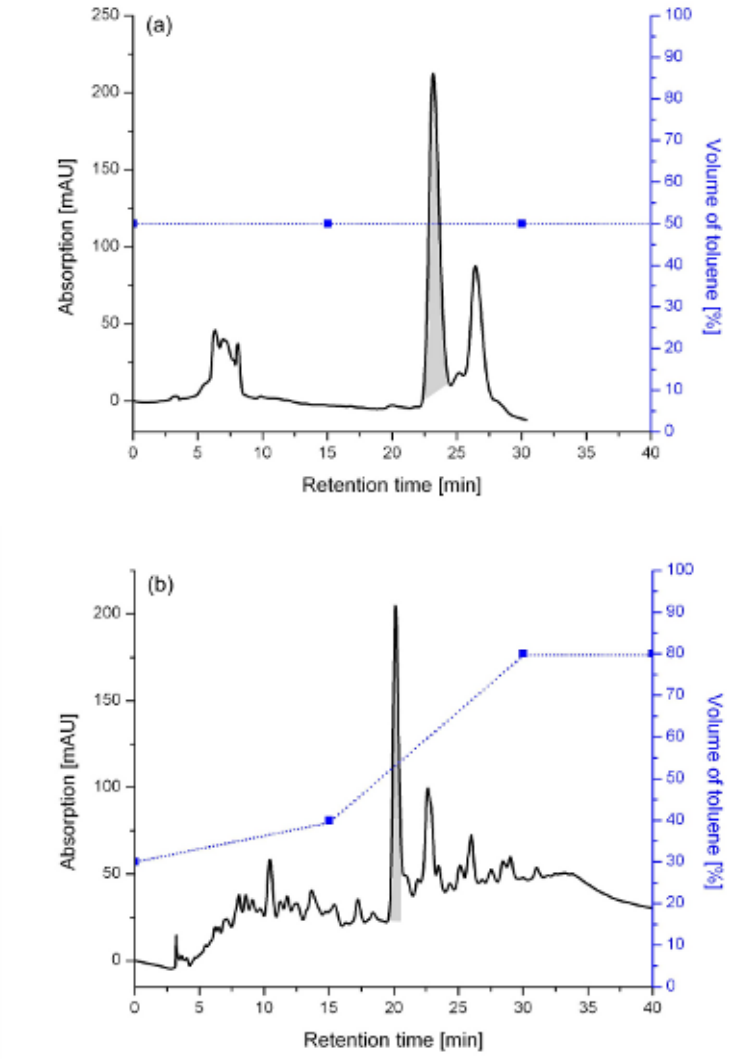

Figure 4.6.: Chromatograms for the isolation of species 84(22)/12-II using isocratic (a) and gradient elution (b). The pure fractions of 84(22)/12-II are highlighted in gray. Condition (a): 25°C, eluent H/T = 50/50; (c): 35°C, eluent H/T = 70/30 to 60/40 to 20/80 in 15 and 30 min, hold at H/T = 20/80 for 10 min.

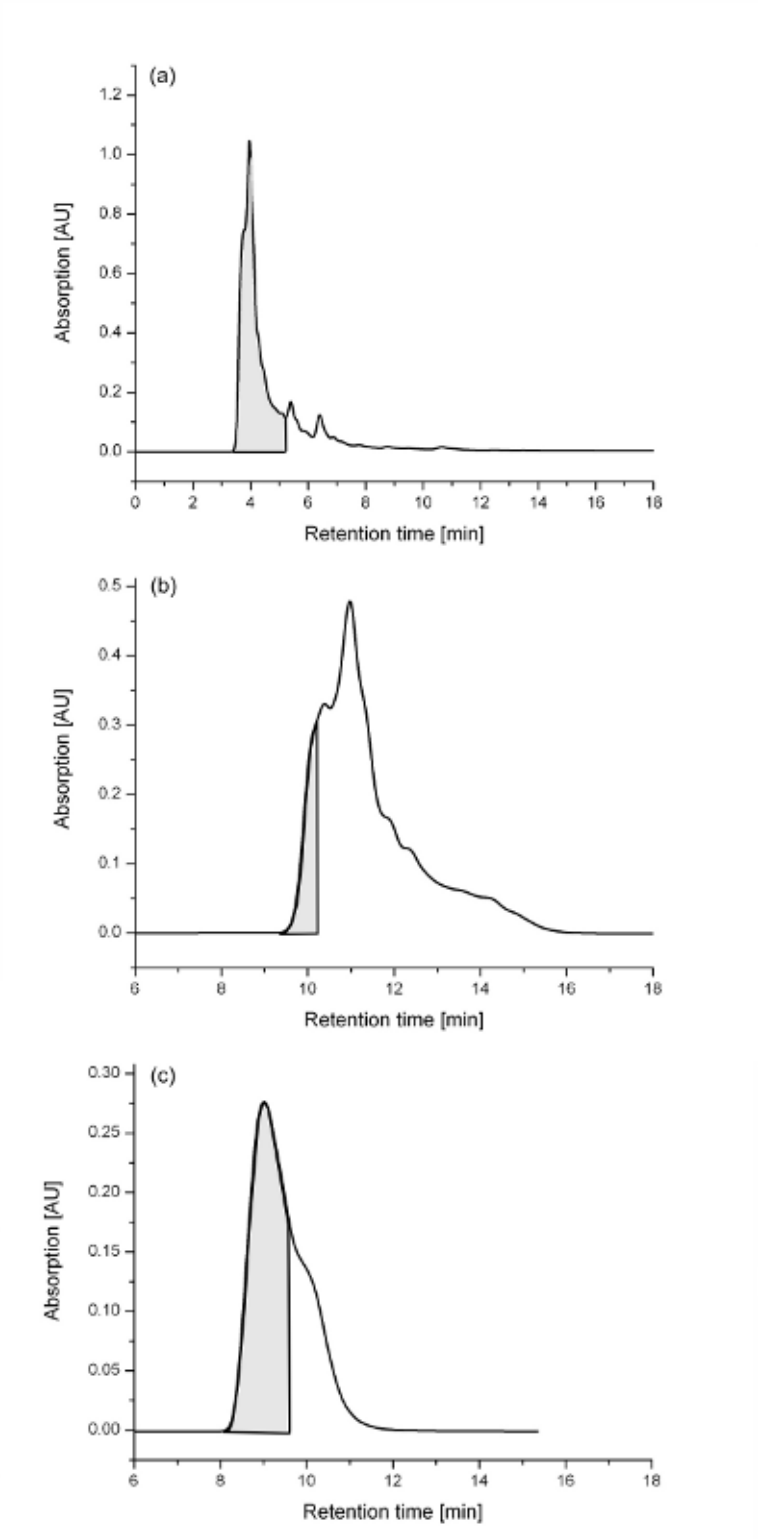

Figure 4.7.: Chromatograms for the isolation of compound 84(22)/20-I. The separation is carried out with flow rate at 4.6 (a) and 2.3 ml/min (b) and (c) with hexane as eluent. The collected fractions are highlighted in gray.

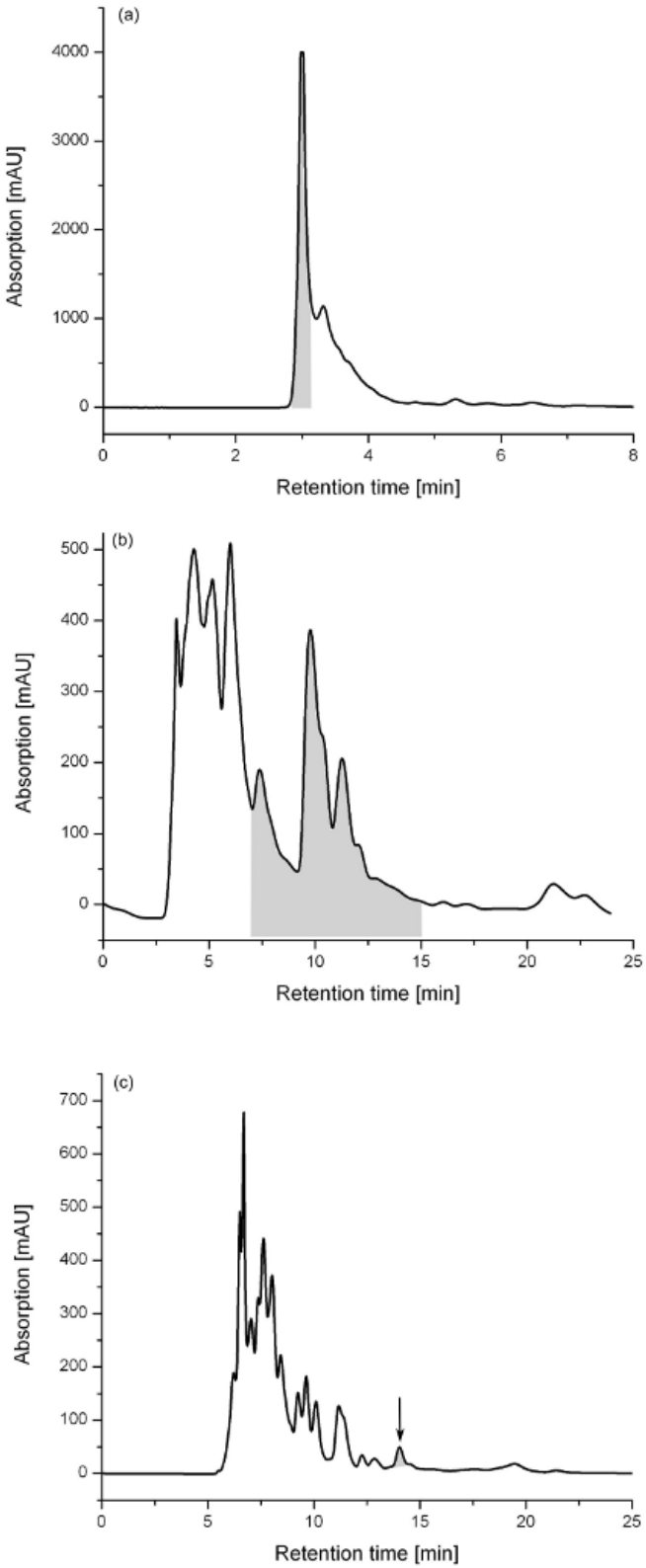

Figure 4.8.: HPLC trace showing 3 steps of separation. Chromatograms (a)-(c) are recorded using toluene, hexane with one column and hexane with 2 columns, respectively. The collected fractions are highlighted in gray. The pure fraction containing species 86(17)/16-I is shown with the arrow in (c).

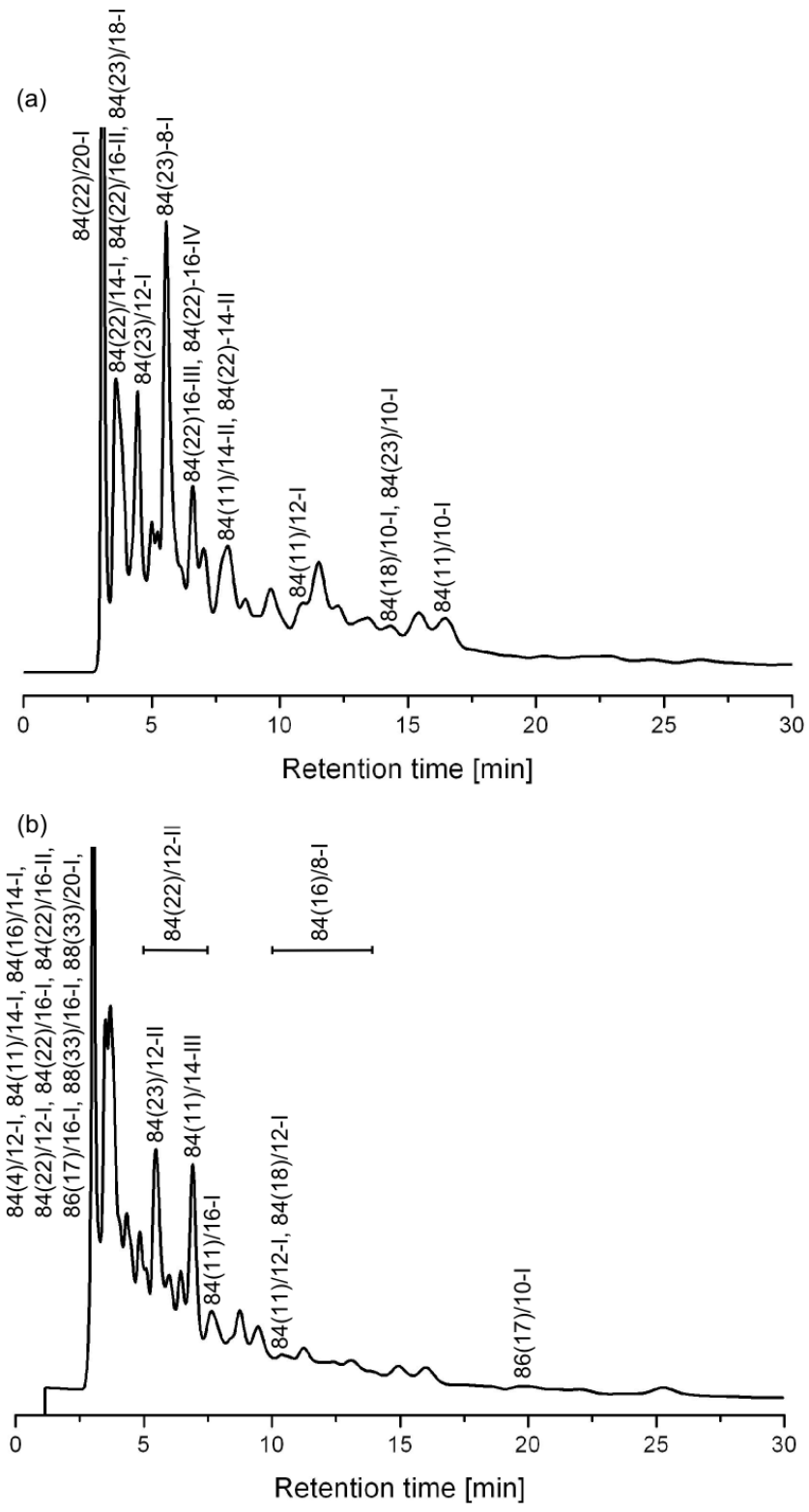

Figure 4.9.: The toluene chromatogram of separation step 1. The crude product mixture is synthesized with fullerene S1, C_{82-84} (a) and S2, C_{76-96} (b) in quartz ampoule. For species 84(11)/14-I and 84(22)/20-I, which are obtained from the synthesis in glass ampoule, the corresponding retention times are given here. The species notation: fullerene (cage isomer)/ number of attached CF_3 groups/ sequential number of isomer in order of increasing elution time. For species 84(22)/12-II and 84(16)/8-I, they are not collected from single toluene fraction but in a period with more peaks and then introduced into further separation step 2.

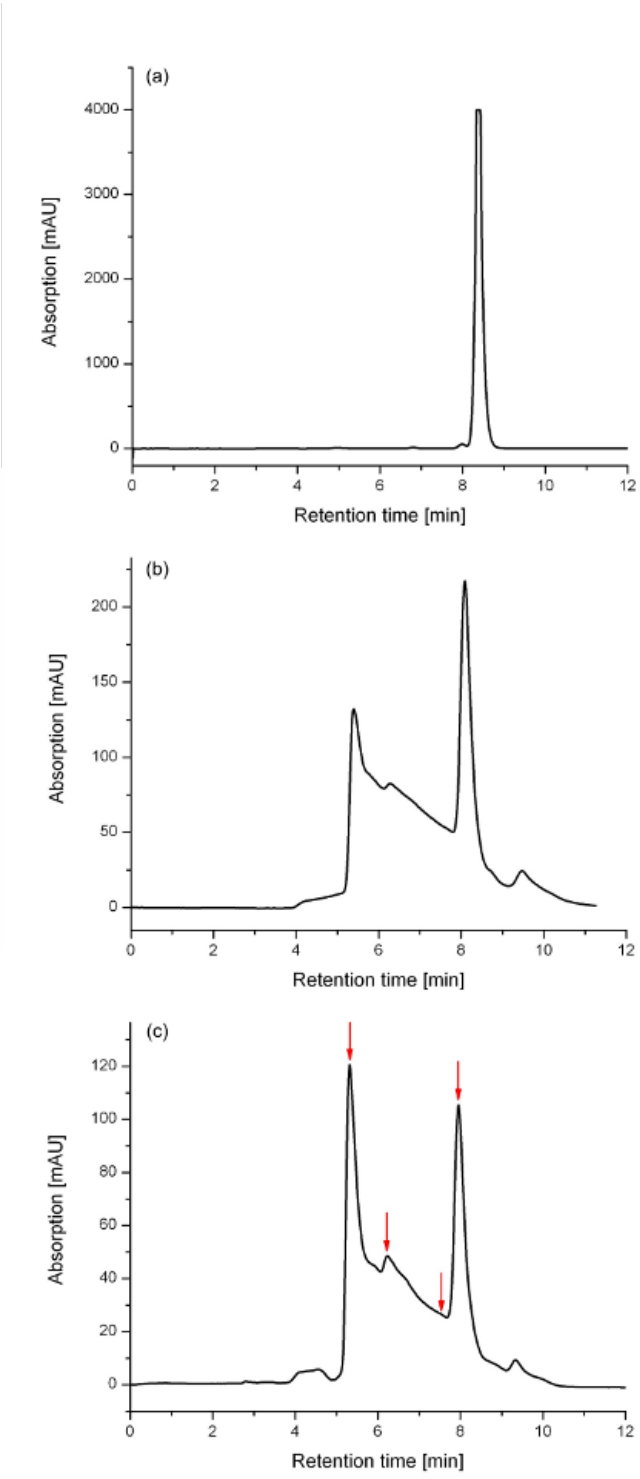

Figure 4.10.: Chromatograms of C_{60} with eluents T1 (a), T2 (b), and T3 (c). Arrows show fractions collected and analyzed with UV/VIS spectroscopy whose spectra are shown in Fig. 4.11

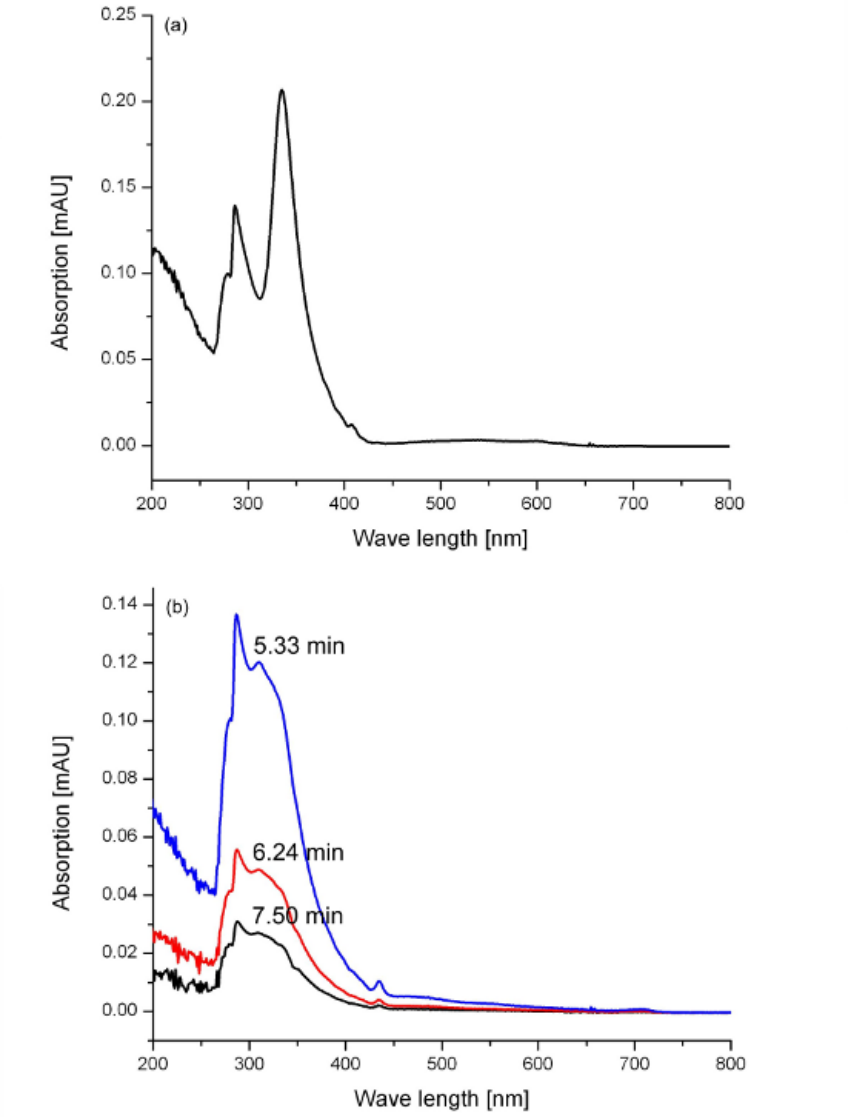

Figure 4.11.: The UV/VIS spectra of HPLC fractions (Fig. 4.10) at 8.3 min (a) and 5.33, 6.24, and 7.50 min (b).

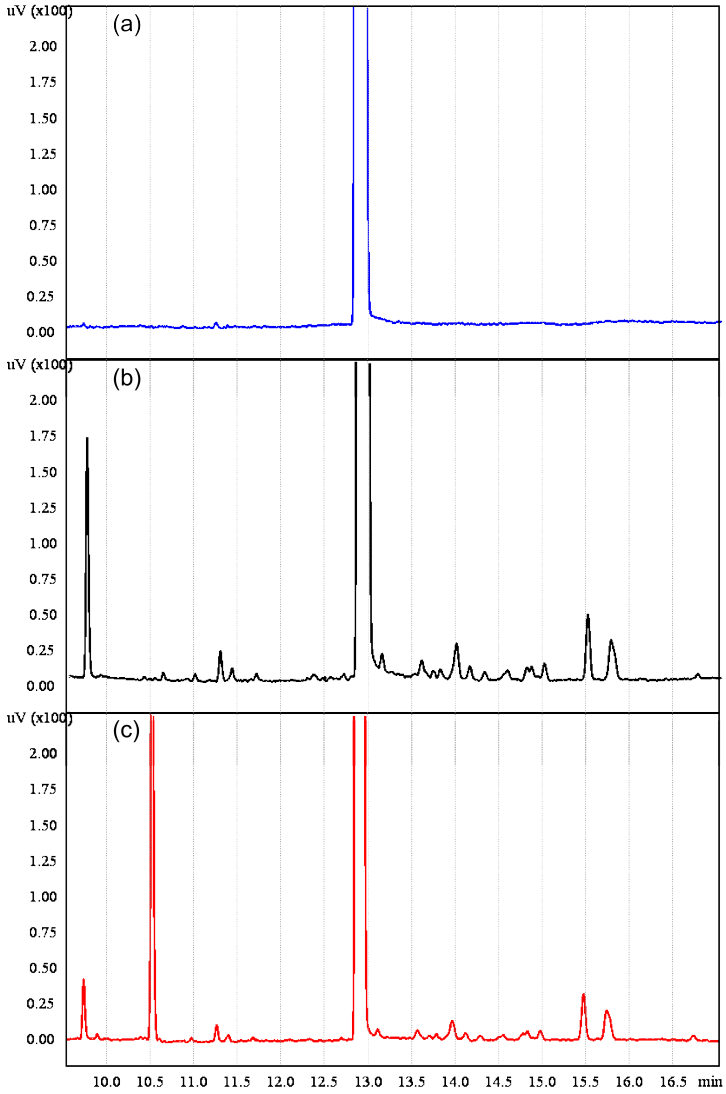

Figure 4.12.: Chromatograms of T1 (a), T2 (b) and T3 (c) in GC. The most intensive peak at 12.8 min is toluene and other peaks are impurities. Analysis via Shimadzu GC-2010, condition: Injector temperature 300°C, HP column (Agilent) with 0.25 mm × 100 m, analysis temperature 120°C, FID temperature 350°C.

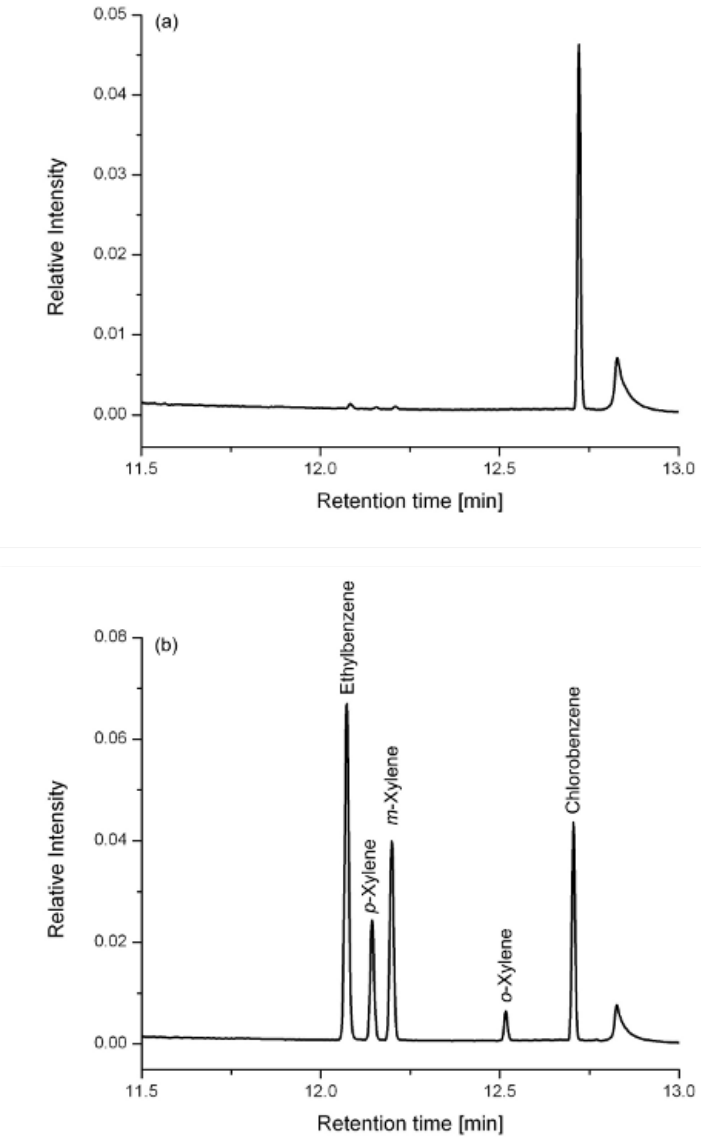

Figure 4.13.: The Chromatograms of T1 (a) and T2 (b) in GC-MS. Chlorobenzene is used as the detergent for injector. The toluene is eluent at about 10 min, which is not shown here. Analysis via Varian GC3800-MS4000, condition: Injector 25°C, Varian VF-waxms column with 0.25 mm $\times$ 30 m, temperature program: 6 min 25°C, with 1°C/min to 30°C, with 60°C/min to 250°C.

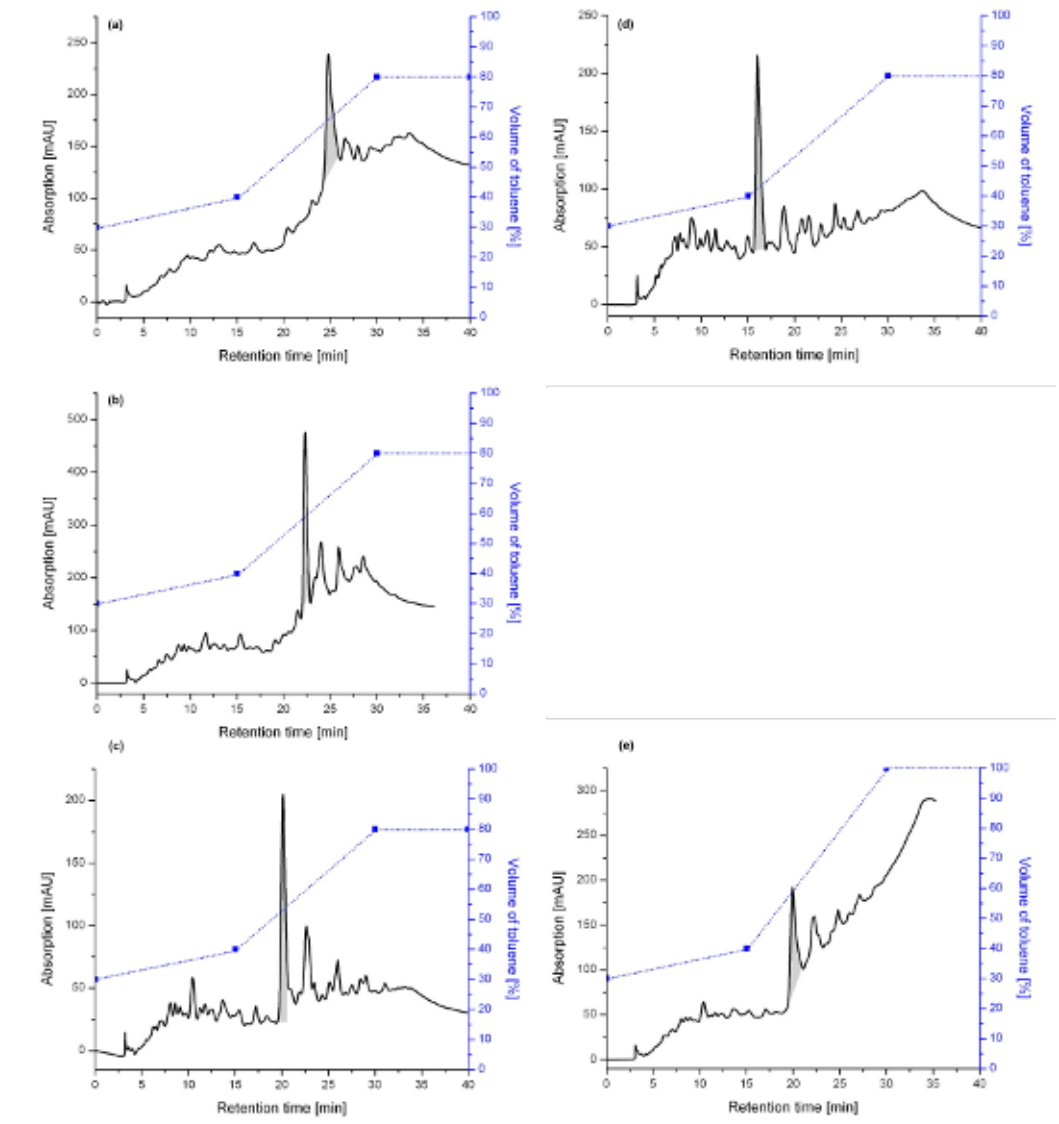

Figure 4.14.: Chromatograms using gradient elution at different temperatures. The marked fraction of 84(22)/12/II is highlighted in gray. Condition of chromatogram (a)-(d): 15°C; 25°C; 35°C; 50°C, respectively; eluent H/T= 70/30 to 60/40 to 20/80 in 15 and 30 min; hold at H/T= 20/80 for 10 min. Condition of chromatogram (e): 35°C; eluent: H/T = 70/30 to 60/40 to 0/100 in 15 and 30 min; hold at H/T = 0/100 for 10 min.

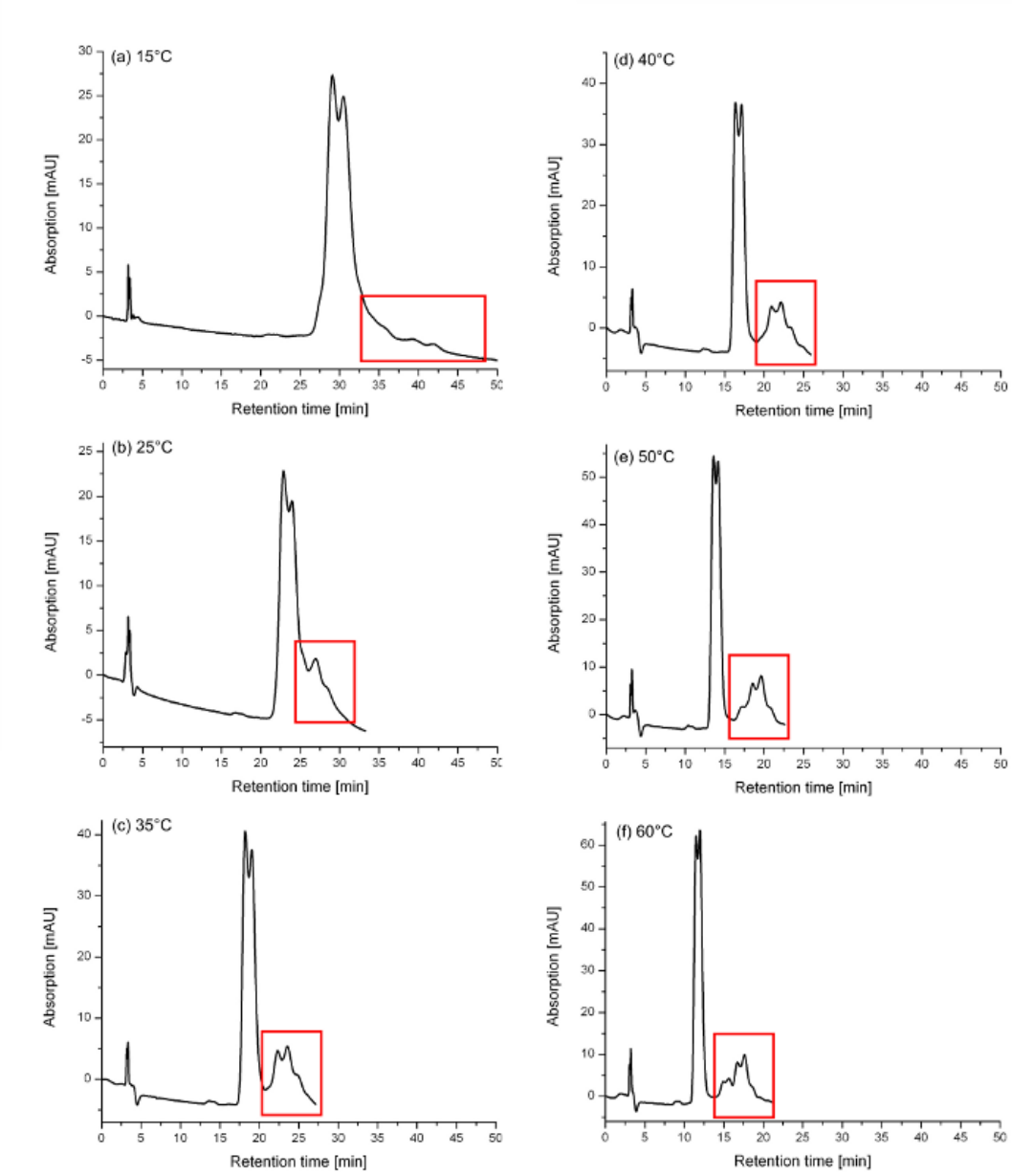

Figure 4.15.: Chromatograms using isocratic elution at different temperatures. Condition of separation (a)-(f): 15°C, 25°C, 35°C, 40°C, 50°C and 60°C, respectively; eluent H/T = 60/40. The retention time of species decreases depending on increasing temperatures. The resolutions of the species with lower amount shown in the red box vary at different temperatures.

Chapter 5.

Results and discussion: Molecular structures

In this chapter, the structures of the fullerene derivatives that have been synthesized and isolated within this study are presented. For each fullerene, there is a set of cage isomers that can be distinguished by the cage topology that is determined by the network of pentagons and hexagons forming the cage surface. In raw products of the fullerene synthesis such cage isomers usually occur as a mixture. Starting from the bare, hollow carbon cage, the addition products are formed by the addition of CF_3 groups on the fullerene surface. For simplification, they are briefly called CF_3 isomers or CF_3 derivatives. For each composition, the different isomers and structures are discussed and compared with each other in the following sections. For some cases, they are further compared with the C_2F_5 derivatives. Each molecular structure is presented as ball-and-stick model and Schlegel diagram using the same orientation. The names given for the CF_3 derivatives follow the IUPAC recommendations for fullerenes and their lowest locant rules.[17] These names are also used in the tables of the calculated relative energies in Appendix D.

5.1. Fullerene C_{84}

The fullerenes C_{60} and C_{70} are formed as the main products of fullerene synthesis using the arc-discharge method. Beside them, fullerene C_{84} is obtained in amounts that make a broad spectrum of investigations possible. Thus, it is the most well-known candidate in the family of higher fullerenes. C_{84} contains a number of cage C atoms which is an integer multiple of 6, i.e., $6n$ with $n = 14$. Such cage compositions are called *magic numbers*. The magic numbers indicate a higher probability to find the compositions C_{6n} in the fullerene raw product.[60] C_{84} has 24 IPR cage isomers.[15] The well-characterized isomers 22 and 23 (the numbering based on the spiral algorithm[15]) are the main products with the amount ratio of 2:1.[13,14] Minor products are the cage 4, 11 and 16. In addition, cage 5, 13, 14, 18 and 19 are known experimentally[54,61]. 26 CF_3 derivatives of fullerene C_{84} are isolated via HLPC and structurally characterized in this thesis (see Tab. 5.1).

Table 5.1.: Overview of isolated trifluoromethylated C_{84} derivatives.

Cage isomer	Number of attachments	Number of CF_3 derivatives
4	12	1
11	10/12/14/16	1/1/3/1
16	8/14	1/1
18	10/12	1/1
22	12/14/16/20	2/2/4/1
23	8/10/12/14/18	1/1/1/2/1

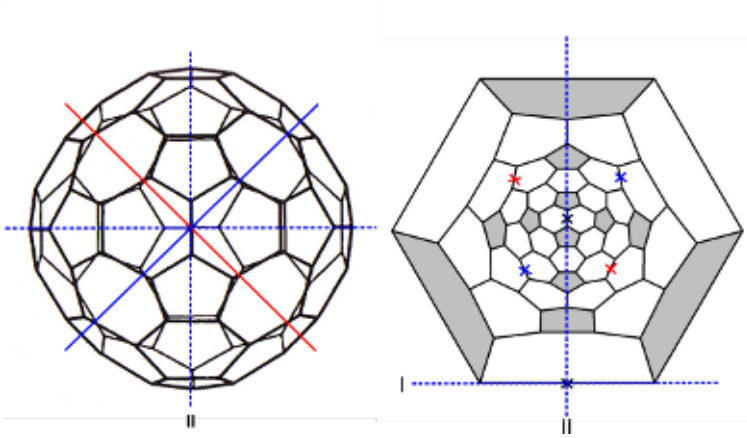

Figure 5.1.: The molecular structure (left) and the corresponding Schlegel diagram (right) of the $C_{84}(4)$. One C_2 axis points to the reader and the remaining two C_2 axes are shown as blue and red solid lines in left and crosses in right. The dashed lines show the mirror planes I and II. Plane I is parallel to one C-C bond and bisects another one.

5.1.1. C_{84}, cage isomer 4

The cage isomer 4 of fullerene C_{84} has high D_{2d} symmetry, which contains three C_2 axes and two mirror planes that are parallel with the principle axes (showing in Fig. 5.1).

$C_{84}(4)$ is one of the minor products of the fullerene synthesis . The experimental results about this cage are limited. Computational results suggest at the first the existence of this cage isomer by Bühl and co-workers.[62] Later, the structural determination of isomer $C_{84}(4)(CF_3)_{12}$ served as directly proof of the cage and supported obviously prediction.[1] This isomer is quite stable and thus can be found in every synthesis. Only one isomer with cage 4 has been found in this work.

$C_{84}(4)(CF_3)_m$ derivatives

$C_{84}(4)(CF_3)_{12}$ For this composition, only one CF_3 isomer $C_{84}(4)(CF_3)_{12}$ has been isolated in this work. This isomer with symmetry point group C_2 contains twelve CF_3 groups that are arranged in four sets that are distributed symmetrically on the parent fullerene (see Fig. 5.2). Each set contains three CF_3 groups and is attached on the three *para* positions of two edge-sharing hexagons. The addition pattern is noted as four times *para*^{2}, i.e., *para*^{2},*para*^{2},*para*^{2},*para*^{2}, where commas denote that each pair of edge-sharing hexagons is isolated from the others. In $C_{84}(4)(CF_3)_{12}$, all CF_3 groups are connected to cage C atoms of pentagon-hexagon-hexagon junctions (PHJs) so that each pentagon bounds one CF_3 group. The attachments on PHJs are preferred compared to those on triple hexagon junctions (THJs). In case of a C atom lying on an idealized planar (THJs) with bond angle of 120°, perfect sp^2 hybridization is retained. Attachment on THJs, however, leads to sp^3 hybridization, i.e., pyramidalization, which increases the steric strains. The same effects have been found for the high order fullerene derivatives of $C_{74}(1)(CF_3)_{12}$ and $C_{78}(5)(CF_3)_{12}$.[63] Such derivatives with 12 attached groups are quite stable and are obtained from every synthesis.

5.1.2. C_{84}, cage isomer 11

The isomer 11 of C_{84} exhibits C_2 symmetry. The C_2 axis passes through two C-C bonds on the opposite sides of fullerene cage (Fig. 5.3). Five IPR isomers of C_{84} with the same symmetry have been

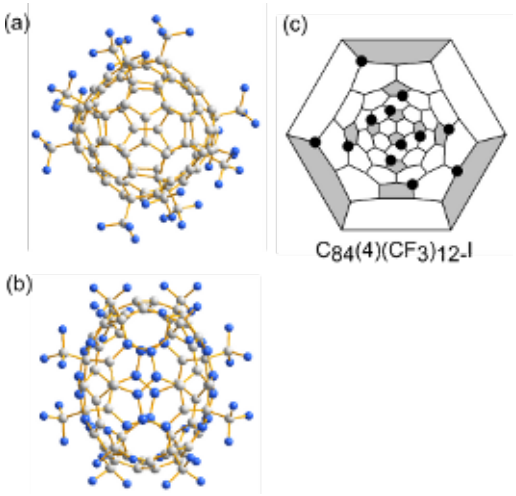

Figure 5.2.: Molecular structure and Schlegel diagram of $C_{84}(4)(CF_3)_{12}$. The projection (a) top view, (b) side view and Schlegel diagram are shown along a C_2 axis.

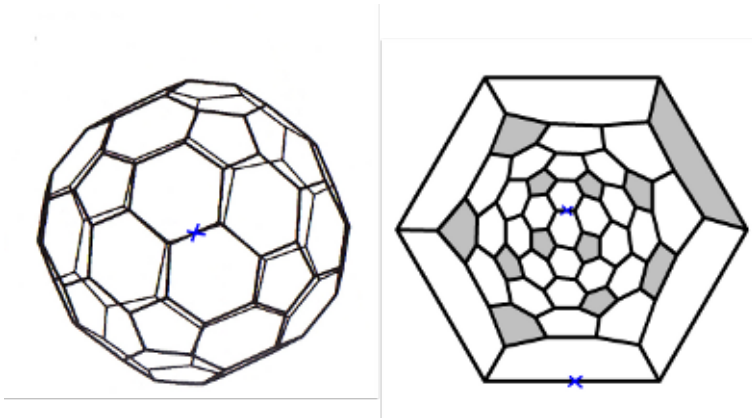

Figure 5.3.: The molecular structure (left) and the corresponding Schlegel diagram (right) of the $C_{84}(11)$. The C_2 axis passes through the cage is shown as cross.

presented earlier in theoretical and experiment studies.[61,64–66] The first trifluoromethylated $C_{84}(11)$ has been reported using ^{19}F NMR by Kareev *et al.*.[67] Tamm *et al.* presented $C_{84}(11)(C_2F_5)_{12}$.[1] In this work, five isomers of $C_{84}(11)(CF_3)_m$ with compositions range from m = 10-16 are isolated and structurally characterized.

$C_{84}(11)(CF_3)_m$ derivatives

$C_{84}(11)(CF_3)_{10}$

One isomer with ten CF_3 groups was isolated. On the cage surface, the CF_3 groups are divided into two sets, each of them containing five CF_3 groups. In each set, all groups attach on the *para* positions in a chain of four hexagons that share the edge with the neighbor hexagons. The addition pattern is denoted as p^5,p^5 (Fig. 5.4). In this way, due to the two symmetry equivalent sets of attachments, the structure of isomer $C_{84}(11)(CF_3)_{10}$ remains the C_2 symmetry of the parent fullerene.

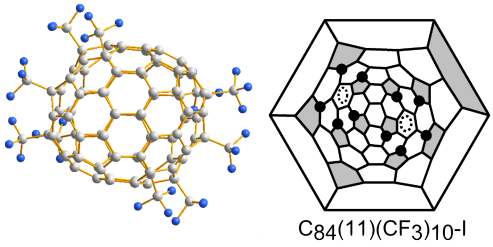

Figure 5.4.: Molecular structure and Schlegel diagram of $C_{84}(11)(CF_3)_{10}$. The projection and Schlegel diagram are shown along a C_2 axis.

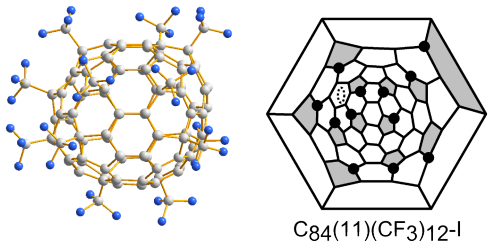

Figure 5.5.: Molecular structure and Schlegel diagram of $C_{84}(11)(CF_3)_{12}$-I. The projection and Schlegel diagram are shown along a C_2 axis of the parent fullerene.

$C_{84}(11)(CF_3)_{12}$ This isomer $C_{84}(11)(CF_3)_{12}$-I exhibits an asymmetric p^6,p^2,p addition pattern of 12 CF_3 groups (see Fig. 5.5). It has been reported for the first time by I. E. Kareev *et al.*.[3] This pattern differs from the p^5,p,p,p structure of the related C_2F_5 derivative $C_{84}(11)(C_2F_5)_{12}$.[2]

In order to compare the stability of different structures, the calculations are carried out for the experimental isomer $C_{84}(11)(CF_3)_{12}$-I and hypothetical isomer $C_{84}(11)(CF_3)_{12}$, denoted as 84(11)/12-2, whose structure corresponds to the one of isomer $C_{84}(11)(C_2F_5)_{12}$. For the discussion purpose, the full compound names of experimental isomers are used for the structure discussion while theoretically considered isomers are labeled as 84(11)/m-N, where even Arabic numbers m and Arabic numbers N denote the number of attached CF_3 groups and sequential number of isomer with increasing relative formation energies. The relative formation energies of the experimental isomer $C_{84}(11)(CF_3)_{12}$-I and hypothetical isomer 84(11)/12-2 are calculated and compared to obtain more insight into the relative stability of both isomers. The computational results show that the energy of isomer 84(11)/12-2 is 4.5 kJ/mol higher than the isolated product $C_{84}(11)(CF_3)_{12}$-I (the difference is very small). Therefore, the isomer 84(11)/12-2 was expected to be found also experimentally. There are several possible explanations of why this isomer has not been found. First, the reaction barrier to form isomer 84(11)/12-2 is higher than that one to from isomer $C_{84}(11)(CF_3)_{12}$-I. Second, the barrier to form higher addition product, i.e., isomer with 14 CF_3 groups, is lower for isomer 84(11)/12-2 than for isomer $C_{84}(11)(CF_3)_{12}$-I. The calculated lower HOMO-LUMO gap of isomer 84(11)/12-2 (1.44 eV) compared to that of isomer $C_{84}(11)(CF_3)_{12}$-I (1.55 eV) can be interpreted as an indication to support this assumption. Indeed, the higher trifluoromethylated fullerene products $C_{84}(11)(CF_3)_{14}$-II and III have been found experimentally which could be obtained from isomer 84(11)/12-2 by addition of two CF_3 groups. A combination of both cases is also possible, i.e., if the molecule has to overcome a quite high barrier to form isomer 84(11)/12-2 then it holds a lot of vibration energy. If this energy is not released fast enough then this may increase the probability to overcome a low barrier for the next addition. It is not excluded the possibility that there are small amounts of isomer 2 in the raw product which do not yield enough materials to form single crystals after the HPLC

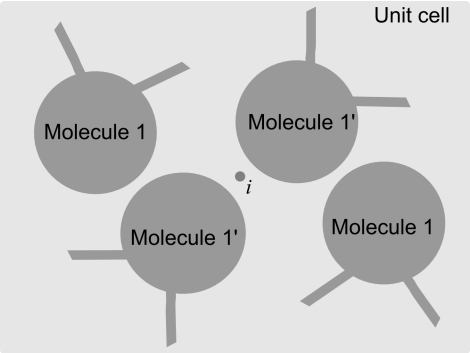

Figure 5.6.: Model of a single crystal containing two crystallographically independent molecules. Molecule 1 (or molecule 1') have been generated by an *inversion center*, *i*. Molecule 1 and 1' are crystallographically independent.

Table 5.2.: Relative formation energy E [kJ/mol] and HOMO-LUMO gap Δ [eV] of the isomer $C_{84}(11)(CF_3)_{14}$

Isomer	I	II	III
E	6.8	8.5	0
Δ	1.53	1.58	1.69

separation.

Another interesting detail of the study of the isolated isomer $C_{84}(11)(CF_3)_{12}$-I is related to its crystal structure. As only one case in this work, a crystal structure of a perfluoromethylated fullerene is formed with two crystallographically independent molecules of the same isomer (see Fig. 5.6).

$C_{84}(11)(CF_3)_{14}$ Three isomers with 14 CF_3 groups are presented in Fig. 5.7. All of their structures are denoted by p^5,p^5,p. $C_{84}(11)(CF_3)_{14}$-I and II have eight CF_3 attached to the same positions, while $C_{84}(11)(CF_3)_{14}$-II and III have 12 common occupied sites. According to the DFT calculations, $C_{84}(11)(CF_3)_{14}$-III is the most stable structure (0 kJ/mol) followed by isomer $C_{84}(11)(CF_3)_{14}$-I and II (6.8 and 8.5 kJ/mol, respectively). $C_{84}(11)(CF_3)_{14}$-II and III are possible precursors for isomer $C_{84}(11)(CF_3)_{16}$ via addition of two more CF_3 groups, but isomer $C_{84}(11)(CF_3)_{14}$-II might be the preferred candidate due to its thermodynamic (higher relative formation energy) and kinetic (smaller HOMO-LUMO gap) instabilities (see Tab. 5.2).

$C_{84}(11)(CF_3)_{16}$ The addition pattern of isomer $C_{84}(11)(CF_3)_{16}$ consists of two chains. One chain contains six and the other ten CF_3 groups. This is denoted by p^9,p^5 and illustrated in Fig. 5.8. On the fullerene cage, four pairs of CF_3 groups are attached on four of the twelve pentagons because the total number of addends is larger than the number of pentagons (12). In such addition patterns, isolated C=C bonds are formed with the bond distance of about 1.32 Å between two pentagons. The isolated C=C bonds are obtained when the fullerene cage is overcrowded with a large numbers of the addends. It can be considered as a stabilizing effect. The formation of the four partially 'aromatic' rings with C-C bond distances between 1.37-1.42 Å is another balancing effect in this structure. Compared with the normal sp^2-hybridized carbons with C=C bond length about 1.34 Å, the bond lengths of C=C on the fullerene cage vary between 1.30 and 1.36 Å. For the partially 'aromatic' rings (or benzenoid ring) on the fullerene cage, the bond lengths also vary, but the average C-C bond length is about 1.40 Å closed to the bond

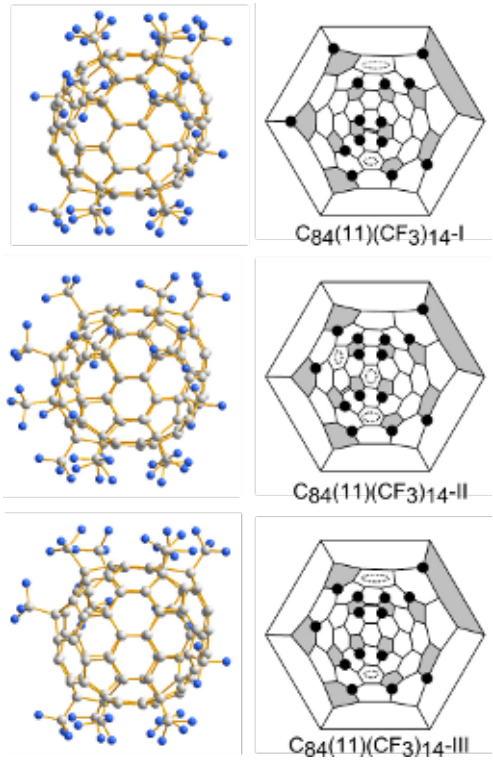

Figure 5.7.: Molecular structure and Schlegel diagram of $C_{84}(11)(CF_3)_{14}$-I, -II and -III. The projection and Schlegel diagram are shown along a C_2 axis of the parent fullerene. The circles with dashed line show the partially 'aromatic' rings.

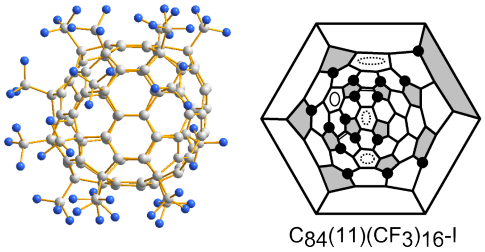

Figure 5.8.: Molecular structure and Schlegel diagram of $C_{84}(11)(CF_3)_{16}$. The projection and Schlegel diagram are shown along a C_2 axis of the parent fullerene. The circles with dashed line show the partially 'aromatic' rings.

length of benzene [1] The variation is caused by (i) the 'quasi planarity' environment of the fullerene cage and (ii) rehybridization. These considerations are applied for the all structures discussed in this work.

General aspects of trifluoromethylation of fullerene: $C_{84}(11)(CF_3)_{10-16}$

In total, six isomers of $C_{84}(11)(CF_3)_m$ (m = 10-16) were isolated in this work. Possible pathways of the $C_{84}(11)$ trifluoromethylation cannot be determined just based on these six structures. Therefore, some structures, mainly with 10-12 CF_3 groups, have been selected under the requirement that they fit into possible reaction pathways. For the discussion of the structures, the full compound names of experimentally observed isomers are used. Isomers investigated only in the calculations are labeled with 84(11)/*m*-N where *m* and N are Arabic numbers. *m* denotes the number of attached CF_3 groups and N consecutively labels isomers of increasing relative formation energies.

In order to find the common feature, the addition patterns of isomers $C_{84}(11)(CF_3)_{14-16}$ are compared. All of them have a p^5-*para*-chain showing on the lower part of their Schlegel diagrams (see Fig. 5.7 and Fig. 5.8). This chain is taken as the fixed feature of the addition pattern. By this way, possible structures formed by the further addition of six CF_3 groups along the reaction pathway only vary in the upper part of the Schlegel diagrams. Two more possible isomers 84(11)/12-3 and 84(11)/12-4 are shown in Fig. 5.9. For the isomers with ten CF_3 groups, three isomers are chosen based on the addition pattern of isomer 84(11)/12-2. The selection rule is the same as before: the p^5-*para*-chain is maintained, and the remaining CF_3 attached positions are varied. It follows that three CF_3 pairs are isolated on the addition pattern of the isomer 84(11)/12-2. The addition patterns of three chosen isomers with ten groups correspond to the one of isomer 84(11)/12-2 without one of the three isolated CF_3 pairs.

For the experimentally obtained isomer $C_{84}(11)(CF_3)_{10}$-I, the lowest formation energy and biggest HOMO-LUMO gap (1.28 eV) are predicted among selected isomers with ten CF_3 groups. That indicates the lower reactivity of this experimental isomer. On the contrary, thermodynamic and kinetic instabilities of the model structures 84(11)/12-2,3,4 were predicted (corresponding relative formation energies [kJ/mol] 30.6 / 37.0 / 67.9 and HOMO-LUMO gaps [eV] 0.65 / 1.02 / 0.36, respectively), and might explain the ongoing reaction to the observed products by addition of two more CF_3 groups. The same explanation holds for isomer with twelve groups. The experimental isolated isomer $C_{84}(11)(CF_3)_{12}$-I might not serve as a precursor for the higher trifluoromethylated products because its reaction barrier might be higher. However, the calculated isomers represent the perfect pathways from lower trifluoromethylated fullerene derivatives to higher ones. According to computational results, the experimental isolated isomers are the most stable. Based on the structural similarities, the possible reaction pathways

[1] For sp^2-hybridized carbons, C=C bonds are about 1.34 Å. For sp^3-hybridized carbons, C-C bond lengths are about 1.47 Å. For molecule benzene, all C-C bond lengths are the same, ca. 1.40 Å.[68]

of $C_{84}(11)(CF_3)_{12-16}$ are suggested in Fig. 5.9.

5.1.3. C_{84}, cage isomer 16

Cage isomer 16 of fullerene C_{84} is one of the minor isomers (4, 5, 11, 14, 16, and 18) found in the usual fullerene mixture. Among these minor isomers, the isomers 14 and 16 have C_s symmetry, i.e., have one symmetry plane (see Fig. 5.10). This is determined by ESR, ^{13}C NMR analysis and predicted by theoretical DFT calculation.[66,69] However, these ESR and NMR experiments cannot distinguish between isomers 14 and 16. For this purpose, the first X-ray crystallographic investigation of isomer 14 was presented as its co-crystal with silver tetraphenylporphyrin by Epple and co-workers.[70] Isomer 16 was found as a pentafluoroethylated derivative in previous studies.[1,71]

$C_{84}(16)(CF_3)_m$ derivatives

$C_{84}(16)(CF_3)_8$ and $C_{84}(16)(CF_3)_{14}$ Two new structures of the trifluoromethylated fullerene $C_{84}(16)$ with 8 and 14 CF_3 groups were determined in this work. The addition patterns in both structures exhibit an overall C_s symmetry and long chains denoted by p^7 and p^{13}. Their structures are shown in Fig. 5.11. Comparing the addition pattern of both CF_3 isomers, the *para* chain orientation differs slightly. That means that eight CF_3 groups can attack the carbon atoms to form the *para* chains in the two different ways due to similar local environment. The prolongation of the *para* chain in isomer $C_{84}(16)(CF_3)_8$ by further addition of CF_3 groups seems to be energetically disfavored. This can be explained by unfavored reaction positions on the THJs on which next possible attachment occurs. For further CF_3 additions, this means that the long *para* chain has to change its orientation to make the chain prolongation possible as realized in the isomer $C_{84}(16)(CF_3)_{14}$. Another way to circumvent the addition of CF_3 to THJs is the formation of multiple short *para* chains. A good example for this is found for $C_{84}(16)(C_2F_5)_{12}$-I in the literature.[1,71] In this isomer (see Fig. 5.12), eleven C_2F_5 groups are arranged on the *para* positions in hexagons and one C_2F_5 is isolated. Six among twelve groups attached on the same position to form a long chain as one of isomer $C_{84}(16)(CF_3)_8$, and the remaining five groups consisted of two more chains with three and two members. A comparison between the isomers $C_{84}(16)(C_2F_5)_{12}$ and $C_{84}(16)(CF_3)_{14}$-I is that ten CF_3 groups of both structures are attached on the same positions.

5.1.4. C_{84}, cage isomer 18

Cage isomer 18 is one of the 24 isomers with higher relative formation energy (65.65 kJ/mol at the B3LYP/6-31G level).[69] [2] Thus, it represents only a small fraction of the fullerene product mixture. The isomer 18 of C_{84} exhibits C_{2v}-symmetry with one C_2 axis and two mirror planes (Fig. 5.13).

$C_{84}(18)(CF_3)_m$ derivatives

$C_{84}(18)(CF_3)_{10}$ and $C_{84}(18)(CF_3)_{12}$ The structures of isomers $C_{84}(18)(CF_3)_{10}$ and $C_{84}(18)(CF_3)_{12}$ exhibit the C_s (see Fig. 5.14). Ten CF_3 groups of both isomers are symmetrically attached on same positions on the cage. For isomer $C_{84}(18)(CF_3)_{12}$, beside ten groups attached to the same positions as isomer $C_{84}(18)(CF_3)_{10}$, the remaining two groups are also located on the *para* position in a hexagon. The addition patterns are described as p^9 and p^9,p for isomer $C_{84}(18)(CF_3)_{10}$ and $C_{84}(18)(CF_3)_{12}$, respectively. Comparing the structures between isomer $C_{84}(18)(CF_3)_{12}$ obtained in this work and isomer $C_{84}(18)(C_2F_5)_{12}$ in previous work[1], the attached positions on the fullerene cage were different. They have only four attachments on the same positions. Otherwise, comparing CF_3 and C_2F_5 isomers, CF_3

[2] The overviews of the relative energy and the HOMO-LUMO gaps of cage isomers C_{84} are shown in Appendix D.

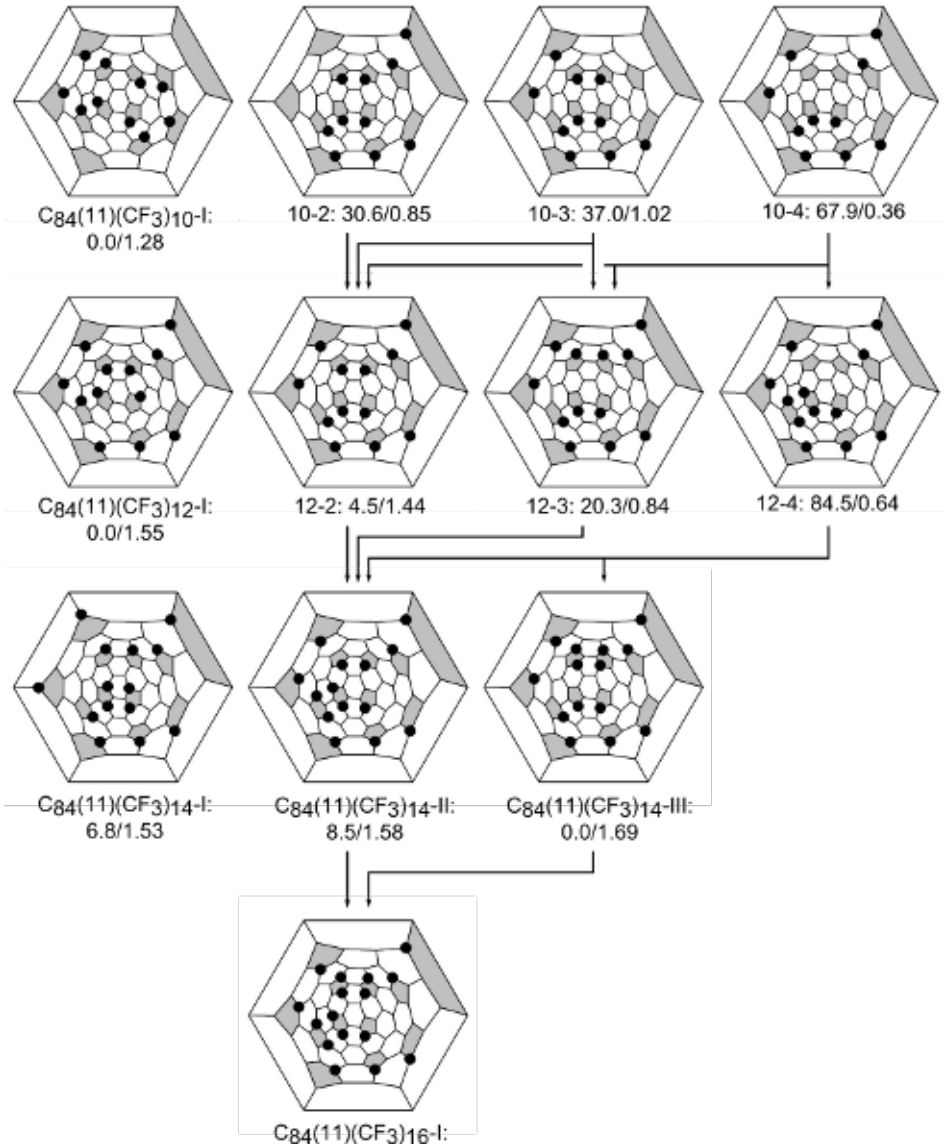

Figure 5.9.: Possible reaction pathways of the trifluoromethylation for isomers $C_{84}(11)(CF_3)_m$ (m = 10-16) shown as Schlegel diagrams. For each isomer m-N (m = no. of CF_3 groups, N = no. of isomer ordered by increasing formation energy), the relative formation energy [kJ/mol] and the HOMO-LUMO gap [eV] are given following the isomer notation. m-N is used as name for the calculated isomers, while full formula is used for experimentally isolated isomers.

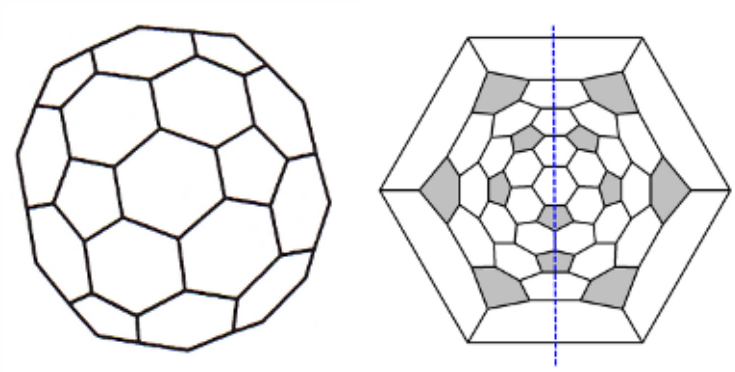

Figure 5.10.: The molecular structure (left) and the corresponding Schlegel diagram (right) of the $C_{84}(16)$. The symmetry plane is shown as dashed lines.

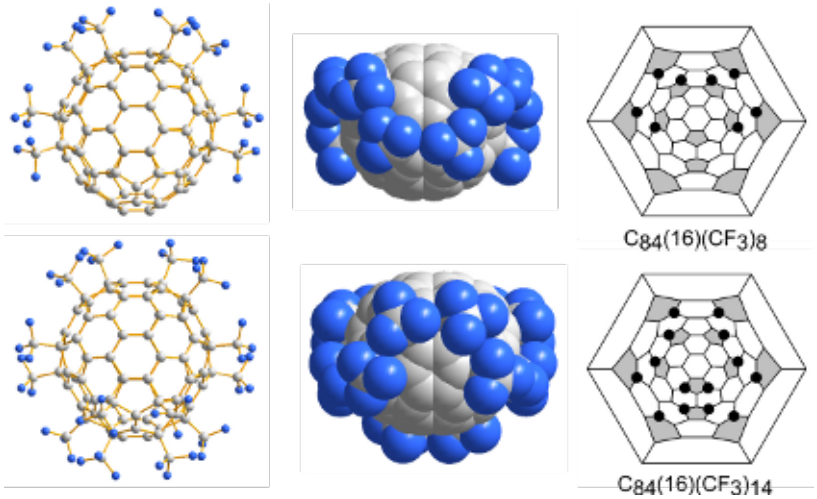

Figure 5.11.: Molecular structures and Schlegel diagrams of $C_{84}(16)(CF_3)_8$ and $C_{84}(16)(CF_3)_{14}$. The projections of the top and side view are shown in the left and middle column, respectively.

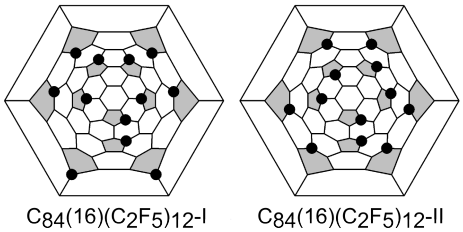

Figure 5.12.: Two isomers of experimentally isolated $C_{84}(16)(C_2F_5)_{12}$ in literature.[1,71]

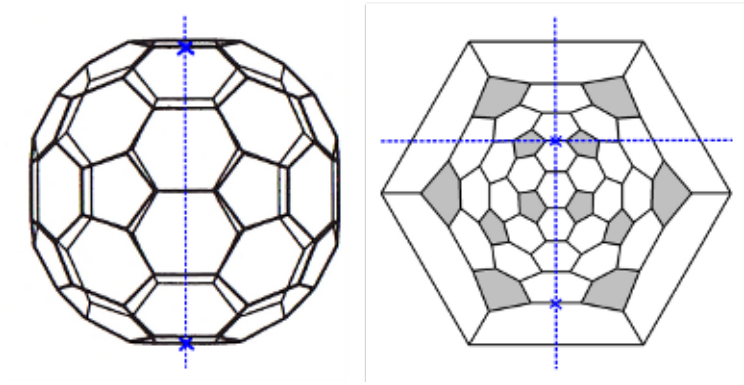

Figure 5.13.: The molecular structure (left) and the corresponding Schlegel diagram (right) of the $C_{84}(18)$. The C_2 axis is shown with crosses, and the symmetry planes are shown with dashed lines.

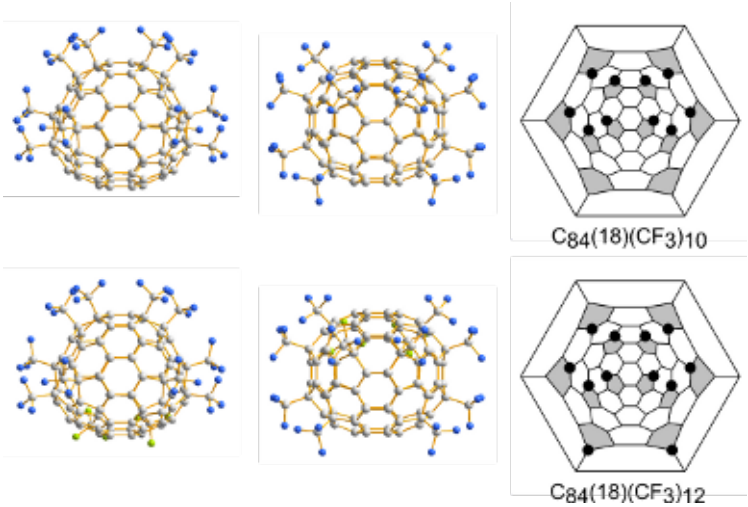

Figure 5.14.: Molecular structures and Schlegel diagrams of $C_{84}(18)(CF_3)_{10}$ and $C_{84}(18)(CF_3)_{12}$. The projections of the top and side view are shown in the left and middle column, respectively.

groups are distributed compactly due to the small size, while the bulky C_2F_5 groups are attached more uniformly on the fullerene cage.

5.1.5. C_{84}, cage isomer 22

The D_2-symmetric isomer 22 of C_{84} has three C_2 axes with two of them passing through the centers of two hexagons shown in Fig. 5.15. The third C_2 axis (marked with a black cross) passes through two C-C bonds. Because of the relative higher yield during the fullerene production, this cage isomer is the most isolated derivative species whose structures are determined in this thesis.

This isomer is a major product of the fullerene mixture from the arc-discharge method because its relative formation energy is the second lowest among all C_{84} cage isomers.[69,72] In earlier studies, the cage isomer 22 was characterized by circular dichroism spectroscopy, ^{13}C NMR and ^{19}F NMR.[73] As CF_3 isomers, $C_{84}(22)(CF_3)_{16}$ and $C_{84}(22)(C_2F_5)_{12}$ are already known and their structures have been determined via X-ray structure analysis.[1] Kareev *et al.* reported two isomers of $C_{84}(22)(CF_3)_{12}$ using

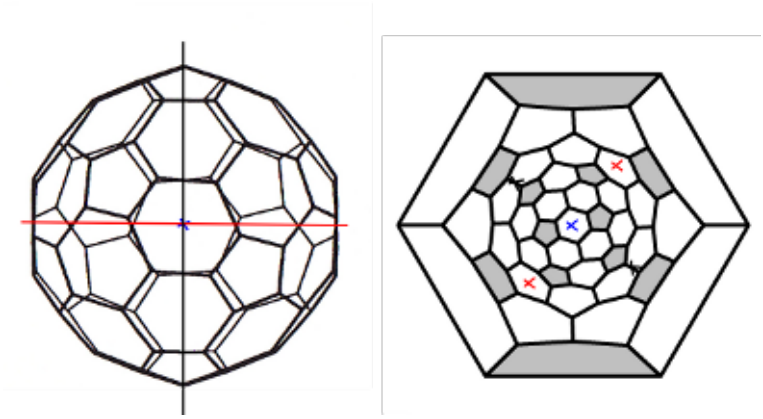

Figure 5.15.: The molecular structure (left) and the corresponding Schlegel diagram (right) of $C_{84}(22)$. The C_2 axes are shown as lines and as crosses.

^{19}F NMR data with DFT-optimized potential structures.[2] In this section, nine isomers are discussed containing 12 to 20 CF_3 groups. Their molecular symmetries belong to D_2, C_2 and C_1, due to the asymmetric attachments of CF_3 groups. In order to compare the isomers, their structures are displayed with the same orientation in the projections and Schlegel diagrams, i.e., along the same C_2 axis of the parents $C_{84}(22)$ cage isomer (blue cross in Fig. 5.15). Their IUPAC lowest locant numbers are summarized in Appendix C. The nomenclature 84(22)/*m*-N for CF_3 isomers is taken from the section of $C_{84}(11)$.

$C_{84}(22)(CF_3)_m$ derivatives

$C_{84}(22)(CF_3)_{12}$ Two isomers, D_2-$C_{84}(22)(CF_3)_{12}$-I and C_2-$C_{84}(22)(CF_3)_{12}$-II are isolated and structurally characterized (Fig. 5.16). In both cases, the CF_3 groups form two separated chains each containing six groups in *para* position of the hexagons. These addition patterns are denoted both by p^5,p^5. One of the two chains has exactly the same position in both isomers. The different arrangement of the second chain leads to the D_2-symmetric isomer I and the C_2-symmetric isomer II. This second chain is shown in the center of Schlegel diagram, and the space-filling models illustrate the differences of the two isomers. The same addition patterns have been deduced earlier for two $C_{84}(22)(CF_3)_{12}$ isomers from ^{19}F NMR spectra (denoted as 84-12-1 and 84-12-3 within the publication).[2] In addition, the only pentafluoroethylated species $C_{84}(22)(C_2F_5)_{12}$ characterized so far exhibits the same addition pattern as isomer D_2-$C_{84}(22)(CF_3)_{12}$-I.[1]

As an expectation from the similar structures of isomer I and II, their formation energies predicted by DFT calculation differ only by 2.2 kJ/mol: C_2-$C_{84}(22)(CF_3)_{12}$-II is energetically favored. A model isomer denoted as 84(22)/12-3 (see Appendix D) exhibits a p^{11} addition pattern showing a long chain of twelve CF_3 groups. This isomer is predicted by calculation as third stable structure with relative formation energy of 18.9 kJ/mol.

$C_{84}(22)(CF_3)_{14}$ Two isomer I and II have been found for $C_{84}(22)(CF_3)_{14}$. In both, 14 CF_3 groups are attached to *para* positions in hexagons on the fullerene cage. They form two chains, one is in the middle and one in the edge of Schlegel diagrams. An isolated C=C bond was formed between two pentagons because a large number of the addends (more than 12) attached on the fullerene cage (see Fig. 5.17). The isomer I and II differ only in one position of the CF_3 group which prolongs one of the two CF_3 chains (comparing the isomer I and II, 13 CF_3 occupied positions are identical). In isomer I,

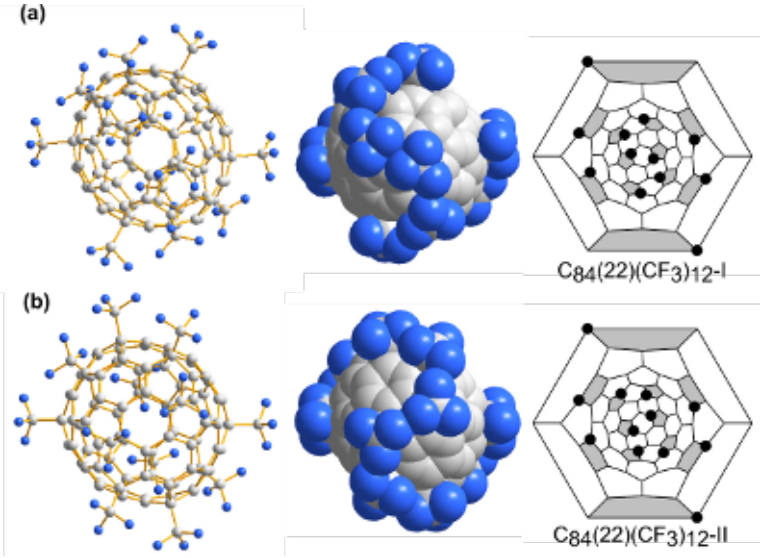

Figure 5.16.: Molecular structures and Schlegel diagrams of (a) $C_{84}(22)(CF_3)_{12}$-I and (b) $C_{84}(22)(CF_3)_{12}$-II. The projection with different models and Schlegel diagram are shown along a C_2 axis.

the two chains consisted of eight and six CF_3 groups, whereas in isomer II of nine and five CF_3 groups. The molecular symmetry is lowered by unsymmetrical attachments. Therefore, both isomers are C_1-symmetric. Theoretical calculations predict their relative formation energies of 4.7 and 0 kJ/mol for isomer I and II, respectively. The model isomer 84(22)/14-3 (see Appendix D) is predicted to have the next higher formation energy of 13.5 kJ/mol. Compared to the isomer II, a pair of CF_3 groups attach on the different positions in hypothetical isomer 84(22)/14-3.

C_{84}(22)$(CF_3)_{16}$ Four isomer $C_{84}(22)(CF_3)_{16}$-I to -IV are characterized, and are denoted as p^9,p^5; p^{10},p^4; p^{11},p^3; p^{11},p^3, respectively. All 16 CF_3 groups are attached in *para* position of hexagons. These *para* chains in the middle of Schlegel diagrams with six to nine attached groups on the fullerene cage are observed for isomers $C_{84}(22)(CF_3)_{12}$ and $C_{84}(22)(CF_3)_{14}$, and have been described in the previous sections. In the four isomers containing 16 CF_3 groups, the principal C_2 axis passes through the central and outer hexagon of the Schlegel diagram. For isomer I to III, they can be distinguished by four CF_3 positions marked with different colors in Fig. 5.18. In comparison to the isomer I and II, II and III, both pairs show a high structural similarity with 15 CF_3 positions in common, while isomer IV has ten positions only, eleven and twelve same attached positions comparing with the isomer I, II, and III, respectively. The comparison of isomer III and IV is displayed using the back views of the molecular structures in Fig. 5.19. The orientation of the four-membered chains differs for isomer III and IV (i.e., anti-S-like and S-like). The formation of different CF_3 isomers through a chain re-orientation is also observed for isomer $C_{84}(22)(CF_3)_{12}$ (see Fig. 5.16). Due to the similar structures, similar stabilities of four isomers can be expected. The formation energies of isomers I-IV are predicted by the DFT method with values of 13.5, 0, 7.7 and 7.7 kJ/mol, respectively. The isomer 84(22)/16-5 served as fifth stable isomer has a relative formation energy of 25.5 kJ/mol. Its addition pattern is also denoted as p^{14},p^2 and contains two isolated benzenoid rings. (see Appendix D)

C_{84}(22)$(CF_3)_{20}$ The only isomer with 20 CF_3 groups found in this study belongs to the symmetry point groups D_2 as its parent fullerene $C_{84}(22)$. The fullerene is covered almost completely by CF_3 groups

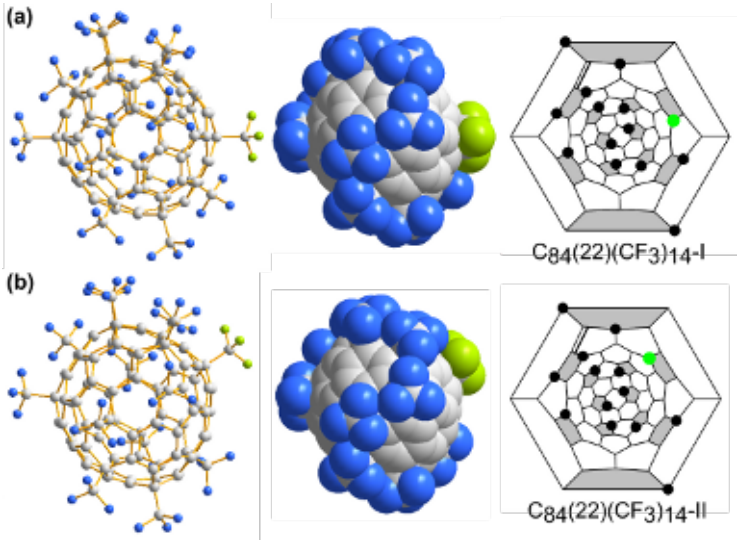

Figure 5.17.: Molecular structures and Schlegel diagrams of (a) $C_{84}(22)(CF_3)_{14}$-I and (b) $C_{84}(22)(CF_3)_{14}$-II. The projection with different models and Schlegel diagram are shown along a C_2 axis. The non-equivalent CF_3 position between the two isomers is shown in green. C=C bonds are shown with double lines.

(see Fig. 5.20). Hence, the retention time of this isomer is short (almost the same with the dead time of the HPLC system). In order to find out if the experimentally obtained structure is the most stable one, four model structures of composition $C_{84}(22)(CF_3)_{20}$ have been generated from the structures of the experimentally isomers $C_{84}(22)(CF_3)_{16}$-I to -IV by addition of four more CF_3 groups. The four groups are added in two pairs to the structures with 16 groups. Each couple of CF_3 groups occupies the para position in hexagons on the fullerene cages. This leads to the formation of the isolated double bonds. The calculation predicts a higher relative formation energy of 69.2 kJ/mol for the experimental isomer $C_{84}(22)(CF_3)_{20}$-I, compared to other four assumed isomers 84(22)/20-2, -1, -5 and -3 of 7.2, 0, 83.9 and 40.4 kJ/mol, respectively. Thus, the formation of the experimental isomer $C_{84}(22)(CF_3)_{20}$-I must be explained by underlying kinetic effects. A possible explanation might be connected with the higher volatility of isomers with numerous attached CF_3 groups. The volatile isomer $C_{84}(22)(CF_3)_{20}$ could immediately migrate out of the hot zone, and the chemical equilibrium can not be reached due to the temperature gradient. It leads to the product formation via the energetically favored reaction pathway with lower activation barrier. This isomer has been obtained only from the reaction at lower temperatures (reaction in glass ampoules). As the reaction temperature increases, the higher activation barrier can be overcome. The thermodynamic products are preferably generated.

Comparison among the isomers with different numbers of attached groups

For common features of all nine isomers $C_{84}(22)(CF_3)_m$ with m = 12,14,16,20, all attachments of CF_3 groups are in *para* positions in hexagons, and all attached positions belong to the PHJs. The addition on THJs is considered to be energetically unfavored because of the steric strain induced by sp^3 hybridization and happens only if the reaction surface of fullerene cage is overcrowded (more than 12 addends). This restriction has been found in earlier studies on trifluoromethylated C_{60} or C_{70}.[74,75]

Comparing the structures of isomers, the similarity of the addition patterns suggests a sequential reaction from the fullerenes with less CF_3 groups to those with more ones. The isomer $C_{84}(22)(CF_3)_{14}$-I is derived from the lower trifluoromethylated derivative $C_{84}(22)(CF_3)_{12}$-II by addition of two more

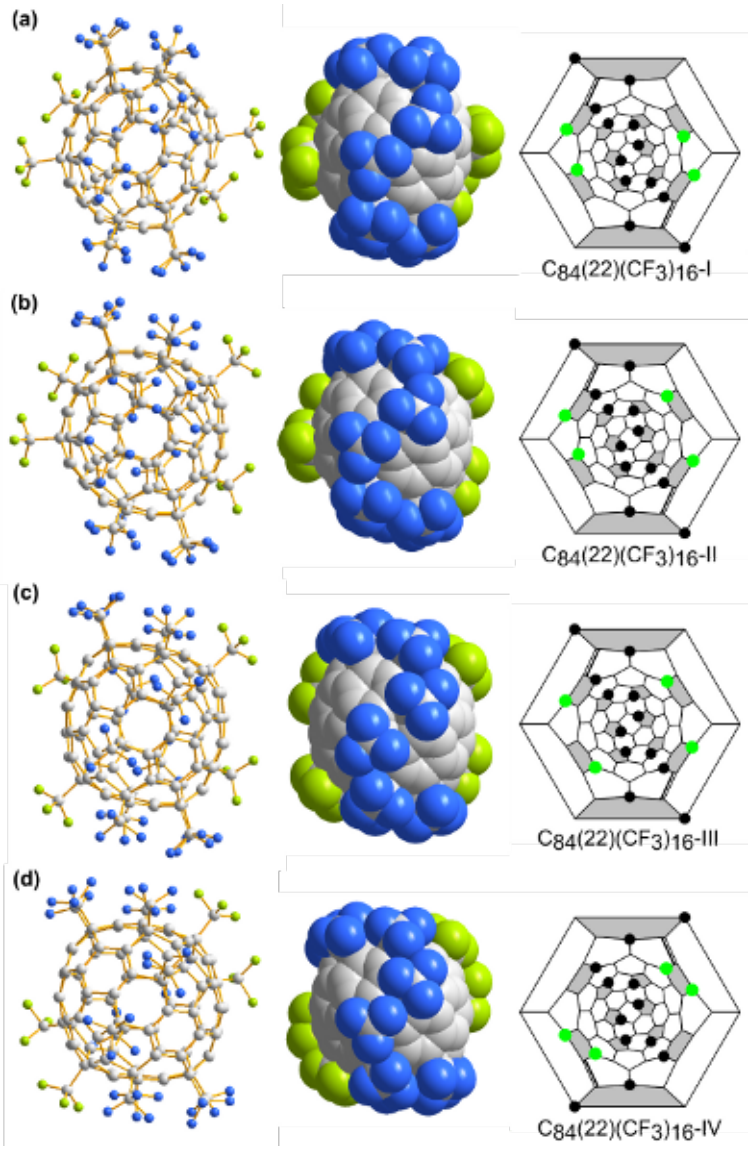

Figure 5.18.: Molecular structures and Schlegel diagrams of (a)-(d) $C_{84}(22)(CF_3)_{14}$-I to -IV. The projection with different models and Schlegel diagrams are shown along a C_2 axis. A chain of four isomers in common is shown in blue color, and the varied positions of four CF_3 groups are shown in green color. C=C bonds are shown with double lines.

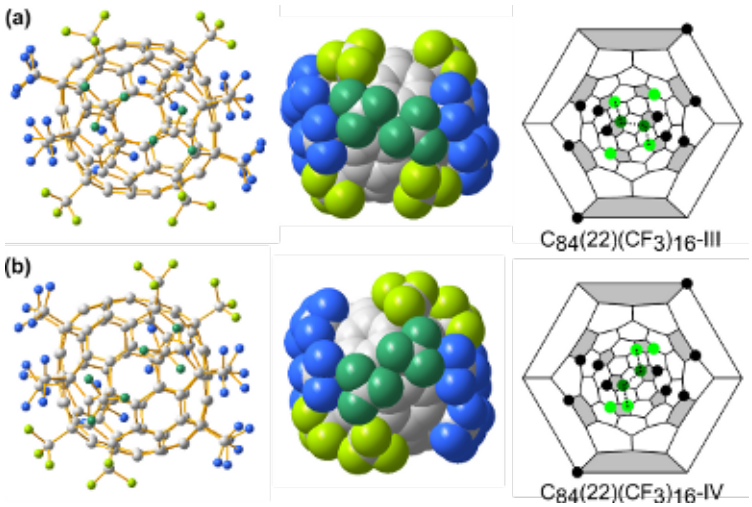

Figure 5.19.: Molecular structures and Schlegel diagrams in back views of (a) $C_{84}(22)(CF_3)_{16}$-III and (b) $C_{84}(22)(CF_3)_{16}$-IV. The projection with different models and Schlegel diagram are shown along a C_2 axis. A chain of four isomers in common is shown in blue color, and the varied positions of six CF_3 groups are shown in green color. The four-membered chains are shown with dotted lines.

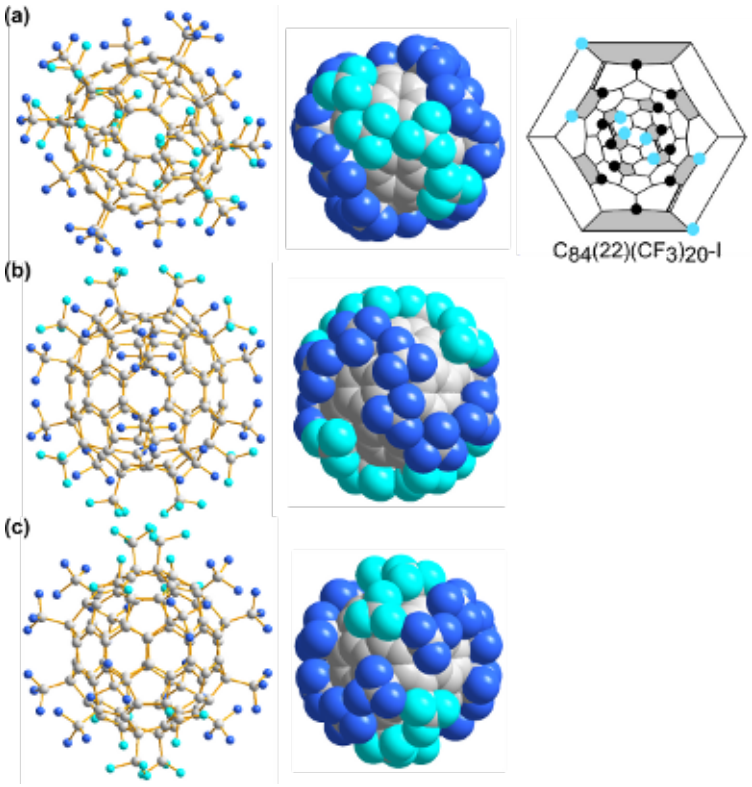

Figure 5.20.: Molecular structures and Schlegel diagram of $C_{84}(22)(CF_3)_{20}$. The projections with different models and Schlegel diagram are shown along a C_2 axis. Different blue colors are used to show the orientation of the molecule in (a) top view and (b)-(c) side views. Four isolated C=C bonds are shown with double lines.

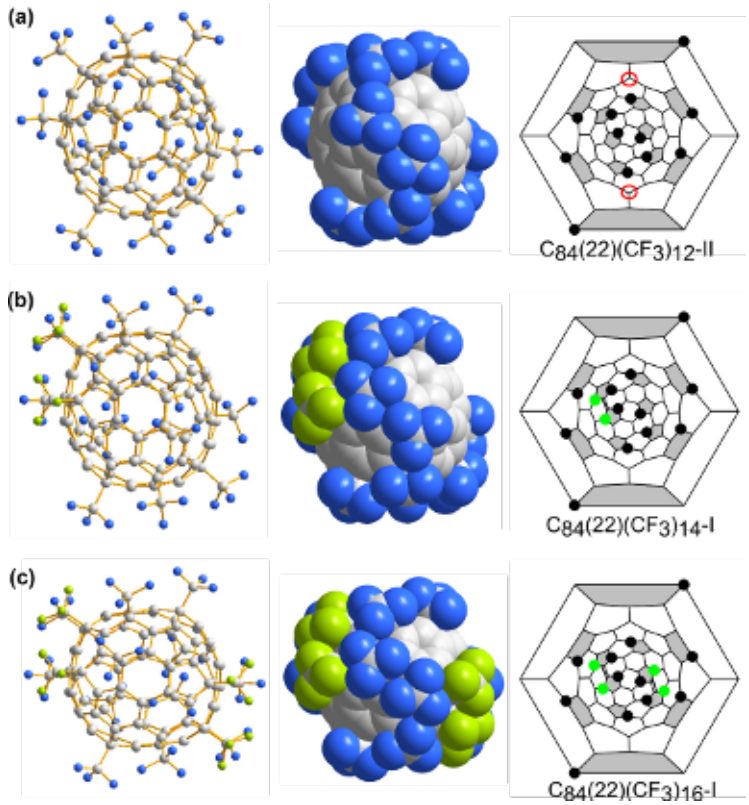

Figure 5.21.: Molecular structures and Schlegel diagrams in back views of (a) $C_{84}(22)(CF_3)_{12}$-II, (b) $C_{84}(22)(CF_3)_{14}$-I and (c) $C_{84}(22)(CF_3)_{16}$-I. The projection with different models and Schlegel diagram are shown along a C_2 axis. The isomer connections are related by a simple addition of two CF_3 groups shown with green color. Isolated C=C bonds are shown with double lines, and C atoms belonging to THJs are shown by red circles.

CF_3 groups. These two additional CF_3 groups prolong one of the six-membered chains (on the edge of the Schlegel diagram) and form an isolated C=C bond (see Fig. 5.21). In the same way, isomer I of $C_{84}(22)(CF_3)_{14}$ is converted into isomer $C_{84}(22)(CF_3)_{16}$-I where eight-membered chain is prolonged with two CF_3 groups thereby forming an additional C=C bond. The 'genetic' relationship among the isomer $C_{84}(22)(CF_3)_m$ by a simple addition of two CF_3 groups from m = 12-16 is shown in Fig. 5.21. In this case, it is worth to note that only one six-membered chain can be prolonged since the addition to THJs is unfavored. This demonstrates how important the basic rules are for addition reactions on fullerenes for the overall reaction pathway.

The set of isolated structures makes it possible to draw a general picture of the reaction pathways for CF_3 group addition on the fullerenes. The CF_3 groups attached on THJs are strongly unfavored while the prolongation of existing CF_3 chains in *para* positions (PHJ) is preferred. Thus, not every lower trifluoromethylated fullerene serves as a suitable precursor for further reaction. The isomer $C_{84}(22)(CF_3)_{12}$-I is an example where all possible attached position for the chain prolongation belong to THJs (see Fig. 5.21). The two isomers of $C_{84}(22)(CF_3)_{14}$ contain substructure of isomer $C_{84}(22)(CF_3)_{12}$-II and can be the precursors for the isomers $C_{84}(22)(CF_3)_{16}$-I and -II. In addition, the model structures 84(22)/12-3, 84(22)/14-3 and 84(22)/14-4 are related to isomers $C_{84}(22)(CF_3)_{16}$-III and -IV with the assistance of calculations. The modeled isomer 84(22)/12-11 with a rather higher relative formation energy (57.7 kJ/mol) can be a possible precursor for the kinetic product $C_{84}(22)(CF_3)_{20}$-I. This assumption is supported by the

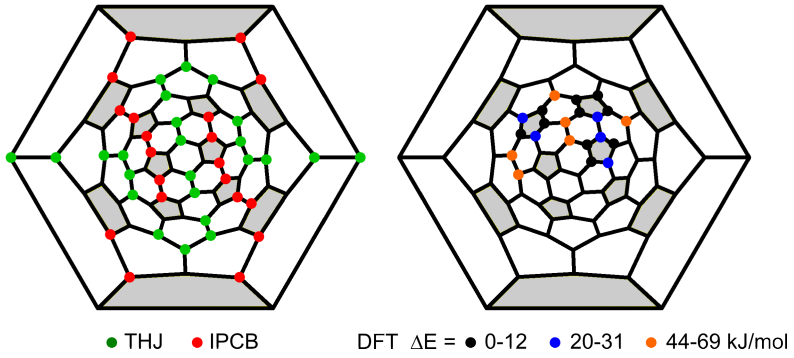

Figure 5.22.: Schlegel diagrams of $C_{84}(22)$. Left: 24 triple hexagon junctions (THJs) as green points and 20 C atoms belonging to the interpentagonal C-C bonds (ICCBs) as red points. Right: different attached positions of CF_3 radical are shown as points, where the points with different colors display the three categories of the relative formation energies.

low HOMO-LUMO gap of isomer 84(22)/12-11 (0.7 eV), which is an indication for the high reactivity.

General aspects of trifluoromethylation for fullerene C_{84}(22)

According to the MALDI-MS results (see the section separation), products of the compositions $C_{84}(CF_3)_m$ with m = 2-10 are obtained from the syntheses at high reaction temperature. Due to the difficulties of the separation and crystallization, only four molecular structures with less than twelve attachments are determined in this work, i.e., $C_{84}(11)(CF_3)_{10}$, $C_{84}(18)(CF_3)_8$, $C_{84}(18)(CF_3)_{10}$ and $C_{84}(23)(CF_3)_8$. These isomers with composition of $C_{84}(CF_3)_m$ with $m < 12$, have been generated only in relatively small amounts compared to isomers with 12-16 attachments. Calculations predicted the experimentally isolated species $C_{84}(CF_3)_{12-16}$ are relative stable in each CF_3 isomer category. That motivates to find the possible reaction pathways of the fullerene trifluoromethylation. Similar approaches were applied for the fullerene C_{60}.[74] and C_{70}[75] For the higher fullerene C_{84}, such approach was realized for the first time while significant experimental CF_3 isomers have been obtained.

Fullerene D_2-$C_{84}(22)$ consists of 60 and 24 C atoms on the PHJs and THJs, respectively. A further important structure feature is that, 20 C atoms form ten interpentagonal C-C bonds (ICCBs) (see Fig. 5.22), i.e., the bond connecting two pentagons, and each one has THJs on *meta* and *para* positions. Determined by the D_2 symmetry, $C_{84}(22)$ has 21 non-equivalent C atoms in which 15 C atoms belong to the PHJs including five atoms of ICCBs, and remaining six C atoms belong to the THJs. To study the trifluoromethylation of fullerenes theoretically, relative formation energies were calculated for the radical species $[C_{84}(22)(CF_3)]^{\bullet}$. For the model structures, the 21 non-equivalent cage C atoms are selected as possible positions of the single attached CF_3 group on the cage. Ordered by relative energies, they can be categorized into three groups:

(1) favored positions (PHJs) with 0-11.9 kJ/mol,
(2) less favored positions (C atoms belong to ICCBs) with 19.8-31.2 kJ/mol,
(3) unfavored positions (THJs) with more than 40 kJ/mol.

Therefore, attachments on C atoms belonging to the ICCBs and the THJs are excluded for further calculations.

The addition of the second CF_3 group to the radical species of $\mathbf{C_{84}(22)(CF_3)}$ should be considered by electron density localization. The CF_3 radical activates the benzene ring by increasing electron density

through a resonance effect. The second CF_3 group prefers to attach on the *ortho* or *para* positions of the first CF_3 groups. A further consideration of the steric effect is that the *para* position is more favored than *ortho* position. The attachment on the THJs is energetically unfavored because such 'quasi plane' of C atoms with bond angles of about 120° should be maintained for sp^2 hybridization. Calculations predicted that CF_3 attachments on the *meta* and *ortho* positions are also not stable, like on the THJs (the energies are >60 (*meta* positions), >40 (*ortho* positions) and >50 (THJs) kJ/mol, respectively). The CF_3 attachment on ICCBs yields the isomer with the relative higher energy of 33.4 kJ/mol, compared to the *para* attachment with lower energies of 0-17 kJ/mol. Based on the same considerations, the calculations were performed for compositions of $C_{84}(22)(CF_3)_{2-20}$. The results and the selection rules are provided in Appendix D.

For the isomers of $\mathbf{C_{84}(22)(CF_3)_4}$, the two most stable structures exhibit addition patterns containing one four-membered *para* chain (0 and 6.9 kJ/mol). Less stable structures with energies in the range of 11.3-18.3 kJ/mol contain three separated *para*-$C_6(CF_3)_2$ motifs. The isomer with three-membered *para* chain and one single CF_3 group has a even higher energy 20.6 kJ/mol. Furthermore, attachments on the *ortho* positions and THJs are as expected exhibiting much higher energy of 50.4 and 67.5 kJ/mol, respectively.

Calculations for isomers $\mathbf{C_{84}(22)(CF_3)_6}$ excluded THJs and *ortho* attachments in the addition patterns. The most stable structures 84(22)/6-1 and 84(22)/6-2 contain a six-membered chain of which four attachments are at the same positions on the cage. Both of them are found as substructures for the experimentally isolated isomers. Furthermore, the isomer 84(22)/6-5 is a possible precursor of 84(22)/12-11 on the way to C84(22)(CF3)20-I.

Most of the isomers $\mathbf{C_{84}(22)(CF_3)_8}$ contain the substructures of the isomers $C_{84}(22)(CF_3)_6$. Their structures are obtained by addition of two CF_3 groups to the corresponding isomer $C_{84}(22)(CF_3)_6$. The structures of 84(22)/8-1, -2, -5, -6 and 84(22)/8-3, -7, -14 are obtained from 84(22)/6-1 and 84(22)/6-2, respectively. The energy differences are small, the 20 relative stable isomers have relative formation energies within 20 kJ/mol.

The most stable isomers of $\mathbf{C_{84}(22)(CF_3)_{10}}$ contain substructures of the lower CF_3 derivatives. They can be separated into two groups. One group contains a six-membered *para* chain as S-type and another one as anti-S-type. For the most stable isomer 84(22)/10-1, the S-type chain is elongated by two more CF_3 groups on the both terminus. The elongation of anti-S-type chain in isomer 84(22)/12-2, -3 is energetically unfavored.

For the isomers of $\mathbf{C_{84}(22)(CF_3)_{12}}$, the structures of the two most stable isomers 84(22)/12-1 and -2 with the energies of 0 and 2.3 kJ/mol have been found experimentally. For isomer 84(22)/12-2, i.e., $C_{84}(22)(CF_3)_{12}$-I, two six-membered chains can not be elongated by further addition reactions due to the attached position on THJs. In contrast, one *para* chain of isomer 84(22)/12-1, i.e., $C_{84}(22)(CF_3)_{12}$-II, has two free attached positions on PHJs. For this reason, isomer $C_{84}(22)(CF_3)_{12}$-II is able to yield 'genetic' isomers with m = 14, 16, which contain the same para chain as $C_{84}(22)(CF_3)_{12}$-II elongated up to 8 and 10 CF_3 groups. Isomer 84(22)/12-11 has two chains each consisting of six CF_3 groups. Although model isomer 84(22)/12-11 (the relative energy of 57.7 kJ/mol) is not thermodynamically stable comparing to isomer $C_{84}(22)(CF_3)_{12}$-I and -II, it is considered to be a possible reactive precursor for isomer $C_{84}(22)(CF_3)_{20}$-I, due to its small HOMO-LUMO gap (0.6 eV).

Based on the experimental and computational results, possible reaction pathways from $C_{84}(22)(CF_3)_2$ to $C_{84}(22)(CF_3)_{20}$ are provided in this work. They are shown as Schlegel diagrams in Fig. 5.23. For the isomer $C_{84}(22)(CF_3)_{14}$-II, it still requires further experimental and theoretical data to confirm the possible reaction pathways.

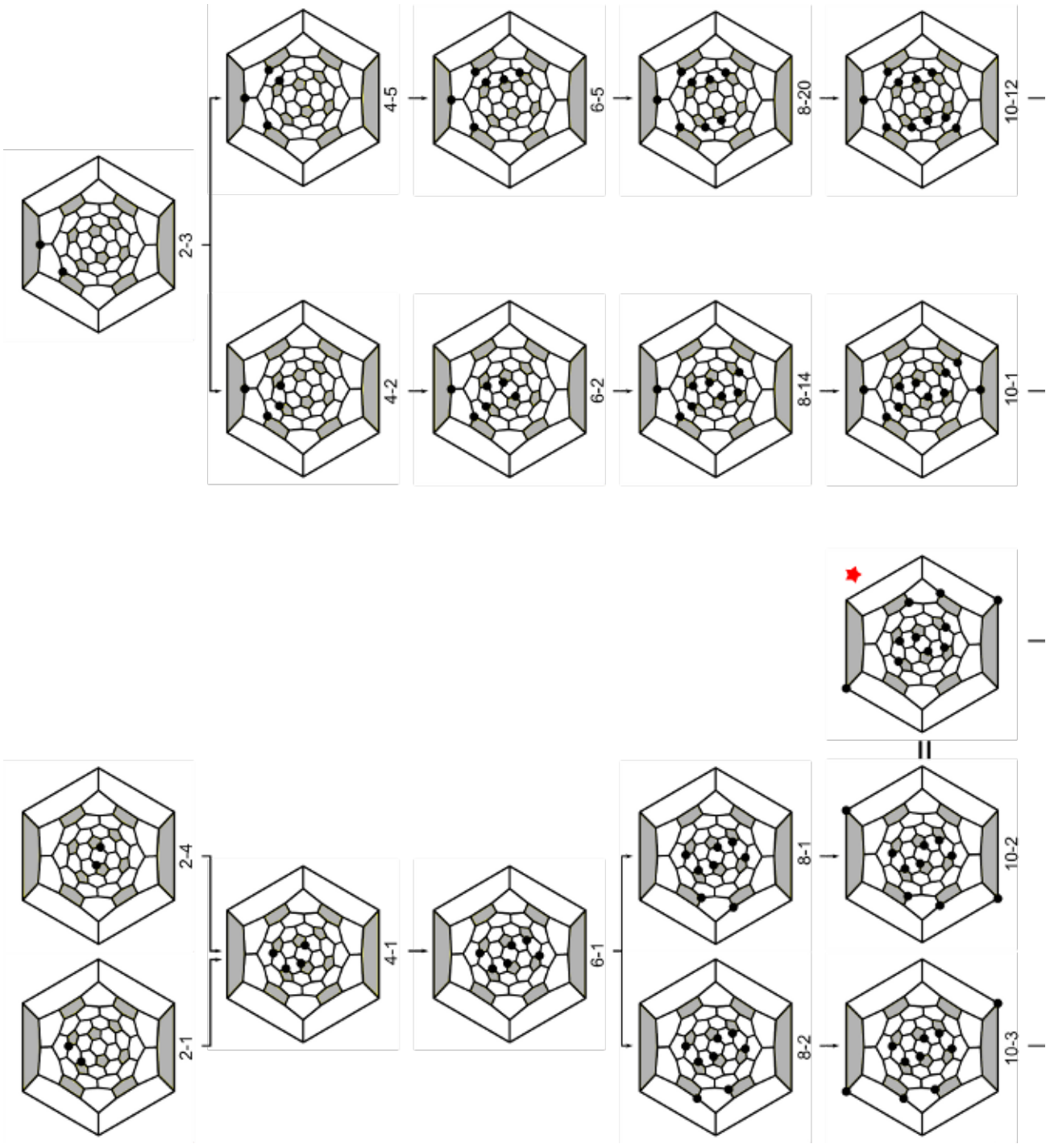
2-3
4-5
6-5
8-20
10-12
4-2
6-2
8-14
10-1
2-4
2-1
4-1
6-1
8-1
8-2
10-2
10-3

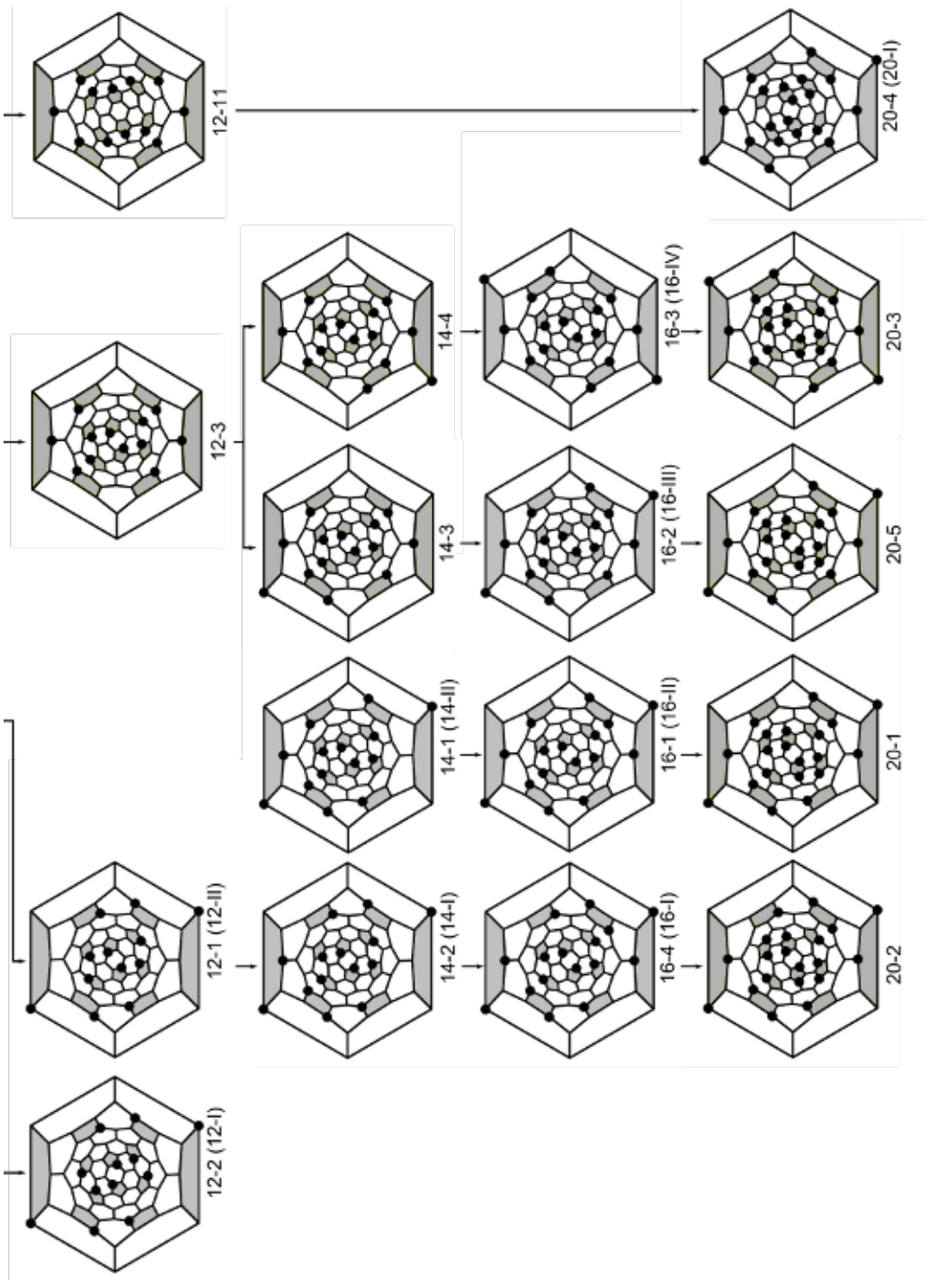

Figure 5.23.: Possible reaction pathways of the trifluoromethylation for isomers $C_{84}(22)(CF_3)_m$ (m = 2-20) shown as Schlegel diagrams., m-N (m = no. of CF_3 groups, N = no. of isomer ordered by increasing formation energy) is used as name for the calculated isomers, while experimentally isolated isomers are given with Latin numbers in the brackets. The Schlegel diagram marked with red star shows a reflection of isomer 10-2, whose orientation of the addition pattern corresponds to the sub-pattern of the isomer 12-1.

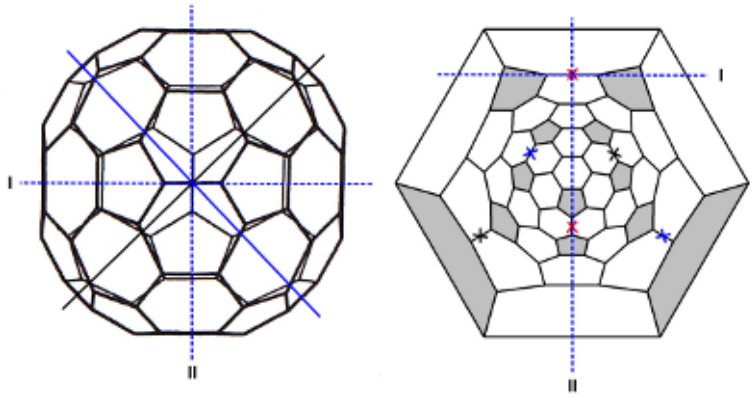

Figure 5.24.: The molecular structure (left) and the corresponding Schlegel diagram (right) of the $C_{84}(23)$. One C_2 axis points to the reader and the remaining two C_2 axes are shown as solid lines in left and crosses in right. The dashed lines show the mirror planes I and II. Plane I is parallel to one C-C bond and bisects another one.

5.1.6. C_{84}, cage isomer 23

Cage isomer 23 is one of the most abundant cage isomers of C_{84}. Its amount ratio is about 2:1 to the isomer 22 discussed in the previous section. Compared to the isomer 22, isomer 23 has the symmetry D_{2d}. The D_{2d}-isomers have been intensively studied within last 20 years with different experimental and theoretical methods. As an iridium derivative, the structure of $[C_{84}(23)Ir(CO)Cl(PPh_3)_2]\cdot 4C_6H_6$ is determined by single crystal X-ray diffraction.[76] The scandium complex $Sc_2@C_{84}(23)$ was analyzed by ^{13}C NMR.[77] The physical properties of $C_{84}(23)$ have been characterized by electron spin resonance (ESR), cyclic voltammetry (CV), VIS/NIR spectroscopy and DFT-calculations.[65,69,78–80] One structure of the trifluoromethylated derivative, $C_{84}(23)(C_2F_5)_{12}$, was shown in a previous study.[1] The cage isomer $C_{84}(23)$ exhibits three C_2 axes and two mirror planes. This intersection of both planes is the C_2 principle axis in Fig. 5.24

$C_{84}(23)(CF_3)_m$ derivatives

$C_{84}(23)(CF_3)_8$ For this molecule, the CF_3 groups are attached on the parent fullerene in a way which leads to a lower molecular symmetry. All addition positions belong to 1,4- (*para*) positions in hexagons and are divided into two main sets to form two four-membered *para* chains, i.e., an p^3,p^3 addition pattern (see Fig. 5.25). The chain prolongation of isomer $C_{84}(23)(CF_3)_8$ to yield isomer $C_{84}(23)(CF_3)_{10}$ is not possible, because the four potential addition positions belong to the energetically unfavored THJs. The possible attached positions are shown as red circles in Fig. 5.25. Therefore, it is reasonable to predict that the structures of the isomer with ten groups consisting of $C_{84}(23)(CF_3)_8$ as substructure and one pair of CF_3 groups attached on the *para* positions in a hexagon.

$C_{84}(23)(CF_3)_{10}$ Ten CF_3 groups of this species are divided into two sets of six- and four-membered chains. The addition pattern is denoted as p^5,p^3 (see Fig. 5.26). The molecular structure of this species has been determined after carrying out of quantum chemical calculations, i.e., this structure appeared originally as a modeled structure in this thesis. Ten modeled structures with ten CF_3 groups have been selected for the calculations. Nine of ten possible modeled isomers have been selected based on the experimentally isolated isomer $C_{84}(23)(CF_3)_{12}$: ten of twelve CF_3 groups have been maintained their attached positions, and the positions of two other CF_3 groups were varied. These nine modeled isomers

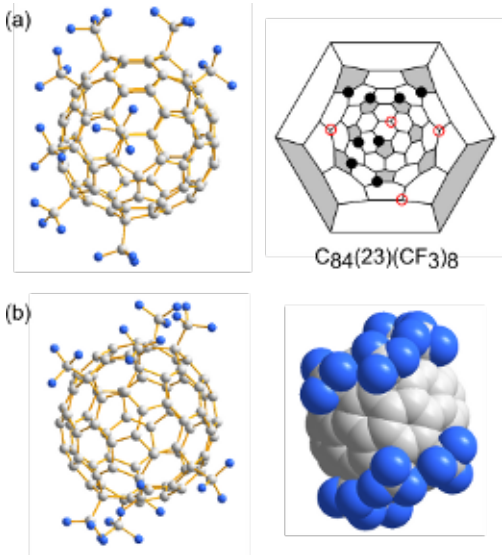

Figure 5.25.: Molecular structures and Schlegel diagram of $C_{84}(23)(CF_3)_8$. The projections (b) with different models are shown along a C_2 axis. The C atom belonging to THJs are shown with red circles.

have been denoted as 84(23)/10-1 and 84(23)/10-3 to 84(23)/10-10 (see Appendix D). Besides those nine isomers, the modeled isomer 84(23)/10-2 is a special case. This isomer is selected based on the modeled isomer 84(23)/12-2, which has been predicted as a possible isomer involved in the trifluoromethylation pathways of fullerene $C_{84}(23)$ (see Fig. 5.33). Isomer 84(23)/10-2 is thermodynamically stable (the relative formation energy of 0.8 kJ/mol), but is considered to be able to react quickly further with CF_3 radicals due to its kinetic instability (HOMO-LUMO gap of 0.8 eV). Such kinetic instability can also explain why this species can not be isolated experimentally. Compared to isomer 84(23)/10-2, modeled isomer 84(23)/10-1 is not only thermodynamically but also kinetic stable (the relative formation energy of 0 kJ/mol and HOMO-LUMO gap of 1.3 eV). Hence, the experimental isolation and structural determination of this species could be achieved. The structural determination of the experimental isomer $C_{84}(23)(CF_3)_{10}$ supported this statement. It is considered as the possible precursor for the formation of isomer $C_{84}(23)(CF_3)_{12}$ with the addition of two more CF_3 groups. According to the empirical rules of the addition reaction on the fullerene cages, the existing CF_3 chains in precursor should be prolonged by attachments on the *para* positions in hexagons. In the case of isomer $C_{84}(23)(CF_3)_{10}$, four possible attached positions for the chains prolongation can be discussed (see Fig. 5.26). Two of them belong to the THJs (attachments on such position are energetically unfavored). Two attachments in a pentagon are also unfavored (theoretical calculations carried out for modeled isomers 84(23)/12 in next paragraph approved this statement). The remaining one position is only one possible attached position. Therefore, the second CF_3 group is forced to attach on the PHJs of another pentagon as an isolated attachment (denoted as *i*). That means that twelve attachments attach on the twelve pentagons of fullerene cages, i.e., one attachment per one pentagon. This empirical rule of the distribution of attachments can be applied to all functional fullerenes with twelve attachments. The results of calculations carried out for isomer 84(23)/12 show that the isomers with the isolated attachment is energetically more preferred than isomers with two attachments in a pentagon. Thus, the structure of isomer $C_{84}(23)(CF_3)_{10}$ is an example to confirm the rule of selecting stable modeled isomers $C_{84}(CF_3)_m$ for calculations: there is only one attachment per pentagon of cages, when the number of attachments between 2-12.

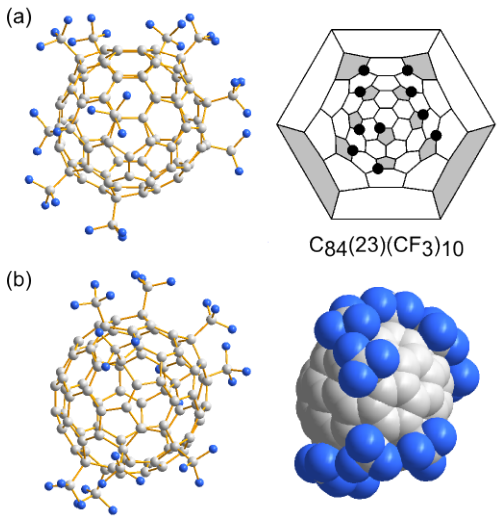

Figure 5.26.: Molecular structures and Schlegel diagram of $C_{84}(23)(CF_3)_{10}$. The projections (b) with different models are shown along a C_2 axis.

C_{84}(23)$(CF_3)_{12}$ This isomer represents a rare case in the stereochemistry of fullerene derivatives. Eleven of twelve CF_3 groups attached on the *para* positions in hexagons. Thus two *para* chains with the notation of p^6,p^3 for the addition pattern were obtained. The remaining one CF_3 group attached alone on the C atom that belongs to the PHJs (see Fig. 5.27). Such isolated attachment is denoted as *i*. A similar isolated attachment was also found in the addition patterns of $C_{70}(C_2F_5)_{10}$ [81] and $C_{84}(23)(C_2F_5)_{12}$ [1] with the notation of p^3,p^2,*p*,*i* and p^3,p^2,*p*,*p*,*i*, respectively . This single attachment is encountered mainly in the addition patterns with bulkier C_2F_5 groups rather than with CF_3 groups in the previous studies. But the isomer $C_{84}(23)(CF_3)_{12}$ shows the possibility that the isolated attachment occurs not only with C_2F_5 but also with less bulkier CF_3 groups.

This isolated attachment is considered as energetically unfavored based on theoretical calculations. The modeled isomers C84(22)/12-2, -3 and -4 in the previous section served as examples. Attachments as a pair on *para* positions of a hexagon for isomer C84(22)/2 have lower relative energies up to 17.1 kJ/mol compared to two isolated CF_3 groups attaching on two PHJs with more than 25 kJ/mol. Isomers C84(22)/3 and 84(22)/4 process isolated CF_3 groups with relative energies larger than 9 and 20 kJ/mol, respectively. Due to the instability, such isolated attachment is considered as the last attachment in the formation process of isomer $C_{84}(23)(CF_3)_{12}$. The calculations for the energy of several isomers have been carried without such isolated attachment. The structures selection is based on the following rules:

(1) eleven of twelve groups stay on the same positions as the experimental isolated isomer, only one single attached CF_3 group varies,
(2) the existing *para* chains will be prolonged,
(3) new attachment should occur on the *para* position of the hexagon and
(4) unfavored attachments on THJs have been excluded.

There are two chains on the addition pattern of isomer $C_{84}(23)(CF_3)_{12}$. Thus, additions on four carbons on the ends of the two chains to yield four new structures are possible (Fig. 5.28). Additions on two of four possible positions which belong to PHJs yield the isomers with relative energies ranging between 23-45 kJ/mol. The other two isomers with addition on THJs are excluded from the discussion. The same calculation is further carried out for model isomer 84(23)/12-5 whose structure is the same as the experimentally obtained isomer $C_{84}(23)(C_2F_5)_{12}$ in a previous study.[1] The results showed that the

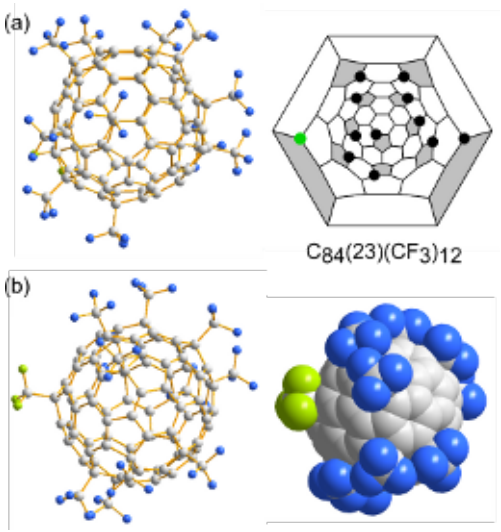

Figure 5.27.: Molecular structures and Schlegel diagram of $C_{84}(23)(CF_3)_{12}$. The projections (b) with different models are shown along a C_2 axis of the parent fullerene. The isolated attachment is shown with green color.

energies of nine model isomers (36-147 kJ/mol) are much higher than the experimental isomers with the isolated attachment (Addition patterns and the energies are shown in Fig. 5.29).

The energy enhance of hypothetic isomers is caused by high strain located in the small area of fullerene cage. Two CF_3 groups attached in a pentagon leads to thermodynamical instability. Therefore, the last attached group is forced to become an isolated attachment. Otherwise, such isolated attachment might occur on the five positions in the pentagon. The calculations have been carried out for other four possible structures. All of hypothetic isomers were predicted more instable than the experimental one. Their structures and energies are shown in Fig. 5.30.

Since steric strain is reduced due to the evenly distributed attachments on the surface of fullerene cage, the unpaired CF_3 addition was obtained in this case although the unpaired CF_3 addition was considered as energetically unfavored attachment.

C_{84}(23)$(CF_3)_{14}$ Two isomers of the composition $C_{84}(23)(CF_3)_{14}$ have been found. Both structures exhibit twelve attachments on the same positions. These ten CF_3 groups form a long *para* chain and the remaining four groups attached on the C atoms around the ICCB to form an isolated C=C bond in different sites (Fig. 5.31). Due to the different attached positions of two CF_3 groups, isomer I has symmetry C_s while isomer II C_1.

C_{84}(23)$(CF_3)_{18}$ The isomer of $C_{84}(23)(CF_3)_{18}$ contains $C_{84}(23)(CF_3)_{14}$-I as substructure (see Fig. 5.32). The 18 attached groups are in *para* positions of the hexagons and have been divided into two identical parts on the fullerene cage which leads to C_s symmetry as the isomer I with 14 groups. The structure of the isomer $C_{84}(23)(CF_3)_{18}$ are expected to be an instable molecule due to the high number of addends. However, the instability might be considered to compensate with the formation of the three isolated C=C bond, four partially and one fully isolated benzenoid ring.

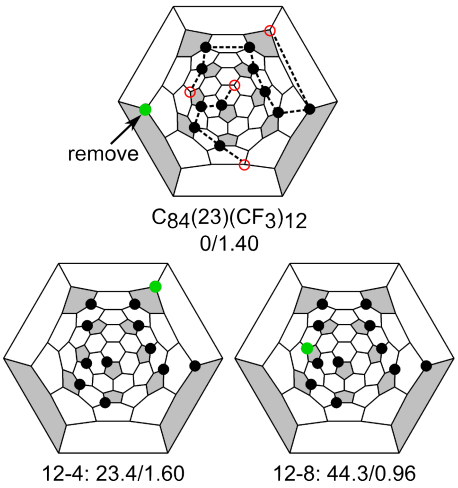

Figure 5.28.: Two possible structures based on the one of the experimental isomer $C_{84}(23)(CF_3)_{12}$. The isomers are denoted as m-N: relative formation energy [kJ/mol] / HOMO-LUMO gap [eV], where m = no. of CF_3 groups, N = no. of isomer ordered by increasing formation energy. The experimental isolated isomers are shown with the formula.

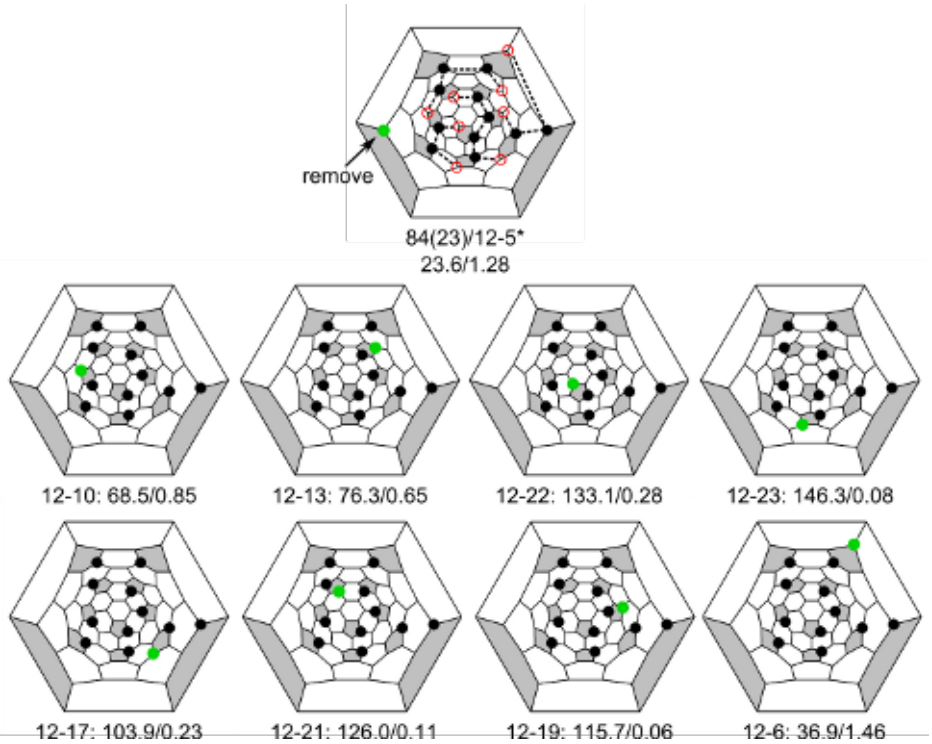

Figure 5.29.: Eight possible structures based on the one of the experimental isomer. The isomers are denoted as m-N: relative formation energy [kJ/mol]/HOMO-LUMO gap [eV], where m = no. of CF_3 groups, N = no. of isomer ordered by increasing formation energy. *The same addition pattern with the experimental isomer $C_{84}(23)(C_2F_5)_{12}$.[1]

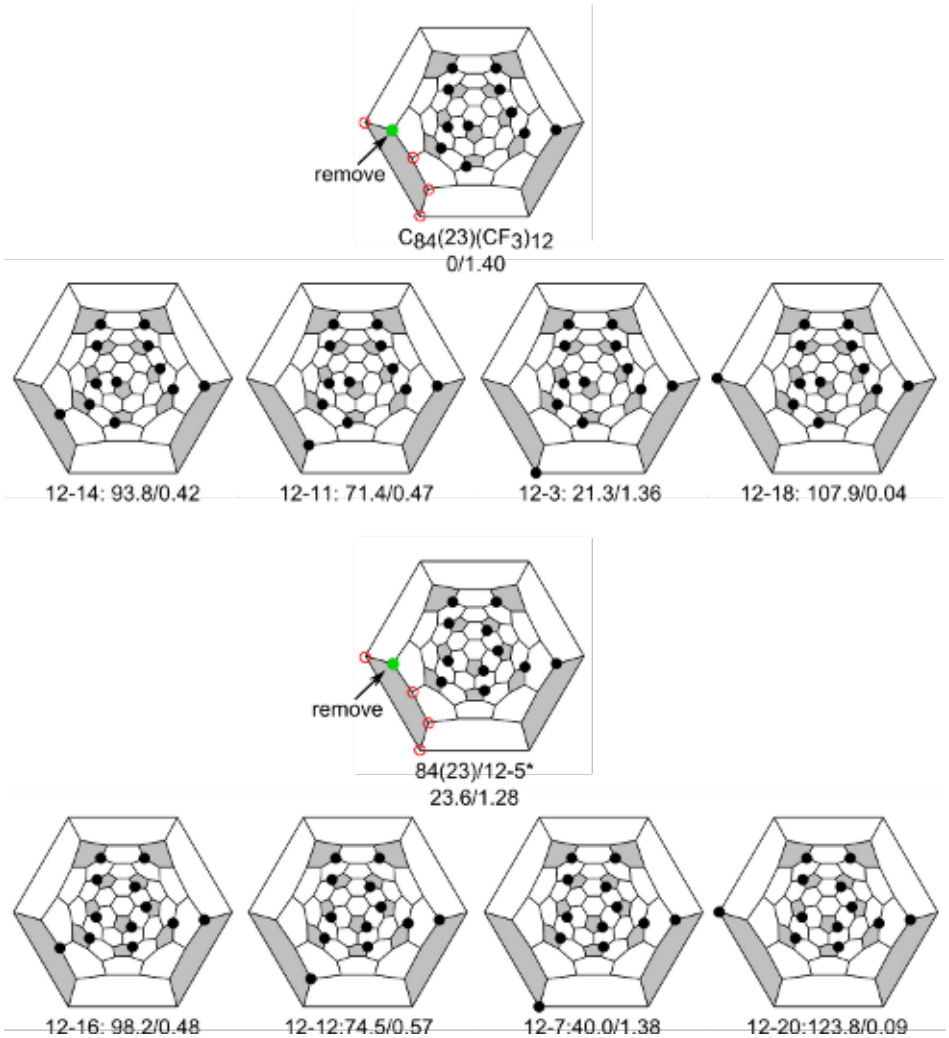

Figure 5.30.: Eight possible structures based on the one of the experimental isomers $C_{84}(23)(CF_3)_{12}$ and $C_{84}(23)(C_2F_5)_{12}$. The isomers are denoted as *m*-N: relative formation energy [kJ/mol] / HOMO-LUMO gap [eV], where N is a sequential number of isomer in order of increasing relative formation energy. *The same addition pattern with the experimental isomer $C_{84}(23)(C_2F_5)_{12}$ [1].

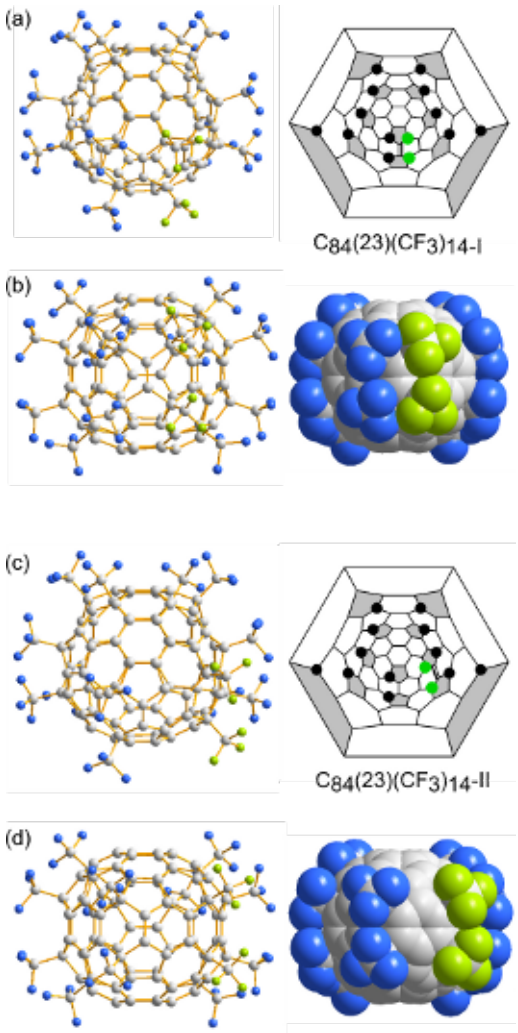

Figure 5.31.: Molecular structures and Schlegel diagrams of $C_{84}(23)(CF_3)_{14}$-I and $C_{84}(23)(CF_3)_{14}$-II. The projections (b) with different models are shown along a C_2 axis of the parent fullerene. The attachments which distinguish two isomers are shown with the green color. C=C bonds are shown with double lines.

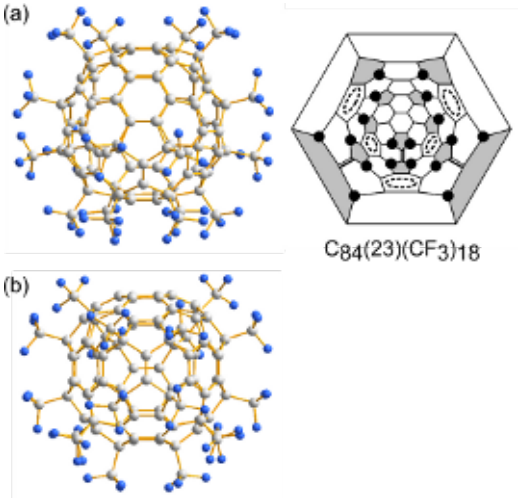

Figure 5.32.: Molecular structure and Schlegel diagram of $C_{84}(23)(CF_3)_{18}$. The projection (b) is shown along a C_2 axis of the parent fullerene. The three C=C bonds are shown with double lines, and the circles with dashed line show the partially 'aromatic' rings.

The possible reaction pathways

Some similar substructures are found among the isomers $C_{84}(23)(CF_3)_{14}$-I,II and $C_{84}(23)(CF_3)_{18}$-I. Therefore, these structures might be connected by a reaction path. In order to reconstruct the possible reaction pathways, some structures based on the experimental isomers are selected for the calculations. The optimized structures of the selected models are supposed to form local minimal along the pathways of experimentally found isomers (see Fig. 5.33). The addition pattern of the isomer 84(23)/12-2 is generated from the experimental isomer $C_{84}(23)(CF_3)_{14}$-I by removing two groups beside a ICCB, while the addition pattern of the isomer 84(23)/12-7 lacks one group at both ends of the *para* CF_3 chain. The isomer 84(23)/12-10 results from the isomer $C_{84}(23)(CF_3)_{14}$-II without two CF_3 groups. According to the calculation results, three chosen precursors show the thermodynamic and kinetic instabilities. They can exist only as intermediate products and miss their experimental identification. For the model isomer 84(23)/16-1, two groups are removed based on the addition pattern of $C_{84}(23)(CF_3)_{18}$-I. The calculated HOMO-LUMO-gap of 1.5 eV is large enough to expect that the synthesis and isolation of this isomer might be possible. The possible reaction pathways of isomers $C_{84}(23)(CF_3)_{12-18}$ are shown in Fig. 5.33.

5.2. Fullerene C_{86}, cage isomer 17

Fullerene C_{86} exists in 19 possible IPR isomers.[15] The ^{13}C NMR spectra with help of the DFT calculations showed the possibility of the existence of the isomer 16 with C_s symmetry and 17 with C_2 symmetry as a mixture in the HPLC fraction. Isomer 17 is the most stable cage isomer of C_{86}, whereas isomer 16 is less stable by 25-33 kJ/mol.[82] The relative formation energies of cage isomers with C_2 and C_s are shown in Appendix D. In previous studies, the cage connectivities of C_{86} were confirmed with its trifluoromethylated derivatives $C_{86}(17)(CF_3)_{16,18}$ via X-ray analysis.[4] In this work, two structures of CF_3 isomers with 10 and 16 groups are presented. Molecule projection and corresponding Schlegel diagram of the $C_{86}(17)$ are shown in Fig. 5.34).

For the structure of the isomer $C_{86}(17)(CF_3)_{10}$ (see Fig. 5.35), ten CF_3 groups can be divided into two sets, and they attach on the symmetrical positions on the fullerene cage. This leads to the isomer

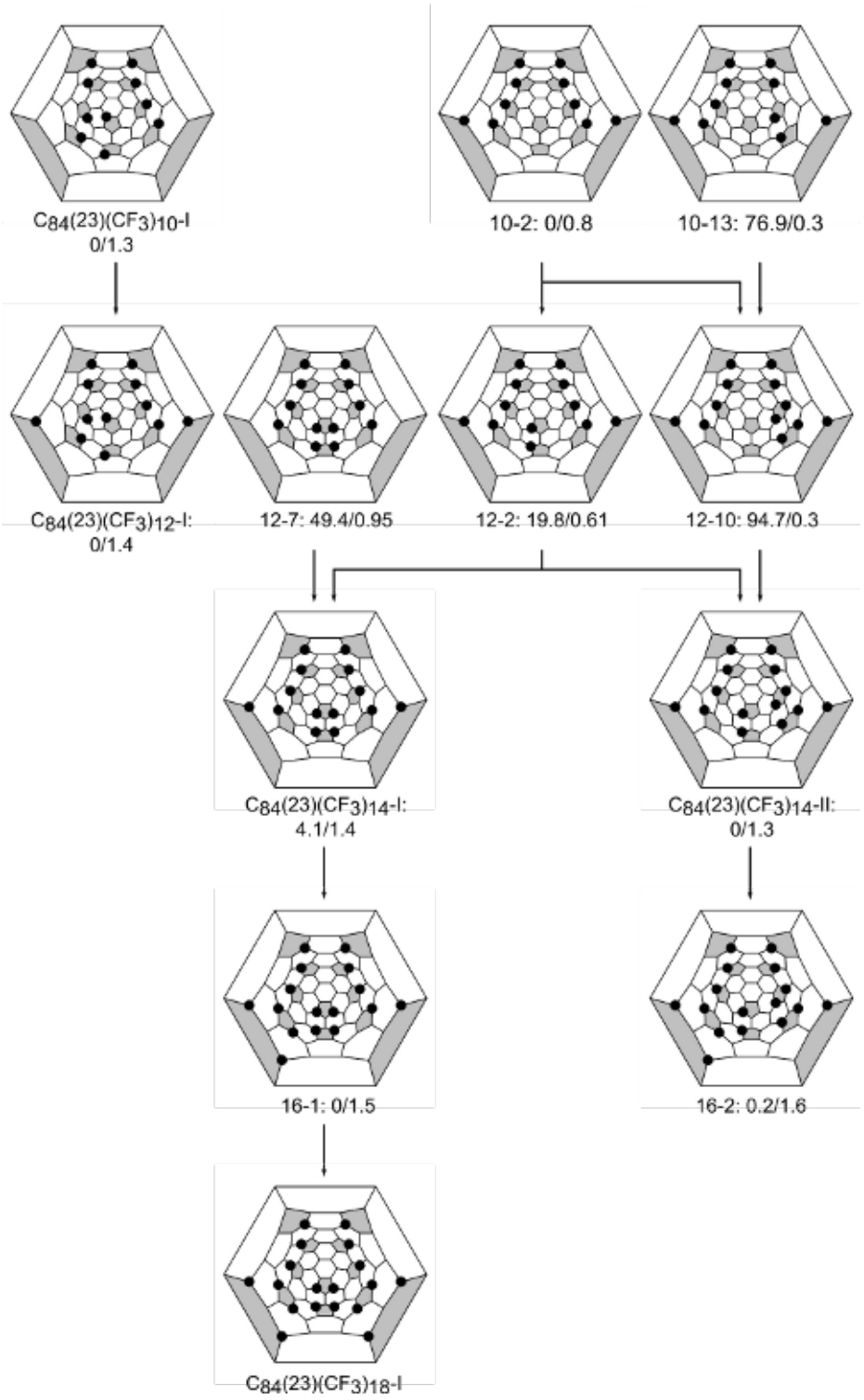

Figure 5.33.: The possible pathways of the trifluoromethylation for isomers $C_{84}(23)(CF_3)_m$ (m = 10-18). The isomers are denoted as m-N, where m = no. of CF_3 groups, N = no. of isomer ordered by increasing formation energy. The relative formation energy [kJ/mol] / HOMO-LUMO gap [eV] are given following the isomer notation. The experimental isolated isomers are shown with the formula.

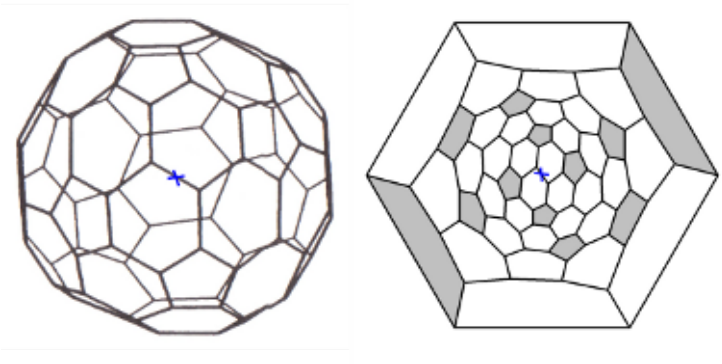

Figure 5.34.: The molecular structure (left) and the corresponding Schlegel diagram (right) of the $C_{86}(17)$. The C_2 axis passing through the cage is shown as crosses.

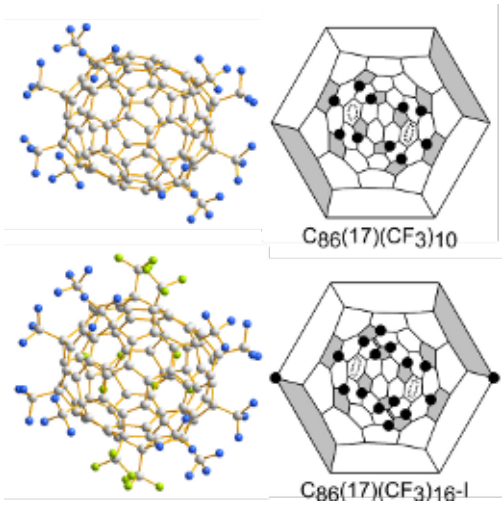

Figure 5.35.: Molecular structures and Schlegel diagrams of $C_{86}(17)(CF_3)_{10}$ and $C_{86}(17)(CF_3)_{16}$. The projection and Schlegel diagram are shown along to the C_2 axis. The extra attachments which distinguish two isomers are shown with the green color. C=C bonds are shown with double lines, and the circles with dashed line shows the partially 'aromatic' rings.

retaining the C_2 symmetry as the parent fullerene. Its addition pattern with two chains is described as p^4,p^4. The isomer $C_{86}(17)(CF_3)_{16}$-I with structure description p^6,p^6,p, contained the substructure of the isomer $C_{86}(17)(CF_3)_{10}$. Two five-membered chains of substructure are prolonged with two extra CF_3 groups in one terminus of one chain, and two CF_3 groups attach on the *para* positions in an isolated hexagon. Compared to the isomers $C_{86}(17)(CF_3)_{16}$-II[4] (see Fig. 5.36), the attachments of isomer I is more symmetric than isomer II, but they have 14 groups in common sites. For isomer $C_{86}(17)(CF_3)_{18}$, it contained the substructure of $C_{86}(17)(CF_3)_{16}$-II with 15 attachments on the same attached positions. Comparing the four isomers of $C_{86}(17)(CF_3)_{10}$, $C_{86}(17)(CF_3)_{16}$-I, -II and $C_{86}(17)(CF_3)_{18}$, two benzenoid rings are found in each isomer, whereas different numbers of isolated C=C bonds have been presented. Two C=C bonds for the isomer with 16 CF_3 groups and three for the isomer with 18 CF_3 groups are shown in Fig. 5.35 and Fig. 5.36. The possible reaction pathways of $C_{86}(17)(CF_3)_{10-16}$ are suggested in Fig. 5.37.

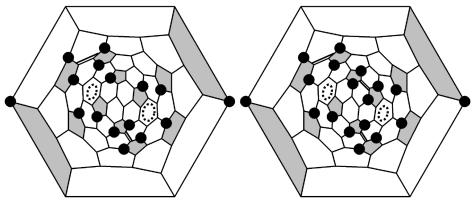

Figure 5.36.: Schlegel diagrams of $C_{86}(17)(CF_3)_{16}$-II and $C_{86}(17)(CF_3)_{18}$-I.[4] C=C bonds are shown with double lines, and the circles with dashed line show the partially 'aromatic' rings.

5.3. Fullerene C_{88}, cage isomer 33

The fullerene C_{88} exhibits 35 cage isomers.[15] The isomers 7 with C_s, 17 with C_2 and 33 with C_2 symmetries have been separated and studied with ^{13}C NMR and UV/VIS/NIR absorption spectra by Achiba *et al.*.[83] The predicted simulated spectra are in agreement with the experimental ones. Moreover, the C_{88} fullerene isomers 7, 17 and 33 are predicted as the most stable structures.[84–86] It explains why experimentally obtained isomers always consisted of these three cage isomers. So far the exact cage connectivity is confirmed by X-ray crystallographic study using its derivatives like $C_{88}(33)(CF_3)_{18}$.[5] In this work, one isomer with 18 CF_3 groups and the further two new structures with 16 and 20 CF_3 groups are reported. Cage isomer 33 has C_2 symmetry, and the C_2 axis passes through two C-C bonds that lie on the opposite sides of fullerene cage. The cage structure projection and the corresponding Schlegel diagram are shown in Fig. 5.38.

Separation and crystal growing is difficult for the C88 derivatives. The small orange crystals of the isomer $C_{88}(33)(CF_3)_{20}$ and $C_{88}(33)(CF_3)_{18}$ were obtained after recrystallization from o-dichlorobenzene (o-DCB) and toluene, respectively. For isomer of $C_{88}(33)(CF_3)_{16}$ is presented as the yellow-orange crystals in the mixture with small amount of $C_{84}(CF_3)_{16}$ and $C_{90}(CF_3)_{14}$ according to MALDI-MS results.

The projections of three molecular structures along C_2 symmetry of the bare C_{88} fullerene and the corresponding Schlegel diagrams are given in Fig. 5.39. Isomer $C_{88}(33)(CF_3)_{18}$ can be derived from isomer $C_{88}(33)(CF_3)_{16}$; $C_{88}(33)(CF_3)_{20}$ can be subsequently derived from $C_{88}(33)(CF_3)_{18}$ by addition of two more CF_3 groups. This confirms that isomer $C_{88}(33)(CF_3)_{20}$ contains only two CF_3 groups in different positions compared to isomer $C_{88}(33)(CF_3)_{18}$ assumed previously.[5] Similar relationship was also found for the other fullerene derivatives, e.g. $C_{84}(22)(CF_3)_{12-16}$ and $C_{76}(1)(CF_3)_{14-18}$.[87] Due to the unsymmetrical distribution of CF_3 groups, the symmetry of $C_{88}(33)(CF_3)_{18}$ is reduced to C_1 compared to that of the bare C_{88} fullerene, whereas the symmetries of the isomer $C_{88}(33)(CF_3)_{16}$ and $C_{88}(33)(CF_3)_{20}$ remain as C_2.

The addition patterns can be discussed in two ways. First, all 16 CF_3 groups of isomer $C_{88}(33)(CF_3)_{16}$ are attached on *para* positions in hexagons, while CF_3 attachments on *meta* position in a hexagon have been found in derivatives $C_{88}(33)(CF_3)_{18,20}$. Such attachments on *meta* position in a hexagon is obtained only when a large number of groups is attached to the fullerene cage. For the same reason, the attachments on *ortho* position in a hexagon is found for the isomer $C_{76}(1)(CF_3)_{18}$.[87] Second, two types of attached positions are distinguished, namely, carbon atoms belong to PHJs and THJs. All CF_3 groups are attached to cage atoms belonging to the PHJs. Such addition is considered to be energetically favored due to the release of steric strains. Comparing to the carbon atoms on the PHJs, attachment to carbon atoms belonging to THJ is energetically unfavored.

The increasing energy created by the unfavored attachment is probably compensated by the formation of isolated C=C bonds and π-conjugated system, such as benzenoid ring. The structures confirm that

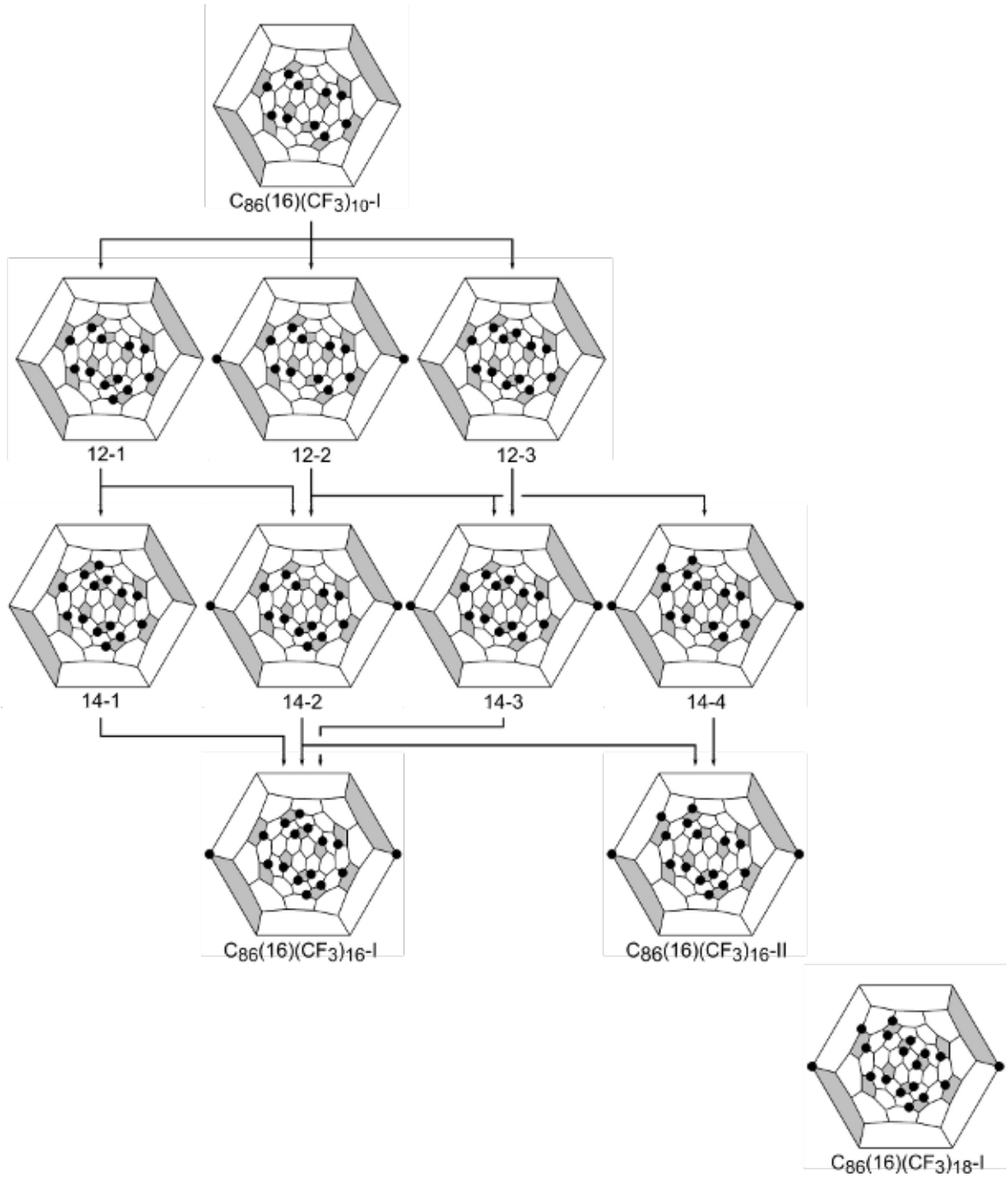

Figure 5.37.: The possible pathways of the trifluoromethylation for isomers $C_{86}(17)(CF_3)_m$ (m = 10-16). The isomers are denoted as m-N, where m = no. of CF_3 groups, N = no. of isomer ordered by increasing formation energy. The relative formation energy [kJ/mol] / HOMO-LUMO gap [eV] are given following the isomer notation. The experimental isolated isomers are shown with the formula.

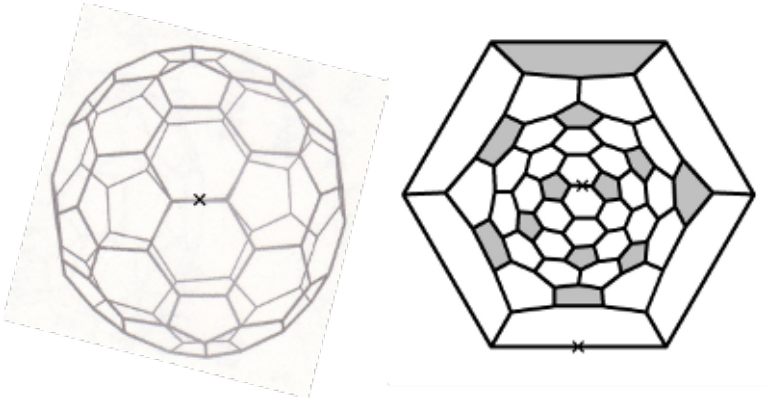

Figure 5.38.: The molecular structure (left) and the corresponding Schlegel diagram (right) of the $C_{88}(33)$. The C_2 axis passes through the cage is shown as crosses.

isomers $C_{88}(33)(CF_3)_{16}$, $C_{88}(33)(CF_3)_{18}$ and $C_{88}(33)(CF_3)_{20}$ have two partial isolated benzenoid rings each, with increasing number of two, three and four isolated carbon double bonds, respectively.

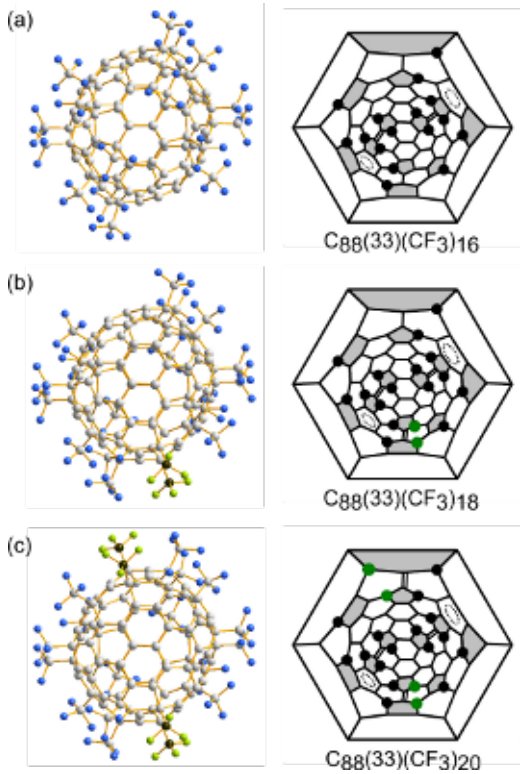

Figure 5.39.: Molecular structures and Schlegel diagrams of $C_{88}(33)(CF_3)_{16}$, $C_{88}(33)(CF_3)_{18}$ and $C_{88}(33)(CF_3)_{20}$. The projections and Schlegel diagrams are shown along the C_2 axis of the parent fullerene. The isomer connections are related by a simple addition of two CF_3 groups that are shown with green color. C=C bonds are shown with double lines, and circles with dashed lines show the partial 'aromatic' rings.

Chapter 6.

Conclusion and outlook

The work presents trifluoromethylated higher fullerenes synthesized from different fullerene sources at different temperatures and isolated *via* multi-step HPLC. The structures have been confirmed by single crystal X-ray analysis. The obtained main species are trifluoromethylated C_{84} fullerenes, but also trifluoromethylated C_{86} and C_{88} fullerenes have been characterized.

Trifluoromethylated higher fullerene (TMFs) were synthesized in glass and quartz ampoules at different reaction temperatures. The product mixtures from the radical addition reactions in glass ampoules at 400-420°C contained $C_n(CF_3)_m$ with n = 60,70,76-96 and m = 12-20, whereas TMFs with m = 2-20 were obtained in quartz ampoules at 500-600°C. The higher TMF species, i.e., $C_n(CF_3)_{m>12}$ sublimed and deposited in the cold region of the ampoule due to their higher volatility. In contrast, the lower TMF species, $C_n(CF_3)_{m\leq12}$, with lower volatility remained in the hot region. The TMF distribution depended significantly on temperature and reaction time. The product composition in the hot zone varied between species with 2-20 CF_3 groups at 550°C and species with 4-10 CF_3 groups at 600°C. The distribution of TMF species showed a significant broadening (from m = 10-20 to m = 2-20) with increasing temperatures (from 400 to 550°C) and the yield of higher TMF species increased with longer reaction time. However, the reaction performed at high temperature (600°C) yielded limited amounts of sublimed products, and the distribution of TMF species in the hot zone was significantly narrow comparing with that at 550°C.

In addition to the common one-step HPLC separation, several modifications have been tested. The separation with two columns using isocratic elution is suitable for the isolation of species with extremely short retention time. The gradient elution saved time and the separation at higher temperature delivered better resolution in some cases. A 'recycling system' has been used for the first time to isolate the TMF species. This technique is applied for the species with extremely close retention times. This multiple separation was very useful, if the species isolation was not achieved by the procedures described before in this paragraph.

Once the products have been isolated from the product mixtures, most of the crystals grew directly in the collected HPLC fractions. For some species, the crystal had to be recrystallized several times in different solvents. Due to the small crystal size, the structure determination was achieved only by using synchrotron radiation. The 28 structures of $C_{84}(CF_3)_m$ for cage isomers 11, 16, 18, 22, 23, one for $C_{86}(17)(CF_3)_{10}$, and two for $C_{88}(33)(CF_3)_{16,20}$ have been obtained for the first time. Based on these molecular structures and their addition patterns, principles of regioselectivity on higher fullerenes are suggested. The addition of CF_3 groups on the fullerene cage releases the steric strain due to the change of hybridizations. Hence, bond angles between C atoms belonging to PHJs of the fullerene cage vary from 109° to 110° and favor addition reactions on PHJs under rehybridization to sp^3. In contrast, C atoms in the quasi-flat fragments of THJs prefer to keep their sp^2 hybridization, and CF_3 addition is energetically unfavored. The conjugation between π-bonds increase if the local environment on the cage approaches planarity. Therefore, the stability of fullerene derivatives depends on the formation of isolated aromatic systems. Another stabilization effect is the formation of isolated C-C double bonds because of restricted rehybridization.

In order to predict possible pathways of trifuoromethylation from the lower derivatives to the higher

ones, quantum chemical calculations have been performed for experimental species $C_{84}(22)(CF_3)_m$ (up to $m = 16$) and some selected model structures of isomers $C_{84}(11)(CF_3)_{10-14}$ and isomers $C_{84}(23)(CF_3)_{10-16}$. The results revealed that TMF species with attachments in *para*-positions of hexagons are more stable than species with attachments in *ortho*- and *meta*-positions. In addition, all experimentally isolated isomers have been predicted as the most stable species in every category of CF_3 isomers with the same compositions. Based on the stable CF_3 isomers, the possible pathways are predicted by stepwise addition of two CF_3 groups. The product mixtures contain many lower TMF species whose structures remain experimentally unconfirmed. Based on the experimentally isolated CF_3 isomers, the general rules for the theoretical calculation can be set up in order to reduce the number of modeled CF_3 isomers from several millions to several hundreds. Although the investigation on synthesis, separation and structural characterization of trifluoromethylated higher fullerenes still remains a challenge, this work is a valuable contribution to the chemistry of higher fullerenes.

Chapter 7.

Experimental part

7.1. Synthesis route

Trifluoromethylated higher fullerenes are obtained through the reaction between fullerene substrates and excess CF_3I. As fullerene substrates, a C_{82-84} mixture (S1) [1] and a mixture of C_{76-96} which contained small amounts of C_{60} and C_{70} (S2) (*MER Corporation*, USA) have been used. The HPLC chromatograms and MALDL MS spectrum are shown in Fig. 7.1.

The fullerene S1 was synthesized with the arc-discharge method and purified by multi-step HPLC on a preparative level. The reactions are accomplished in quartz and glass ampoules. In the quartz ampoules, drastic reaction conditions of 510-600°C allow for a chemical conversion in a short time of 0.5-3 h, while in glass ampoules lower reaction temperatures of 390-410°C are applied for a longer time of about 2-3 days.

The operation system is shown in Fig. 7.2. There are three valves in this system. The valve I connects the ampoule and the system, the valve II connects the gas controller with the system and the valve III connects the system with the vacuum pump.

20-40 mg of the fullerene mixture is placed in a glass/quartz ampoule. The ampoule has been bent (about 120°) and divided into three sections with a narrowing (see Fig. 7.2). These three sections of the ampoule correspond to the hot, cold zones and room temperature section mentioned in the following chapters. The ampoule with the fullerene mixture is heated *in vacuo* to remove the water or gas that adsorbs on the surface of the ampoule or fullerene mixture. In this step, the valve I and III are opened and the valve II is closed. In the next step, the valve I and III are closed and valve II is opened for 1-2 sec to fill this closed system with CF_3I gas (Apollo, 98 %). With the vacuum gauge, the system pressure can be controlled. After opening of the valve I, CF_3I is condensed into the ampoule under cooling with liquid nitrogen. This procedure is carried out several times until about 0.5 ml of CF_3I has been filled into the ampoule.

After water and air as impurities, which interfere in target reactions, have been removed, the ampoule is sealed *in vacuo* and placed in a gradient furnace. While the fullerene mixture is heated within the furnace (hot zone), the liquid CF_3I stays at room temperature outside the furnace (cold zone). During the reaction, brown to orange fullerene products and the dark violet I_2 deposit between the hot and cold zone. A schematic presentation is shown in Fig. 7.3. For the reaction in quartz ampoule, fullerene products are also found with small amounts of black residue of the fullerene substrate in the hot zone. However, large amounts of non-reacted substrate are found typically for the reactions accomplished in glass ampoules.

The ampoule is opened after the reaction has finished and cooled to room temperature. Excess CF_3I vaporizes at room temperature and I_2 has been removed by vaporization by heating at 200°C for ca. 1 h. The raw products are the dark brown powders obtained from the deposit at the border between hot and cold zone and the black solid products from the hot zone. Both of them can be dissolved in organic

[1] S1 was obtained from our corporation partner at the Hefei National Laboratory for Physical Sciences at Microscale Department of Materials Science and Engineering, University of Science and Technology of China in Hefei, P. R. China.

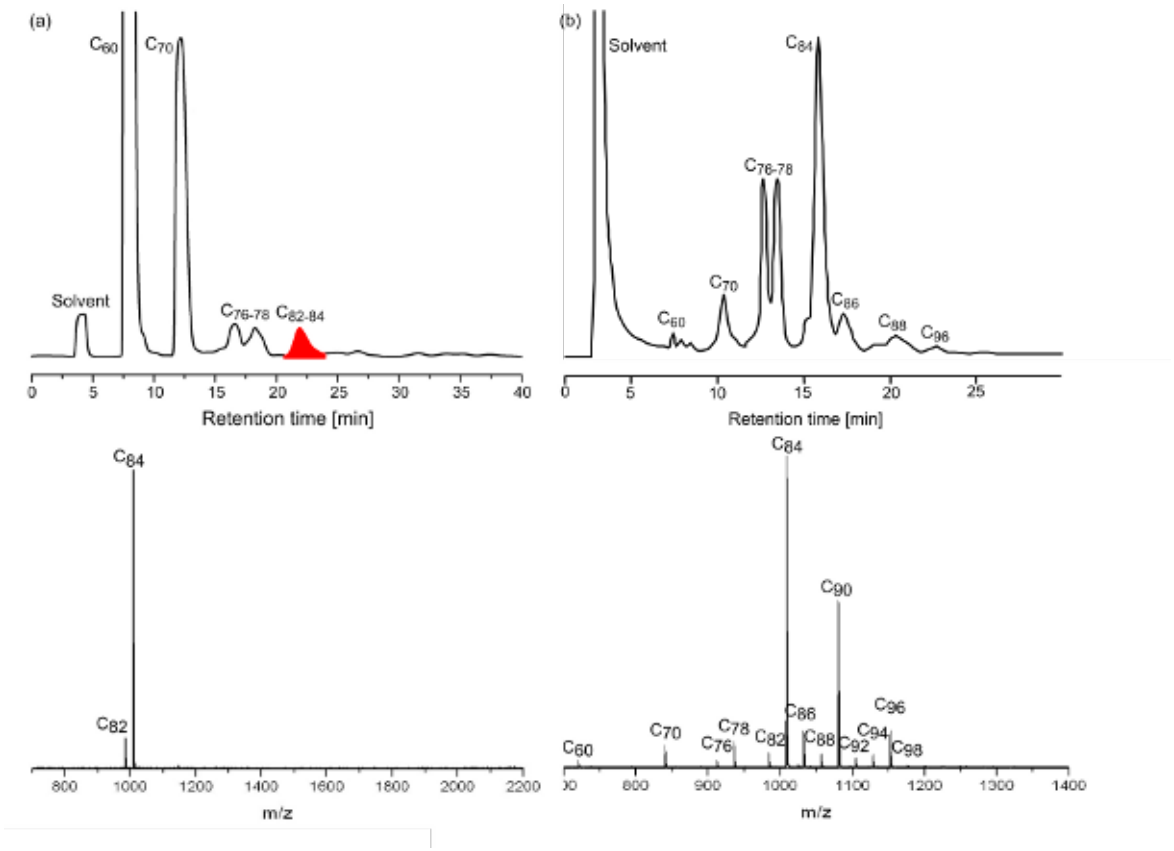

Figure 7.1.: HPLC trace of the fullerene S1 (a) and S2 (b). The spectrum of MALDI-MS analysis of the collected fraction marked with red color in (a) shows the prevailing abundance of fullerene C_{84} (m/z=1008) and smaller abundance of fullerene C_{82} (m/z=984).

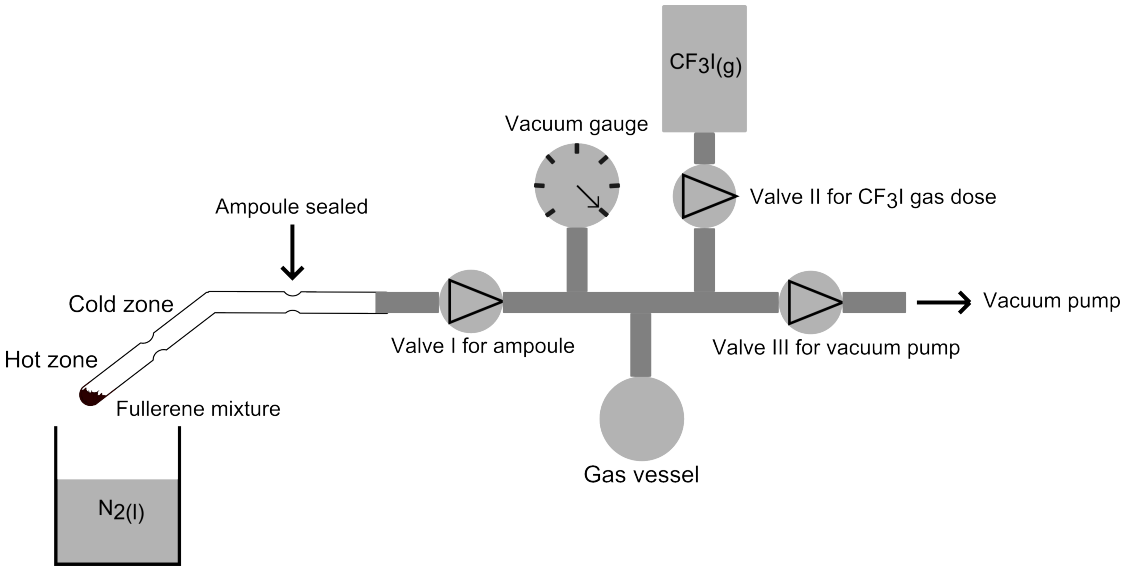

Figure 7.2.: Operation system of trifluoromethylation for fullerenes.

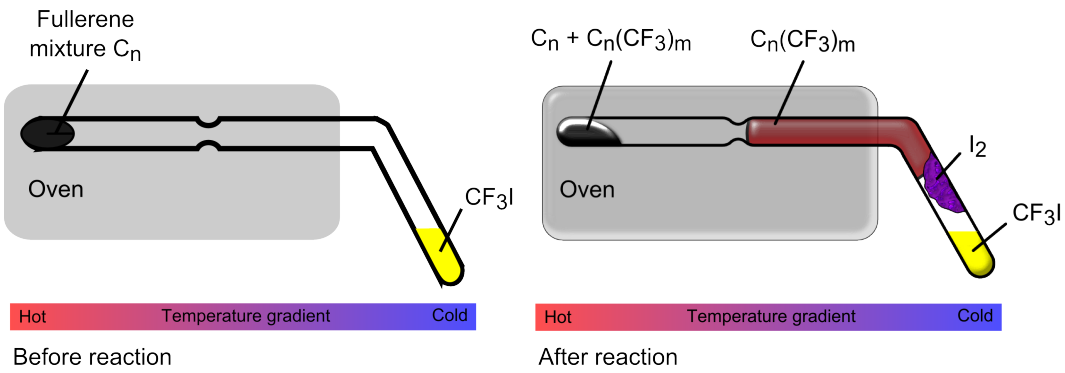

Figure 7.3.: The presentation of a reaction ampoule before and after trifluoromethylation.

solvents and the separation has been carried out by HPLC.

7.2. Product separation and isolation of isomers via HPLC

The product mixture containing several derivatives was obtained from the synthesis that is described in the above section. To get individual compounds for the next step of the crystallization, separation of trifluoromethylated fullerene isomers using HPLC techniques play a key role. For this, two HPLC systems from *Shimadzu Prominence series* (*Shimadzu Corporation*, Japan) have been used.

The crude products are filtered through a PTFE membrane (0.2 μm pore, *Carl Roth GmbH*, Karlsruhe, Germany) to remove the unreacted fullerene substrate that has a lower solubility in toluene. The filtrate is further purified using toluene as eluent in the first step of the HPLC [2]. The separation of the crude product is performed at 25°C with a flow rate of 4.6 ml/min. Subsequently, the toluene fractions undergo several HPLC steps with toluene / n-hexane mixtures as eluents. The eluent mixtures are adjusted for each fraction depending on their retention time in toluene. The n-hexane / toluene ratio is lowered as the retention time increases.

7.3. Composition analysis with MALDI-MS

MALDI-MS is used to determine the compositions of the raw products and the fractions obtained from the reactions and the HPLC separations, respectively. The products are mixed with a matrix, trans-2-[3-(4-butylphenyl)-2-methyl-2-propenylidene]malononitrile (DCTB), (*Sigma-Aldrich*, Germany, 99.9 %), to prepare the MALDI samples on a target. The analyte can be dissolved in toluene, hexane, their mixture or o-dichlorobenzene (o-DCB). The matrix dissolved in toluene at concentrations of 400 mM (about 1 mg matrix in 10 μl toluene). The analyte and the matrix solution mixed together at the volume ratio of ca. 1:10 in a 0.5 ml plastic tube and transferred to a sample target [3].

The samples are irradiated with laser pulses (N_2 laser, 337 nm, 1 ns pulse) in an *AutoFlex III Smart-beam spectrometer* (*Bruker Daltonics*, Germany). Depending on the product concentrations in the samples, the laser intensity is varied between 5-20 %. The spectra are recorded between *mass-to-charge ratios* (*m/z*) of 700 and 3000 Dalton (Da) in *negative*-ion mode.

[2] Several sources for toluene were used in this work. Their different impurities influenced the separation results. For details see Chapter 4. *Acros*, HPLC-grad with purity 99.85 %; *ROTH*, *ROTISOLV*© HPLC-quality, 99.9 %; *Stockmeier*, 99.5 %

[3] A sandwich technique can also be used for a sample preparation. The analyte was deposited between two matrix layers that carried out directly on the sample target.

7.4. Structure determination by single crystal X-ray diffraction

The solvent evaporates from the HPLC fraction within several days leaving single crystals of mainly small sizes in the sample vials (size variation between 0.01 and 0.05 mm). Therefore, synchrotron radiation with wavelength between 0.8434 and 0.9050 Å is used to achieve a sufficiently high resolution for the diffraction patterns of the crystals. The data are collected at 100 K using the *MAR225 image plate detector* (*Bruker*) at the *BESSY* (Working station BL 14.2, Protein Structure Factory of the Freie Universität Berlin, Germany) [4].

For larger single crystals, the diffraction patterns are recorded on an *Image Plate Stoe Diffractometer* (IPSD) at 100 K using Mo Kα radiation with a wavelength of 0.71073 Å. The structures are determined using the programs *SHELXS97* or *SHELXD* and refined with *SHELXL97*[88].

7.5. Theoretical calculations

Computational data of the fullerene derivatives are used to interpret the experimental results. The optimized structures, their relative formation energies and the HOMO-LUMO gaps are obtained by *density functional theory* (DFT) and the *semi-empirical Austin Model 1* (AM1)[89]. The DFT calculations are performed by the software *PRIRODA* with the *exchange-correlation functional* (PBE)[90] using *triple zeta basis sets with polarization functions* (TZ2P). DFT methods within the formulation of Kohn and Sham[90,91] provide currently the most accurate *ab initio* energies and structures with affordable computational demand for large molecules. The AM1 method is a parameterized semi-empirical model based on the neglect of differential overlap. The calculations were carried out by Dr. A. A. Goryunkov in Chemistry Department of Moscow State University.

[4] German: Berliner Elektronspeicherring-Gesellschaft für Synchrotronstrahlung m.b.H; English: Berlin Electron Storage Ring Society for Synchrotron Radiation.

Appendices

Appendix A.

Crystallographic data

Table A.1: $C_{84}(4)(CF_3)_{12}$ and $C_{84}(11)(CF_3)_{10-12}$

Molecule name	84(4)/12-I	84(11)/10-I	84(11)/12-I	84(11)/12-I
Empirical formula	$C_{84}(CF_3)_{12}$	$C_{84}(CF_3)_{10}$	$C_{84}(CF_3)_{12}$	$C_{84}(CF_3)_{12}$
Solvent in the lattice	2 C_6H_{14}	2 $C_6H_5CH_3$	1 $C_6H_5CH_3$	2 $C_2Cl_4H_2$
Molar mass (g/mol)	2009.3	1791.07	1929.09	2124.59
Crystal system	Monoclinic	Triclinic	Triclinic	Triclinic
Space group	$R\bar{3}c$	$P\bar{1}$	$P\bar{1}$	$P\bar{1}$
Unit cell dimensions a (Å), α (°)	30.739(1), 90	10.936(1), 85.94(1)	17.852(1), 87.54(1)	13.434(1), 93.31(1)
b , β	30.739(1), 90	14.587(1), 85.74(1)	19.826(1), 89.99(1)	14.502(1), 98.65(1)
c , γ	42.241(1), 120	21.014(1), 74.56(1)	29.420(2), 68.59(1)	19.314(1), 100.49(1)
Unit cell volume (Å^3)	34565.6(18)	3210.8(12)	9701.5(10)	3643.7(4)
Z	18	2	4	2
Measurement temperature (K)	100(2)	100(2)	100(2)	100(2)
Data collection (θ) (°) at radiation λ (Å)	2.4-37.0 / 0.8856	2.4-36.8 / 0.8856	1.7-36.9 / 0.9050	2.7-38.4 / 0.9050
Crystal color	orange	black	orange	orange
Crystal size (mm)	$0.03 \times 0.02 \times 0.01$	$0.2 \times 0.05 \times 0.01$	$0.04 \times 0.04 \times 0.01$	$0.02 \times 0.02 \times 0.01$
Crystal density (g/cm^3)	1.737	1.853	1.321	1.936
F(000)	18000	1768	3800	2808
Radiation type	Synchrotron	Synchrotron	Synchrotron	Synchrotron
hkl-index	$-41 \leq h \leq 41$	$-14 \leq h \leq 14$	$-22 \leq h \leq 22$	$-18 \leq h \leq 17$
	$-39 \leq k \leq 39$	$-18 \leq k \leq 18$	$-24 \leq k \leq 24$	$-19 \leq k \leq 19$
	$-54 \leq l \leq 54$	$-28 \leq l \leq 28$	$-36 \leq l \leq 36$	$-23 \leq l \leq 26$
Data / parameter	9519 / 651	12668 / 1168	35137 / 2433	18035 / 1277
Refls. collected / R(int)	157340 / 0.031	46408 / 0.667	115656 / 0.153	31120 / 0.238
Completeness to $\theta = 25°$ (%) *	98.7	89.1	87.5	93.6
Goodness of fit	1.157	2.836	2.019	0.765
Reliability factor R1 / *w*R2	0.0692 / 0.237	0.145 / 0.395	0.195 / 0.462	0.115 / 0.301
Different electron density max / min (e Å^3)	1.07 / -0.74	3.00 /-0.94	1.15 / -0.58	1.66 / -1.46

* Recalculated for Mo K_α.

Table A.2: $C_{84}(11)(CF_3)_{14-16}$

Molecule name	84(11)/14-I	84(11)/14-II	84(11)/14-III	84(11)/16-I
Empirical formula	$C_{84}(CF_3)_{14}$	$C_{84}(CF_3)_{14}$	$C_{84}(CF_3)_{14}$	$C_{84}(CF_3)_{16}$
Solvent in the lattice	2.45 $C_6H_5CH_3$	1 $C_6H_5CH_3$	1 o-$C_6Cl_2H_4$	1 $C_6H_5CH_3$
Molar mass (g/mol)	2200.71	2067.11	2121.97	2297.27
Crystal system	Triclinic	Triclinic	Triclinic	Triclinic
Space group	$P\bar{1}$	$P\bar{1}$	$P\bar{1}$	$P\bar{1}$
Unit cell dimensions a (Å), α (°)	13.007(1), 80.67(1)	14.042(1), 93.31(1)	13.297(1), 95.18(1)	13.416(1), 84.78(1)
b , β	14.182(1), 88.95(1)	14.431(1), 94.97(1)	14.796(5), 91.28(1)	14.714(1), 78.74(1)
c , γ	25.595(2), 68.24(1)	20.153(2), 103.44(1)	19.278(2), 112.63(1)	21.918(2), 75.11(1)
Unit cell volume (Å^3)	4322.5(8)	3944.2(6)	3479.8(5)	4097.1(6)
Z	2	2	2	2
Measurement temperature (K)	100(2)	100(2)	100(2)	100(2)
Data collection (θ) (°) at radiation λ (Å)	2.2-36.9 / 0.9050	3.3-36.8 / 0.9050	1.9-36.8 / 0.8920	2.3-37.0 / 0.8920
Crystal color	yellow-orange	light orange	orange	yellow
Crystal size (mm)	$0.01 \times 0.01 \times 0.01$	$0.03 \times 0.02 \times 0.01$	$0.02 \times 0.02 \times 0.01$	$0.06 \times 0.03 \times 0.01$
Crystal density (g/cm^3)	1.691	1.741	2.025	1.862
F(000)	2177	2032	2080	2264
Radiation	Synchrotron	Synchrotron	Synchrotron	Synchrotron
hkl-index	$-15 \leq h \leq 14$	$-17 \leq h \leq 17$	$-17 \leq h \leq 17$	$-15 \leq h \leq 15$
	$-17 \leq k \leq 17$	$-17 \leq k \leq 17$	$-19 \leq k \leq 19$	$-19 \leq k \leq 19$
	$-32 \leq l \leq 31$	$-26 \leq l \leq 26$	$-24 \leq l \leq 24$	$-28 \leq l \leq 28$
Data / parameter	15398 / 1309	13645 / 1277	12998 / 1361	15773 / 1461
Refls. collected / R(int)	57818 / 0.206	50408 / 0.078	48146 / 0.193	47085 / 0.035
Completeness to $\theta = 25°$ (%) *	80.2	85.0	87.0	88.9
Goodness of fit	1.369	1.128	1.046	1.373
Reliability factor R1 / wR2	0.116 / 0.317	0.119 / 0.356	0.106 / 0.366	0.078 / 0.229
Different electron density max / min (e Å^3)	0.97 / -0.44	1.16 / -0.40	0.73 / -1.12	3.13 / -0.56

* Recalculated for Mo K_α.

Table A.3: $C_{84}(16)(CF_3)_{8,14}$ and $C_{84}(18)(CF_3)_{10,12}$

Molecule name	84(16)/8-I	84(16)/14-I	84(16)/14-I	84(18)/10-I	84(18)/12-I
Empirical formula	$C_{84}(CF_3)_8$	$C_{84}(CF_3)_{14}$	$C_{84}(CF_3)_{14}$	$C_{84}(CF_3)_{10}$	$C_{84}(CF_3)_{12}$
Solvent in the lattice	2 $C_6H_5CH_3$	1 $C_6H_5CH_3$	1 $C_6H_5CH_3$	0.5 *p*-$C_6H_4(CH_3)_2$	1 $C_6H_5CH_3$
Molar mass (g/mol)	1745.19	2003.14	2067.11	1952.02	1929.09
Crystal system	Triclinic	Orthorhombic	Triclinic	Triclinic	Triclinic
Space group	$P\bar{1}$	*Pbcn*	$P\bar{1}$	$P\bar{1}$	$P\bar{1}$
Unit cell dimensions a (Å), α (°)	11.022(1), 90.35(1)	29.583(2), 90	13.285(1), 106.56(1)	11.526(1), 95.20(1)	13.739(1), 93.19(1)
b , β	15.301(1), 100.56(1)	20.249(1), 90	13.299(1), 94.11(1)	15.400(1), 102.17(1)	13.816(1), 96.85(1)
b , γ	19.254(1), 96.93(1)	24.122(1), 90	23.318(2), 109.19(1)	17.650(1), 103.05(1)	17.568(1), 103.92(1)
Unit cell volume (Å^3)	3167.5(5)	14449.7(17)	3666.9(5)	2951.8(4)	3201.4(4)
Z	2	8	2	2	2
Measurement temperature (K)	100(2)	100(2)	100(2)	100(2)	100(2)
Data collection (θ) (°) at radiation λ (Å)	1.7-36.9 / 0.8856	1.9-37.1 / 0.9050	2.1-36.9 / 0.9050	2.8-36.9 / 0.9050	1.9-37.0 / 0.8856
Crystal color	orange	yellow	yellow	orange	red
Crystal size (mm)	$0.02 \times 0.01 \times 0.01$	$0.2 \times 0.01 \times 0.01$	$0.02 \times 0.02 \times 0.01$	$0.05 \times 0.02 \times 0.02$	$0.04 \times 0.02 \times 0.01$
Crystal density (g/cm^3)	1.830	1.842	1.872	1.971	2.001
F(000)	1736	7868	2032	1726	1900
Radiation type	Synchrotron	Synchrotron	Synchrotron	Synchrotron	Synchrotron
hkl-index	$-13 \leq h \leq 13$	$-36 \leq h \leq 36$	$-16 \leq h \leq 16$	$-13 \leq h \leq 13$	$-17 \leq h \leq 17$
	$-20 \leq k \leq 20$	$-26 \leq k \leq 26$	$-15 \leq k \leq 15$	$-20 \leq k \leq 20$	$-18 \leq k \leq 18$
	$-24 \leq l \leq 24$	$-29 \leq l \leq 29$	$-30 \leq l \leq 30$	$-21 \leq l \leq 21$	$-23 \leq l \leq 23$
Data / parameter	12438 / 1217	15785 / 1581	12389 / 1279	10726 / 1154	12652 / 1253
Refls. collected / R(int)	46398 / 0.054	176809 / 0.058	34856 / 0.179	39150 / 0.042	47514 / 0.023
Completeness to $\theta = 25°$ (%) *	88.7	99.9	81.9	87.1	87.8
Goodness of fit	1.144	1.040	1.686	1.025	1.019
Reliability factor R1 / *w*R2	0.093 / 0.263	0.101 / 0.293	0.162 / 0.394	0.105 / 0.298	0.069 /0.191
Different electron density max / min (e Å^3)	2.34 / -0.82	0.93 / -1.09	1.33 / -0.78	0.66 / -0.64	1.02 / -0.55

* Recalculated for Mo K_α.

Table A.4: $C_{84}(22)(CF_3)_{12,14}$

Molecule name	84(22)/12-I	84(22)/12-II	84(22)/12-II	84(22)/14-I	84(22)/14-I
Empirical formula	$C_{84}(CF_3)_{12}$	$C_{84}(CF_3)_{12}$	$C_{84}(CF_3)_{12}$	$C_{84}(CF_3)_{14}$	$C_{84}(CF_3)_{14}$
Solvent in the lattice		1 $C_6H_5CH_3$		3 $C_6H_5CH_3$	2 $C_6H_5CH_3$
Molar mass (g/mol)	1836.96	1929.09	1836.96	2251.38	2159.25
Crystal system	Tetragonal	Monoclinic	Tetragonal	Monoclinic	Monoclinic
Space group	$p4_1$/a	$P2_1$/n	$P4_2$/bc	$P2_1$/n	$P2_1$/n
Unit cell dimensions a (Å), α (°)	16.610(1), 90	10.921(1), 90	16.028(1), 90	21.440(2), 90	18.014(1), 90
b , β	16.610(1), 90	26.171(3), 92.25(1)	16.028(1), 90	19.580(2), 118.80(1)	22.820(1), 107.031(8)
c , γ	43.550(2), 90	23.441(3), 90	45.983(3), 90	21.890(2), 90	19.067(1), 90
Unit cell volume (Å^3)	12016.5(12)		11813(1)		7494.3(7)
Z	8	4	8	4	4
Measurement temperature (K)	100(2)	100(2)	100(2)	100(2)	100(2)
Data collection (θ) (°) at radiation λ (Å)	1.6-36.2 / 0.8856	2.2-37.0 / 0.8856	2.3-37.0 / 0.9050	2.3-37.0 / 0.9050	1.8-34.8 / 0.8793
Crystal color	yellow	orange	orange	orange	orange
Crystal size (mm)	$0.03 \times 0.01 \times 0.01$	$0.03 \times 0.02 \times 0.01$	$0.02 \times 0.01 \times 0.01$	$0.6 \times 0.2 \times 0.1$	$0.4 \times 0.4 \times 0.01$
Crystal density (g/cm^3)	2.031	1.914	2.066	1.857	1.914
F(000)	7200		7200		4264
Radiation type	Synchrotron	Synchrotron	Synchrotron	Synchrotron	Synchrotron
hkl-index	$-21 \leq h \leq 21$	$-13 \leq h \leq 13$	$-21 \leq h \leq 21$	$-25 \leq h \leq 29$	$-23 \leq h \leq 23$
	$-21 \leq k \leq 21$	$-33 \leq k \leq 33$	$-21 \leq k \leq 21$	$-26 \leq k \leq 26$	$-29 \leq k \leq 29$
	$-54 \leq l \leq 54$	$-30 \leq l \leq 29$	$-60 \leq l \leq 60$	$-29 \leq l \leq 27$	$-24 \leq l \leq 24$
Data / parameter	7218 / 596	15049 / 1304	13810 / 1217	20910 / 1418	15229 / 1526
Refls. collected / R(int)	89285 / 0.069	98661 / 0.074	159259 / 0.061	82634 / 0.115	106282 / 0.025
Completeness to $\theta = 25°$ (%) *	98.8	96.3	99.4	97.2	91.6
Goodness of fit	1.059	1.066	1.050	1.034	1.024
Reliability factor R1 / *w*R2	0.187 / 0.421	0.108 / 0.282	0.058 / 0.163	0.082 / 0.203	0.048 / 0.116
Different electron density max / min (e Å^3)	0.74 / -0.66	0.86 / -0.47	0.42 / -0.39	2.45 / -0.73	0.46 / -0.30

* Recalculated for Mo K_α.

Table A.5: $C_{84}(22)(CF_3)_{14,16}$

Molecule name	84(22)/14-II	84(22)/16-I	84(22)/16-II	84(22)/16-III	84(22)/16-IV
Empirical formula	$C_{84}(CF_3)_{14}$	$C_{84}(CF_3)_{16}$	$C_{84}(CF_3)_{16}$	$C_{84}(CF_3)_{16}$	$C_{84}(CF_3)_{16}$
Solvent in the lattice	0.5 $C_6H_5CH_3$	1.7 $C_6H_5CH_3$	1.3 $C_6H_5CH_3$	1 $C_6H_4CH_3(CHO)$	0.8 p-$C_6H_4(CH_3)_2$
Molar mass (g/mol)	2021.05	2268.90	2233.17	2356.49	2198.92
Crystal system	Triclinic	Monoclinic	Triclinic	Monoclinic	Triclinic
Space group	$P\bar{1}$	$C2$/c	$P\bar{1}$	$C2$/c	$P\bar{1}$
Unit cell dimensions a (Å), α (°)	13.7011(6), 94.843(2)	15.677(1), 90	14.3777(6), 74.141(2)	17.5142(6), 90	13.2413(8), 80.832(5)
b , β	14.8432(6), 94.101(2)	24.675(2), 90.546(8)	14.4859(6), 72.150(2)	23.8456(9), 92.799(2)	13.2610(9), 74.73(9)
c , γ	17.2820(17), 109.41(1)	20.4170(20), 90	21.1530(21), 66.29(1)	19.6284(3), 90	22.7910(10), 80.561(7)
Unit cell volume (Å^3)	3284.5(3)	7829.5(9)	3785.8(3)	8187.8(5)	3780.4(4)
Z	2	4	2	4	2
Measurement temperature (K)	100(2)	100(2)	100(2)	100(2)	100(2)
Data collection (θ) (°) at radiation λ (Å)	2.7-36.9 / 0.9050	2.4-36.9 / 0.8793	2.0-36.9 / 0.9050	2.2-36.5 / 0.9050	2.0-36.9 / 0.9050
Crystal color	orange	orange	yellow	yellow-orange	orange
Crystal size (mm)	$0.03 \times 0.03 \times 0.02$	$0.04 \times 0.01 \times 0.01$	$0.03 \times 0.03 \times 0.01$	$0.04 \times 0.003 \times 0.001$	$0.03 \times 0.02 \times 0.01$
Crystal density (g/cm^3)	2.044	1.925	1.959	1.912	1.932
F(000)	1982	4466	3384	4646	2158
Radiation type	Synchrotron	Synchrotron	Synchrotron	Synchrotron	Synchrotron
hkl-index	$-16 \leq h \leq 16$	$-21 \leq h \leq 21$	$-17 \leq h \leq 17$	$-22 \leq h \leq 22$	$-15 \leq h \leq 15$
	$-19 \leq k \leq 19$	$-33 \leq k \leq 33$	$-18 \leq k \leq 18$	$-29 \leq k \leq 29$	$-16 \leq k \leq 16$
	$-22 \leq l \leq 22$	$-27 \leq l \leq 27$	$-27 \leq l \leq 27$	$-25 \leq l \leq 25$	$-30 \leq l \leq 30$
Data / parameter	12052 / 1378	9019 / 816	14158 / 1427	8076 / 814	13759 7 1472
Refls. collected / R(int)	45656 / 0.031	57127 / 0.026	53678 / 0.042	56156 / 0.040	52002 / 0.104
Completeness to $\theta = 25°$ (%) *	88.1	96.1	89.2	92.0	89.0
Goodness of fit	1.088	1.041	1.064	1.035	1.020
Reliability factor R1 and wR2	0.053 / 0.142	0.067 / 0.173	0.068 / 0.178	0.065 / 0.169	0.185 / 0.411
Different electron density max / min (e Å^3)	0.35 / -0.40	0.75 / -0.81	0.75 / -0.62	0.68 / -0.50	0.74 / -0.76

* Recalculated for Mo K_α.

Table A.6: $C_{84}(22)(CF_3)_{20}$ and $C_{84}(23)(CF_3)_{8-12}$

Molecule name	84(22)/20-I	84(23)/8-I	84(23)/10-I	84(23)/12-I
Empirical formula	$C_{84}(CF_3)_{20}$	$C_{84}(CF_3)_8$	$C_{84}(CF_3)_{10}$	$C_{84}(CF_3)_{12}$
Solvent in the lattice				2 $C_6H_5CH_3$
Molar mass (g/mol)	2389.04	1560.92	1698.94	2021.23
Crystal system	Monoclinic	Monoclinic	Monoclinic	Triclinic
Space group	$C2$/c	$C2$/c	$P2_1$/n	$P\bar{1}$
Unit cell dimensions a (Å), α (°)	23.073(2), 90	44.659(1), 90	11.501(1), 90	12.023(1), 89.04(1)
b , β	14.586(1), 108.24(1)	11.320(1), 119.73(1)	28.207(1), 90.54(1)	14.869(1), 85.25(1)
c , γ	24.270(2), 90	24.053(1), 90	41.466(2), 90	21.191(2), 68.87(1)
Unit cell volume (Å^3)	7757.5(11)	10559.7(11)	13451.3(14)	3521.1(5)
Z	4	8	8	2
Measurement temperature (K)	100(2)	100(2)	100(2)	100(2)
Data collection (θ) (°) at radiation λ (Å)	2.3-36.0 / 0.9050	2.2-39.6 / 0.9050	2.4-37.0 / 0.9050	1.8-37.1 / 0.8856
Crystal color	yellow	red	black	orange
Crystal size (mm)	$0.03 \times 0.02 \times 0.01$	$0.03 \times 0.03 \times 0.02$	$0.08 \times 0.01 \times 0.01$	$0.03 \times 0.02 \times 0.01$
Crystal density (g/cm^3)	2.046	1.964	1.678	1.906
F(000)	4656	6144	6672	2000
Radiation type	Synchrotron	Synchrotron	Synchrotron	Synchrotron
hkl-index	$-28 \leq h \leq 29$	$-61 \leq h \leq 61$	$-13 \leq h \leq 13$	$-16 \leq h \leq 16$
	$-18 \leq k \leq 18$	$-15 \leq k \leq 15$	$-34 \leq k \leq 34$	$-19 \leq k \leq 19$
	$-31 \leq l \leq 31$	$-31 \leq l \leq 31$	$-54 \leq l \leq 53$	$-28 \leq l \leq 28$
Data / parameter	7633 / 920	13573 / 1127	26044 / 2343	13987 / 1437
Refls. collected / R(int)	29470 / 0.137	85201 / 0.065	185004 / 0.070	52621 / 0.025
Completeness to $\theta = 25°$ (%) *	95.3	99.0	90.6	88.5
Goodness of fit	1.062	1.036	1.095	1.115
Reliability factor R1 / wR2	0.095 / 0.225	0.069 / 0.198	0.098 /0.275	0.070 / 0.208
Different electron density max / min (e Å^3)	0.75 / -0.62	0.62 /-0.39	1.25 / -0.66	1.90 / -1.04

* Recalculated for Mo K_α.

Table A.7: $C_{84}(23)(CF_3)_{14,18}$

Molecule name	84(23)/14-I	84(23)/14-II	84(23)/18-I
Empirical formula	$C_{84}(CF_3)_{14}$	$C_{84}(CF_3)_{14}$	$C_{84}(CF_3)_{18}$
Solvent in the lattice	0.77 $C_6H_5CH_3$	1 $C_6H_5CH_3$	2 $C_6H_5CH_3$
Molar mass (g/mol)	2039.89	2067.11	2435.29
Crystal system	Triclinic	Triclinic	Triclinic
Space group	$P\bar{1}$	$P\bar{1}$	$P\bar{1}$
Unit cell dimensions a (Å), α (°)	13.640(1), 83.18(1)	14.389(1), 93.66(1)	13.517(1), 89.02(1)
b , β	14.322(1), 82.68(1)	15.291(1), 90.06(1)	14.458(1), 88.63(1)
c , γ	20.678(1), 89.05(1)	18.577(1), 98.91(1)	21.981(2), 67.81(1)
Unit cell volume (Å^3)		4029.5(4)	3976.3(7)
Z	2	2	2
Measurement temperature (K)	100(2)	100(2)	100(2)
Data collection (θ) (°) at λ (Å)	2.4-36.3 / 0.9050	2.3-34.9 / 0.8920	2.3-36.8 / 0.8856
Crystal color	red	yellow	yellow
Crystal size (mm)	$0.04 \times 0.02 \times 0.02$	$0.08 \times 0.01 \times 0.01$	$0.03 \times 0.02 \times 0.01$
Crystal density (g/cm^3)	1.703	1.704	2.034
F(000)	2003	2032	2396
Radiation type	Synchrotron	Synchrotron	Synchrotron
hkl-index	$-17 \leq h \leq 17$	$-18 \leq h \leq 18$	$-18 \leq h \leq 18$
	$-17 \leq k \leq 17$	$-19 \leq k \leq 19$	$-17 \leq k \leq 18$
	$-23 \leq l \leq 24$	$-23 \leq l \leq 13$	$-29 \leq l \leq 29$
Data/parameter	11903 / 1290	14698 / 1278	15536 / 1571
Refls. collected / R(int)	37312 / 0.185	49211 / 0.087	48184 / 0.139
Completeness to $\theta = 25°$ (%) *	78.4	82.6	88.7
Goodness of fit	1.232	1.178	1.102
Reliability factor R1 / wR2	0.164 / 0.477	0.096 / 0.266	0.099 / 0.297
Different electron density max / min (e Å^3)	0.68 / -0.49	1.28 / -0.48	0.90 / -0.60

* Recalculated for Mo K_α.

Table A.8: $C_{86}(17)(CF_3)_{10,16}$ and $C_{88}(33)(CF_3)_{16-20}$

Molecule name	86(17)/10-I	86(17)/16-I	88(33)/16-I	88(33)/18-I	88(33)/20-I
Empirical formula	$C_{86}(CF_3)_{10}$	$C_{86}(CF_3)_{16}$	$C_{88}(CF_3)_{16}$	$C_{88}(CF_3)_{18}$	$C_{88}(CF_3)_{20}$
Solvent in the lattice		2 $C_6H_5CH_3$		1.5 $C_6H_5CH_3$	
Molar mass (g/mol)	1722.96	2321.29	2161.04	2437.26	2437.08
Crystal system	Monoclinic	Triclinic	Monoclinic	Triclinic	Triclinic
Space group	$P2_1/c$	$P\bar{1}$	$C2/c$	$P\bar{1}$	$P\bar{1}$
Unit cell dimensions a (Å), α (°)	10.881(1), 90	13.982(1), 74.28(1)	30.813(1), 90	13.632(1), 86.15(1)	16.331(1), 104.81(1)
b , β	29.776(3), 93.328(1)	14.060(1), 83.28(1)	12.548(1), 123.42(1)	13.822(1), 85.84(1)	22.273(1), 90.04(1)
c , γ	20.419(2), 90	23.724(2), 65.56(1)	21.576(1), 90	22.888(1), 74.49(1)	22.835(1), 102.60(1)
Unit cell volume (Å^3)	6604.4(11)	4086.9(5)	6962.8(7)	4139.0(3)	7828.8(6)
Z	4	2	2	2	4
Measurement temperature (K)	100(2)	100(2)	100(2)	100(2)	100(2)
Data collection (θ) (°) at λ (Å)	2.4-35.9 / 0.9050	2.0-36.9 / 0.8434	2.0-36.9 / 0.9050	2.3-36.8 / 0.9050	1.9-36.7 / 0.9050
Crystal color	black	orange	orange	yellow	yellow
Crystal size (mm)	$0.1 \times 0.01 \times 0.01$	$0.04 \times 0.04 \times 0.02$	$0.02 \times 0.02 \times 0.01$	$0.05 \times 0.05 \times 0.01$	$0.04 \times 0.04 \times 0.02$
Crystal density (g/cm^3)	1.733	1.886	2.062	1.956	2.068
F(000)	3384	2288	4224	2394	4752
Radiation type	Synchrotron	Synchrotron	Synchrotron	Synchrotron	Synchrotron
hkl-index	$-12 \leq h \leq 12$	$-17 \leq h \leq 17$	$-36 \leq h \leq 37$	$-17 \leq h \leq 17$	$-19 \leq h \leq 19$
	$-36 \leq k \leq 36$	$-18 \leq k \leq 18$	$-16 \leq k \leq 16$	$-17 \leq k \leq 17$	$-29 \leq k \leq 29$
	$-24 \leq l \leq 24$	$-32 \leq l \leq 32$	$-27 \leq l \leq 27$	$-30 \leq l \leq 30$	$-29 \leq l \leq 29$
Data / parameter	12507 / 1135	17174 / 1479	7279 / 685	15249 / 1624	28568 / 3109
Refls. collected / R(int)	78828 / 0.235	57421 / 0.034	39609 / 0.036	57204 / 0.036	97709 / 0.072
Completeness to $\theta = 25°$ (%) *	96.0	85.9	95.5	88.7	88.5
Goodness of fit	1.618	1.016	1.118	1.015	1.131
Reliability factor R1 / *w*R2	0.194 / 0.496	0.067 / 0.217	0.083 / 0.230	0.061 / 0.165	0.083 / 0.219
Different electron density max / min (e Å^3)	1.17 / -0.65	3.17 / -0.49	0.56 / -0.59	0.64 / -0.40	0.91 / -0.46

* Recalculated for Mo K_α.

Appendix B.

Isolation conditions and UV/VIS specta

Table B.1: Retention time and isolation conditions of trifluoromethylated higher fullerenes

Compound				*Separation step 1*	*Separation step 2*				*Separation step 3*			
Fullerene	**IPR** cage	CF_3 groups	Isomer no.	t_R(min) toluene	t_R(min) mixture	*v*% of the eluent hexane	toluene	Special conditions	t_R(min) mixture	*v*% of the eluent hexane	toluene	Special conditions
82	3	12	x	3.09	7.51	100	0	2 columns				
84	4	12	I	3.01	10.84	100	0					
	11	10	I	16.45	38.04	35	65					
				15.18	19.90	10	90		80.54	10	90	recycling
		12	I	10.89	23.60	40	60					
				10.48	17.90	40	60	40 °C				
		14	I	3.02	16.55	100	0	2 columns				
			II	8.1	7.4	30	70					
			III	6.8	19.0	50	50					
		16	I	8.1	26.6	50	50					
	16	8	I	10-14	41.50	35	65					
		14	I	3.32	11.94	70	30					
	18	10	I	14.31	33.46	35	65					
		12	I	10.7	21.9	90	10					
	22	12	I	3.12	8.9	100		2 columns				
			II	5-10	71.97	80	20		24.52	50	50	
				5-7.5	19.66			gradient,35°C †				
		14	I	3.60	30.35	90	10	2 columns				
			II	8.0	25.3	50	50					
		16	I	3.01	8.41	100	0					
			II	3.32	14.64	30	70					
				3.60	35.09	90	10	2 columns				
			III	6.0	13.5	50	50					
			IV	6.6	7.4	10	90					
		20	I	3.1	4.4	100	0		8.5	100	0	2.3 ml/min
	23	8	I	5.38	27.51	60	40					
		10	I	10.6	28.0	40	60					
		12	I	4.4-5.1	17.6	70	30					
			II	5.7	13.5	50	50					
		18	I	3.60	39.84	10	90	2 columns				
86	17	10	I	19.90	47.17	30	70					
		16	I	3.01	7-15	100	0		13.98	100	0	2 columns
88	33	16	I	3.32	16.85	70	30					
		18	I		47.0	100						
		20	I		8.9	100						

† The composition of eluent varied at 0/15/30 min with toluene v% of 30/40/80.

The separations via HPLC are carried out with the following parameters:

Cosmosil Buckyprep (250 × 10 mm i.d.) column; flow rate 4.6 mL^{-1}; 25°C (if no special mention in the table).

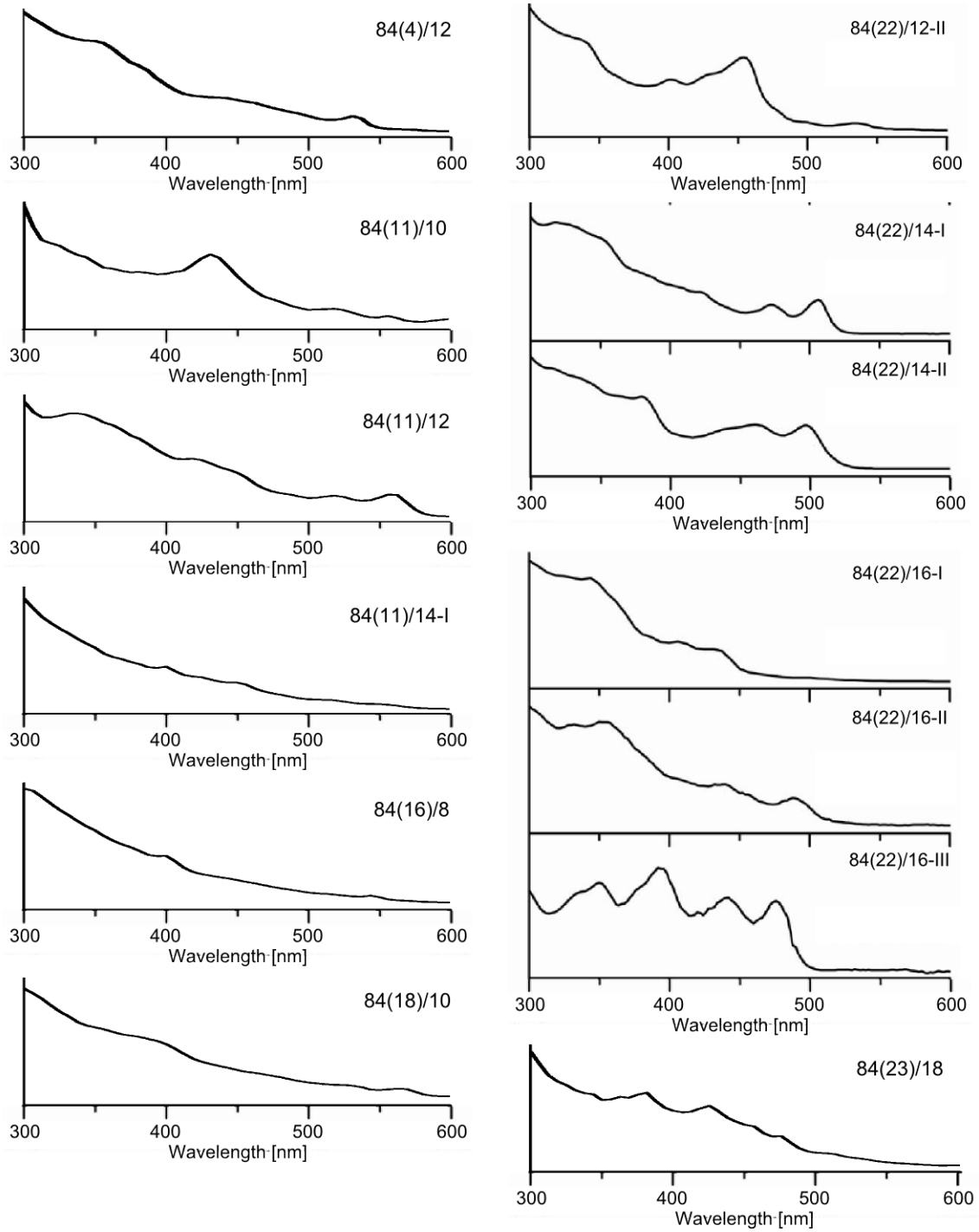

Figure B.1.: UVU/VIS spectra of selected TMF species

Appendix C.

IUPAC lowest locants of Fullerene$(CF_3)_n$

Table C.1: IUPAC lowest locants of the experimentally isolated fullerene(CF_n) compounds

Fullerene	IPR cage	Compound	Reaction product	Sym of compd	Add. pat.	IUPAC lowest locants
84	4	12-I	2*qs*	C_2	p^2,p^2,p^2,p^2	5,12,20,26,31,37,44,50,56,62,70,79
	11	10-I	1*qs*	C_2	p^4,p^4	24,35,44,48,55,59,65,69,74,78
		12-I	1*qr*,2*qr*	C_1	p^6,p^2,p	7,18,21,29,35,50,55,59,67,78,83,84
		14-I	2*qs*	C_1	p^5,p^5,p	7,14,18,21,29,32,50,62,65,71,74,79,82
		14-II	1*qr*, 2*qr*	C_1	p^5,p^5,p	7,18,21,29,35,39,50,55,59,62,65,78,83,84
		14-III	2*qs*	C_1	p^5,p^5,p	7,18,21,29,35,39,50,55,62,65,71,74,83,84
		16-I	2*qs*	C_1	p^9,p^5	7,18,21,29,35,39,50,55,59,62,65,71,74,78,83,84
	16	8-I	2*qr*	C_s	p^7	7,10,13,20,32,41,52,65
		14-I	2*qr*, 2*qs*	C_s	p^3,p^3,p^2,p^2	2,5,11,22,30,43,54,63,68,70,74,79,82,84
	18	10-I	2*qr*	C_s	p^9	2,5,14,19,24,29,33,42,45,54
		12-I	2*qs*	C_s	p^{10},p	2,5,14,19,24,29,33,42,45,54,77,80
	22	12-I	2*qr*	D_2	p^5,p^5	3,6,9,17,29,39,44,54,66,74,81,84
		12-II	2*qr*	C_2	p^5,p^5	2,5,11,19,27,37,44,54,66,74,81,84
		14-I	1*qr*	C_1	p^7,p^5	2,5,11,19,27,37,44,48,54,66,69,74,81,84
		14-II	1*qs*	C_1	p^8,p^4	2,5,11,19,27,37,44,48,62,66,69,74,81,84
		16-I	1*qr*, 2*qs*	C_2		2,5,11,19,27,37,44,48,54,58,66,69,74,77,81,84
		16-II	1*qr*, 2*qs*	C_1		2,5,11,19,27,37,44,48,52,58,66,69,74,77,81,84
		16-III	1*qs*	C_2		2,5,11,19,27,37,48,52,58,62,68,69,74,77,81,84
		16-IV	1*qr*	C_2		2,5,11,19,27,37,48,52,58,62,64,69,72,77,79,82
		20-I	1*qs*	D_2		3,6,9,14,17,22,25,31,35,41,48,52,58,62,66,69,74,77,81,84
	23	8-I	1*qr*	C_2	p^3,p^3	8,14,17,23,27,33,46,58
		10-I	1*qr*	C_1	p^5,p^3	3,6,16,21,28,35,52,56,69,72
		12-I	1*qr*	C_1	p^4,p^3,p,i	3,6,16,21,28,35,41,52,56,69,72,79
		14-I	2*qs*	C_{2v}		3,6,16,21,26,35,41,47,50,56,70,75,79,84
		14-II	2*qs*	C_1		3,6,8,16,21,23,35,41,50,56,70,75,79,84
		18-I	1*qs*	C_{2v}		3,6,9,12,16,21,23,35,38,41,44,50,53,60,65,70,81,83
86	17	10-I	2*qr*	C_{2v}	p^4,p^4	31,42,45,52,56,63,68,72,76,80
		16-I	2*qs*	C_{2v}		2,5,27,31,38,42,45,49,52,56,60,63,68,72,76,80
88	33	16-I	2*qs*	C_{2v}		17,21,25,28,32,36,43,47,55,59,67,70,77,80,84,87
		18-I	1*gs*	C_1		17,19,21,25,28,32,36,41,43,47,55,59,67,70,77,80,84,87
		18-I	1*gs*	C_2		17,19,21,25,28,30,32,36,41,43,47,53,55,59,67,70,77,80,84,87

Appendix D.

Computational results

Following products of the exohedral addition of CF_3 group(s) to $C_{84}(22)$ cage were considered:

1. all possible $C_{84}(22)(CF_3)$ and $C_{84}(22)(CF_3)_2$ diastereomers,
2. two sets of $C_{84}(22)(CF_3)_m$ diastereomers with m = 3 and 4 which were constructed as all possible products of addition of m-th CF_3 group to any sp^2 carbon atoms of each $C_{84}(22)(CF_3)_{m-1}$ isomer of the corresponding isomer set within AM1 energy gap of 50 kJ/mol (without rearrangement of the initial (m-1) CF_3 groups),
3. set of $C_{84}(22)(CF_3)_6$ diastereomers: all possible *para* additions of six CF_3 groups at non-THJ cage carbon atoms with excluding isomers with *ortho*-situated CF_3 groups,
4. sets of $C_{84}(22)(CF_3)_m$ diastereomers with m = 8, 10, and 12: all possible *para* additions of m CF_3 groups at non-THJ cage carbon atoms with excluding isomers with *ortho*-situated CF_3 groups and containing no more than (m-12) *meta*-$C_5(CF_3)_2$ moieties,
5. sets of $C_{84}(22)(CF_3)_m$ diastereomers with m = 14 and 16: satisfy restrictions in (4.) as well as containing the most energetically preferable 3,6,9,17,29,39- or 2,5,11,27,48,69-$C_{84}(22)(CF_3)_6$ diastereomers as a substructure,
6. set of $C_{84}(22)(CF_3)_{20}$ diastereomers: experimentally found isomer 20-I and four isomers constructed by addition of four CF_3 groups to the experimentally found isomers $C_{84}(22)(CF_3)_{16}$, 16-I, 16-II, 16-III, and 16-IV, accompanied by formation of two interpentagonal double bonds.

The total number of isomers as well as the numbers of isomers considered at the AM1, single point DFT (*sp*DFT), and DFT levels of theories are given in the Table D.1. Initially, molecular geometry of the isomers was optimized by TINKER 4.2 molecular mechanic package with MM2 parameter sets[92]. Further, preliminary geometry optimization for these molecules was carried out at the AM1 level of theory with the use of the Firefly QC software (7.1.C,[93] partially based on GAMESS (US) source code[94]). Single point DFT calculation of AM1 optimized geometries and final optimizations at the DFT level of theory were performed with the use of the **PRIRODA** v. 6 software.[95] PBE exchange-correlation functional[90] and an original basis set of triple zeta quality with (11s6p2d)/[6s3p2d] contraction scheme for atoms of the second row were used.

Table D.1: Considered isomer sets at the AM1, single point DFT (*sp*DFT), and DFT levels of theories

$C_{84}(22)(CF_3)_m$	Precursors		Generated	Considered methods			Theoretical
m =	ΔE^{AM1}, [kJ/mol]	Isomer count	isomer count	AM1	spDFT[a]	DFT[a]	Possibility
1	-	-	21	21	21	21	21
2	-	-	903	903	-	20^{50AM1}	903
3	50	20	1439	1439	110^{30AM1}	$17^{20spDFT}$	23821
4	50	278	16985	16985	30^{40AM1}	$17^{20spDFT}$	$\sim 4.8{\cdot}10^5$
Restrictions							
6	*para* addition, excluding THJ sites and *ortho* addition		1314	131430	35^{50AM1}	$14^{30spDFT}$	$\sim 1.0{\cdot}10^8$
8			2228	2228	31^{40AM1}	$28^{30spDFT}$	$\sim 1.1{\cdot}10^{10}$
10	+ no more than (m-12)*meta*-$C_5(CF_3)_2$ patterns		2451	2451	18^{50AM1}	$18^{50spDFT}$	$\sim 6.9{\cdot}10^{11}$
12	+ no more than (m-12)*meta*-$C_5(CF_3)_2$ patterns		433	433	-	13^{100AM1}	$\sim 2.8{\cdot}10^{13}$
14	+ $C_{84}(22)(CF_3)_6$-1 or 2 substructures		887	887	30^{60AM1}	$9^{30spDFT}$	$\sim 7.9{\cdot}10^{14}$
16	+ $C_{84}(22)(CF_3)_6$-1 or 2 substructures		4892	4892	42^{50AM1}	$17^{30spDFT}$	$\sim 1.6{\cdot}10^{16}$

[a] Subscribes denote energy gap of selected isomers (kJ/mol) at given level of theory

Table D.2: 84(22)/1

Isomer number	IUPAC lowest locants	Relative formation energy [kJ/mol]
1-1	9	0
1-2	11	2.0
1-3	31	2.2
1-4	30	3.7
1-5	25	3.8
1-6	14	6.0
1-7	3	8.3
1-8	29	9.2
1-9	2	9.3
1-10	27	11.9
1-11	13	19.8
1-12	12	22.7
1-13	7	25.8
1-14	26	27.5
1-15	8	31.2
1-16	23	44.3
1-17	24	50.2
1-18	10	65.3
1-19	1	65.3
1-20	28	68.6
1-21	32	69.4

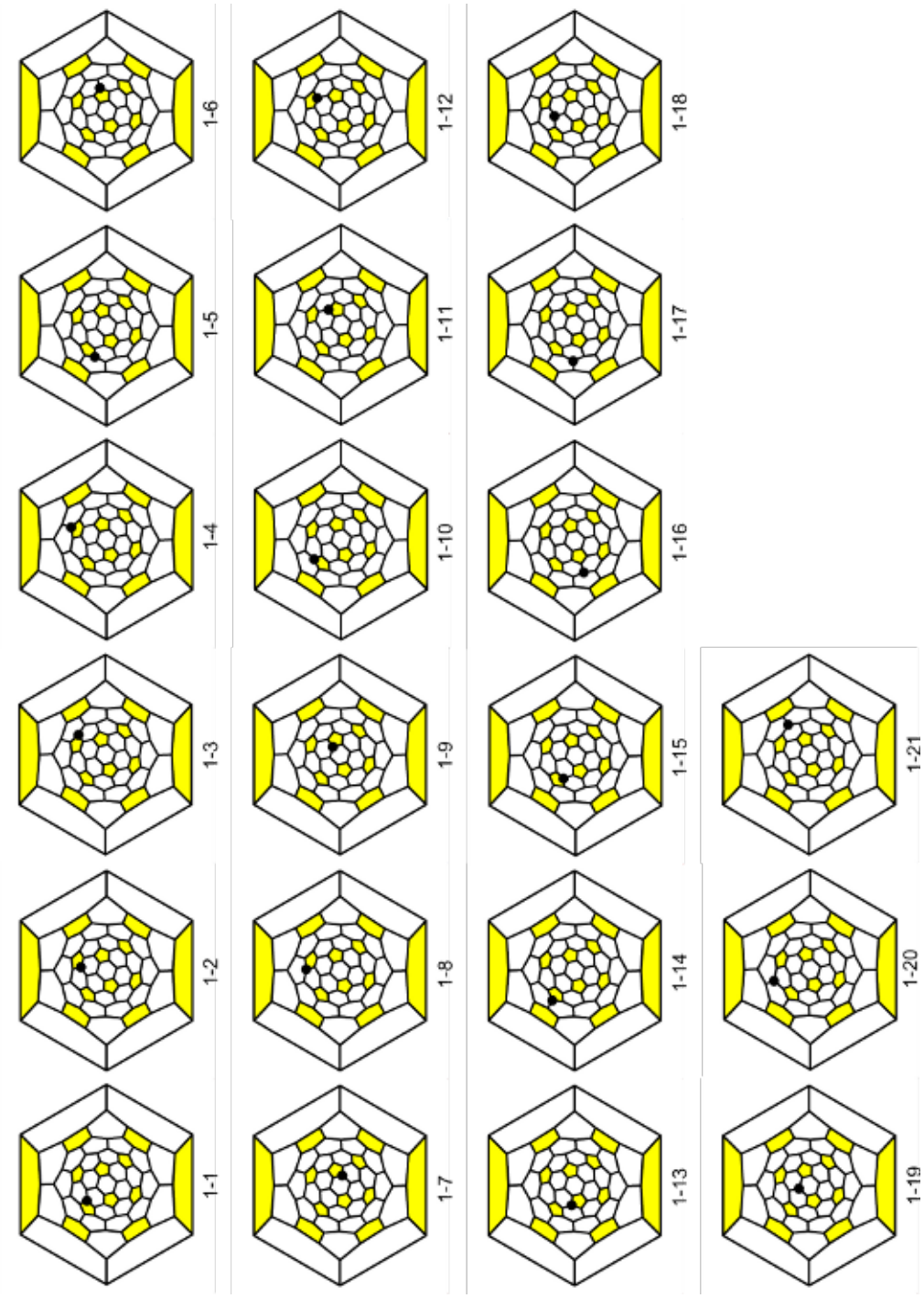

Figure D.1.: 84(22)/1

Table D.3: 84(22)/2

Isomer number	IUPAC lowest locants	Relative formation energy [kJ/mol]
2-1	9,29	0
2-2	30,53	0.2
2-3	14,35	4.6
2-4	3,6	5.4
2-5	2,5	5.6
2-6	11,27	13.9
2-7	31,52	17.1
2-8	9,53	25.4
2-9	11,53	27.3
2-10	9,31	28.8
2-11	12,35	33.4
2-12	11,29	44.3
2-13	8,23	53,4
2-14	11,31	63.2
2-15	12,13	68.1

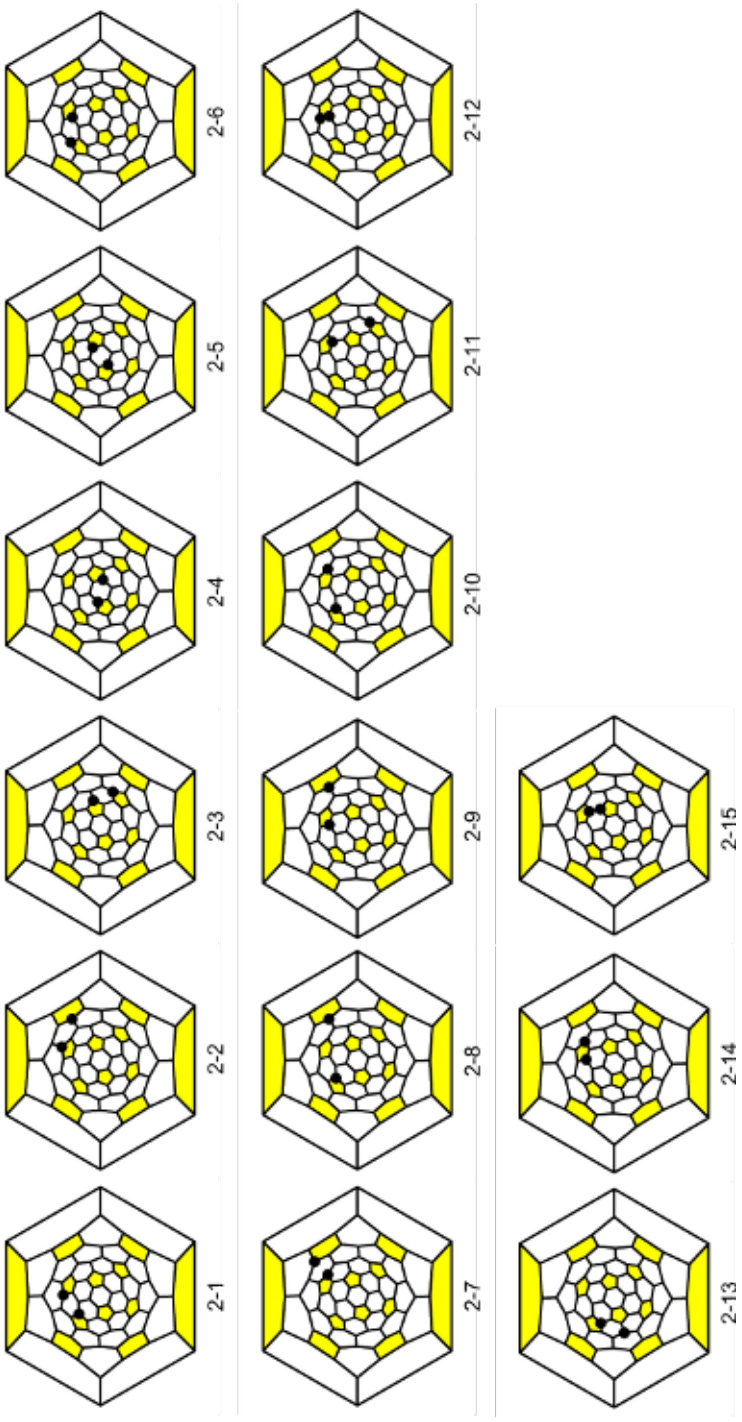

Figure D.2.: 84(22)/2

Table D.4: 84(22)/3

Isomer number	IUPAC lowest locants	Relative formation energy [kJ/mol]
3-1	3,6,9	0
3-2	14,31,35	4.4
3-3	2,5,11	5.5
3-4	3,17,39	7.2
3-5	9,19,29	9.2
3-6	11,27,48	9.4
3-7	9,17,29	11.7
3-8	3,6,66	12.0
3-9	9,29,41	12.3
3-10	2,5,66	12.5
3-11	9,29,40	13.7
3-12	14,35,56	13.8
3-13	9,40,43	15.8
3-14	9,29,66	17.2
3-15	25,30,53	17.9
3-16	30,40,43	18.5
3-17	3,9,29	19.7

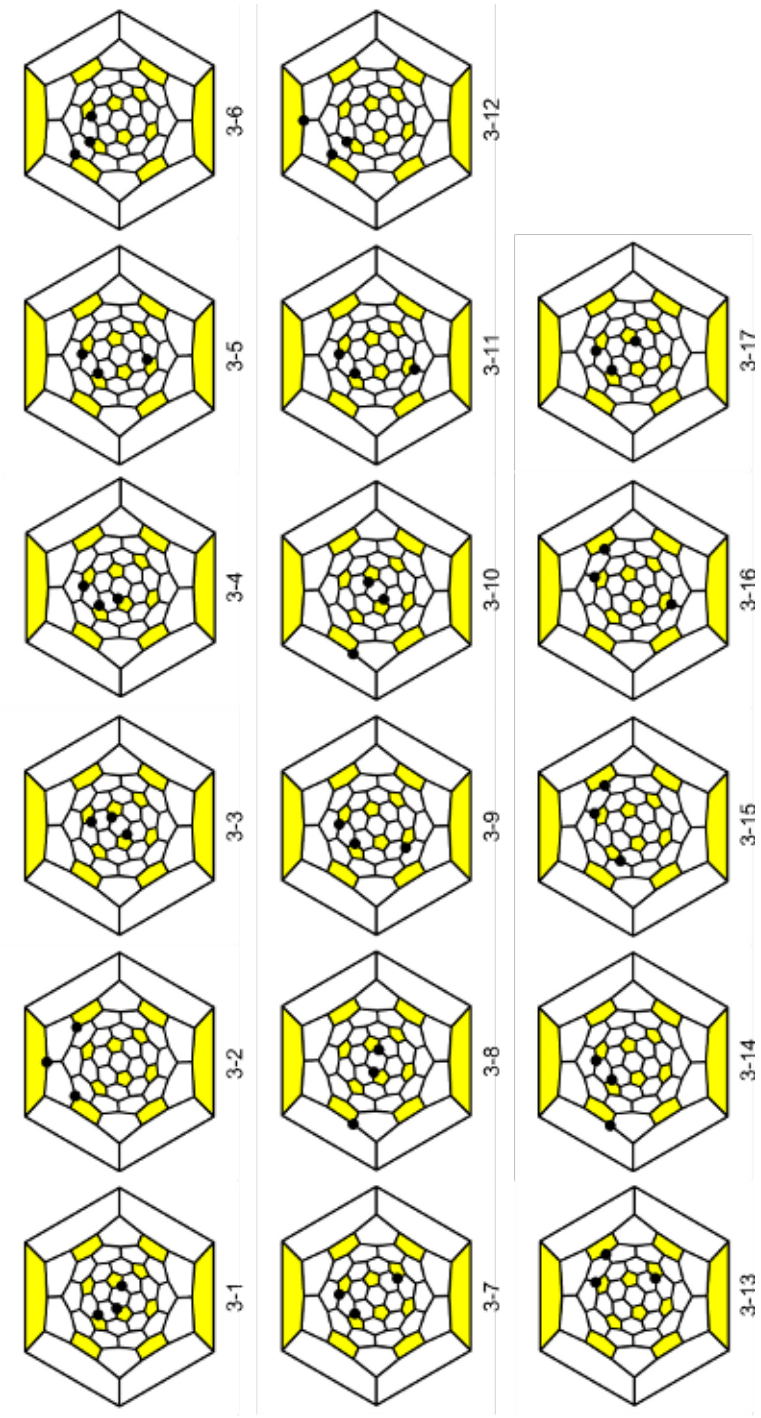

Figure D.3.: 84(22)/3

Table D.5: 84(22)/4, 6

Isomer number	IUPAC lowest locants	Relative formation energy [kJ/mol]
4-1	3,6,9,29	0
4-2	11,27,48,69	6.9
4-3	9,17,29,39	7.8
4-4	9,29,40,43	11.3
4-5	14,31,35,52	11.4
4-6	9,29,54,74	12.2
4-7	30,40,43,53	12.4
4-8	9,29,44,66	13.1
4-9	2,5,30,53	13.3
4-10	9,19,29,37	13.9
4-11	2,5,44,66	15.8
4-12	2,5,11,27	16.2
4-13	3,6,81,84	17.2
4-14	9,29,46,64	18.3
4-15	3,6,44,66	18.3
4-16	3,6,9,53	20.6
4-17	2,3,17,39	50.4
4-18	8,23,44,66	67.5
6-1	3,6,9,17,29,39	0
6-2	2,5,11,27,48,69	12.7
6-3	3,6,9,29,58,77	15.3
6-4	9,19,29,37,58,77	17.2
6-5	14,31,35,48,52,69	17.5

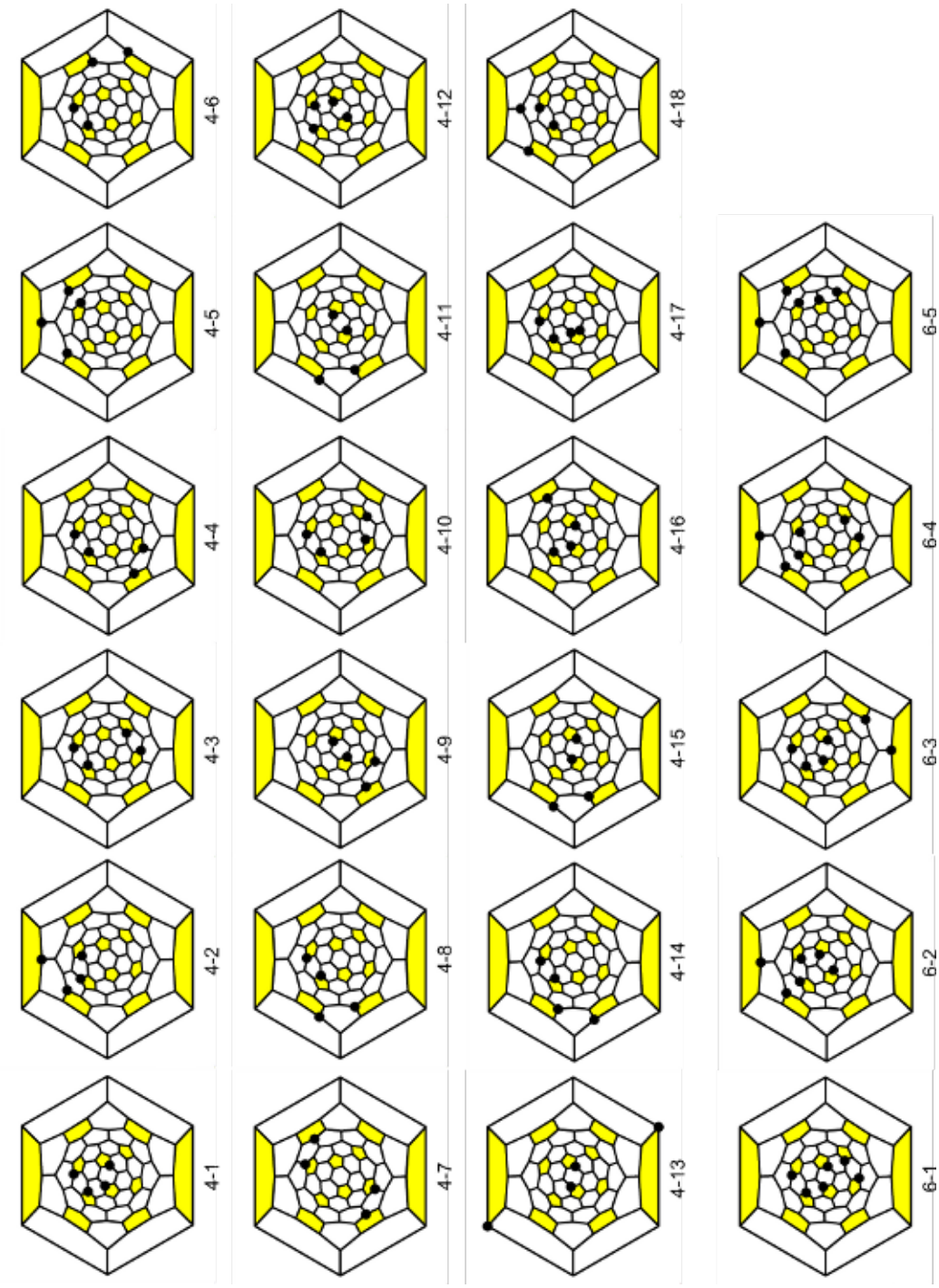

Figure D.4.: 84(22)/4, 6

Table D.6: 84(22)/8

Isomer number	IUPAC lowest locants	Relative formation energy [kJ/mol]
8-1	3,6,9,17,29,39,46,64	0
8-2	3,6,9,17,29,39,44,66	0.4
8-3	2,5,11,27,48,54,69,74	1.8
8-4	3,6,9,41,58,62,77	1.9
8-5	2,5,44,54,66,74,81,84	1.9
8-6	3,6,9,17,29,39,81,84	3.4
8-7	2,5,11,27,40,43,48,69	4.9
8-8	3,6,9,29,54,74,81,84	5.9
8-9	2,5,11,27,44,66,81,84	9.7
8-10	3,6,9,29,44,66,81,84	9.8
8-11	9,14,29,35,44,56,66,72	10.3
8-12	3,6,9,29,46,54,64,74	10.8
8-13	3,6,9,17,29,41,62,77	11.2
8-14	2,5,11,19,27,37,48,69	11.7
8-15	3,6,9,29,44,58,66,77	12.6
8-16	2,5,11,27,54,74,81,84	13.1
8-17	2,5,11,19,27,37,81,84	14.6
8-18	2,5,11,19,27,37,44,66	15.0
8-19	9,14,29,35,40,43,56,72	15.7
8-20	14,22,25,31,35,48,52,69	24.9

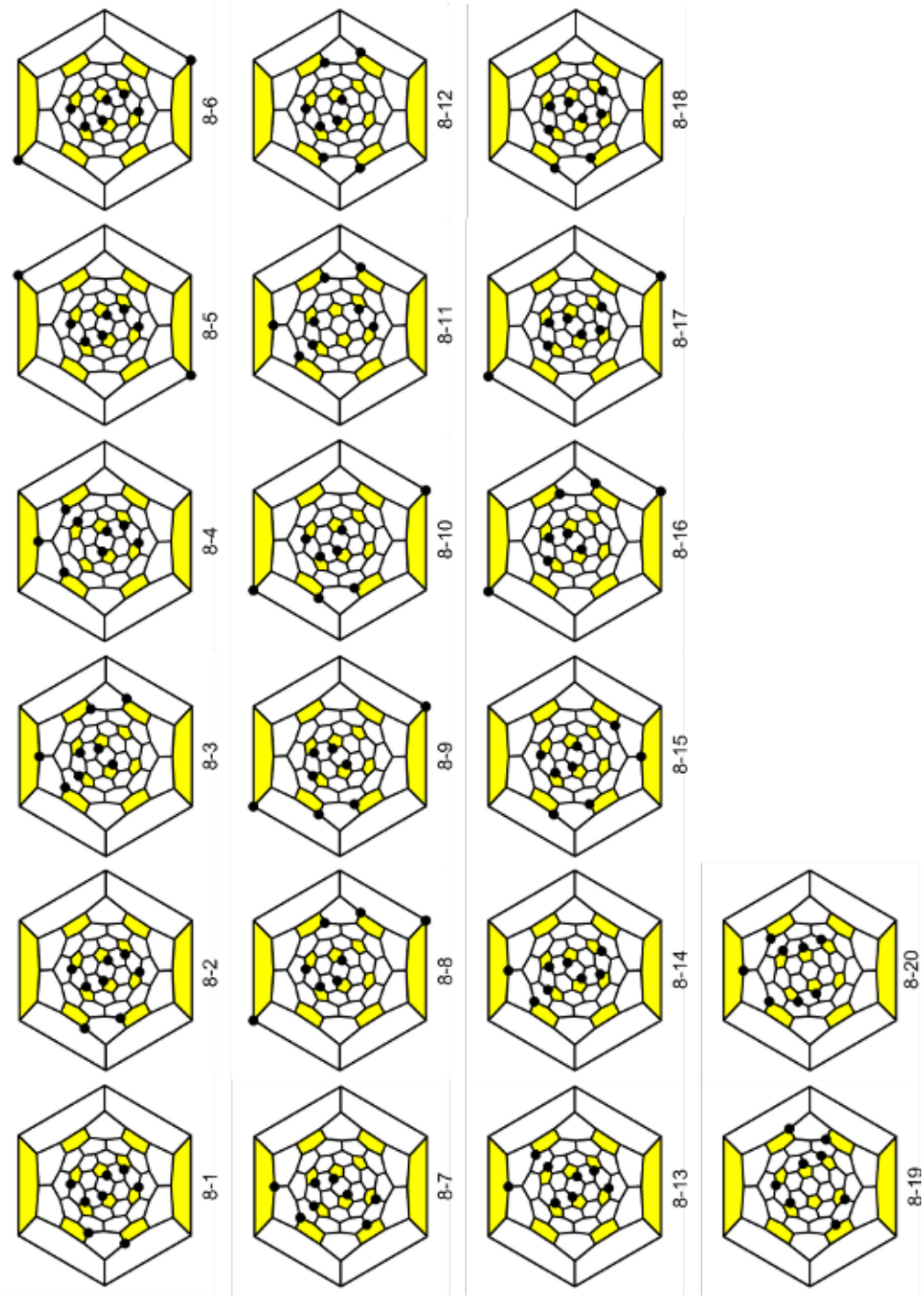

Figure D.5.: 84(22)/8

Table D.7: 84(22)/10, 12

Isomer number	IUPAC lowest locants	Relative formation energy [kJ/mol]
10-1	2,5,11,19,27,37,48,58,69,77	0
10-2	2,5,11,27,44,54,66,74,81,84	1.1
10-3	3,6,9,17,29,39,44,66,81,84	1.5
10-4	2,5,11,19,27,37,44,58,66,77	8.0
10-5	2,5,11,19,27,37,44,66,81,84	8.1
10-6	3,6,9,17,29,39,44,56,66,72	10.2
10-7	2,5,11,27,40,43,48,54,69,74	10.3
10-8	2,5,11,19,27,37,44,54,66,74	15.4
10-9	3,6,9,17,29,41,56,62,72,77	17.9
10-10	3,6,9,17,29,39,44,54,66,74	19.5
10-11	3,6,9,17,29,39,46,56,64,72	20.9
10-12	14,22,25,31,35,41,48,52,62,69	27.6
12-1	2,5,11,19,27,37,44,54,66,74,81,84	0
12-2	3,6,9,17,29,39,44,54,66,74,81,84	2.3
12-3	2,5,11,19,27,37,48,52,58,62,69,77	18.9
12-4	2,5,11,27,35,40,43,48,56,72,79,82	27.0
12-5	2,5,11,19,25,37,46,58,62,72,77,82	27.4
12-6	3,6,9,17,29,39,44,56,66,72,81,84	42.7
12-7	2,5,9,19,29,37,44,54,66,74,81,84	44.0
12-8	14,22,25,31,35,41,48,52,58,62,69,77	57.7

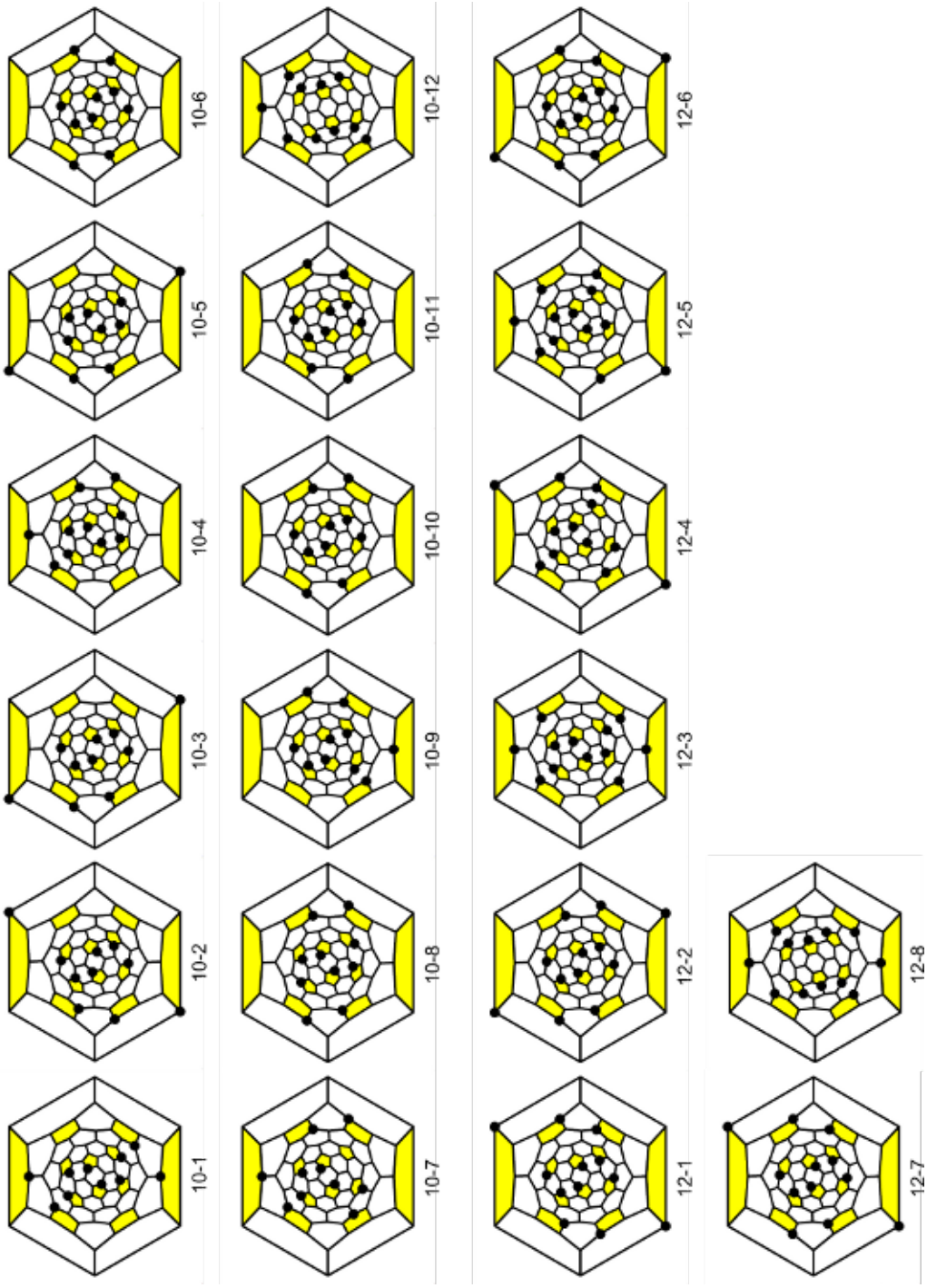

Figure D.6.: 84(22)/10, 12

Table D.8: 84(22)/14, 16

Isomer number	IUPAC lowest locants	Relative formation energy [kJ/mol]
14-1	2,5,11,19,27,37,44,48,52,66,69,74,81,84	0
14-2	2,5,11,19,27,37,44,48,54,66,69,74,81,84	4.7
14-3	2,5,11,19,27,37,48,52,58,62,66,69,77,81	13.5
14-4	2,5,11,19,27,37,48,52,58,62,64,69,77,79	14.6
14-5	2,5,11,14,19,27,31,35,48,56,64,72,79,82	15.5
14-6	2,5,11,19,27,37,44,48,52,58,66,69,77,81	18.6
14-7	2,5,11,14,27,31,35,40,43,48,56,72,79,82	18.9
14-8	2,5,11,14,19,25,31,35,46,56,64,72,79,82	20.3
16-1	2,5,11,19,27,37,44,48,52,58,66,69,74,77,81,84	0
16-2	2,5,11,19,27,37,48,52,58,62,66,69,74,77,81,84	7.7
16-3	2,5,11,14,19,22,25,31,35,41,46,56,64,72,79,82	7.7
16-4	2,5,11,19,27,37,44,48,54,58,66,69,74,77,81,84	13.5
16-5	2,5,11,14,19,27,31,35,48,52,56,64,69,72,79,82	19.0
16-6	2,5,11,14,19,25,31,37,46,58,62,64,72,77,79,82	19.3
16-7	2,5,11,19,25,27,37,46,48,52,58,62,64,69,77,79	19.8
16-8	2,5,11,14,19,25,27,31,35,46,48,56,64,72,79,82	20.7

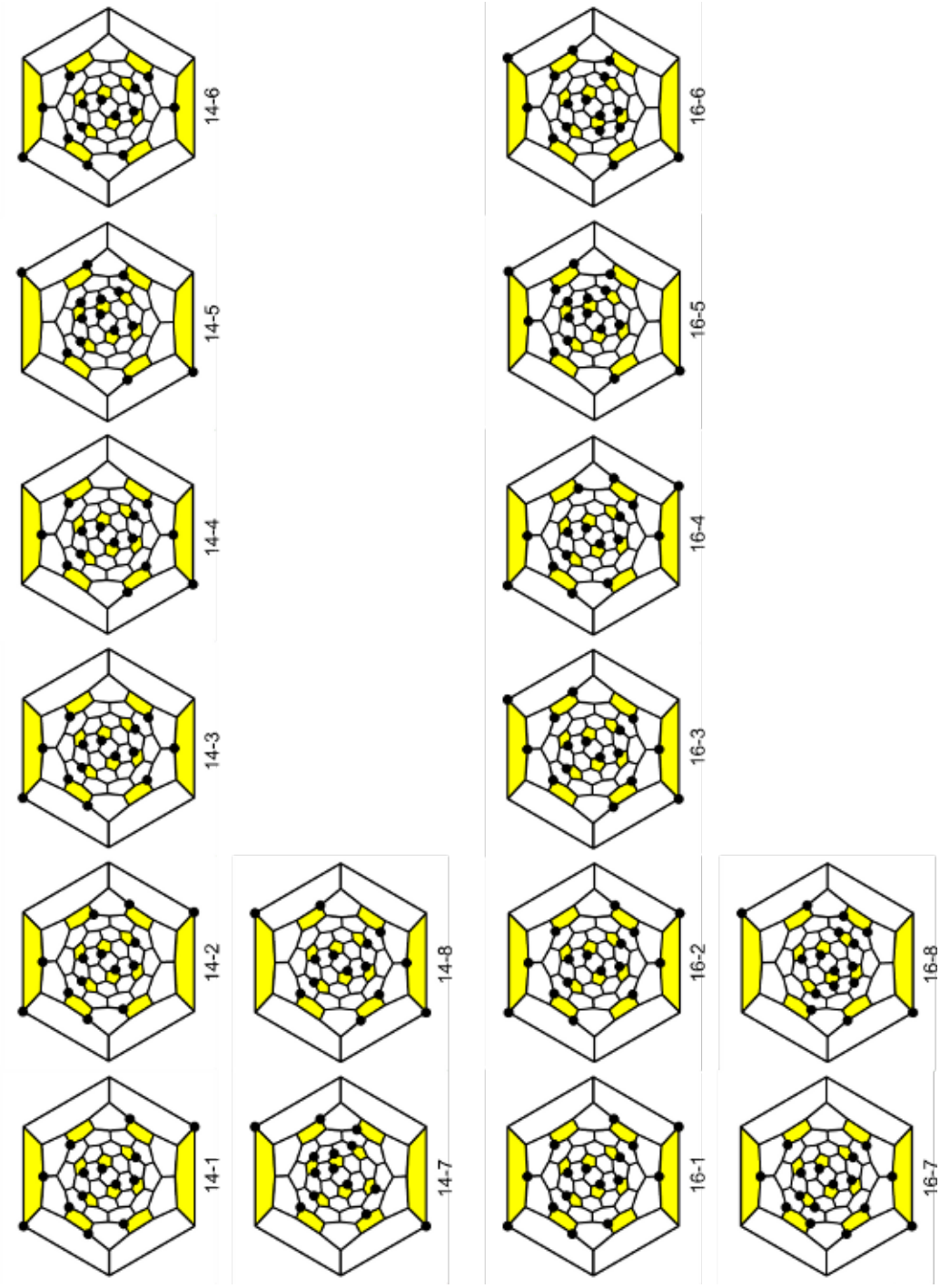

Figure D.7.: 84(22)/14, 16

Table D.9: 84(22)/20

Isomer number	IUPAC lowest locants	Relative formation energy [kJ/mol]
20-1	2,5,11,14,19,22,27,31,37,41,44,48,52,58,66,69,74,77,81,84	0
20-2	2,5,11,14,19,22,27,31,37,41,44,48,54,58,66,69,74,77,81,84	7.2
20-3	2,5,11,14,19,22,25,31,35,41,46,52,56,62,64,69,72,77,79,82	40.3
20-4	3,6,9,14,17,22,25,31,35,41,48,52,58,62,66,69,74,77,81,84	69.2
20-5	2,5,11,14,19,22,27,31,37,41,48,52,58,62,66,69,74,77,81,84	83.9

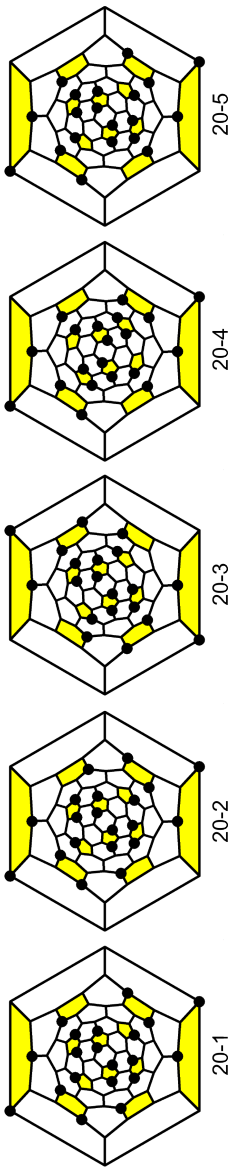

Figure D.8.: 84(22)/20

Table D.10: 84(23)/10

Isomer number	IUPAC lowest locants	Relative formation energy [kJ/mol]	HOMO-LUMO gap [eV]
10-1	3,6,16,21,28,35,52,56,69,72	0	1.3
10-2	3,6,16,21,35,41,56,75,79,84	0	0.8
10-3	3,6,16,21,35,4156,69,72,79	10.3	1.1
10-4	3,6,16,21,28,35,41,52,56,79	13.0	1.1
10-5	3,6,16,28,35,52,56,69,72,79	34.4	0.9
10-6	3,6,16,21,28,35,41,52,56,72	44.7	0.4
10-7	3,6,16,21,35,41,52,56,72,79	76.9	0.3
10-8	3,6,16,21,28,35,52,69,72,79	100.4	0
10-9	3,6,16,21,28,41,52,69,72,79	129.0	0.7
10-10	3,6,16,21,28,35,41,52,69,72	138.0	0.6

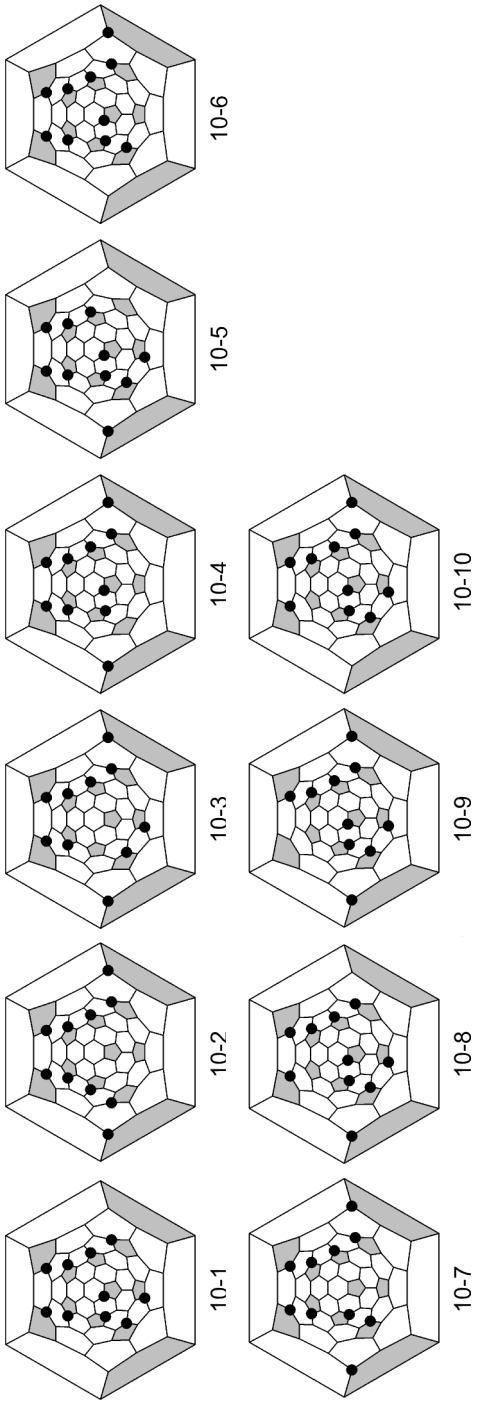

Figure D.9.: 84(23)/10

Table D.11: 84(23)/12

Isomer number	IUPAC lowest locants	Relative formation energy [kJ/mol]	HOMO-LUMO gap [eV]
12-1	3,6,16,21,28,35,41,52,56,69,72,79	0	1.4
12-2	3,6,16,21,26,35,41,47,56,75,79,84	19.8	0.61
12-3	3,6,16,21,28,35,41,52,56,63,69,72	21.3	1.36
12-4	3,6,16,21,28,35,38,41,52,56,69,72	23.4	1.60
12-5	3,6,16,26,31,35,40,44,47,53,62,83	23.6	1.28
12-6	3,6,16,26,31,35,40,44,47,50,53,62	36.9	1.46
12-7	3,6,16,26,31,35,40,44,47,53,62,73	40.0	1.38
12-8	3,6,8,16,23,27,35,46,56,75,79,84	44.3	0.96
12-9	3,6,16,21,26,35,47,50,56,70,75,84	49.4	0.95
12-10	3,6,8,16,23,31,35,50,53,70,79,84	68.5	0.85
12-11	3,6,16,21,28,35,41,52,56,69,72,81	71.4	0.47
12-12	3,6,16,26,31,35,40,44,47,53,62,84	74.5	0.57
12-13	3,6,9,16,26,31,35,40,44,47,53,62	76.3	0.65
12-14	1,14,17,33,44,50,53,58,65,70,81,83	93.8	0.42
12-15	3,6,8,16,21,23,35,41,56,75,79,81	94.7	0.30
12-16	1,14,33,38,44,50,53,60,65,70,79,84	98.2	0.48
12-17	3,6,9,26,38,44,47,52,60,65,72,79	103.9	0.23
12-18	3,6,16,21,28,35,41,52,56,62,69,72	107.9	0.04
12-19	3,6,12,16,26,31,35,40,44,47,53,62	115.7	0.06
12-20	3,6,16,26,31,35,40,44,47,53,62,72	123.8	0.09
12-21	3,6,16,21,26,31,35,40,44,47,53,62	126.0	0.11
12-22	3,6,16,18,26,31,35,40,44,47,53,62	133.1	0.28
12-23	3,6,16,26,31,35,40,44,47,53,59,62	146.2	0.08

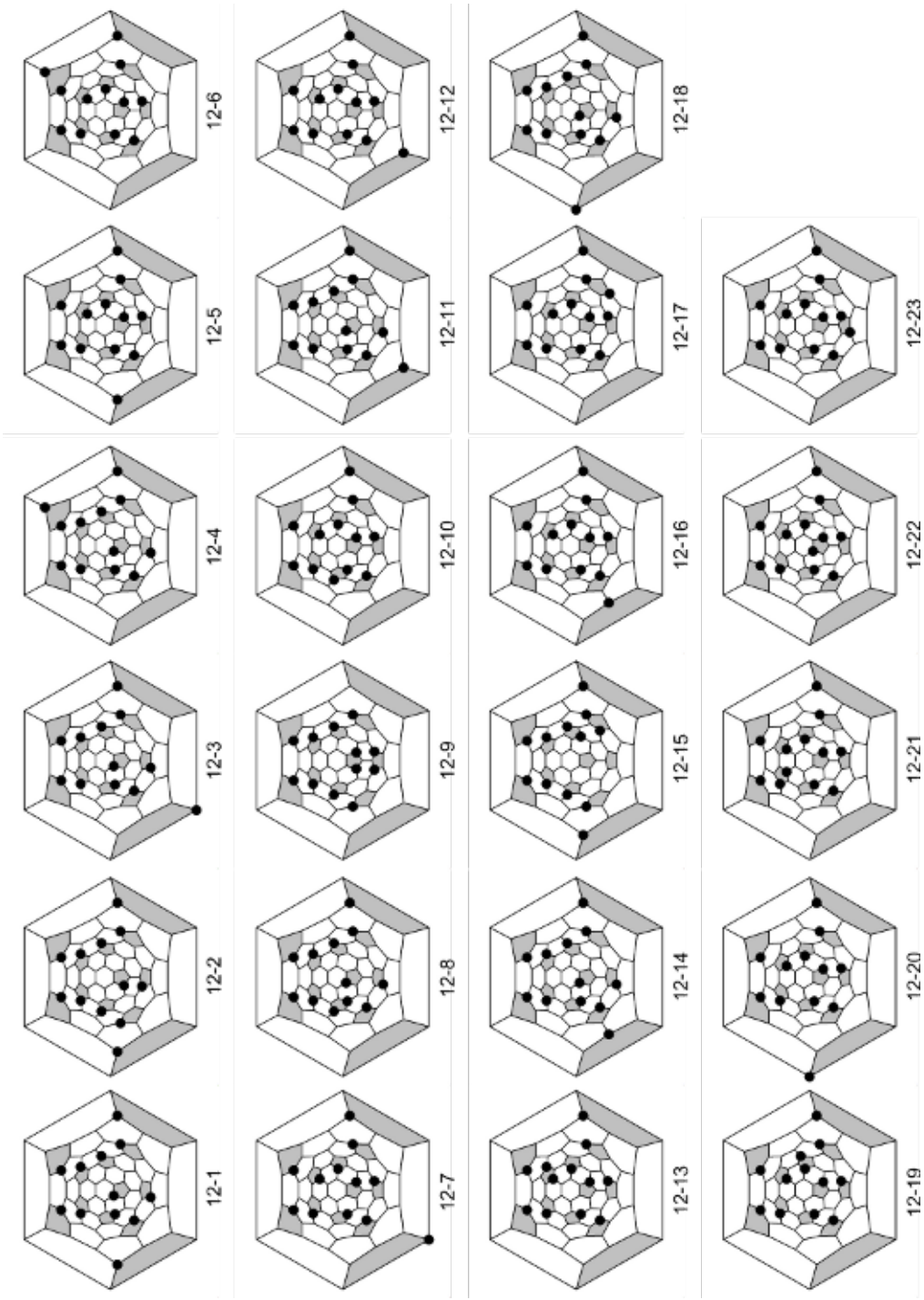

Figure D.10.: 84(23)/12

Table D.12: 84(11)/10-16

Isomer number	IUPAC lowest locants	Relative formation energy [kJ/mol]	HOMO-LUMO gap [eV]
10-1	24,35,44,48,55,59,65,69,74,78	0	1.28
10-2	7,18,21,29,39,50,62,65,83,84	30.6	0.85
10-3	7,18,21,35,39,55,62,65,83,84	37.0	1.02
10-4	7,18,21,29,35,39,50,55,62,65	67.9	0.36
12-1	7,18,21,29,35,50,55,59,67,78,83,84	0	1.55
12-2	7,18,21,29,35,39,50,55,62,65,83,84	4.5	1.44
12-3	7,18,21,29,35,39,50,55,62,65,71,74	20.3	0.84
12-4	7,18,21,29,35,39,50,55,59,62,65,78	84.5	0.64
14-1	7,18,21,29,35,39,50,55,62,65,71,74,83,84	0	1.69
14-2	7,14,18,21,29,32,39,50,62,65,71,74,79,82	6.8	1.53
14-3	7,18,21,29,35,39,50,55,59,62,65,78,83,84	8.5	1.58
16-1	7,18,21,29,35,39,50,55,59,62,65,71,74,78,83,84		

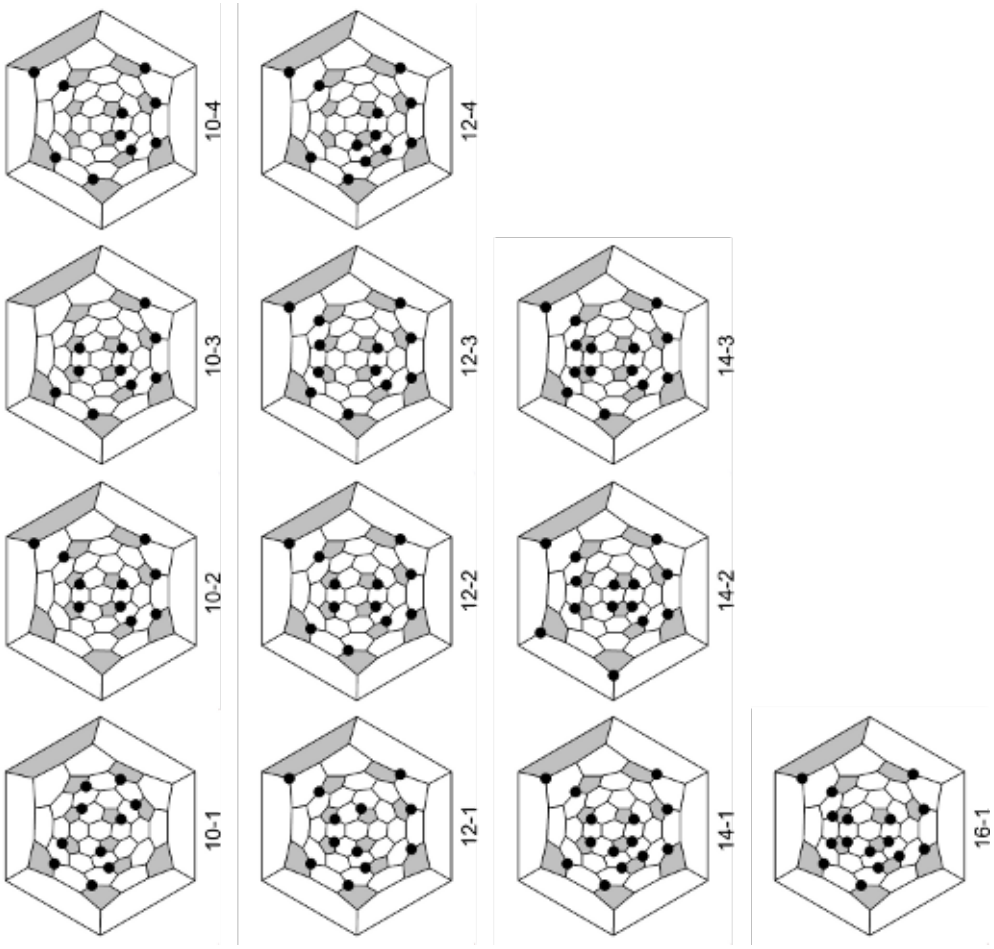

Figure D.11.: 84(11)/10-16

Table D.13: Spiral code, relative energies E [kJ/mol] and HOMO-LUMO gap Δ [eV] of fullerene cage isomers

Fullerene	Cage	Spiral code	E	Δ
84	4	1,7,9,11,14,22,27,30,35,39,41,43	61.25	2.13
	11	1,7,9,12,20,24,26,28,30,33,36,44	35.10	1.64
	16	1,7,9,13,20,22,25,28,30,34,37,44	33.64	1.78
	18	1,7,9,13,20,22,25,28,34,37,39,41	65.65	1.96
	22	1,7,10,13,18,22,25,27,31,34,38,44	0.33	1.98
	23	1,7,10,13,18,22,25,27,31,38,41,43	0	2.05
86	17	1,7,9,12,20,24,26,29,33,38,40,43		
88	33	1,7,9,12,21,24,26,29,38,41,43,45		

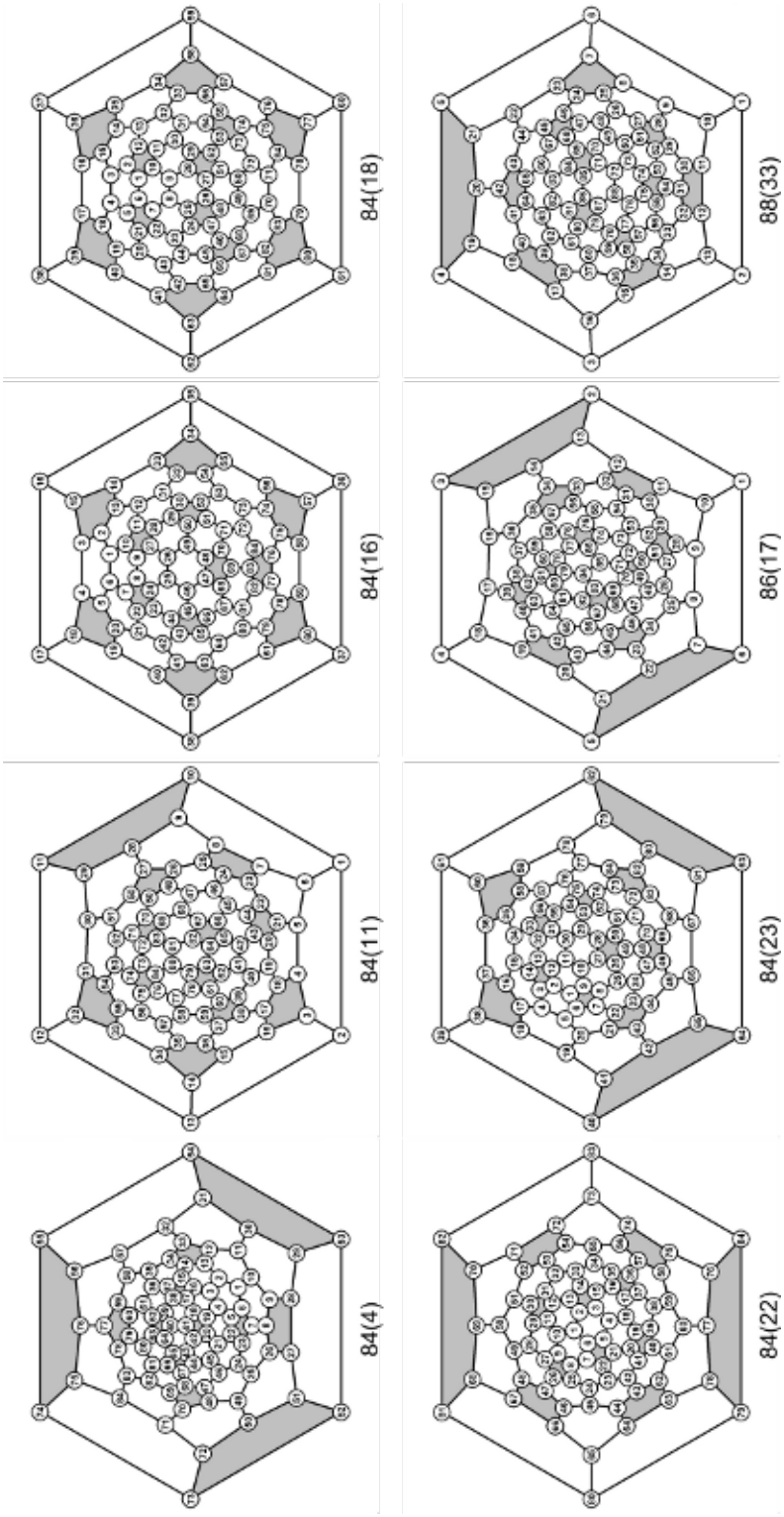

Figure D.12.: Schlegel diagram of fullerenes

Table D.14: Spiral code, relative energies E [kJ/mol] and HOMO-LUMO gap Δ [eV] of fullerene C_{86} cage isomers

Cage	Symmetry	Spiral code	E	Δ
2	C2	1,7,9,11,13,24,28,32,37,39,41,43	122.30	2.10
3	C2	1,7,9,11,13,25,29,31,34,38,43,45	87.24	1.12
4	C2	1,7,9,11,14,22,28,31,34,37,39,43	92.13	0.90
6	C2	1,7,9,11,14,23,28,31,33,37,39,43	66.40	0.99
8	Cs	1,7,9,11,22,24,27,29,32,37,40,43	152.93	0.82
14	C2	1,7,9,12,14,21,28,31,35,37,39,42	93.26	0.98
15	Cs	1,7,9,12,14,28,30,32,34,36,38,45	94.94	1.07
16	Cs	1,7,9,12,20,24,26,28,34,39,41,44	27.53	1.91
17	C2	1,7,9,12,20,24,26,29,33,38,40,43	0	1.56

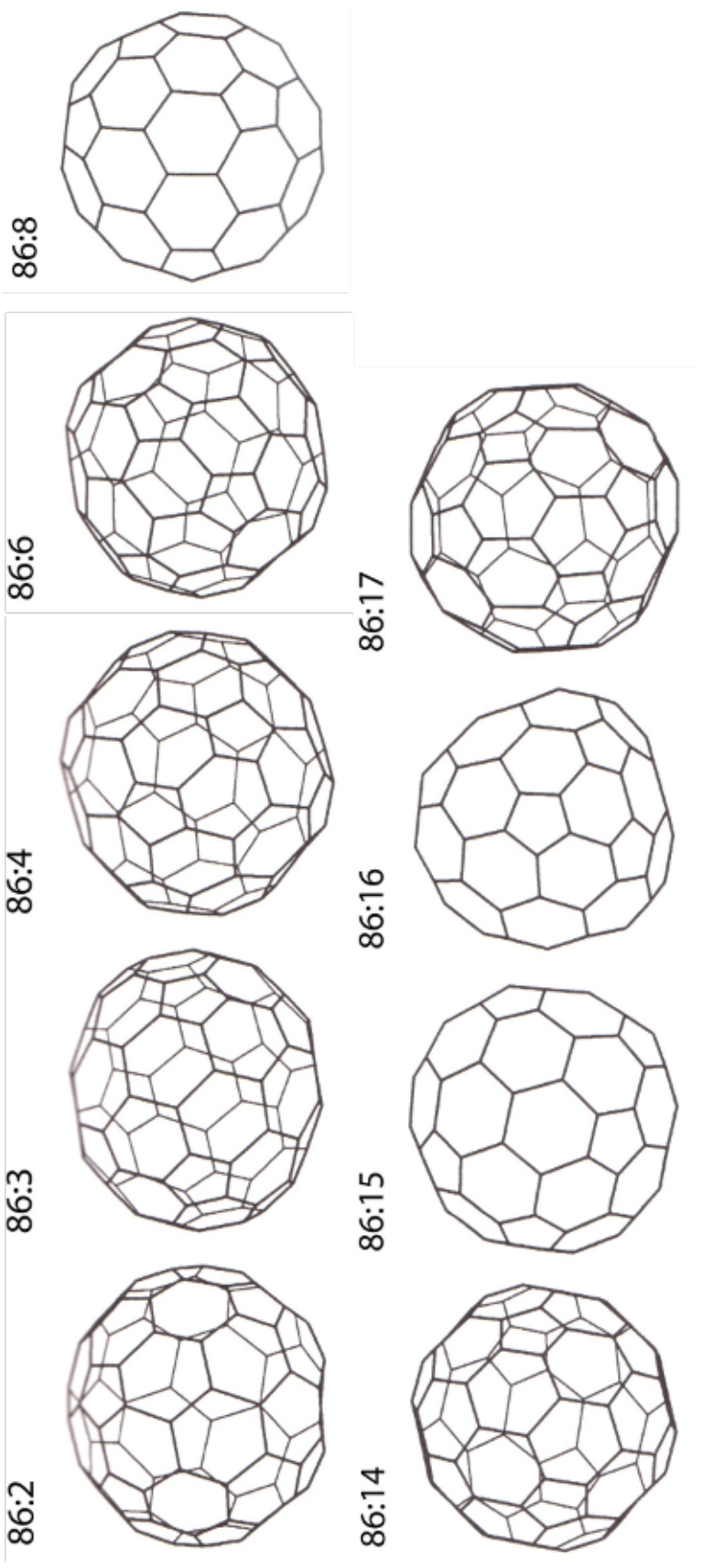

Figure D.13.: Cage isomers of fullerene C_{86}

Abbreviations and acronyms

AU	Absorption unit
AM1	semi-empirical Austin Model 1
BESSY	Berlin Electron Storage Ring Society for Synchrotron Radiation
B-LYP	Becke-Lee, Yang, Parr; related to the exchange-correlation energy functional in DFT
CCD	Charge coupled device
CHCA	α-Cyano-4-hydroxycinnamic acid
CV	Cyclic voltammetry
DCB	Dichlorobenzene
DCTB	*trans*-2-[3-(4-Butylphenyl)-2-methyl-2-propenylidene]malononitrile
DFT	Density functional theory
DHB	2,5-Dihydroxybenzonic acid
ESR	Electron spin resonance
FID	Flame ionization detector
FTICR	Fourier transfer ion cyclotron resonance
HIV	Human immunodeficiency virus
HOMO	Highest occupied molecular orbital
HPLC	High performance liquid chromatography
ICCB	Interpentagonal C-C bonds
IPR	Isolated pentagon rules
IUPAC	International Union of Pure and Applied Chemistry
LUMO	Lowest occupied molecular orbital
MALDI-TOF-MS	Matrix-assisted laser desorption ionization time-of-flight mass spectrometry
MP	Mobile phase
NMR	Nuclear magnetic resonance
NP	Normal phase
ODS	Octadecylsilica
PA	Picolinic acid
PBE	Perdew, Burke, Ernzerhof; related to the exchange-correlation energy functional in DFT
PDA	Photodiode array
PHJ	Pentagon-hexagon-hexagon junction
PTFE	Polytetrafluoroethylene
RP	Reversed phase
SP	Stationary phase
TFA	Trifluoroacetic acid
THJ	Triple hexagon junction
3D-projections	Three-dimensional projections
TMF	Trifluoromethylated fullerenes derivatives
2D-projections	Two-dimensional projections

UV/VIS	Ultraviolet/visible
TZP	Triple zeta basis sets with polarization functions

Bibliography

[1] N. B. Tamm, L. N. Sidorov, E. Kemnitz, and S. I. Troyanov, Chem. Eur. J. **15**, 10486 (2009).

[2] I. E. Kareev, A. A. Popov, I. V. Kuvychko, N. B. Shustova, S. F. Lebedkin, V. P. Bubnov, O. P. Anderson, K. Seppelt, S. H. Strauss, and O. V. Boltalina, J. Am. Chem. Soc. **130**, 13471 (2008).

[3] I. E. Kareev, I. V. Kuvychko, N. B. Shustova, S. F. Lebedkin, V. P. Bubnov, O. P. Anderson, A. A. Popov, O. B. Boltalina, and S. H. Strauss, Angew. Chem. Int. Ed. **47**, 6204 (2008).

[4] S. I. Troyanov and N. B. Tamm, Crystallogr. Rep. **54**, 598 (2009).

[5] S. I. Troyanov and N. B. Tamm, Chem. Commun. , 6035 (2009).

[6] D. R. Huffman, Phys. Today **11**, 22 (1991).

[7] W. Kraetschmer, Nanoscale **3**, 2485 (2011).

[8] W. Kraetschmer, L. D. Lamb, K. Fostiropoulos, and D. R. Huffman, Nature **347**, 354 (1990).

[9] A. Hirsch, *The chemistry of the fullerenes*, Thieme, 1994.

[10] H. W. Kroto, J. R. Heath, S. C. O'Brien, R. F. Curl, and R. E. Smalley, Nature **318**, 162 (1985).

[11] R. Ettl, I. Chao, F. Diederich, and R. L. Whetten, Nature **353**, 149 (1991).

[12] F. Diederich, R. L. Whetten, C. Thilgen, R. Ettl, I. Chao, and M. M. Alvarez, Science **254**, 1768 (1991).

[13] K. Kikuchi, N. Nakahara, T. Wakabayashi, S. Suzuki, H. Shiromaru, Y. Miyake, K. Saito, O. Ikemoto, M. Kainosho, and Y. Achiba, Nature **357**, 142 (1992).

[14] D. E. Manolopoulos, P. Fowler, R. Taylor, H. W. Kroto, and D. W. Walton, J. Chem. Soc. Faraday Trans **88**, 3117 (1992).

[15] P. W. Fowler and D. E. Manolopoulos, *An atlas of fullerenes*, Dover Publication, Inc., 2007.

[16] H. W. Kroto, Nature **329**, 529 (1987).

[17] F. Cozzi, W. H. Powell, and C. Thilgen, Pure Appl. Chem. **77(5)**, 843 (2005).

[18] A. D. Hayment, Chem. Phys. Lett. **122**, 421 (1985).

[19] R. C. Haddon, L. E. Brus, and K. Raghavechari, Chem. Phys. Lett. **125**, 459 (1986).

[20] S. Stapathy, Chem. Phys. Lett. **130**, 545 (1986).

[21] P. D. Hale, J. Am. Chem. Soc. **108**, 6087 (1986).

[22] S. Larsson, A. Volosov, and A. Rosen, Chem. Phys. Lett. **137**, 501 (1987).

[23] Q. Xie, E. Perez-Cordero, and L. Echegoyen, J. Am. Chem. Soc. **114**, 3978 (1992).

[24] F. Fhou, C. Jehoulet, and A. J. Bard, J. Am. Chem. Soc. **114**, 11004 (1992).

[25] I. S. Uzkikh, E. I. Dorozhkin, O. V. Boltalina, and A. Boltalina, Dokl. Chem. **379**, 204 (2001).

[26] I. E. Kareev, I. V. Kuvychko, S. F. Lebedkin, S. M. Miller, O. P. Anderson, S. H. Strauss, and O. V. Boltalina, Chem. Commun. , 308 (2006).

[27] N. Shinohara, K. Matsumoto, S. Endoh, J. Maru, and J. Nakanishi, Toxicol. Lett. **191**, 289 (2009).

[28] S. H. Friedman, D. L. DeCamp, R. P. Sijbesma, G. Srdanov, F. Wudl, and G. L. Kenyon, J. Am. Chem. Soc. **115**, 6506 (1993).

[29] R. P. Sijbesma, G. Srdanov, F. Wudl, J. A. Castro, C. Wilkins, S. H. Friedman, D. L. DeCamp, and G. L. Kenyon, J. Am. Chem. Soc. **115**, 6510 (1993).

[30] G. L. Marcorin, T. D. Ros, S. Castellano, G. Stefancich, I. Bonin, S. Miertus, and M. Prato, Org. Lett. **2**, 3955 (2000).

[31] V. W. und D. Wechsler, *Technologiefrueherkennung, Technologieanalyse, Nanobiotechnologie II: Anwendungen in der Medizin und Pharmazie*, VDI Technologiezentrum, 2004.

[32] J. Kanicki, *Handbook of conducting polymer*, Dekker, New york, 1986.

[33] S. Glenis, G. Tourllon, and F. Garnier, Thin Solid Films **111**, 93 (1984).

[34] S. Karg, W. Riess, V. Dyakonov, and M. Schwoerer, Synth. Metals **54**, 427 (1993).

[35] H. Antoniadis, B. R. Hsieh, M. A. Abkowitz, S. A. Jenekhe, and M. Stolka, ibid **64**, 265 (1994).

[36] R. N. Marks, J. J. M. Halls, D. D. D. C. Bradley, R. H. Friedl, and A. B. Holmes, J. Phys. Condens. Matter **6**, 1379 (1994).

[37] G. Yu, C. Zhang, and A. J. Heeger, Appl. Phys. Lett. **64**, 1540 (1994).

[38] G. Yu, J. Gao, J. C. Hummelen, F. Wudl, and A. Heeger, Science **270**, 1789 (1995).

[39] C. Deibel and V. Dyakonov, Rep. Prog. Phys. **73**, 096401 (2010).

[40] V. R. Meyer, *Practical high-performance liquid chromatography*, Wiley, 2004.

[41] H. H. Perkampus, *UV-VIS spectroscopy and its application*, Springer, 1992.

[42] M. Karas, D. Bachmann, U. Bahr, and F. Hillenkamp, Int. J. Mass Spectrum, Ino Proc **78**, 53 (1987).

[43] M. Karas, D. Bachmann, U. Bahr, and F. Hillenkamp, Int. J. Mass Spectrum. Ion Proc **92**, 231 (1989).

[44] M. Karas and F. Hillenkamp, Anal. Chem. **60**, 2299 (1988).

[45] K. Tanaka, H. Waki, Y. Ido, S. Akita, and Y. Yoshida, Rapid Commun. Mass Spectrom **2**, 151 (1998).

[46] R. Ekman, J. Silberring, A. M. Westman-Brinkmalm, and A. Kraj, *Mass spectrometry: instrumentation , interpretation and application*, John Wiley & sons, Inc, 2008.

[47] C. G. Herbert and R. A. W. Johnstone, *Mass Spectrometry basic*, CRC Press LLC, 2000.

[48] K. Strupat, M. Kara, and F. Hillenkamp, Int. J. Mass Spectrum. Ion Proc. **111**, 89 (1991).

[49] R. C. Beavis, T. Chaudhary, and B. T. Chait, Org. Mass Spectum **27**, 156 (1992).

[50] K. Tanaka, N. I. Taranenko, S. L. Allman, L. Y. Chang, and C. H. Chen, Rapid Commun. Mass Spectrom **8**, 727 (1994).

[51] L. Ulmer, J. Mattay, H. G. Torres-Garcia, and H. Luftmann, Eur. J. Mass. Spectrom **6**, 49 (2000).

[52] W. Massa, *Crystal structure determination*, Spring-Verlag, 2004.

[53] P. J. Krusic, E. Wasserman, P. N. Keizer, J. R. Morton, and K. F. Preston, Science **254**, 1183 (1991).

[54] N. B. Tamm, L. N. Sidorov, and S. I. Troyanov, Moscow Univ. Chem. Bull. **64**, 327 (2009).

[55] T. Mutig, E. Kemnitz, and S. I. Troyanov, Mendeleev Commun. **19**, 30 (2009).

[56] J. P. Hare, H. W. Kroto, and R. Taylor, Chem. Phys. Lett. **177**, 394 (1991).

[57] P. K. Zarzycki, H. Ohta, Y. Saito, and K. Jinno, Chromatographia **64**, 79 (2006).

[58] H. Ohta, Y. Saito, N. Nagae, J. J. Pesek, M. T. Matyska, and K. Jinno, J. Chromatogr. A **883**, 55 (2000).

[59] R. S. Ruoff, D. S. Tse, R. Malhotra, and D. C. Lorents, J. Phys. Chem. **97**, 3379 (1993).

[60] K. Kikuchi, N. Nakahara, T. Wakavayashi, M. Honda, H. Matsumiya, T. Moriwaki, S. Suzuki, H. Shiromaru, K. Saito, K. Yamauchi, I. Ikemoto, and Y. Achiba, Chem. Phys. Lett. **188**, 177 (1992).

[61] H. Yang, M. Yu, H. Jin, Z. Liu, M. Yau, B. Liu, M. M. Olmstead, and A. L. Balch, J. Am. Chem. Soc. **134**, 5331 (2012).

[62] M. Buehl and C. van Wuellen, Chem. Phys. Lett. **247**, 63 (1995).

[63] N. B. Shustova, B. S. Newell, S. M. Miller, O. P. Anderson, R. D. Bolskar, K. Seppelt, A. A. Popov, O. B. Boltalina, and S. H. Strauss, Angew. Chem. Int. Ed. **46**, 4111 (2007).

[64] X. Lu, Z. Slanina, T. Akasaka, T. Tsuchiya, N. Mizorogi, and S. Nagase, J. Am. Chem. Soc. **132**, 5896 (2010).

[65] M. Zalibera, P. Rapta, A. A. Popov, and L. Dunsch, J. Phys. Chem. C **113**, 5141 (2009).

[66] J. A. Azamar-Barrios, T. J. S. Dennis, S. Sadhukan, H. Shinohara, G. E. Scuseria, and A. Penicaud, J. Phys. Chem. A **105**, 4627 (2001).

[67] B. C. Thompson and J. M. Frechet, Angew. Chem. Int. Ed. **47**, 58 (2008).

[68] P. M. Dewick, *Essentials of organic chemistry*, John Wiley & Son Ltd., 2006.

[69] G. Sun and M. Kertesz, J. Phys. Chem. A **105**, 5212 (2001).

[70] L. Epple, K. Amsharov, K. Simeonov, I. Dix, and M. Jansen, Chem. Commun. , 5610 (2008).

[71] M. A. Lanskikh, N. B. Tamm, L. N. Sidorov, and S. I. Troyanov, Inorg. Chem. **51**, 2719 (2012).

[72] J. Cioslowski, N. Rao, and D. Moncrieff, J. Am. Chem. Soc. **122**, 8265 (2000).

[73] J. Crassous, J. Rivera, N. S. Fender, L. Shu, L. Echegoyen, C. Thilgen, A. Herrmann, and F. Diederich, Angew. Chem. Int. Ed. **38**, 1613 (1999).

[74] E. I. Dorozhkin, A. A. Goryunkov, I. N. Ioffe, S. M. Avdoshenko, V. Y. Markov, N. B. Tamm, D. V. Ignat'eva, L. N. Sidorov, and S. I. Troyanov, Eur. J. Org. Chem , 5082 (2007).

[75] E. I. Dorozhkin, D. V. Ignat'eva, N. B. Tamm, A. A. Goryunkov, P. A. Khavrel, I. N. Ioffe, A. A. Popov, I. V. Kuvychko, A. V. Streletskiy, V. Y. Markov, J. Spandl, S. H. Strauss, and O. V. Boltalina, Chem. Eur. J. **12**, 3876 (2006).

[76] A. L. Balch, A. S. Ginwalla, J. W. Lee, B. C. Noll, and M. M. Olmstead, J. Am. Chem. Soc. **116**, 2227 (1994).

[77] E. Yamamoto, M. Tansho, T. Tomiyama, and H. Shinohara, J. Am. Chem. Soc. **118**, 2293 (1996).

[78] P. Boulas, M. T. Jones, K. M. Kadish, R. S. Ruoff, D. C. Lorents, and D. S. Tse, J. Am. Chem. Soc. **116**, 9393 (1994).

[79] P. L. Boulas, M. T. Jones, R. S. Ruoff, D. C. Lorents, R. Malhotra, D. S. Tse, and K. M. Kadish, J. Phys. Chem. **100**, 7573 (1996).

[80] Y. Yang, F. Arias, L. Echegoyen, L. P. Chibante, S. Flanagan, A. Robertson, and L. J. Wilson, J. Am. Chem. Soc. **117**, 7801 (1995).

[81] N. B. Tamm, I. N. Ioffe, E. Kemnitz, and S. I. Troyanov, Dalton Trans. , 2740 (2009).

[82] G. Sun and M. Kertesz, Chem. Phys. Lett. **276**, 107 (2002).

[83] Y. Achiba, K. Kikuchi, Y. Wakabayashi, Y. Miyake, and M. Kainosho, in *Science and technology of Fullerene Materials, MRS Symposia Proc.Pittsburgh: Materials Research Society*, 1995.

[84] G. Sun, Chem. Phys. Lett. **289**, 371 (2003).

[85] Z. Slanina, F. Uhlik, M. Yoshida, and E. Osawa, Full. Sci. Tech. **8**, 417 (2000).

[86] M. Watanabe, D. Ishimaru, N. Mizorogi, M. Kiuchi, and J. Aihara, J. Mol. struct.: Theochem **726**, 11 (2005).

[87] M. A. Lanskikh, Y. M. Belova, N. B. Tamm, K. Chang, E. Kemnitz, and S. I. Troyanov, Crystallogr. Rep. **56**, 1107 (2011).

[88] G. M. Sheldrick, Acta Cryst. **A64**, 112 (2008).

[89] M. S. J. Dewar, E. G. Zoebisch, E. F. Healy, and J. J. P. Stewart, J. Am. Chem. Soc. **107**, 3902 (1985).

[90] J. P. Perdew, K. Burke, and M. Ernzerhof, Phys. Rev. Lett. **77**, 3865 (1996).

[91] W. Kohn and J. J. Sham, Phys. Rev. **140**, A1113 (1965).

[92] T. molecular modeling software version 4.2, http://dasher.wustl.edu/tinker/index.html .

[93] A. A. Granovsky, Firefly version 7.1C, http://classic.chem.msu.su/gran/firefly/index.html .

[94] W. M. Schimdt, K. K. Baldridge, J. A. Boatz, S. T. Elbert, M. S. Gordon, J. J. Jensen, S. Koseki, N. Matsunaga, K. A. Nguyen, S. Su, T. L. Windus, M. Dupuis, and J. A. Montgomery, J. Comput. Chem. **14**, 1347 (1993).

[95] D. N. Laikov, Chem. Phys. Lett. **281**, 151 (1997).

Publications by the Author

The author is involved in the following publications:

(I) **Chang, K.** ; Fritz, M. A. ; Tamm, N. B. ; Goryunkov, A. A.; Sidorov, L. N.; Chen, C.; Yang, S.; Kemnitz, E. ; Troyanov, S. I.: Synthesis, Structure, and Theoretical Study of Trifluoromethyl Derivatives of C_{84}(22) Fullerene. In: *Chem. Eur. J* DOI: 10.1002/chem.201202568

(II) Lanskikh, M. ; **Chang, K.** ; Tamm, N. B. ; Kemnitz, E. ; Troyanov, S. I.: Trifluoromethyl derivatives of C_{88}(33)fullerene: $C_{88}(CF_3)_{16,18,20}$. In: *Mendeleev Commun.* 22 (2011), S. 136

(III) Lanskikh, M. ; Belova, Yu. ; Tamm, N. B. ; **Chang, K.** ; Kemnitz, E. ; Troyanov, S. I.: Crystal and molecular structures of tirfluoromethyl derivatives of fullerene C_{76} and C_{82}. In: *Crystallography Reports* 56 (2011), S. 1107

Presentation:

(IV) **Chang, K.** ; Lanskikh, M. ; Troyanov, S. I. ; Kemnitz, E. : Synthesis and Investigation of trifluoromethylated high order fullerenes: New trifluoromethyl derivatives of C_{76}. In: *Graduate School 1582/1 - Fluorine as a key element, PhD students workshop, Burg(Spreewald), Germany* (2011)

(V) **Chang, K.** ; Mutig, T. ; Troyanov, S. I. ; Kemnitz, E. : Synthesis and Investigation of trifluoromethylated high order fullerenes. In: *Graduate School 1582/1 - Fluorine as a key element, colloquium, Berlin, Germany* (2011)

(VI) **Chang, K.** ; Mutig, T. ; Troyanov, S. I. ; Kemnitz, E.: Synthesis and isolation of heptafluoropropylated fullerenes: Molecular structures of $C_{60}(n\text{-}C_3F_7)_{6-10}$ and $C_{60}(CF_3)(i\text{-}C_3F_7)$. In: *14. Deutscher Fluortag, Schmitten, Germany* (2010)

Poster:

(VII) Lanskikh, M. ; **Chang, K.** ;Belova, Yu. ; Tamm, N. B. ; Kemnitz, E. ; Troyanov, S. I.: New trifluoromethyl derivatives of C_{76} and C_{82} In: *ACN - Advanced Carbon Nanostructures, St. Perstersburg, Russia* (2011)

(VIII) **Chang, K.** ; Mutig, T. ; Troyanov, S. I. ; Kemnitz, E.: Synthesis and isolation of heptafluoropropylated fullerenes: Molecular structures of $C_{60}(n\text{-}C_3F_7)_{6-10}$ and $C_{60}(CF_3)(i\text{-}C_3F_7)$. In: *16th ESFC - European Symposium on Fluorine Chemistry, Ljubljana, Slovenia* (2010)

Selbständigkeitserklärung

Ich erkläre, dass ich die vorliegende Arbeit selbständig und nur unter Verwendung der angegebenen Literatur und Hilfsmittel angefertigt habe.

Berlin, den 08. Oktober 2012 Kai-Chin Chang

Acknowledgments

I would like to take this opportunity to express my gratitude to Prof. Dr. Erhard Kemnitz for the available resources and the generous support for my scientific work. I would like to thank also my co-supervisor Prof. Dr. Sergey Troyanov for his patience, advice and valuable discussion.

It gives my great pleasure to thank Dr. Steffen Weidner and Ms. Rosemarie Laging in Federal Institute for Materials Research and Testing (BAM) for MALDI-Mass analysis.

My special thanks go to Dr. Johannes Noack, Dr. Asbjörn Burow, Dr. David Zhang, Larissa Schmidt, Matthias Karg and Ying Guo for the thesis correction.

At last but not least, i would like to thank the colleagues of Kemnitz's group for the support and keeping nice atmosphere.